A-20 Chimera

Final Report
Austere Field Light Attack Aircraft
DSE Group 4

Delft University of Technology, Faculty of Aerospace Engineering

TU Delft

A-20 Chimera

Austere Field Light Attack Aircraft

by

DSE Group 4

Version Number	Date	Comment
0.1	January 21, 2021	Draft
1.0	January 26, 2021	Final

Tutor:	Dr. Ir. R. Vos	
Coaches:	G. B. L. Tosti Balducci	
	Dr. S. J. de Vet	
Students:	J. M. Hinsenveld	4368908
	M. Jansens	4444515
	M. T. de Keijzer	4496701
	F. Kuhnert	4353811
	L. van der Mark	4535839
	A. Moghaddam	4536932
	S. P. van Oosterhout	4536711
	T. H. Y. Tom	4650174
	D. G. Velds	4549244
	Y. Watabe	4669797

TU Delft

Acknowledgement

This report is the result of the education we have received in the Bachelor courses on the Aerospace Engineering Faculty of the Delft University of Technology. As a group we have learned a lot during our years as Bachelor students and will learn much more on the path we will take after this report. Therefore, we would like to thank every employee of the Aerospace Engineering Faculty whom have made this Bachelor program available.

A special thank goes out to Dr. Ir. Roelof Vos, Dr. Sebastiaan J. de Vet and Giorgio B. L. Tosti Balducci for their help and guidance throughout the process of designing this aircraft. They helped us bring this design to a higher level with their insights and feedback. They also provided us with guidance where ever needed during the design phase.

We also want to thank Richard Helsdingen and Pascal Smaal, former F-16 pilot and current F-35 pilot respectively. For their help and insight in the pilots view on flying fighter aircraft and the information they gave about current war scenarios. They aided us in making choices based on real-life feedback, which we believe was of tremendous help to our project.

Last but certainly not least we would like to thank the OSCC and especially our TA, Robert Coenen, to provide us with the information we needed to perform this DSE in these challenging times.

Delft, January 2021

J. M. Hinsenveld
M. Jansens
M. T. de Keijzer
F. Kuhnert
L. van der Mark
A. Moghaddam
S. P. van Oosterhout
T. H. Y. Tom
D. G. Velds
Y. Watabe

Contents

List of Symbols

Abbreviations

ADSEE	Aerospace Design and Systems Engineering Elements
AIAA	American institute of aeronautics and astronautics
APU	Auxiliary Power Unit
c.g.	Center of gravity
CAS	Close Air Support
CBR	California Bearing Ratio
CD	Cockpit Distributor
CFD	Computational Fluid Dynamics
COVID-19	Corona Virus Disease 2019
CPI	Consumer Price Index
CVR	Cockpit Voice Recorder
DAPCA	Development And Production Costs Of Aircraft
DOD	Department of defense
DSE	Design Synthesis Exercise
EAS	Equivalent Airspeed
EBAS	Engine Based Air System
ECS	Environmental Control System
EHA	Electro-Hydrostatic Actuation
EHA-CPU	EHA Processor
FBS	Functional Breakdown Structure
FCC	Flight Control Computer
FCMS	Fuel Control and Monitoring System
FFD	Functional Flow Diagram
FLIR	Forward-Looking Infrared
FQIS	Fuel Quantity Indication System
GPS	Global Positioning System
GPWS	Ground Proximity System
HUD	Head-up display
ISA	International Standard Atmosphere
JTAC	Joint Terminal Attack Controller
LiDAR	Light Detection and Ranging
MAC	Mean Aerodynamic Chord
MANPADS	MAN-Portable Air-Defense Systems
MAW	Missile Approach Warning
MMOI	Mass Moment of Inertia
MNS	Mission Need Statement
MTOW	Maximum Take Off Weight
NATO	North Atlantic Treaty Organization
OEW	Operational Empty Weight
OFAT	One Factor At a Time
PD	Power Delivery system
PID	Proportional-Integral-Derivative
POS	Project Objective Statement
QDF	Quantity Discount Factor
RDT&E	Research, Development, Testing & Evaluation
RFP	Request for Proposal
ROI	Return On Investment
S.M.	Stick fixed stability margin
S/G	Starter-Generator
SEAD	Systems Engineering and Aerospace Design
SWOT	Strength, Weakness, Opportunities and Threats
TBO	Time Between Overhauls
TPM	Technical Performance Measures
TRL8	Technology Readiness Level 8
US	United States

Greek symbol

α	Angle of attack	[°]
α_{fuel}	correction factor for lateral fuel position	[-]
$\Delta C_{\text{L}_{\text{flap}}}$	Incremental lift coefficient due to flaps	[-]
δ_{a}	Aileron deflection	[°]
δ_{LD}	Flap deflection during landing	[°]
δ_{TO}	Flap deflection during takeoff	[°]
δ_{ac}	Actuator commanded aileron deflection	[°]
ϵ_{t}	Twist angle	[rad]
η	Drag ratio of a finite cylinder over an infinite cylinder	[-]
η_{h}	Horizontal tail ratio to the wing dynamic pressure	[-]
$\frac{\partial \alpha_h}{\partial \alpha}$	Horizontal tailplane angle of attack derivative with respect to angle of attack	[-]
$\frac{d\varepsilon}{d\alpha}$	Downwash effect of the wing on the tail	[-]
Γ	Dihedral	[°]
λ	Taper ratio	[-]
$\Lambda_{\text{hinge line}}$	Sweep angle of the flap hinge line	[°]
$\Lambda_{c/4}$	Quarter-chord sweep angle	[°]
μ	Viscosity coefficient of air	[kg/ms]
ϕ	Roll angle	[°]
ρ	Air density	[kg/m^3]
ρ_0	Air density at sea level (ISA)	[kg/m^3]
ρ_s	Air density at begin of tropopause	[kg/m^3]
τ	Aileron efficiency	[-]
τ	Time constant	[s^{-1}]

Nomenclature

μ_{g}	Ground friction coefficient	[-]
A	Wing aspect ratio	[-]
b	wing span	[m]
b_1	Inboard span position of aileron	[m]
b_2	Outboard span position of aileron	[m]
b_{cw}	Center section span	[m]
c	Chord length	[m]
$(c_{l_\delta})_{\text{theory}}$	Lift effectiveness plain control surface	[-]
$\bar{c}$	MAC length	[m]
$\left(\frac{c_{l_\delta}}{(c_{l_\delta})_{\text{theory}}}\right)$	Lift effectiveness correction factor	[-]
$\left(C_{\text{l}_\delta}\right)_{\text{left}}$	Rolling moment contribution of the left aileron	[-]
$\left(C_{\text{l}_\delta}\right)_{\text{right}}$	Rolling moment contribution of the right aileron	[-]
ω	Turn rate	[deg/s]
$c(y)$	Chord function, describing the chord length as a function of y	[m]
C_{fe}	Skin friction coefficient	[-]
C_{D_0}	Zero lift drag coefficient	[-]
$C_{\text{D}_{0_{\text{emp}}}}$	Empenage zero lift drag coefficient	[-]
$C_{\text{D}_{0_{\text{fus-base}}}}$	Base less fuselage drag coefficient	[-]
$C_{\text{D}_{0_{\text{fus}}}}$	Zero lift fuselage drag coefficient	[-]
$C_{\text{D}_{0_{\text{gear}}}}$	Landing gear zero lift drag coefficient	[-]
$C_{\text{D}_{0_{\text{W}}}}$	Zero lift wing drag coefficient	[-]
$C_{\text{D}_{\text{b}_{\text{fus}}}}$	Fuselage base drag coefficient	[-]
$C_{\text{D}_{\text{c}}}$	Canopy drag coefficient	[-]
$c_{\text{d}_{\text{c}}}$	steady state cross-flow drag coefficient	[-]
$C_{\text{D}_{\text{emp}}}$	Empennage drag coefficient	[-]
$C_{\text{D}_{\text{flap}}}$	Flap drag coefficient	[-]
$C_{\text{D}_{\text{fus}}}$	Fuselage drag coefficient	[-]
$C_{\text{D}_{\text{gear}}}$	Landing gear drag coefficient	[-]
$C_{\text{D}_{\text{int}_{\text{flap}}}}$	Flap interference drag coefficient	[-]
$C_{\text{D}_{\text{int}_{\text{flap}}}}$	Two-dimensional profile drag increment	[-]

$C_{D_{int}}$	Interference drag coefficient	[-]
$C_{D_{i_{flap}}}$	Flap induced drag coefficient	[-]
$C_{D_{L_{emp}}}$	Empenage lift drag coefficient	[-]
$C_{D_{L_{fus}}}$	Lift induced fuselage drag coefficient	[-]
$C_{D_{L_W}}$	Lift induced wing drag coefficient	[-]
$C_{D_{misc}}$	Miscellaneous drag coefficient	[-]
$C_{D_{np}}$	Nacelle/ pylon drag coefficient	[-]
$C_{D_{n_{int}}}$	Nacelle / pylon interference drag coefficient	[-]
C_{D_n}	Uninstalled nacelle drag coefficient	[-]
C'_{D_n}	Nacelle interference drag coefficient	[-]
$C_{D_{prof_{flap}}}$	Flap profile drag coefficient	[-]
C_{D_p}	Uninstalled pylon drag coefficient	[-]
$C_{D_{stores}}$	Stores drag coefficient	[-]
$C_{D_{trim}}$	Trim drag coefficient	[-]
$C_{D_{wing}}$	Wing drag coefficient	[-]
C_{d_0}	Zero drag coefficient of the airfoil	[-]
$C_{f_{fus}}$	Fuselage skin friction coefficient	[kg/ms]
C_{f_w}	Skin friction coefficient of the wing	[kg/ms]
$C_{L_{\alpha_{A\text{-}h}}}$	Lift rate coefficient aircraft less tail	[-]
$C_{L_{\alpha_h}}$	Lift rate coefficient horizontal tail	[-]
$C_{L_{\alpha_v}}$	Lift curve slope of the vertical tail	[-]
$C_{l_{\delta_\alpha}}$	Control derivative with respect to δ_α, describing rolling moment	[-]
$C_{l_{\delta_a}}$	Rolling moment due to aileron deflection	[-]
$C_{l_{\delta_r}}$	Rolling moment due to rudder deflection	[-]
$C_{L_{A\text{-}h}}$	Lift coefficient of the aircraft less tail	[-]
C_{L_h}	Lift coefficient of the horizontal tail	[-]
$C_{L_{max_{landing}}}$	Maximum lift coefficient in landing configuration	[-]
$C_{L_{max_{TO}}}$	Maximum lift coefficient in takeoff configuration	[-]
$C_{L_{max}}$	Maximum lift coefficient	[-]
C_{L_W}	Lift coefficient of the wing	[-]
C_{l_p}	Stability derivative with respect to p, describing roll damping	[-]
C_L	Lift coefficient	[-]
C_{m_α}	Static longitudinal stability coefficient	[-]
$C_{m_{\dot{\alpha}}}$	Pitching moment derivative due to the rate of the angle of attack	[-]
$C_{m_{ac}}$	Moment coefficient about the aerodynamic center	[-]
C_{m_q}	Pitching moment coefficients due to the pitch rate	[-]
C_{m_u}	Pitching moment coefficient due to the airspeed	[-]
$C_{n_{\delta_a}}$	Yawing moment due to aileron deflection	[-]
$C_{n_{\delta_r}}$	Yawing moment due to rudder deflection	[-]
C_{X_α}	Drag coefficient due to the angle of attack	[-]
C_{X_u}	Drag coefficient due to the airspeed	[-]
$C_{Y_{\delta_a}}$	Side force due to aileron deflection	[-]
$C_{Y_{\delta_r}}$	Side force due to rudder deflection	[-]
C_{Z_α}	Aerodynamic angle-of-attack derivative	[-]
$C_{Z_{\dot{\alpha}}}$	Lift derivative due to the rate of the angle of attack	[-]
C_{Z_q}	Lift coefficient due to pitch rate	[-]
C_{Z_u}	Lift coefficient due to the airspeed	[-]
$C_{D_{store}}$	Store drag coefficient	[-]
C_{l_β}	Rolling moment due to sideslip derivative	[rad$^-$1]

C_{l_p}	Rolling moment due to roll rate derivative	[rad$^-$1]
C_{l_r}	Rolling moment due to yaw rate derivative	[rad$^-$1]
C_{L_α}	Lift curve slope of aircraft	[rad^{-1}
$C_{l_{\beta_h}}$	Rolling moment due to sideslip derivative for horizontal tail	[rad$^-$1]
$C_{l_{\beta_v}}$	Rolling moment due to sideslip derivative for vertical tail	[rad$^-$1]
$C_{l_{\beta_{wf}}}$	Rolling moment due to sideslip derivative for wing-fuselage	[rad$^-$1]
$C_{l_{p_h}}$	Rolling moment due to roll rate derivative for horizontal tail	[rad$^-$1]
$C_{l_{p_v}}$	Rolling moment due to roll rate derivative for vertical tail	[rad$^-$1]
$C_{l_{p_w}}$	Rolling moment due to roll rate derivative for wing	[rad$^-$1]
$C_{l_{r_v}}$	Rolling moment due to yaw rate derivative for the vertical tail	[rad$^-$1]
$C_{l_{r_w}}$	Rolling moment due to yaw rate derivative for the wing	[rad$^-$1]
$C_{m_{\alpha_{fus}}}$	Pitching moment due to angle of attack derivative	[[rad^{-1}]
C_{n_β}	Yawing moment due to sideslip derivative	[rad$^-$1]
C_{n_p}	Yawing moment due to roll rate derivative	[rad$^-$1]
C_{n_r}	Yawing moment due to yaw rate derivative	[rad$^-$1]
$C_{n_{\beta_f}}$	Yawing moment due to sideslip derivative for fuselage	[rad$^-$1]
$C_{n_{\beta_v}}$	Yawing moment due to sideslip derivative for vertical tail	[rad$^-$1]
$C_{n_{\beta_w}}$	Yawing moment due to sideslip derivative for wing	[rad$^-$1]
$C_{n_{p_v}}$	Yawing moment due to roll rate derivative for vertical tail	[rad$^-$1]
$C_{n_{p_w}}$	Yawing moment due to roll rate derivative for wing	[rad$^-$1]
$C_{n_{r_v}}$	Yawing moment due to yaw rate derivative for the vertical tail	[rad$^-$1]
$C_{n_{r_w}}$	Yawing moment due to yaw rate derivative for the wing	[rad$^-$1]
C_{y_β}	Sideforce due to sideslip derivative	[rad$^-$1]
C_{y_p}	Sideforce due to roll rate derivative	[rad$^-$1]
C_{y_r}	Sideforce due to yaw rate derivative	[rad$^-$1]
$C_{y_{\beta_f}}$	Sideforce due to sideslip derivative for fuselage	[rad$^-$1]
$C_{y_{\beta_v}}$	Sideforce due to sideslip derivative for vertical tail	[rad$^-$1]
$C_{y_{\beta_w}}$	Sideforce due to sideslip derivative for wing	[rad$^-$1]
d_b	Fuselage base diameter	[m]
d_f	Fuselage diameter	[m]
e	Oswald efficiency factor	[-]
F_{a_2}	Factor including area rulling effects	[-]
k	Quantity factor	[-]
k'	Rudder effectiveness constant	[-]
K_a	Correlation constant for the yawing moment due to aileron deflection	[-]
K_b	Control surface span factor	[-]
k_{fair}	Correction factor for the fairing	[-]
L'	Airfoil thickness location parameter	[-]
l_f	Fuselage length	[m]
l_h	Tail length	[m]
l_v	Distance between c.g. and the a.c. of the vertical tail in x-direction	[m]
M	Mach number	[-]
m	Mass	[kg]
p	Roll rate	[°/s]
P_s	Specific Excess Power	[m/s]
R_{LS}	Lifting surface correction factor	[-]
R_N	Reynolds number	[-]

R_{wf}	Wing/fuselage interference factor	[-]
S	Surface area of the wing	[m^2]
S_1	Reference area 1 for wing box side panel	[m]
S_2	Reference area 2 for wing box side panel	[m]
$S_{b_{fus}}$	Fuselage base area	[m^2]
S_{fus}	Fuselage frontal area	[m^2]
S_{gear}	Reference area for the zero lift gear drag coefficient	[m^2]
S_h	Surface area of the horizontal tail	[m^2]
S_n	Nacelle frontal area	[m^2]
$S_{plf_{fus}}$	Fuselage planform area	[m^2]
s_{TOG}	Maximum allowable ground run	[m]
s_{TO}	Takeoff distance	[m]
S_v	Surface area of the vertical tail	[m^2]
$S_{wet_{fus}}$	Wetted fuselage area	[m^2]
S_{wet}	Wetted surface area	[m^2]
S_{wf}	Wing area effected by flaps	[m^2]
$S_{w_{net}}$	Net exposed wing area	[m^2]
t	Time	[s]
$\left(\overline{t/c}\right)_w$	Thickness ratio of the wing	[-]
T_0	Thrust at sea level	[N]
$T_a v$	Thrust available	[N]
T_s	Thrust at begin of tropopause	[N]
V	Airspeed	[m/s]
$\bar{V}_h$	Horizontal tail volume coefficient	[-]
$\left(\frac{V_h}{V}\right)$	Tail/wing speed ratio	[-]
W_F	Fuel Weight	[N]
W_{TO}	Take off weight	[N]
$\bar{x}_{ac_h}$	Aerodynamic center location of the horizontal tail with respect to wing MAC	[-]
$\bar{x}_{ac}$	Aerodynamic center position relative to the MAC	[%MAC]
$\bar{x}_{cg}$	Center of gravity position relative to the MAC	[%MAC]
$\bar{x}_{np}$	Neutral point location expressed as percentage MAC	[-]
$x_{cg_{ammo}}$	c.g. location of the ammo	[m]
$x_{cg_{fuel}}$	c.g. location of the fuel	[m]
$x_{cg_{payload,hardpoint}}$	c.g. location of the payload on the hardpoints	[m]
x_{LEMAC}	Position of the leading edge of the MAC	[m]
x_{cg}	Longitudinal position of the center of gravity	[m]
y	Variable describing position along wingspan	[m]
y_{cg}	Lateral position of the center of gravity	[m]
z_v	Distance between c.g. and the a.c. of the vertical tail in z-direction	[m]
R	Turn radius	[m]

Executive Overview

Challenge

A concrete Mission Need Statement and Project Objective Statement is stated which are used for this project.

MNS: To provide close air support to ground forces from short, front-line, austere fields at short notice, while being affordable.
POS: To design an affordable light attack aircraft, within 10 weeks by 10 students, which can operate from short austere fields close to the front lines.

Missions, Functions and Requirements

The missions, the A-20 should perform, are listed below.

1. CAS (Close Air Support) against infantry
2. CAS against vehicles
3. CAS against structures
4. Tactical bombing
5. Reconnaissance
6. Armed patrol

Additionally, for these missions, the threats are identified. These threats were taken into account when designing the protection of the pilots in the aircraft, and what the aircraft should be capable of during such missions. Hot-pit refueling is a primary example of such a scenario, where the aircraft has to re-arm and re-fuel within a short time span. This meant that the loading pattern had to be taken into account when sizing the aircraft regarding its balance.

Market Analysis

In the market definition, the stakeholders involved in designing a fighter aircraft was evaluated. This was used to find requirements that came from the stakeholder, which can drive the design or give new insights on how the aircraft should function.
Additionally, the market trend for military aircraft fixed wing aircraft was looked at. The market trend showed that there will be more demand for multi-role aircraft that fulfill multiple roles by 2025. These include reconnaissance, surveillance and attack aircraft. This yielded the aircraft to be as flexible as possible, in order to fill the gap in the market.
Moreover, the competition showed what aircraft manufacturers are involved in the current market and the aircraft that these manufacturers will provide in the near future. In this market, it showed that the F-35 (provided by Lockheed Martin) will contribute roughly 45% to the expected 3 400 fighters by 2025. From these aircraft manufacturers, a reference aircraft had been listed that provide a similar mission profile or are currently in demand. An analysis within these reference aircraft confirmed that the ones solely designed for attack purposes are out of production or are even upgraded to perform as a multi-role aircraft, like the F-4 Phantom.
Lastly, the buyers behavior showed the rationale of the buyer. These determined that political and cost reasons have the biggest impact to the buyer.

Design Approach and Trade-off

In order to design the aircraft, a step-by-step design approach was determined. These steps were:

Class I

1. Drag polar analysis
2. Class I weight estimation
3. Wing/power loading diagrams
4. Propulsion, fuselage, and wing geometry
5. Component weight analysis
6. Empennage sizing
7. Landing gear placement & sizing

Class II

1. Aerodynamic analysis
2. High lift devices design
3. Control surfaces sizing
4. Class II weight estimation
5. Stability & control analysis

In the Class I design phase, four different concepts were sized in an iterative process. The four concepts were based on different characteristics. Concept 1 was focused on survivability and redundancy, where an H-tail and two turboprop engines allowed the aircraft to keep operating when one of the engines or vertical tails malfunction. The second concept was based on a canard configuration, which focused on high maneuverability and redundancy. This concept was the only concept with two turbojet engines. The third concept was based on affordability, where it was primarily based on reducing costs and simplicity. The fourth concept was a hybrid propulsion aircraft. It was powered by a gas turbine, which generates electricity for the propellers. It utilized three propellers, two on the wingtips and the third as a push propeller.

With survivability, costs, flexibility, sustainability, and performance as trade off criteria, the four concepts were assessed. As a result, a fifth concept was made, which was a hybrid solution of the first four concepts. Therefore, it is designed for survivability and redundancy, and uses a turbofan to cope with the high required cruise speed. Taking this fifth concept into account for the trade-off, the conclusion, given in Table 1, showed that the fifth concept was the best concept. This concept was then taken into the Class II design steps.

Table 1: Trade summary table

Criterion	Survivability [30%]	Costs [25%]	Flexibility [20%]	Sustainability [15%]	Performance [10%]	Total score
Concept 1	0.88	0.60	0.75	0.83	0.92	**77.9%**
Concept 2	0.88	0.50	0.70	0.76	0.77	**71.8%**
Concept 3	0.25	1	0.78	1	0.97	**72.7%**
Concept 4	0.63	0.25	0.70	0.74	0.69	**57.0%**
Concept 5	1	0.6	0.85	0.85	0.83	**83.0%**

Weight Estimation

To estimate the weight of the aircraft, two methods were used. First the Class I weight estimation, which estimated the Maximum Take Off Weight (MTOW), Operational Empty Weight (OEW), and Fuel Weight (W_F) based on statistical data of reference aircraft, and statistical fuel usage during each flight phase. It takes into account the required payload, range, and endurance of the aircraft. The payload consists of the required payload and the integrated gun with rounds. Furthermore, the crew, and trapped fuel and oil are included

in the OEW. With the Class I weight estimation, an initial sizing of the aircraft geometry was made. Using the initial sizing, the Class II weight estimation was performed. Class II estimates the weight of individual components of the aircraft, based on the component weight of reference aircraft. This resulted in an updated empty weight, and a more detailed center of gravity analysis. The resulting weight breakdown of the MTOW and OEW is presented in Figure 1.

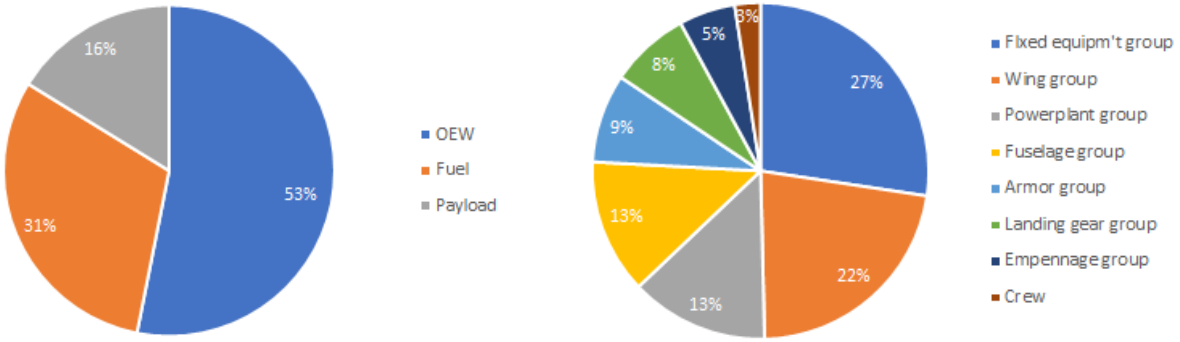

(a) Maximum Take Off Weight Breakdown as percentage of 135 kN

(b) Operational Empty Weight breakdown as a percentage of 71.5 kN

Figure 1: Weight breakdown of the A-20 *Chimera*

Fuselage Design

The fuselage is 15 m long and has an oval shape with flattened sides. It is 1.1 m wide and 1.5 m high (excluding cockpit). The cross section was determined by sizing and modeling the cockpit for ergonomics and viewing angles. The tail cone is 5.3 m long and is angled upwards to provide a ground scrape angle of 16.5 °. The fuselage houses the cockpit including armor, the cannons including ammunition as well as the majority of all electric and hydraulic subsystems as well as the nose landing gear. The rotating cannons are placed below the wing box. They are placed such that the firing barrel sticks out of fuselage. To reduce drag, they are hidden behind an aerodynamic fairing, with small cutouts for the muzzles. The cockpit features thick Steel-Steel Composite Metal Foam (CMF) plates, to armor the crew against rounds of handheld weapons, heavy machine guns and anti aircraft cannons with a caliber of at least 14.5 mm. The cockpit also features a big bubble shaped canopy, to provide the crew with an excellent visibility. Furthermore, it is fitted with big digital screens and modern helmets with integrated displays, instead of a cockpit mounted Head-up display.

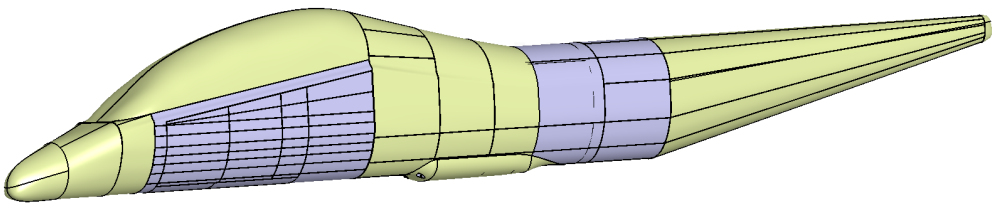

Figure 2: 3D model of the fuselage

Wing Design

The wing was sized using a thrust and weight loading diagram (Figure 3). The take off and landing stall requirements turned out to be the driving factors. A landing C_L of 2.6, and aspect ratio of 7 were selected. This resulted in the wing parameters of Table 2.

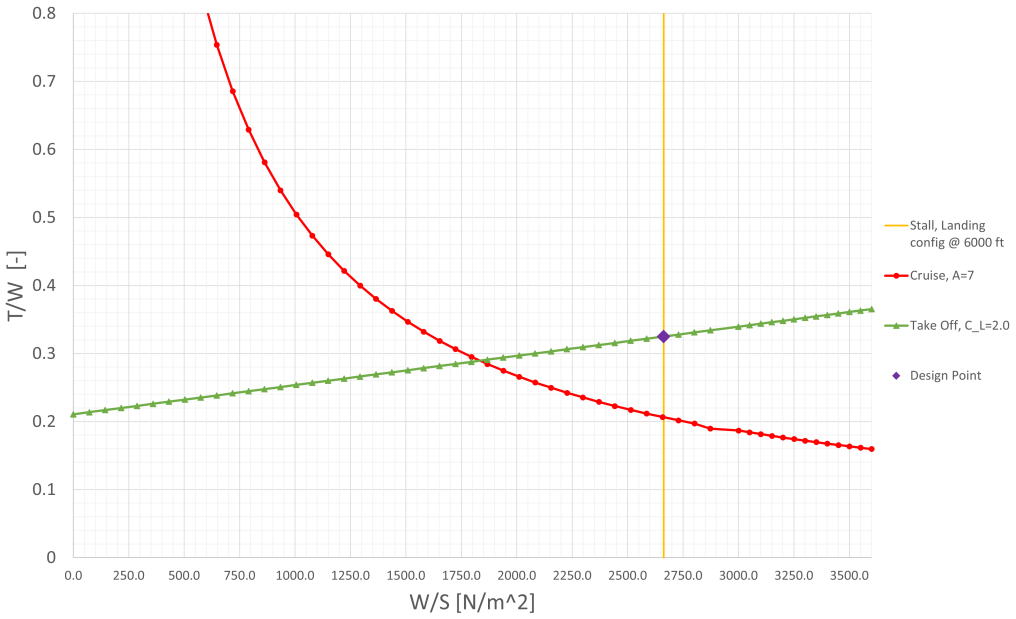

Figure 3: Thrust and wing loading diagram

Table 2: Dimensions of the main wing

parameter	value	unit
S	50.5	[m^2]
b	18.8	[m]
MAC	2.85	[m]
c_r	3.84	[m]
c_t	1.54	[m]
λ	0.4	[-]
$\Lambda_{c/4}$	0	[°]
Γ	3	[°]

Using this data, and the required airspeed at the most fuel-intenstive phase of the mission, the loitering phase, the NACA-44018 airfoil was selected to attain a design lift coefficient of 0.68. The properties of the airfoil in turn were used for sizing the ailerons, ensuring the required roll rate of 90°in 1.3 s. Each aileron has an area of 2.9 m^2, a span of 4.1 m, and cover 35% of the wing chord at the wing tips. The maximum deflection angle of the ailerons is 30°in both directions.

With the airfoil properties, and the required landing C_L, the required increase in maximum lift coefficient ($\delta C_{L_{max}}$) was determined. The flap type was chosen, and was sized accordingly. The double-slotted fowler flaps span 4.3 m, and cover 35% of the wing chord at the wing root. The deflection angle at take off is 20°, and the maximum deflection at landing configuration is 50°.

The wing structure was created, along with three hard points on each wing, and a fairing for the main landing gear. Figure 4 gives an impression of the wing geometry and structure.

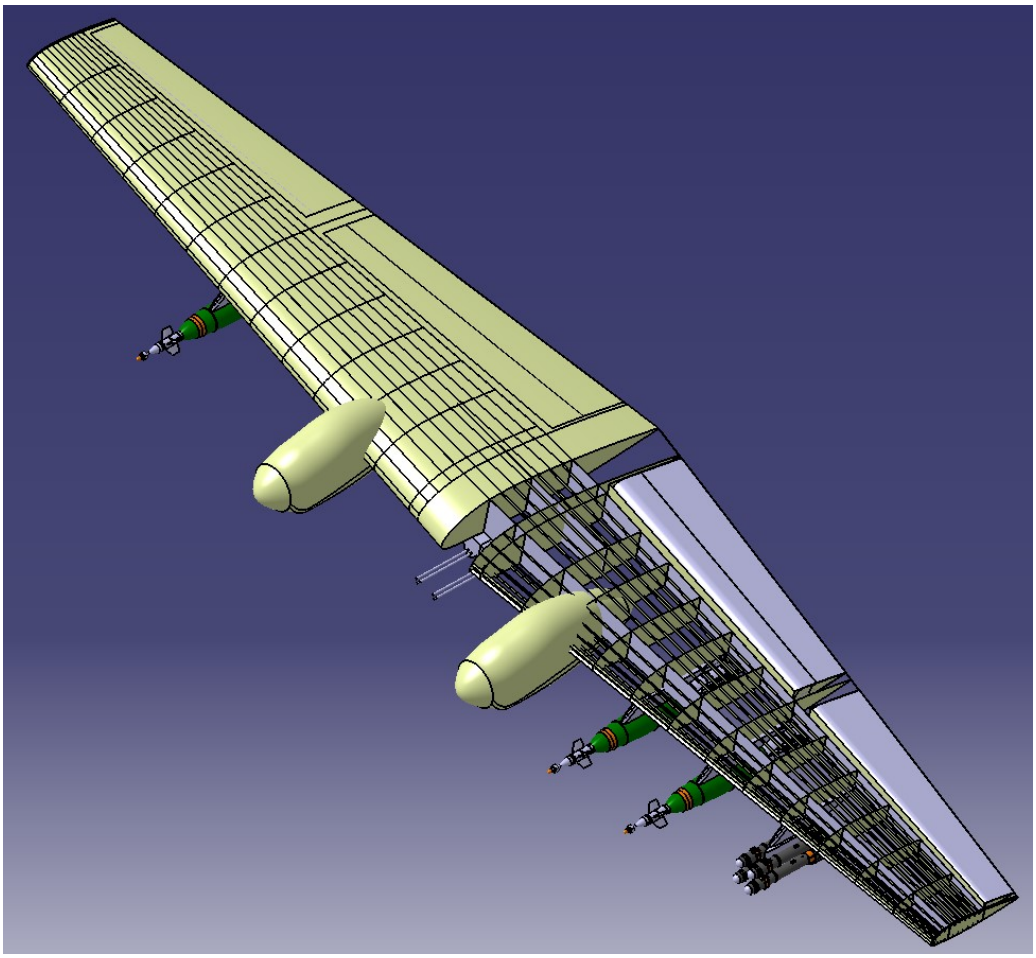

Figure 4: CAD model of the wing including armament, and main landing gear fairing

Empennage Design

The aircraft utilizes an H-tail design, which increases the redundancy regarding its controllability. The empennage was designed using a loading diagram and an X-plot. The loading diagram is a graph that combines each loading procedure of the payload on the aircraft (in this case the fuel, payload on hardpoints and ammo for the integrated gun). Based on the location and the weight a c.g. range is created between the most forward and most aft c.g. Then using these c.g. ranges, the wingposition can be moved to obtain a c.g. range diagram.

Simultaneously, an X-plot is created. In this plot, the stability and control curves of the aircraft is given. The sizing of previous subsystem designs were used as input to determine aerodynamic characteristics of the aircraft to determine the slope and location of these curves.

Both these diagrams were then superimposed and adjusted, such that the c.g. ranges determined in the c.g. range diagram fit between the lines of the controllability and stability. The combines diagrams resulted in an updated location of the wing and horizontal tailsurface sizing.

At last, these values were used as input for the whole design iteration to determine a new weight estimation and new weight and balance estimation (these are used in the class-I estimation). Consequently, the updated values of the class-I estimation are used as input for the class-II. This again yielded in a new empennage design (and wing location). The integrated process of class-I, class-II and empennage sizing was iterated until the output values of the empennage sizing was converged.

Finally, these resulted in a horizontal tailsurface-wingsurface ratio (S_h/S) of 0.22 and wingposition ratio (x_{LEMAC}/l_{fus}) of 0.4369. These values yielded a c.g. range of most forward and most aft c.g. of 0.31 and 0.41 % MAC, respectivel.

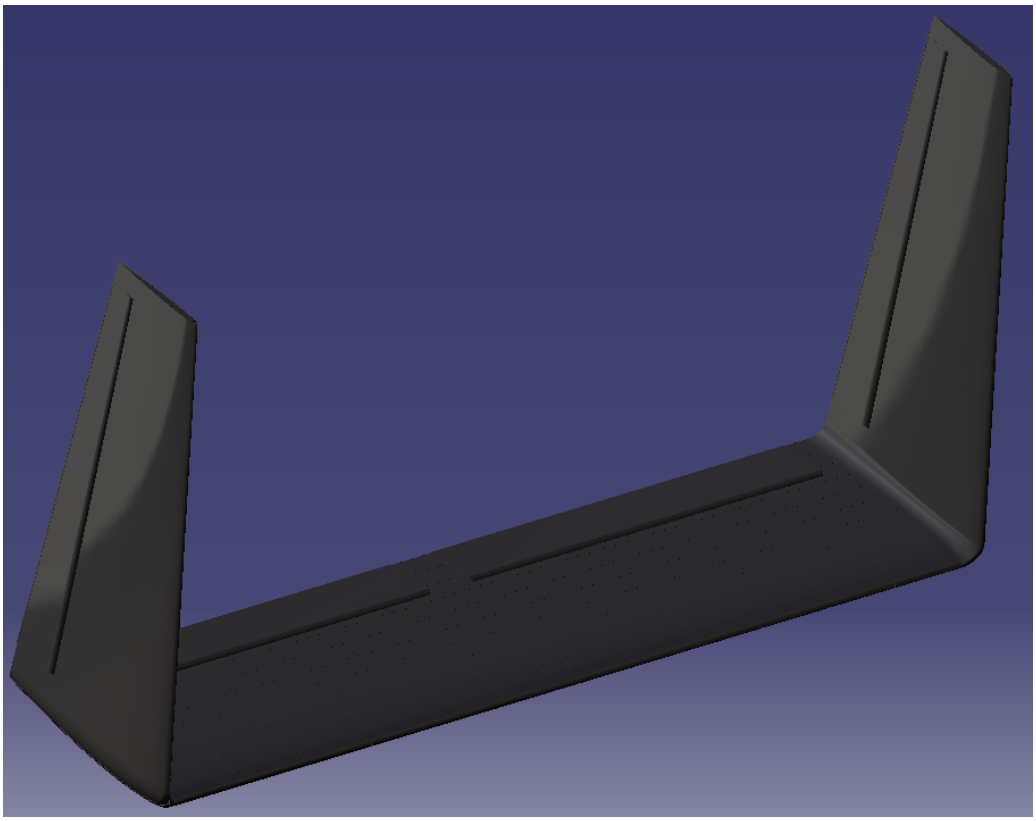

Figure 5: Empennage Design

Propulsion Unit Design

The required thrust of the aircraft was determined from Figure 3. The aircraft will feature two fuselage-mounted engines, with a mixer. Direct line of sight from the ground is limited as the inlets are covered by the wing, and the exhausts are partially covered by the horizontal tail plane. The engines were sized, based on an already existing engine. Each engine provides 21.9 kN of thrust, has a length of 1.78 m, and a diameter of 1.02 m. The nacelle is 2.08 m long. Considerably longer than the engine, because of the inlet and mixer.

Landing Gear Design

The landing gear was designed to be a tricycle retractable configuration, with a strut length of 2202.75mm at the nose and 2099.245mm at the main landing gear. The tyres were determined by static load and CBR 5 requirement, which leads to the nose landing gear tyre with an width of 152.4mm and an outer and inner diameter of 444.5mm and 152.4mm. Furthermore, the main landing gear tyres were chosen to be 220.98mm in width and an outer and inner diameter of 651.51mm and 220.98mm. Moreover, each individual wheel was equipped with carbon brakes to provide the aircraft to braking ability after landing or during taxi.

Additional Subsystems

As additional subsystems the fuel, hydraulic and electrical systems were designed. Next to these, the environmental control system as well as the data handling system were discussed.

The fuel system configuration was mainly determined by the location of the fuel and the location of the engines and Auxiliary Power Unit. It was chosen to have fuel tanks in both the wings and the fuselage in order to reduce the possibility of one big fuel tank being hit in combat. In order to pump the fuel to the two engines, different transfer pumps, for fuel pumping between tanks, as well as high pressure pumps, for fuel pumping to the engines, are used.

For the hydraulic system it was chosen to have a Electric-Hydrostatic Actuation system in the aircraft. The Electric-Hydrostatic Actuation system has multiple self-contained hydraulic systems at the actuation points and is powered by an Electric-Hydrostatic Actuation processor. To ensure redundancy, multiple actuation points were added for some components, such as the main landing gear and the flaps.

The electrical system provides electricity throughout the aircraft. Redundancy was a driving factor for the electrical system design, as the hydraulic system is also dependent on the electrical system. There are two independent electrical systems in the aircraft, to ensure this redundancy. In both electrical systems, a power delivery system makes sure every component is powered, connected to this is a battery. Both flight control computers can be powered from both power delivery systems. For power generation two starter-generators are implemented in the engines, as well as an Auxiliary Power Unit. All power generating components were coupled to both power delivery systems. A general layout for the electrical and hydraulic system was created.

The environmental control system is designed to provide pressurization and thermal control of the cabin for the pilots. The control system is chosen to have an Engine Based Air System, which uses bleed air from the engines, next to this, the cabin is equipped with pressure valves to regulate the cabin pressure. As with similar aircraft, a under-pressurization of the cabin was chosen for altitudes up to 8 000 ft, at higher altitudes the pressure in the cabin will remain at 8 000 ft. It was decided to design the thermal control system at a later stage.

For the data handling of the aircraft the F-35 approach to sensor fusion was taken as inspiration. Where the aircraft is able to obtain data from a vast variety of sensors, including in- and outside of the aircraft. Combining this data the pilot receives information interesting for the mission which is flown. Part of the data will be communicated to the pilot via a F-35 like helmet, as this would be positive for the mission execution.

Aerodynamics

During the designing of the aircraft an simplified approach to the aircraft's drags profile has been used. Where use has been made of simplified analytical equations and assumptions from reference data. This allowed for a much quicker iterative loop during the designing and sizing of all geometries. However, after finalizing the aircraft was finished a more thorough drag analyses was performed.

During this more thorough analysis the aircraft was divided into several subsystems, such as wings, fuselage, empenage, etc.. This allowed for a more detailed analysis of all drag inducing components on the aircraft. Per subsystem both the zero lift drag coefficient and the lift induced drag coefficient were determined. It was however assumed that only the wing, fuselage and horizontal tail create lift.

The next step in the analysis was to set the configurations of the aircraft which were of interest. It was decided to perform the analysis for: clean, stores, landing gear and flapped configuration. The meaning of these configurations are explained below. Clean was found interesting as this would give the lowest drag profile the aircraft could obtain. Stores was of interest as this is the main configuration the aircraft would fly in. Landing gear was of interest as this is a big non-aerodynamic area which the aircraft could deploy. Flapped configuration was of interest as this would yield the maximum drag profiles the aircraft could have.

- **clean**: Where the aircraft is flying clean (without stores), at cruise conditions.
- **stores**: Where the aircraft is flying with stores, at cruise conditions.
- **landing gear**: Where the aircraft is flying with stores and landing gear out, at maximum approach speed.
- **flapped**: Where the aircraft is flying with stores, landing gear out and flaps deflected.

After the analysis was performed, the obtained drag coefficient for different lift coefficients were plotted. Through the data points a trend-line was fitted, from which the zero lift drag coefficients and the Oswald efficiency factors were found. The results of this excursion can be found in Table 3.

Table 3: Values found from trend lines of the drag polars.

Configuration	C_{D_0} [-]	e [-]
Clean	0.017	0.76
Stores	0.028	0.76
Landing gear	0.043	0.78
Flapped	$0.061\Delta C_L + 0.038$	0.57

Stability and Control

Once all subsystems of the aircraft had been designed, they are integrated and evaluated on its aerodynamics, stability and control, and the performance. Here, the stability for longitudinal and lateral directions were analyzed. For each of these directions, they are differentiated between static and dynamic stability. For all cases, they were analyzed for cruise condition (Mach=0.61, clean-configuration), loiter condition (Mach=0.26, clean-configuration) and landing condition (Mach=0.14, flaps extended configuration)

The resulting values for the static stability and control, are given in the tables below. Next to the symbols listed in these table, the sign is given between square brackets that indicate the sign that is expected or required for a statically stable aircraft.

The longitudinal static stability derivative is the stability of the aircraft when there is a change in angle of attack, α. This value is considered stable, when the sign is negative, meaning for a change in angle of attack, the aircraft pitches back to its equilibrium position. Hence, the aircraft is stable according to Table 4

Table 4: Longitudinal Static Stability

Configuration	C_{m_α} **[-]**
Loiter	-0.856
Cruise	-0.895
Landing	-0.699

Similar to the longitudinal static stability, the sign of each derivative coefficient determine whether the aircraft is laterally static stable.

Table 5: Lateral stability derivatives with respect to sideslip angle, roll rate and yaw rate

Configuration	C_{y_β} [-]	C_{l_β} [-]	C_{n_β} [+]
Loiter	-0.438	-0.086	0.123
Cruise	-0.438	-0.083	0.122
Landing	-0.427	-0.072	0.131
	C_{y_p} [-]	C_{l_p} [-]	C_{n_p} [-]
Loiter	-0.092	-0.494	0.000
Cruise	-0.092	-0.499	0.000
Landing	-0.017	-0.513	-0.337
	C_{y_r} [+]	C_{l_r} [+]	C_{n_r} [-]
Loiter	0.269	0.736	-0.180
Cruise	0.269	0.220	-0.174
Landing	0.276	1.737	-0.216

Table 6 provides an overview of the handling qualities during each flight phase. The handling qualities are rated from one to three, where level one corresponds to the most desirable handling quality. This is due to the fact that it does not induce any extra work by the pilot to regain control of the aircraft. The aperiodic spiral did not comply with the desired flying quality, hence a PID controller was designed.

Table 6: Dynamic stability handling quality levels

	Short Period	**Phugoid**	**Aperiodic Roll**	**Dutch Roll**	**Aperiodic Spiral**
Loiter	Level 1	Level 1	Level 1	Level 1	Level 3
Cruise	Level 1	Level 1	Level 1	Level 1	Level 1
Landing	Level 1	Level 1	Level 1	Level 1	>Level 3

The sign of the control derivatives themselves follow naturally from the airplane configuration. However, the magnitude themselves do change according to the design. The results are given in Table 7.

Table 7: Control derivatives due to elevator deflection, aileron deflection and rudder deflection

Configuration	$C_{D_{\delta_e}}$ [+]	$C_{L_{\delta_e}}$ [+]	$C_{m_{\delta_e}}$ [-]
Cruise	0.52	1.10	-1.35
Landing	0.52	0.96	-1.35
Configuration	$C_{Y_{\delta_a}}$ [+]	$C_{l_{\delta_a}}$ [-]	$C_{n_{\delta_a}}$ [+]
Cruise	0	-0.40	0.01
Landing	0	-0.40	0.10
Configuration	$C_{Y_{\delta_r}}$ [-]	$C_{l_{\delta_r}}$ [-]	$C_{n_{\delta_r}}$ [-]
Cruise	1.59	0.20	-0.58
Landing	1.27	0.02	-0.49

Aircraft Performance

For the aircraft performance, the payload range, payload combat radius diagram, the load factor envelope, specific excess power diagrams and turn rate diagrams were made.

From the payload range diagram it was found that the aircraft exceeds the required range by a lot. This is mainly due to the range credit of the loiter mission, which was included in the diagram. From the payload combat radius diagram it was found that the aircraft provides enough range to go to and come back from mission, here the range credit of the loiter was not taken into account. Therefore a more accurate result was obtained.

For the load factor envelope the first step was to determine the limit loads for the aircraft, from MIL-A-8861 it was required to have a upper limit load of 7.5 and a lower limit load of -3. Combining these limit loads with the stall speed requirement, the minimum speed required at a given load factor was determined. From the aerodynamic analysis the C_{D_0} was used to find the drag profile of the aircraft (during a cruise mission), from which the maximum diving speed was obtained. Combining these steps resulted in the maneuvering diagram. The second step was to check for gust loads during flight. Where from the same MIL document as stated before, the gust speeds were obtained. This resulted in gust load lines, which were overlaid with the maneuverability plot. Tracing the limiting cases resulted in the load factor envelope.

Seven flight stages were considered for the performance diagram, namely; take off, clean cruise, cruise with stores, clean loiter, loiter with stores, normal landing, and aborted landing. In a performance diagram the specific excess power is given as a contour plot in a diagram with altitude and speed as its vertical and horizontal axis, respectively. The specific excess power can be used for acceleration, to climb or for sustained turns. The results of the design points for the given flight stages and their configuration are given in Table 8. In the table the weight, flight speed and altitude are given for the specified design points, as a result the specific excess power, P_s, at that point is given. Moreover, the maximum specific excess power is given and at which speed this is achieved. The last two column give the stall speed and maximum speed which can be achieved in level flight.

Table 8: Results from performance diagrams for four flight stages

	W [kN]	V [m/s]	h [m]	P_s [W/N]	$P_{s,max}$ [W/N]	$V_{Ps\,max}$ [W/N]	V_{stall} [m/s]	V_{max} [m/s]
Take off	130	61	1 800	9.7	12	86	51	140
Cruise, stores	130	200	3 000	13	23	140	59	230
Loiter, stores	120	86	910	22	28	130	52	230
Landing	100	50	1 800	11	13	68	39	110

From the excess power plot, turn rate plots were deduced. Using a speed and load factor combination the turn rates were determined. For the same speed and load factor combination the specific excess power was calculated. From these plots it can be deduced what the sustained maneuverability of the A-20 Chimera is. Since maneuverability is the most important during cruise and loiter two plots were produced. For the cruise conditions it was found that the maximum sustained turn rate is 15 deg/s, for loiter it is a bit higher with roughly 18 deg/s.

Operations & Logistics

In addition to missions of the the aircraft, A-20 is also expected to preform hot pit refueling as well as rearming. For rearming, it is mentioned that this procedure would take around 5 minutes per hard point for either missiles or rockets.
For the sake of having the keeping the logistics costs as low as possible, it is decided to transfer the aircraft via containers. After that, the dimensions of the containers are given to be 16.154m X 2.591m X 2.896m. Based on these dimensions and structural integrity of the aircraft, it is decided to have assembled the aircraft at the following:

- Along an axis that is located right after the leading edge and extends from the wing root to wing tip.
- Where the wing roots of the wings meet inside the fuselage.
- Where the engines are mounted to the pylons.
- At the empennage fairing to the fuselage.
- Where the horizontal stabilizers meet the vertical stabilizers.

Based on these assembly configurations, the dimensions of the aircraft and the dimensions of the container, it is concluded to have 2 containers per aircraft.

Production & Assembly Plan

The production and assembly plan is created, such that the aircraft is dissected into smaller parts. These are refined into even smaller components and produced among several manufacturers. The format of this scheme allows several manufacturers to take part in the production of the aircraft. This allows all components to be made by parties that are specialized in their respective field. This leads up to an aircraft with an optimum quality.
The second chapter discusses how the components of the aircraft are connected to each other. This is a function of each component's material, its role in the structure and safety measures. To connect components made from aluminum, it is decided to use Gas Tungsten Arc Welding methods. For skin panels that are made from composites, it is decided to use scarf adhesives to join them. To connect aluminum structures to the composites, it is decided to use 3M Scotch-Weld Epoxy Adhesives. Lastly, for assembly locations, inspection and maintenance panels, bolting is used.

RAMS Analysis

This section covers the RAMS analysis of the aircraft. The aircraft is evaluated with respect to all of Reliability, Availability, Maintainability and Safety matters. These perspectives works together to optimize the aircraft's performance. Reliability of the aircraft relies on the risk mitigation which is analyzed thoroughly through out the whole report. Furthermore for reliability of the aircraft systems, redundancy has been taken in account in their design. For Availability, the readiness of aircraft for operations is the most important parameter. Thus it is recommend to the operators to have an appropriate maintenance schedule. Maintain-

ability consists of providing the aircraft with spare components as well as predictive maintenance such as wear component replacement and lubrication replacement. It also includes maintenance of aircraft computers and software. Lastly Safety focuses on keeping the aircraft and pilots safe from hazards or failure. This is done by again introducing redundancies as well as recommending the operators to make sure the operational environment of the aircraft is safe as possible. Furthermore it is recommend to the operator to run extensive test to evaluate RAMS of the aircraft such as Failure Mode, Effect, and Criticality Analysis (FMECA).

Production Quantity and Cost Analysis

With the market analysis, an estimate of the production quantity can be made, which primarily consists of replacing aircraft that are outdated or too expensive. Based on the reference list that was made, the F-4 and the F-16 is one of the outdated aircraft, which have been converted to a multi-role aircraft. Due to the expensive costs of upgrading those aircraft, the designed aircraft is able to be a cheaper replacement while functioning as a multi-role aircraft. Additionally, due to the expensive cost of the F-35, the designed aircraft will be an aircraft that is able to be a replacement for countries looking for a cheaper alternative.
Political reasons have also withheld countries from buying aircraft developed by another nation.
Consequently, this has led to an estimated 830 aircraft that will be produced.

The cost analysis of the aircraft was performed using the DAPCA-IV method. This method provided estimations for RDT&E costs and the required engineering, tooling and manufacturing labor hours. With these estimations the total production cost of the aircraft had been established, presented in Table 9, which ended up to be $9.96 million per aircraft when producing 830 aircraft. As a selling price of $10.96 was decided upon, this resulted in a ROI of 10% and a break-even when selling 465 units.

Table 9: Summary of the most important values of the cost analysis

Cost factor per unit	**Cost in mln $**
Certification cost	1.26
Production cost	2.37
Engines	2.93
Avionics	2.27
Liability	1.13
Total cost	9.96

The operational and maintenance cost were approximated as well, which led to the cost per flight hour for the aircraft of $1 072. This is however subject to change, as the fuel prices can drastically increase at remote locations. Additionally, the idea of shipping the aircraft in containers turned out to be cheap in comparison with transporting by mid air refueling. The fuel required for flying the same distance as shipping the aircraft would already cost roughly ten times as much.

Lastly a subsystem cost analysis and a comparison to competitors were carried out. The subsystem cost analysis, as presented in Figure 6, shows the most cost intensive parts of the aircraft. The comparison to competitors showed that the aircraft is relatively cheap compared to military aircraft of the same weight class. This strengthens the market position of the aircraft and could lead to better sales.

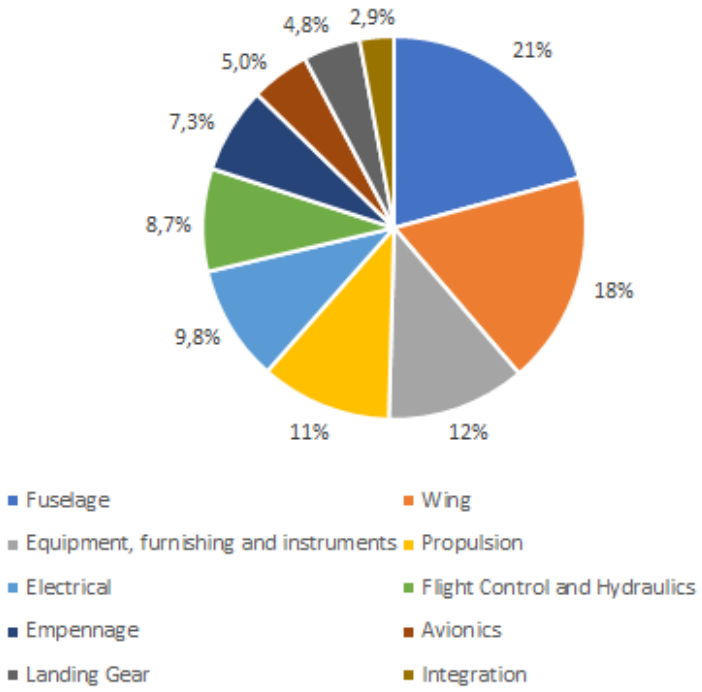

Figure 6: Cost breakdown per subsystem of the aircraft

Sustainability Strategy

The approach to create a sustainable aircraft included, but was not limited to, reducing the greenhouse gas emissions, analyzing material selection, account for recyclability, providing safe working environments, and reducing noise. The emissions were reduced by adding passive turbulent drag reduction methods to the skin, thereby decreasing drag and increasing fuel efficiency, and by shipping the aircraft in containers.

By analyzing the materials and taking into account their recyclability, it was decided that primarily 2XXX and 5XXX series aluminum are used in the aircraft. These aluminum are recyclable with the current recycling methods and provide adequate properties for most structures.

Lastly the social sustainability is accounted for by ensuring safe work environments and educating workers to increase efficiency and quality. This helps workers both in this project and their future work. Noise was also considered for social sustainability. High noise level negatively impact not only civilians when flying near civilian domains, it also impacts the pilots and other military personnel. On top of that, noise can introduce acoustic fatigue into structures, which can lead to more maintenance. Therefore, chevron nozzles are implemented on the engines to reduce their noise.

Post DSE activities

This section focuses on the future steps that should be done after this report. It start from the preliminary design, followed by detailed design, pre-manufacturing, manufacturing, operation and service and end of life stages. These stages are shown in a work break down structure and based on that, a gantt chart is made which shows the distribution of the tasks with respect to time until 2055.

1 Introduction

As warfare has changed from symmetrical to mostly asymmetrical, also the utilization of available aircraft has changed significantly. This results in an A-10 *Thunderbolt* performing CAS missions against terrorist groups, while it was originally designed to assault heavily armored vehicles. The F-35, which is currently one of the most advanced aircraft, is used for the same type of CAS missions. These aircraft are overdesigned for the task at hand. The A-20 *Chimera*, which is presented in this report, aims to combine everything that works on the currently used aircraft, with a 'best-value' design approach in mind. The best value approach for this aircraft is to design it for mission flexibility while being affordable. In order to achieve this goal, a mission need statement (MNS) and project objective statement (POS) were set-up to solve the need of the stakeholder.

MNS: To provide close air support to ground forces from short, front-line, austere fields at short notice, while being affordable.
POS: To design an affordable light attack aircraft, within 10 weeks by 10 students, which can operate from short austere fields close to the front lines.

The purpose of this report is to present the reader with the process followed for the conceptual design of the A-20 *Chimera*. The report is build up in three main parts, first a discussion is presented on the boundaries of the design and how the concept was obtained. Then the design of the aircraft is discussed, including a drag, stability and performance analysis. The last part of the report discusses everything that is not included in the design, such as a market analysis and the sustainable design approach taken.

First, in chapter 2 the mission obtained from the request for proposal (RFP) is analyzed. This discussion entails a thorough threat analysis, combined with a function breakdown of the aircraft system and its key and driving requirements. After this, the design approach to the aircraft is discussed in chapter 4, followed by a trade-off between the obtained concepts. These two chapters conclude the first part of the report.

Chapter 5 discusses both the first and second order weight estimations, combined with a technical drawing of the obtained aircraft. Followed by a more detailed discussion on the design of the fuselage, wing, empennage, propulsion unit, landing gear and additional subsystems, presented in chapter 6 to chapter 11. From these chapters the design is worked out, after which detailed analyses on the drag, chapter 12, stability & control, chapter 13, and performance, chapter 14, are executed. From these chapters the aerodynamic characteristics, and handling and performance qualities become apparent, which concludes the second part of the report.

The final part of the report starts with a discussion on the operations and logistics of the aircraft in chapter 16. This is followed by a production plan presented in chapter 17, and RAMS analysis in chapter 18. In chapter 3 a preliminary market analysis was carried out which looks at different stakeholders and competitors. These results are used in Chapter 19 to get a quantity and breakdown for the cost. This is followed by the sustainability strategy discussed in chapter 20 and the post-DSE activities discussed in chapter 21. The final chapter, chapter 22, shows the reader the compliance of the aircraft to the user requirements set at the beginning of the report and presents the reader with a number of future recommendations.

2
Missions, Functions and Requirements

Before starting the aircraft design, the missions and threats were identified. This was followed by other functions the aircraft shall perform. These were used to determine the requirements the aircraft shall meet. This chapter describes these aforementioned steps.

2.1. Design Missions and Threats

To determine the missions for the A-20, multiple war scenarios were examined. These include anti-terror missions, anti-drug cartel missions, the Gulf war, the Vietnam war, and the Yugoslavia conflict. This section describes the missions the A-20 shall perform, followed by the corresponding threats.

2.1.1. Mission Analysis

Military aircraft may be designed for multiple missions. The most common missions, and whether the A-20 is suited for these missions, are described below.

1. **CAS against infantry:** One of the most important tasks of an attack aircraft is to provide Close Air Support (CAS). The aircraft attacks hostile ground forces, providing support to allied forces close by. A high level of precision is required, because of the proximity of friendly troops. Often, integrated guns or precision guided missiles are used. Less common is the use of unguided missiles, or bombs due to the lower accuracy, hence the increased risk of accidentally targeting friendly forces. Typical guided missiles that are used are the AGM-114 *Hellfire* or the AGM-65 *Maverick*. Guided bombs like the GBU-12 *Paveway* are generally more effective, at a cost of more collateral damage. The A-20 is capable of carrying all three, due to the six NATO standard hardpoints. Because of that, it can carry a wide variety of guided and unguided bombs and missiles, as long as the total weight does not exceed the total payload capacity of 3000 lbs. When using the integrated gun, the aircraft flies low and slow, and engages the hostile forces. This is also called "strafing". The A-20 is well suited for strafing runs. Its low stall speed and good handling qualities allow for an easy targeting, which increases accuracy. Furthermore, it includes two integrated .50 cal GAU-19 rotary cannons with 1200 rounds of ammunition each. The cannons have a fire rate of 1300 rounds per minute and can be used individually or together. Using the cannons individually leads to a total firing time of almost two minutes, while increasing accuracy and reducing collateral damage. When using the guns together, the fire power is increased for greater impact, at cost of accuracy and firing time.

2. **CAS against vehicles:** CAS against vehicles is largely comparable to CAS against infantry. The A-20 *Chimera* is capable of targeting light vehicles, but it is not meant to be used against heavily armored vehicles like tanks. This is due to the smaller caliber of the cannon. However, this was a conscious tradeoff, as smaller caliber ammunition is significantly lighter (115 g vs > 650 g of the A-10 ammunition[1]). This increases the ammunition capacity, allowing for longer support missions without rearming. Furthermore, collateral damage is reduced. The cannon of the A-10 *Thunderbolt II* is more suited for CAS against well armored targets. The A-20 can compensate by having access to a large arsenal of missiles and bombs, like the aforementioned AGM-114, which was developed for anti-armor use.

3. **CAS against structures:** Compared to CAS against infantry, the on board cannon is hardly used, as it is not very effective against structures. However, the A-20 can compensate with the large arsenal of bombs and missiles, again.

4. **Tactical bombing:** The tactical bombing, or air strike, of targets with strategic importance, like bridges, radar sites, or enemy units, may be required. Usually, an air strike is preformed far away from allied troops, possibly behind enemy lines. Accuracy is still valuable, but not an absolute necessity, since

[1] https://www.gd-ots.com/wp-content/uploads/2017/11/30x173mm-Ammunition-Suite-MK44-Cannon-Version-3.pdf, conducted on [19-01-2021]

allied forces are not within range of the impacts. Tactical bombing may be executed by the A-20, but as the payload capacity is limited, other aircraft like the B-2 *Spirit*, or F-18 *Super Hornet* may be better suited. Even though the payload capacity is limited, the A-20 can still be used for long range precision strikes, as it can carry cruise missiles like the AGM-158 JASSM, AGM-158C LRASM and AGM-84E SLAM. They offer a range of up to 1000 km[2], while being stealthy. The large standoff distance also means, that the aircraft often can stay in friendly airspace, where it does not encounter enemy interceptors or advanced surface to air missiles.

5. **Reconnaissance:** To gather intelligence about enemy movements and numbers, infrastructure, or landscapes in enemy territory, reconnaissance missions are performed. The A-20 is capable of performing reconnaissance missions. It features a sensor suite including LiDAR and IR-sensors, as well as optical camera systems, more on this in subsection 11.1.5.

6. **Armed patrol:** In armed patrol missions, the aircraft flies low and slow over critical locations. Sometimes the show of force is enough to discourage the enemy to enter these locations. If this does not help, the patrol identifies, and possibly engages the enemy. The A-20 is well suited for armed patrol missions, due to the slow flight performance, armament and armor, this will be further alluded in subsection 6.4.1.

7. **Air combat:** The A-20 is not suited for air combat. It is too slow and has a low thrust-to-weight ratio. Fighter aircraft like the F-15 *Eagle*, F-16 *Fighting Falcon* or F-22 *Raptor* are designed for air combat missions. Air superiority is assumed in all missions the A-20 performs.

2.1.2. Threat Analysis

In each mission, different threats are encountered. The aircraft performs missions at very low altitude (CAS missions) to high altitude (reconnaissance missions), and the threats at each altitude are different. To identify the threats at different altitudes, the distinction between low, medium, and high altitude was made. An altitude of 500 m and lower was considered a low altitude, at which the aircraft flies during CAS missions, and armed patrol. Medium altitude were considered to be 1 to 5 km, which may be an altitude for tactical bombing, or reconnaissance. The cruise altitude (10 000 ft) and mission loiter altitude (3 000 ft) also lie within this region. An altitude of 10 km was considered high, mainly reconnaissance missions are performed at this altitude. A "kill level" was assigned to each potential threat as per the guidelines of the U.S. Department of Defense [1].

Table 2.1 shows the potential threats against the A-20 at different altitudes, and the corresponding kill level. At low altitude, threats include handheld weapons with a small caliber (below 0.50 cal./12.7 mm). The threat from handheld weapons is relatively small, and only at low altitudes. Bigger threats include anti-aircraft guns, as the caliber, which can go up to 37mm, and effective range are much bigger than that of handheld weapons. AA guns reach low and medium altitudes. Man-portable air-defense systems (MANPADS) are a threat against the A-20 as well. MANPADS like the *Stinger* include heat-seeking missiles, which actively target the hot parts of the aircraft engine. Missiles may also be laser-guided, manually controlled, or unguided. They are a threat a low and medium altitude.
The kill level in Table 2.1 represents the vulnerability level to the threats. Damage from handheld weapons may lead to a Mission Abort (MA). Damage from AA guns may lead to a Forced Landing (FL). As discussed before, damage from MANPADS are the biggest threat, and may result in Attrition (A), or loss of control after five minutes if the engines are hit. If the wing tips or control surfaces are hit, this may lead to loss of control after 30 minutes (B). The damage may be catastrophic (K) if the fuselage, tail, or wing root is hit. There is enough time for the pilots to eject. If the cockpit is directly hit, it may result in an instant loss of vehicle and crew (KK).

[2] https://www.lockheedmartin.com/content/dam/lockheed-martin/mfc/pc/jassm/mfc-jassm-er-pc.pdf, conducted on [19-01-2021

Table 2.1: Threat analysis at different altitudes with designated kill/survivability level.

	Altitude			
Threats	**Low (<500 m)**	**Medium (1-5 km)**	**High (10 km)**	**Kill Level**
Handheld Weapons (<.50 cal)	X			MA
AA guns/cannons	X	X		FL - powered
MANPADS (unguided, heat seeking, laser guided, manually controlled)	X	X		KK - direct hit to cockpit K fuselage, wing root, tail etc B - wing tips, control surfaces A - engine

To achieve these kill levels, the cockpit will be armored to protect the crew (see subsection 6.4.1). To reduce the likelihood of being hit by MANPADS, flare launchers will be included. Flare launchers eject burning pieces of Magnesium (flares) that are very hot compared to the engine exhausts. This makes heat seeking missiles loose their lock on the engines; they lock onto the flares instead, which results in a miss. These flare launchers are stored, flushed with the fuselage surface.

These are not all possible threats to military aircraft in general. As the A-20 was designed for asymmetric warfare, the threats of advanced surface-to-air missiles, and enemy fighter aircraft were not considered. Due to this, enemy airspace surveillance was not considered either.

2.2. Functional Breakdown Structure

In this section, the functional breakdown structure (FBS) is displayed. In Figure 2.1, the first two levels of the FBS are shown with gray boxes representing the life-cycle processes of the aircraft, and the red boxes representing the top-level functions.

A more in-depth FBS for the operations is shown in Figure 2.3. The top-level functions consist of multiple levels of sub-functions, which are represented by the color blue, yellow and green, in the hierarchical order respectively.

2.3. Functional Flow Diagram

In this section, the functional flow diagram (FFD) is displayed. In Figure 2.4, the gray boxes represent the life-cycle processes identified in section 2.2.

However, to understand the operation part of the FFD, a flight profile diagram is required, which is shown in Figure 2.2. The anomalies and alternative missions, such as rejected take offs, aborted landings with go-arounds, loitering periods, and the ferry mission, have been included in the flight profile diagram as well with red and blue line to differentiate from normal flight profile. In addition, the sub-functions were constructed in a hierarchical manner, with *AND* and *OR* blocks as connection. To minimize the size and to improve the clarity of the diagram, the *Fly & Survive* and *Landing & Taxi* blocks have been separated and developed individually.

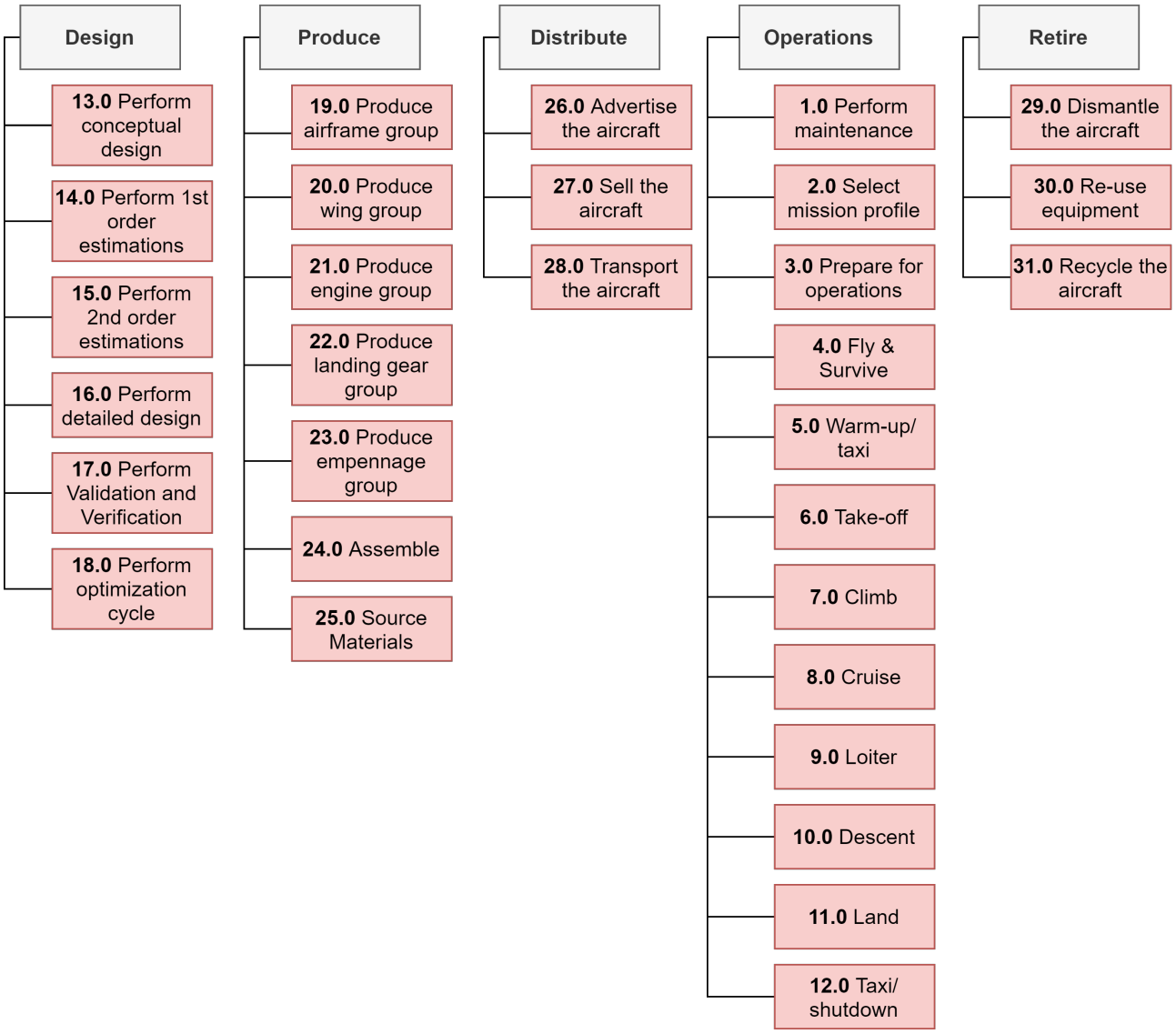

Figure 2.1: Top-level functional breakdown structure

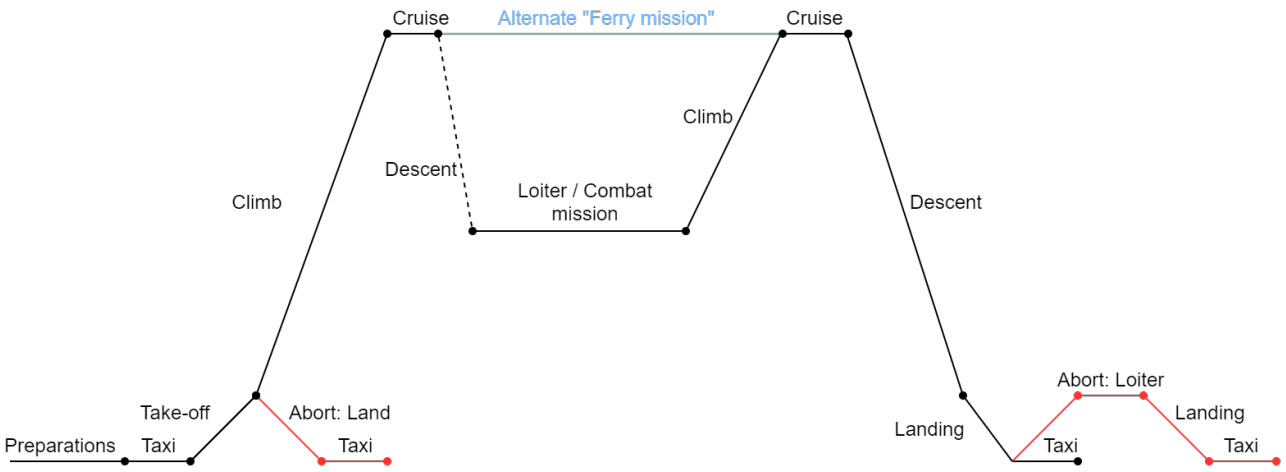

Figure 2.2: Depiction of the flight envelop with main and alternative mission, as well as aborts and go-around

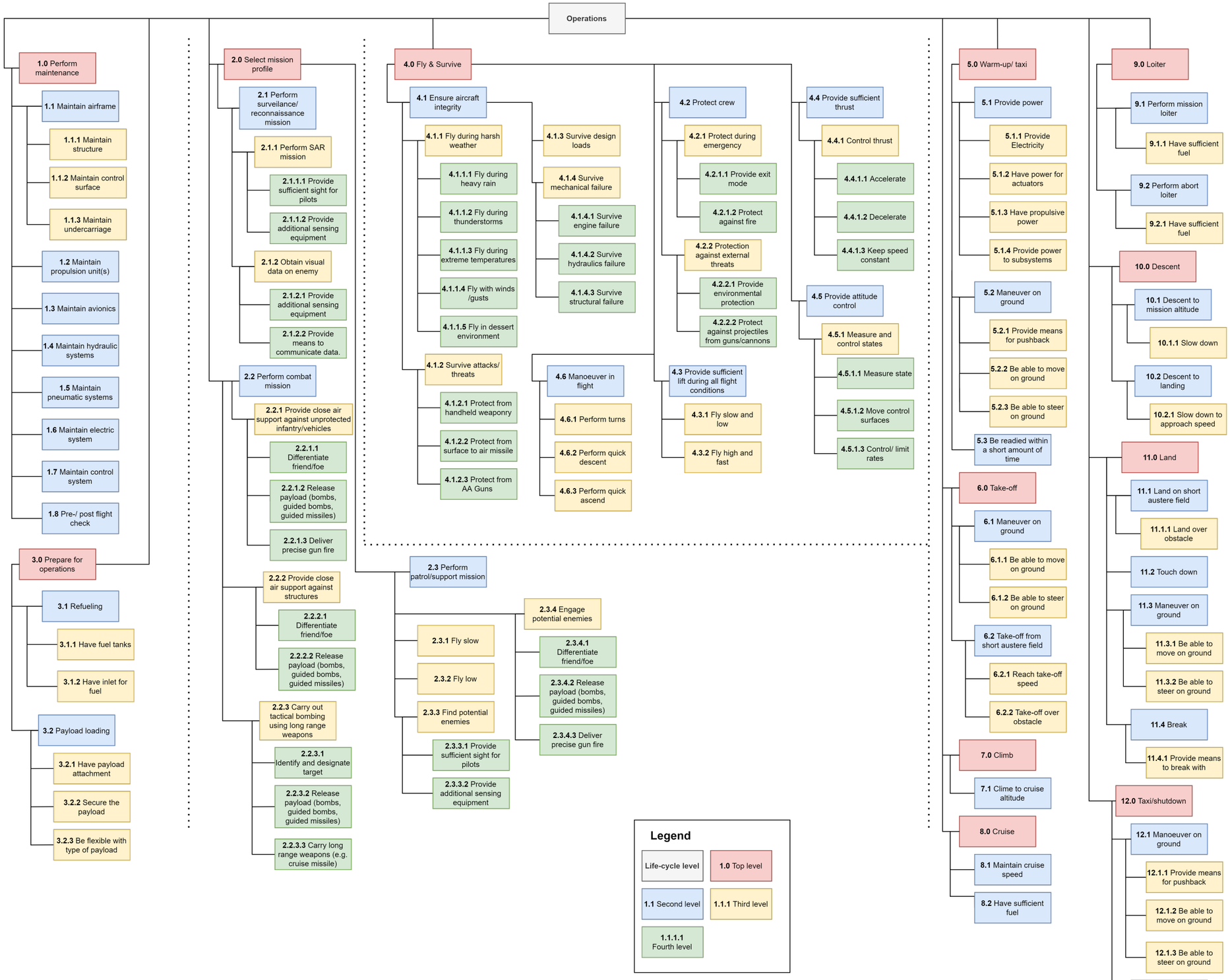

Figure 2.3: Functional breakdown structure

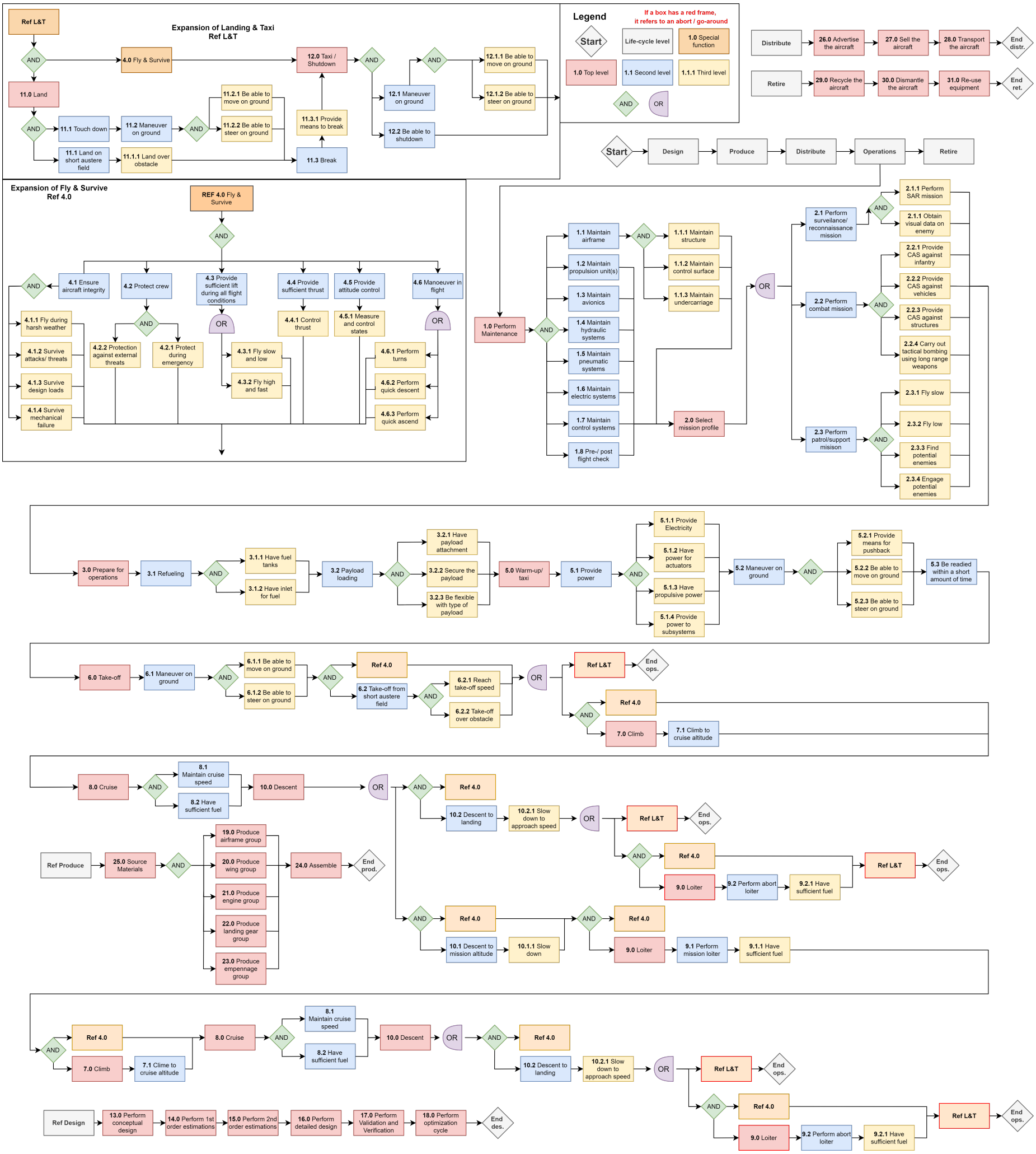

Figure 2.4: Functional flow diagram

2.4. Key and Driving Requirement Analysis

From the mission & threat analysis, and the aircraft functions, the requirements were derived. In this section, only the key and driving requirements are discussed, see Table 2.2, which resulted from the Request for Proposal (RFP) from the American Institute of Aeronautics and Astronautics (AIAA).

The key Requirements are the most important requirements to the customer. The driving requirements drive the design more than other requirements. The requirements listed below were used to set the boundaries on the design space, chapter 22 discusses if the design is compliant to these requirements.

Table 2.2: List of user requirements for the Light Attack Aircraft given by the AIAA

Requirement ID	Description
Payload	
LAA-PAY-WTH-1.1	The aircraft shall be able to carry 1 360.78 kg (3 000 lbs) of armament.
Performance	
LAA-PER-SER-1.1	The service ceiling shall be higher than 9,144 m (30 000 ft).
LAA-PER-FEM-1.1	The cruise distance during a ferry mission shall be at least 1 666.80 km (900 nmi).
LAA-PER-DSM-1.1	Descent to 914.40 m (3 000 ft) shall be completed within 20 minutes of the initial climb to the cruise altitude.
LAA-PER-DSM-2.1	The aircraft shall be able to loiter 4 hours on station without dropping the armament.
LAA-PER-DSM-3.1	The aircraft shall have reserve fuel sufficient for climb to 914.40 m (3 000 ft) and loiter for 45 minutes after the design mission completion.
LAA-PER-DSM-3.3	The aircraft shall have a cruise altitude above 3 048 m (10 000 ft)
LAA-PER-DSM-4.1	The aircraft shall be able to land over a 15.28 m (50 ft) obstacle within a distance of 1 219.2 m (4 000 ft) at most and at a density altitude up to 1 828.80 m (6 000 ft) on runways with California bearing ratio 5.
LAA-PER-DSM-4.2	The aircraft shall be able to take off over a 15.28 m (50 ft) obstacle within a distance of 1 219.2 m (4 000 ft) at most and at a density altitude up to 1 828.80 m (6 000 ft) on runways with California bearing ratio 5.
Power and Propulsion	
LAA-PAP-DSM-1.1	Warm-up shall take no longer than 5 minutes.
LAA-PAP-DSM-1.2	Shutdown shall take no longer than 5 minutes.
Time	
LAA-TIM-SER-1.1	The aircraft shall enter service in 2025.
LAA-TIM-SER-1.2	The aircraft shall have a service life of at least 15,000 hours over 25 years.
Technology	
LAA-TEC-RDY-1.1	Critical technologies shall be above NASA's technology readiness level (TRL) 8 in 2020. & Driving
Structures	
LAA-STR-WPN-1.1	The aircraft shall feature a board canon to engage ground targets.
LAA-STR-CRW-1.1	The aircraft shall be able to fit two crew members.

3
Market Analysis

In this chapter, an updated version of the business analysis is described. First, the market definition was re-evaluated. Additionally, the historical, current, and future market size was analyzed. Then, the competition section looks at the biggest contributors to the fighter market. This also shows an updated reference aircraft list, that is used for the segment analysis.

3.1. Stakeholder list

A stakeholder list is given below to summarize which stakeholders are involved in the design process. The stakeholders have an influence on the product and the cost for the product. In section 19.1, the buyer's behaviour show the stakeholder's rationale for buying a military aircraft.

- **American Institute of Aeronautics and Astronautics (AIAA)**: The AIAA remains an important stakeholder for this project, due to the RFP. The user requirements given here, are the primary focus and direct the aircraft design.
- **Manufacturer**: For producing the aircraft, the manufacturer plays another important role. The manufacturer has to be able to produce the required components, which may be challenging. Additionally, the manufacturing process may be divided into multiple producers, meaning third-party manufacturers may be considered to acquire parts.
- **End-user**: The end-users of the product are mainly the pilots. An F-16 pilot was contacted to discuss his experience as an end-user. From this conversation, one of the most important features mentioned, was that the aircraft should be survivable against any kind of threat. The end-user must be able to operate the aircraft in the safest way possible. A mission and threat analysis was performed (see section 2.1, in order to get an overview of the past and possible future war scenarios. Another important feature, is the ability to perform multiple roles during a mission or in combat. Next to the fighter pilots, other end-users include parties that communicate between pilots and troops Joint Terminal Attack Controller (JTAC).
- **Armed forces**: The countries' armed forces are still one of the key stakeholders that were considered. The purpose of the designed aircraft is to support ground troops. Hence, the countries military remains to be the primary customer.
- **Regulator**: Regulators such as the department of defense (DOD) are another important stakeholder as they evaluate the airworthiness of the aircraft and give the certification requirements. These requirements have been followed from the start of the project and shall be referred back to in order to avoid termination of the project.

Before looking into detail for each of the stakeholder, the market's size has been discussed in order to observe the past and current market situation and then predict the future trends.

3.2. Market Size

The current market size for military fixed wing aircraft suggests that there is very little development of the market's spending per region from 2015 to 2025. Additionally, this analysis shows that North America, Pacific Asia and Europe are the major players contributing to the total spending. North America spends roughly 25-30 %, Asia Pacific spends roughly 30 % and Europe around 20 % of the total [2].

Next, the actual amount of spending per country was analyzed in order to identify the historical, current, and future market size. Only the data for the United States (US) could be found. However, due to the fact that the US has a large dominance over military spending (as data suggest that the US are number one with

a spending of $ 731.8 Billion on the list of military spendings in 2019[1]), it captures a good estimate that other contries also do not increase their military spendings. The data containing the military spendings suggest that from 2015 till 2021, there is a steep climb in the market size, but afterwards (from 2011 till 2025) there is little fluctuation for military fixed-wing aircraft. It is expected that roughly 3 400 fighters will be produced in the coming 10 years [2]) [3].

Additionally, the trend for military fixed wing aircraft categories was investigated. This shows that it is expected that there is more demand for multi-role aircraft, and less for surveillance and reconnaissance aircraft [3]. Although this data is only provided for the US, it captures a good estimate of how other countries are motioned in the same way.

One could reason that, since there is expected to be lower spendings on fixed wing aircraft, there is a higher demand in affordable multi-role aircraft.

3.3. Competition

The data provided in this subsection originates from dsm.forecastinternational.com[2]. The biggest contributors to the fighter market are listed below, Lockheed Martin clearly dominates the market with a market share of almost 60%.

- Lockheed Martin (58 %)
- Boeing (12 %)
- United Aircraft Corporation (8 %)
- Aviation Industry Corporation of China (7 %)
- Dassault (6 %)
- Saab (4 %)
- Eurofighter (3 %)
- Hindustan Aeronautics Limited (1 %)
- Korea Aerospace Industries (0.5 %)

Of the expected 3 400 fighters that will be manufactured, 46 % will be F-35 produced by Lockheed Martin. This aircraft is in demand because of its multi-purpose functionality. However, as can be seen from Table 3.1, the F-35 is very costly, which is why some nations in Europe and Asia rather choose the F-16. Aircraft like the JF-17 built by China in cooperation with Pakistan Aeronatical Complex are offered to Africa and Asia and are less expensive than the F-35.
Table 3.1 show that the Eurofighter is very expensive, too. This lead to the conclusion for Belgium's air force to choose the F-35 over the Eurofighter[3].

In the baseline report, reference aircraft were added that have a similar mission profile and requirements as this project or are seen as competitors in the current market share. Additional aircraft were added of the current in demand aircraft. This gives an updated look on what aircraft are already feasible to satisfy the mission need statement and also the aircraft that are sought after right now. The three additional aircraft are the F-35, JF-17 and the KAI T-50 (not to be confused with the Russian T-50) as mentioned before.

[1] https://www.visualcapitalist.com/mapped-the-countries-with-the-most-military-spending/, conducted on 17-12-2020
[2] https://dsm.forecastinternational.com/wordpress/2019/06/19/fighter-aircraft-market-worth-260b-over-next-10-years/, conducted on 17-12-2020
[3] https://www.reuters.com/article/us-aerospace-belgium/belgium-picks-lockheeds-f-35-over-eurofighter-on-price, conducted on 17-12-2020

Table 3.1: Updated reference aircraft[4]

Aircraft	Unit Price in millions (2020 USD)	OEW (kg)	Units sold	Role	Region
A-10 Thunderbolt	$39.90	10 710	716	Attack	North-America
Super Tucano	$10.63	3 200	220	Attack	South-America
Eurofighter	$105.7[5]	11 000	220	Multi	Europe
F-16	$23.20	12 020	4600	Multi	North-America
A-4 Skyhawk	$35.00	4 469	2960	Attack	North-America
F-4 Phantom II	$16.40 (1965)	13 757	5000	Attack	North-America
AV-8B Harrier II	$25.00	6 336	337	Multi	Europe
Alpha Jet	$17.95	3 515	480	Attack	Europe
Sepecat Jaguar	$9.60	7 000	543	Attack	Europe
Super-Etendard	$37.80	6 500	85	Attack	Europe
Panavia Tornado	$59.60	14 100	990	Multi	Europe
Cessna A-37 Dragonfly	$0.16	2 817	577	Attack	North-America
F-35A	$77.90	13 154	648	Multi	North-America
JF-17 Thunder	$25.00	6 586	54	Multi	Asia
T-50 Golden Eagle	$30.00 (2012)	6 470	72	Multi	Asia

3.4. Segment Analysis

A segment analysis was carried out to further understand the current market trend. The chosen segments are:

- By manufactured region (North America, Europe, Asia-Pacific, Middle East & Africa, Latin America)
- By role (i.e. combat, surveillance, intelligence, reconnaissance, multirole)

For the segmentation, the same aircraft were considered as derived from Table 3.1. Additionally, the segmentation looked at those which are still in on the market.

Firstly, the segmentation according to manufacturing region was looked at. Figure 3.1 shows the segmentation of the aircraft that are produced including ones out of service (this includes all aircraft from Table 3.1) and Figure 3.2 shows the segmentation of what is currently on the market (this only include aircraft that are still in service from Table 3.1[6]). This data shows that there are less aircraft manufactured in Europe that are currently on in service.
Since the A-20 Chimera is an aircraft designed as collaboration with the Delft University of Technology, this would interest European countries to invest in such aircraft. This would mean that European are less dependent on American made Aircraft, which otherwise would go against European interest [7].

[4] https://www.wikipedia.org/, conducted on 17-12-2020
[5] https://militarymachine.com, conducted on 17-12-2020
[6] https://www.wikipedia.org/, conducted on 17-12-2020
[7] https://www.france24.com/en/20181026-france-belgium-aviation-macron-purchase-usa-f35-jets-eurofighter

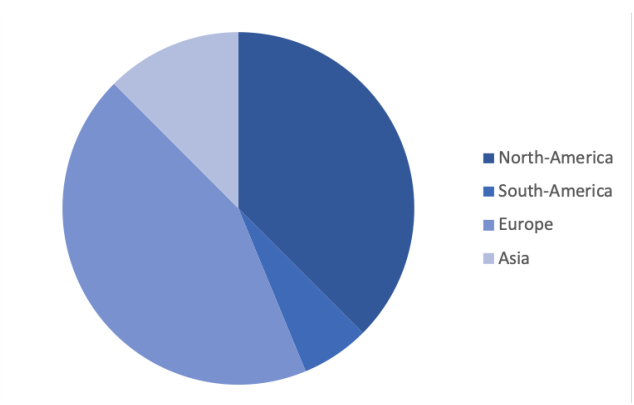

Figure 3.1: Geographical segmentation of reference aircraft that had been produced including ones out of service

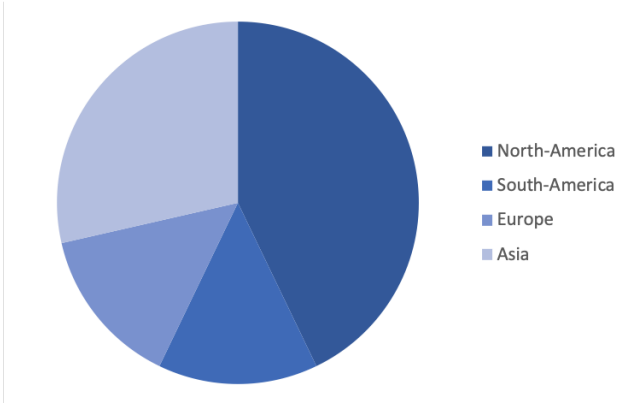

Figure 3.2: Geographical segmentation of reference aircraft that are currently in service

Secondly, the role of the aircraft were analyzed. As can be seen in Table 3.1, the division of the roles of the aircraft consists mainly of multirole and attack aircraft. It should be noted that, when looking at aircraft that are currently still in production, there has been a shift towards multi role fighter aircraft over the last few decades. This can be viewed in Figure 3.3. It should be also noted that some aircraft listed in Table 3.1 and are still in service according to Figure 3.3 have been upgraded from attack role to multi-role, like the F-4 Phantom II. These have not been included in Figure 3.3

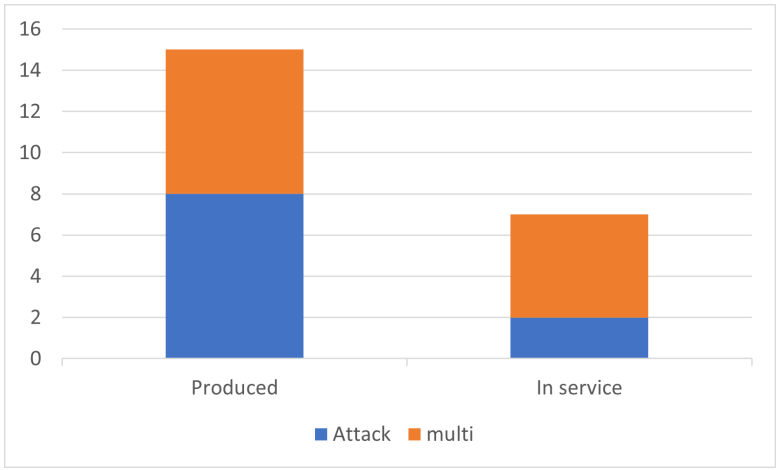

Figure 3.3: Histrogram of aircraft roles, produced vs. in service

4 Design Approach, Design Options Trade-off and Impressions

In this chapter, the design approach and concept trade-off are discussed. The structuring of the design approach in section 4.1 describes the design steps that were taken throughout the project. Next, in section 4.2 a summary of the trade-off for five previously designed different concepts is described.

4.1. Design Approach

To design the aircraft, first an initial sizing for multiple options was made. These were used in the trade-off in section 4.2. The resulting design from the trade off was then used for the next step in conceptual design. In this Class II design phase, more accurate estimations of the drag polar, and aircraft component weights were made. Furthermore, an airfoil for the wing and for the empennage was selected. From this, high lift devices and control surfaces were sized. Finally, all outputs of the design steps were an input for a stability & control analysis. Figure 4.1 shows the design steps in the diagonal, with the inputs of each step on the vertical axis, and the outputs on the horizontal axis. The blue boxes represent design steps of the the Class I phase, which were re-iterated in the Class II phase, which are represented with yellow boxes. The results of the Class II sizing were used to analyze the aircraft performance and stability characteristics. The next chapters explain the design steps of Figure 4.1 in more detail.

4.2. Trade-Off

In this section, the trade-off that was carried out in the mid-term report is summarized. A brief description of all concept designs are given of which a trade-off is made. Next, the trade-off criterion are explained and reasoned why some criterion have higher weight than others. Afterwards, the actual results of the trade-off is given in a summary table.

In the midterm report, four aircraft designed were sized, based on a Class I sizing. This sizing is based on statistical data and, although being a rough estimate of the actual result, gives a general idea of the weight, sizing, some subsystem sizing and the feasibility of the aircraft.

Concept 1: Survivability & Redundancy

Design concept 1 was primarily designed based on survivability and redundancy. By using two turboprop engines and H-tail configuration, it allows the aircraft to keep operating when one of the engines is malfunctioning. Additionally, a mid-wing configuration was chosen to allow easy access to external stores under the wing.

Concept 2: Canard

Design concept 2 was primarily designed based on high maneuverability and redundancy. By having fail-safe set up throughout the whole design, the design tries to achieve redundancy. This concept included 2 turbojet engines, 2 vertical and horizontal stabilizers. The canard configuration was chosen for high maneuverability, which results in better avoidance of threats encountered during the mission.

Concept 3: Affordability

Design concept 3 was primarily designed based on reducing costs. By reducing complexity of the aircraft, and shipping the aircraft in a container. Therefor the aircraft was sized to fit inside a container, this effectively reduces operational and logistic costs.

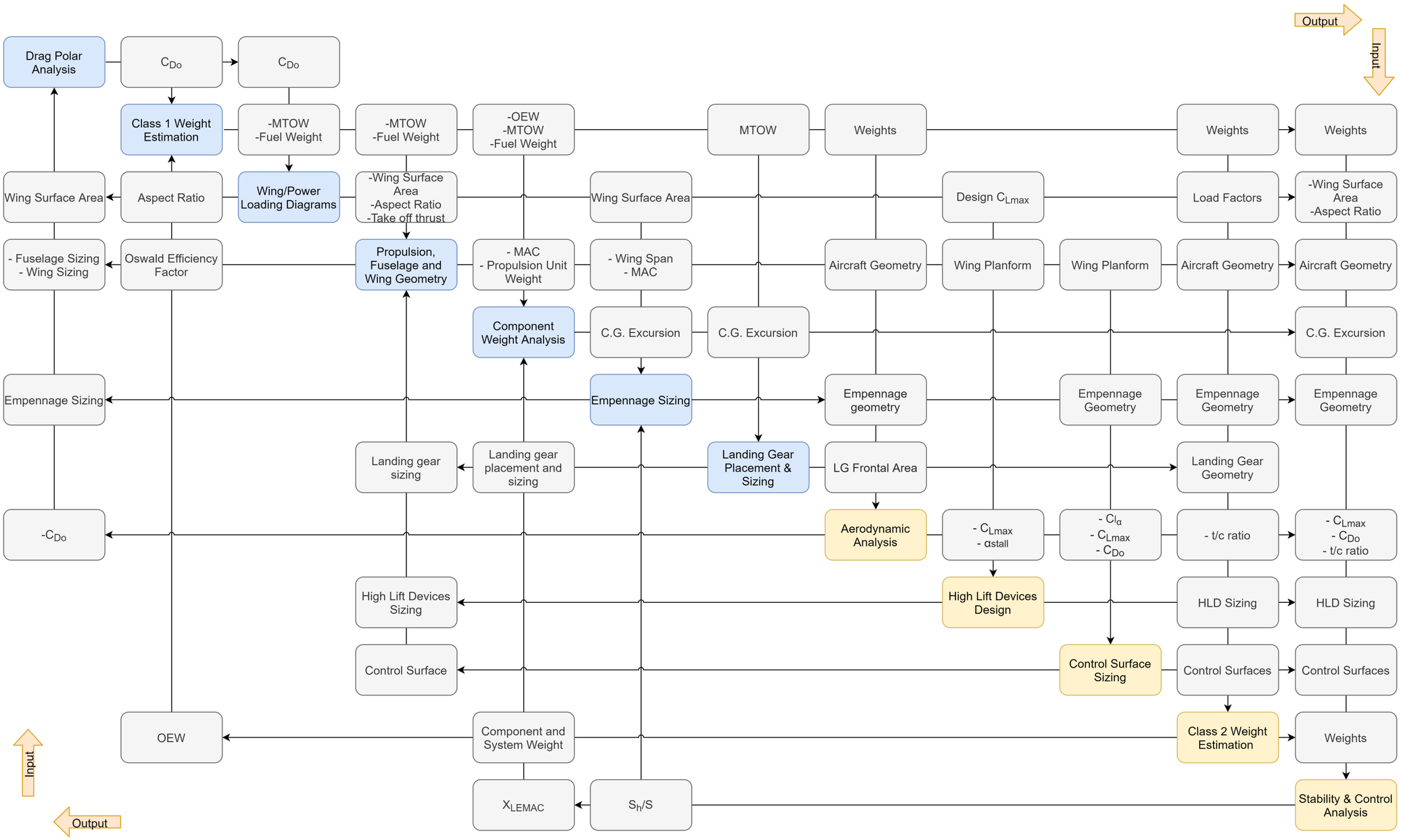

Figure 4.1: N2 chart of the Class II design process.

Concept 4: Hybrid

Design concept 4 was primarily designed on hybrid propulsion and reduced susceptibility. The aircraft was powered by a gas turbine, which generates electricity for the propellers. The aircraft utilizes three propellers of which the one behind the empennage is used as push propeller and the propellers at the wingtips are able to fold in when there is less speed required.

4.2.1. Summary of Trade-off Between 4 Concepts

Survivability was rated the highest, since the aircraft will operate in war zones, the pilots must be able to safely operate the aircraft and be able to return home safely. The survivability is split into susceptibility and vulnerability. The susceptibility is scored on the ability to avoid detection of threats, while vulnerability is the ability to sustain damage and survive when the aircraft is hit.

Another important criteria is the cost. The maintenance costs here has been given a higher weight than its production costs. This is due to the long service life and the maintenance capabilities on austere airfields.

The flexibility takes into account the ability of the aircraft to adapt to different mission profiles. The feasible amount of hardpoints and operations and logistics of aircraft determines this result.

Sustainability of the aircraft is with regards to the environmental and operational considerations. The fuel was considered, due to fuel being expensive in remote locations and also adds environmental impact when used (therefore, less specific fuel consumption is better). The operational empty weight (OEW) was also considered for each aircraft, based on the logic that the OEW is related to the material usage.

Lastly, the performance was evaluated on its turn radius, climb rate at sea level and maximum cruise speed.

Table 4.1 shows the trade-off weight with respect to its criteria. Every concept was given a score between zero and one, based on the feasibility and relative result between the concept designs. For non-quantifiable trade-off criteria , the scores from Table 4.2 were used.

Table 4.1: Trade-off table with assigned scores

Criteria	Weight	Concept 1	Concept 2	Concept 3	Concept 4
Survivability	**30.0%**				
- Susceptibility	15.0%	0.75	1	0.25	0.5
- Vulnerability	15.0%	1	0.75	0.25	0.75
Subtotal Survivability		**26.3%**	**26.3%**	**7.5%**	**18.8%**
Costs	**25.0%**				
- Maintenance costs	15.0%	0.5	0.5	1	0.25
- Production costs	10.0%	0.75	0.5	1	0.25
Subtotal Costs		**15.0%**	**12.5%**	**25.0%**	**6.3%**
Flexibility	**20.0%**				
- Feasible amount of hardpoints	8.00%	0.75	1	1	1
- Operations	6.0%	0.75	0.75	0.5	0.5
- Logistics	6.0%	0.75	0.25	0.75	0.5
Subtotal Flexibility		**15.0%**	**14.0%**	**15.5%**	**14.0%**
Sustainability	**15.0%**				
- Fuel Consumption	10.5%	0.82	0.74	1	0.72
- OEW	4.5%	0.85	0.80	1	0.78
Subtotal Sustainability		**12.4%**	**11.4%**	**15.0%**	**11.1%**
Performance	**10.0%**				
- Turn Radius	3.5%	0.92	0.77	1	0.77
- Climb Rate at sea level	3.5%	0.93	0.56	1	0.44
- Max Cruise Speed	3.0%	0.89	1	0.89	0.90
Subtotal Performance		**9.2%**	**17.7%**	**9.7%**	**6.9%**
Total	**100.0%**	**77.9%**	**71.8%**	**72.7%**	**57.0%**

Table 4.2: Non-quantifiable trade-off scores

	Excellent	Good	Feasible	Bad	Not Feasible
Score	1	0.75	0.5	0.25	0

According to the trade-off table, concept 1 scored overall best through all criterion, making this the winner. A sensitivity analysis of the trade-off was performed to see the impact of changing the weights and removing categories of the trade-off criteria, which can be seen in Table 4.3. Different scenarios were considered; equal weights, the survivability and cost were made less important, the performance and sustainability were made more important and the performance was removed from the trade-off. Nonetheless, concept 1 remained the winner in most scenarios of the sensitivity analysis.

Table 4.3: Sensitivity analysis on the trade-off input parameters

Scenario	Concept 1	Concept 2	Concept 3	Concept 4
Tradeoff	**78%**	72%	73%	57%
Equal	80%	72%	**80%**	60%
Survivability -	76%	68%	**86%**	56%
Cost -	**81%**	75%	71%	64%
Performance +	**81%**	73%	78%	61%
Performance 0	**76%**	71%	71%	56%
Sustainability +	**79%**	73%	78%	60%

4.2.2. Trade-Off Conclusion

Finally, a concept 5 was made, which includes the strengths (survivability and redundancy) that concept 1 contained. However, it also solves the complications that concept 1 had. Therefore, the H-tail, mid-wing, conventional wing configuration, but uses a turbofan engine to cope with the high required cruise speed.

In Table 4.4 another trade-off was performed, which showed that concept 5 indeed had a better result.

Table 4.4: Trade summary table

Criterion	Survivability [30%]	Costs [25%]	Flexibility [20%]	Sustainability [15%]	Performance [10%]	Total score
Concept 1	0.88	0.60	0.75	0.83	0.92	**77.9%**
Concept 2	0.88	0.50	0.70	0.76	0.77	**71.8%**
Concept 3	0.25	1	0.78	1	0.97	**72.7%**
Concept 4	0.63	0.25	0.70	0.74	0.69	**57.0%**
Concept 5	1	0.6	0.85	0.85	0.83	**83.0%**

4.3. Design Impressions and 3-View Drawing

Figure 4.2 shows the three-view drawing of the aircraft. Some impressions of the A-20 are presented in Figure 4.3 to Figure 4.4.[1]

[1] Models of bombs and missiles made by M. Rahnama, https://grabcad.com/m.rahnama-1, conducted on [19-01-2021]

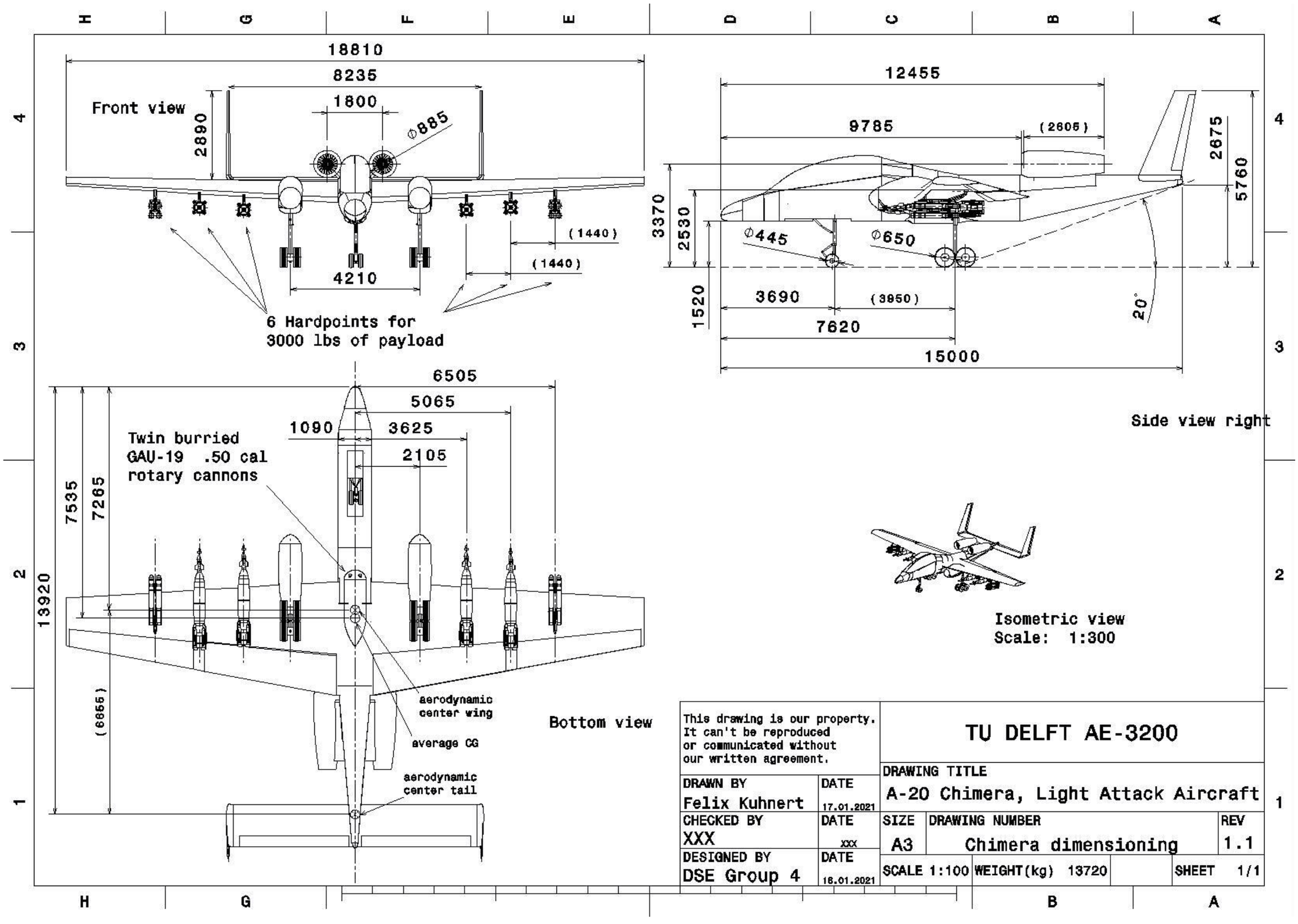

Figure 4.2: Three-view drawing of A-20

Figure 4.3: The A-20 *Chimera* on a mission

Figure 4.4: The A-20 *Chimera* taking off

5 Weight Estimations

In this chapter, an approximation of the aircraft weight is presented. First a rough weight estimation, the Class I weight estimation is discussed. This is followed by a more detailed weight estimation in the class II, based on components weights of comparable aircraft.

5.1. Class I Weight Estimation

The Class I weight estimation finds an initial approximation of the take off weight (W_{TO}), operational empty weight (W_{OE}), and fuel weight (W_F). W_{OE} includes the empty weight of the aircraft, the weight of the trapped fuel and oil, and the weight of the crew. Typical values were taken from Roskam part I, chapter 2 [4].W_F was determined by applying the fuel fraction method of Roskam chapter 2[4], using the mission profile diagram of Figure 2.2, which is explained in more detail in section 2.3. The fuel fractions of the cruise and loiter phases were calculated using Breguet's equations for range and endurance for jet aircraft. A specific fuel consumption of 0.42 lbs/hr/lbf was chosen for these calculations, based on a reference engine (see chapter 9). The L/D ratios were based on the drag polar from chapter 12. W_{TO} is the sum of W_{OE}, W_F, and the payload weight W_{PL}. The payload weight was set by requirement as 1 361 kg.

5.2. Class II Weight Estimation

To provide a more accurate prediction of the empty weight, the weight estimation method of Raymer chapter 15 was used [5]. This method estimates the weight of different components, based on historical data, and sizing methods described in chapter 6 to chapter 10. The resulting empty weight was then used to update the OEW in the Class I estimation, and iterated until the the values for all weights converged to less than 1% difference compared to the previous iteration. The resulting component weights are listed in Table 5.1.

Table 5.1: Component weights from the class II weight estimation with the Raymer method[5], converted to kilograms.

Component Group	Weight [kg]	Component Group	Weight [kg]
Wing	1561	Furnishing	197
Fuselage	948	Vertical Tailplane	146
Engine	936	Air Conditioning and Anti-Ice	105
Armor	626	Instruments	91
Avionics	491	Hydraulics	67
Electrical Systems	361	Engine Mount	24
Main Landing Gear	360	Engine Controls	23
Flight Controls	327	Engine Section	15
Fuel Tank	325	Pneumatic starter	12
Horizontal Tailplane	251	Handling Gear	4
Nose Landing Gear	205	Firewall	3
Empty Weight			**7075**

Compared to the class I weight estimation, the weight increased significantly in class II. The MTOW increased by 73% to 13700 kg. The increase in weight in the iterative process had a large influence on the wing, engine, empennage, and landing gear sizing. The breakdown of the MTOW, and corresponding OEW is presented in Figure 5.1.

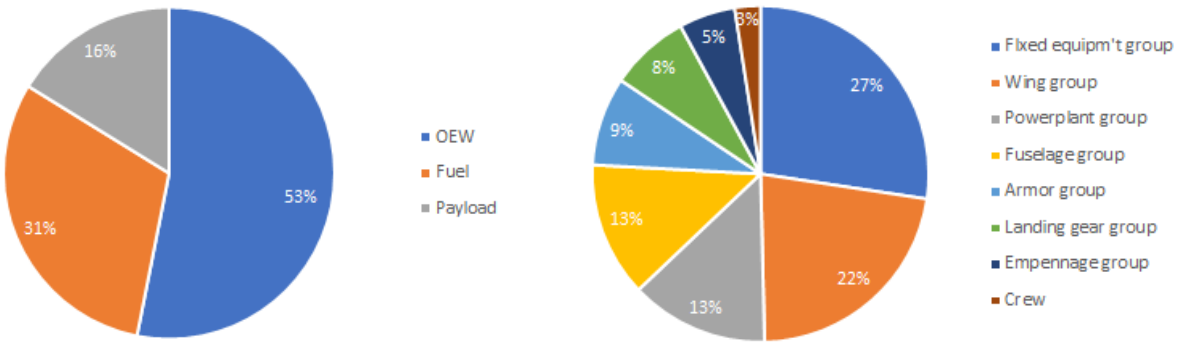

(a) Maximum Take Off Weight Breakdown as percentage of 135 kN

(b) Operational Empty Weight breakdown as a percentage of 71.5 kN

Figure 5.1: Weight breakdown of the A-20 *Chimera*

5.3. Mass Moment of Inertia

From the Class II weight estimation the mass moment of inertia (MMOI) could be calculated. The MMOI's are eventually needed for the stability and control calculations, which can be found in section 13.6. For the MMOI calculations the component group weights from Table 5.1 were used and the approximated location with respect to the most aft center of gravity location axis. In order to make the calculations more accurate, the component weights were split up into a left and right side variant. From the weights and distances, the MMOI could be calculated as per Equation 5.1, where the mass moment of inertia of component i around the x-axis, with mass m_i and distance to the x-axis that originates in the most aft center of gravity of r_x. The same calculation can be done for the y- and z-axis, as per Equation 5.2 and Equation 5.3, respectively. The calculated values around the x-, y- and z-axis were determined to be 72.2 $*10^3$ kg/m^2, 52.1 $*10^3$ kg/m^2 and 117.7 $*10^3$ kg/m^2. These values where verified and validated with a first order MMOI estimation from Roskam [6].

$$I_{xx,i} = m_i * r_x^2 \quad (5.1) \qquad I_{yy,i} = m_i * r_y^2 \quad (5.2) \qquad I_{zz,i} = m_i * r_z^2 \quad (5.3)$$

6
Fuselage Design

This chapter describes the steps taken for the fuselage design. First, an overview of the fuselage is given, followed by a functional analysis of the fuselage. The risks regarding the fuselage design are discussed next. The design methods are discussed, including the design of the structure. Whether the fuselage design is sensitive to changes due to changes in other subsystems is also explained. Finally, the requirement compliance is explained.

6.1. Design Overview

Figure 6.1 shows the fuselage of the aircraft. It is 15 m long and has an oval shape with flattened sides. It is 1.1 m wide and 1.5 m high (excluding cockpit). The tail cone is 5.3 m long and is angled upwards. The fuselage houses the cockpit including armor, the cannons including ammunition as well as the majority of all electric and hydraulic subsystems as well as the nose landing gear. The rotating cannons are placed below the wing box. They are placed such that the firing barrel sticks out of fuselage. To reduce drag, they are hidden behind an aerodynamic fairing, with small cutouts for the muzzles. The cockpit features thick Steel-Steel Composite Metal Foam (CMF) plates, to armor the crew against rounds of handheld weapons, heavy machine guns and anti aircraft cannons with a caliber of at least 14.5 mm. The cockpit also features a big bubble shaped canopy, to provide the crew with an excellent visibility.

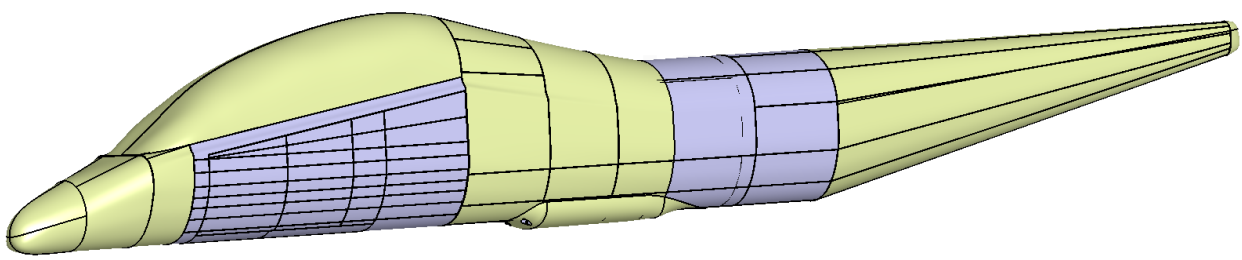

Figure 6.1: 3D modell of the fuselage

6.2. Functional Analysis

The main task of the fuselage is to accommodate the pilots and their cockpit, the majority of the electric and hydraulic subsystems, as well as the cannons and their ammunition. Furthermore, it has to mechanically connect the wing and the empennage, while transferring their loads and being as aerodynamic as possible. Apart from that, it has to fulfill the requirements listed in Table 6.1.

Table 6.1: List of requirements for the fuselage

Requirement ID	Description	Function source
Fuselage		
LAA-SUR-SAF-1	The aircraft shall be fitted with two zero-zero ejection seats.	User
LAA-SUR-VIS-1.1	The cockpit shall provide the pilot 280 degrees horizontal visual range	Mission analysis
LAA-SUR-VIS-1.2	The cockpit shall provide the pilot 30 degrees downward visual range when looking straight ahead	Mission analysis

Table 6.1: List of requirements for the fuselage

Requirement ID	Description	Function source
LAA-SUR-VIS-1.3	The cockpit shall provide the pilot 70 degrees downward visual range when looking to the sides	Mission analysis
LAA-STR-WPN-1.1	The aircraft shall feature a board canon to engage ground targets.	User
LAA-STR-CRW-1.1	The aircraft shall be able to fit two crew members.	User
LAA-SUR-PRJ-1.1	The aircraft shall be able to survive, according to table Table 2.1, impact of projectiles.	JSSG-2001 [1]

6.3. Risk Analysis

The risks found during the risk analysis executed for the design of the A-20 Chimera are stated per design chapter. The identification for probability and impact are given by Table 6.2 and will be used in subsequent chapters as well.

Table 6.2: Scoring system used to quantify risks.

Score	Probability		Impact
1	Highly Unlikely	(0%-10%)	Negligible
2	Unlikely	(10%-25%)	Minor
3	Reasonable chance	(25%-50%)	Moderate
4	Likely	(50%-90%)	Significant
5	Highly Likely	(90%-100%)	Severe

Previously, technical risks have been determined. The risks that are either specific to the fuselage or that are influenced by the fuselage design, can be found in Table 6.3.

Table 6.3: Fuselage related technical risks

ID	Label	Risk	Seq.	Cause	Prob.	Imp.
Fuselage related technical risks						
RIS-042	T	Aircraft does not survive attack of foe.	a	Aircraft is not well protected against defined threats.	1	5
RIS-045	T	Pilot(s) - aircraft interface is poor.	a	Poor view on what end user likes.	1	3
RIS-050	T	Aircraft is too vulnerable when flying low.	a	Protection is not sufficient for close attacks.	1	4
			b	Critical areas badly protected.	1	4

During the design of the fuselage, steps were taken to mitigate these risks. For RIS-042 and RIS-50 a CMF tub was designed to make sure the pilots will be protected against projectiles, this is explained in more detail in the section below. For RIS-045 two Dutch pilots were interviewed, from these interviews a lot of information was obtained about the user perspective. During the design these steps were considered to be sufficient enough to mitigate the risks.

6.4. Design Approach

The design of the fuselage is majorly influenced by the shape and size of the cockpit. Thus, this section is separated into two parts, the design of the cockpit and the design of the remaining fuselage.

6.4.1. Cockpit

The cockpit design is based on the crew that has to be accommodated as well as their vision angles and general ergonomics. The starting point of design of the cockpit were the two zero-zero ejection seats. Three dimensional models [1] were imported into CATIA. After that, two average American male mannequins from the CATIA Ergonomics & Design workbench were placed in the seats. The tool bench allows full manipulation of the mannequins to check, whether modeled control elements are reachable or not. Based on that, basic control elements like side stick, rudder pedals, thrust lever and screens were placed as well. A head-up display (HUD) was not implemented, as the crew will be equipped with modern helmets, featuring integrated displays, as discussed in subsection 11.1.5. However, the cockpit is equipped with big digital screens, reducing clutter and increasing overview.

It was decided to place the crew members behind each other and to have one pilot and one Weapons Systems Officer (WSO). It was decided to have only one pilot, because the work load of piloting a modern attack aircraft is small enough, that a second pilot does not add any benefits. This was also confirmed during the interviews with Pascal Smaal and Richard Helsdingen. They were placed behind each other, because the fuselage had become to wide having them next to each other. Next, the seats, including crew and controls, were placed on the longitudinal axis of the aircraft and spaced such that there is a sufficient amount of leg room for the crew (i.e. they can stretch their legs past the rudder pedals/feet rests without colliding with the front wall). According to Roskam, the rear crew member needs a downward viewing angle of at least 5 °[7]. Thus, the rear seat was raised, to achieve the downward angle. After that, a dummy fuselage cross section was placed around the seats, to determine the required seat height, so that the pilot has a sideways downwards viewing angle of 45 °[7]. Next, the cross section was trimmed to size, while keeping enough free space for the nose landing gear wheel-well and armor plating.

As armor, 54.3 mm thick Steel-Steel Composite Metal Foam (CMF) was chosen. Steel-Steel CMF consists of hollow steel spheres embedded in a steel matrix. It has shown to be able to absorb a large amount of impact energy and to stop 14.5 mm armor piercing incendiary rounds (API) as used in anti tank rifles and anti aircraft guns. It is likely to stop even larger calibers. However, this was not tested yet. Even though the CMF is made of steel, it is only slightly heavier than Aluminum (3.0 g/cm^3) [8]. The armor was placed below, in front and to the sides of the cockpit, protecting the crew of ground based projectiles. The armor adds a weight of 625.7 kg. This is a significant weight, but compared to the armor of an A-10, this is relatively light. The Titanium armor of the A-10 weighs 540 kg [9], while only protecting a single pilot. Furthermore, as steel has significantly lower material and production costs, the armor will be cheaper, too.

Next, a big bubble shaped canopy was placed on top of the cockpit, to maximize the crew's visibility. It was shaped by trying to avoid big slopes, while giving the pilots enough room overhead. Lastly, the cockpit fuselage was closed off with a nosecone. Focus has been put on rounding all interfaces between segments.

The cockpit does not satisfy the vision angle requirements as set before. However, as discussed in subsection 11.1.5, it was decided to augment the viewing angles by using fuselage mounted cameras and screens in the cockpit.

6.4.2. Fuselage

Based on the fuselage shape of the cockpit, the rest of the fuselage was constructed. The fuselage was originally designed to be 12 m long to fit in a 53 ft shipping container. However, during the empennage sizing, as further discussed in chapter 16, the decision was made to increase the fuselage to 15 meters. This decision was made to increase the tail arm, which would then result in a smaller empennage. The fuselage will still fit in a shipping container, as specified in chapter 16. However, the container has to be larger. The task of the remaining fuselage is to connect cockpit, wing and empennage while also housing the electric and hydraulic subsystems and cannons.

To be able to remove the wing for transport, the wingbox is not continuous, but split along the center line. This way, the wing can be transported in halves. To connect the halves to the fuselage, a 'socket' of the shape of the wingbox is fixed to large ribs, which connect to the fuselage. The halves can be slid in the 'socket' and fixed by using bolts. The two GAU-19 rotary .50 cal cannons and their ammunition were placed below the

[1] https://grabcad.com/library/ejection-seat-2, conducted on [17-01-2021]

wingbox. They were placed such that the firing barrel sticks out of the cross section of the fuselage. To reduce drag, a fairing with cutout was placed over the cannons. To increase the tail strike angle and to lift the empennage out of the downwash of the wing, the tail cone was sloped upwards.

Even though this method of sizing the fuselage might seem arbitrary, the determined fuselage diameter, length and tail cone shape fit very well into the range of reference values provided by Roskam[7].

6.4.3. Fuselage Structural Overview

The structural type used for this aircraft's fuselage is a conventional stiffened skin. This choice was made based on a comparison with an aircraft with similar fuselage dimensions [10]. With respect to other fuselage architectures such as Sandwich fuselage fuselage concept, this model is also known for its favorable distribution of tensile stresses over its structure. Furthermore this model promises a lighter fuselage structure as well as offering more resistance to buckling. This design has stiffened hat stringers that run along the fuselage. Additionally, the design is equipped with frames that are curved around the longitudinal axis of fuselage [11]. Again looking at similar aircraft, it was decided that the main materials used in the construction of the fuselage would be an aluminum 2024 alloy due to its light weight, high tensile strength and resistance against corrosion with respect to other materials such as steel or even other aluminum alloys. [2]. In addition to aluminum, carbon/epoxy composites are also used thanks to their high strength over weight ratio. The skin of the aircraft is made of these composites, in quasi-isotropic configuration. This means that the fibers of the composites are put in directions that will lead the component to have an isotropic response to in plane loads [11]. The skin of the fuselage consists of multiple layers of the carbon/epoxy composites which are put in various orientations to obtain a quasi-isotropic layup. The purpose of this configuration is to provide sufficient axial, shear and torsional strength as well as stiffness for the skin section. To protect the instruments inside the nosecone such as the antenna and radars, the radome of the aircraft is made from glass fiber epoxy. Furthermore, the radome is coated to protect itself from high temperatures, rain, snow, sunlight, and high voltages for static electricity. Another advantage of using glass fiber is its remarkable resistance against deformation[3]. Given that aircraft is expected to operate from austere fields, it is important to make sure the fuselage skin is protected against impacts from the ground such as gravel. For that, it is decided to apply silica particle coating on composite skin of the fuselage [12].

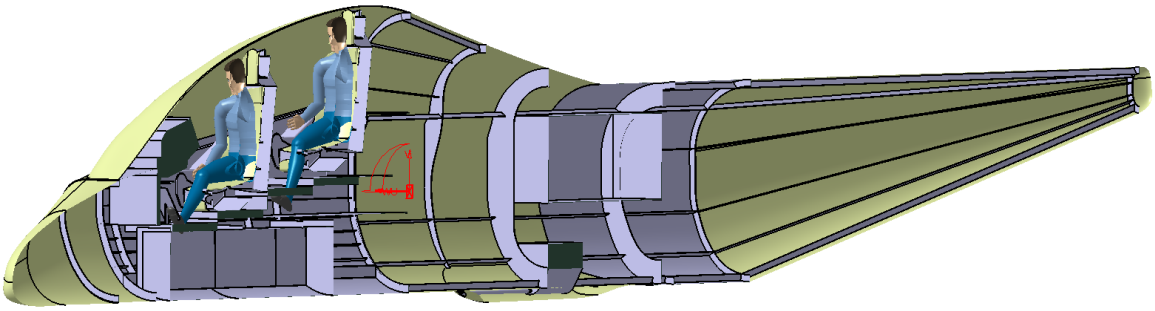

Figure 6.2: Section view of the fuselage

6.5. Sensitivity Analysis

The fuselage design is not very sensitive to changes. It's shape is mostly determined by the amount of systems that has to be fitted, as well as the required tail arm.
If the landing gear was placed inside of the fuselage, the fuselage would have to include big aerodynamic fairings and wheel wells, that might interfere with other systems, like the cannons. Furthermore, it would require extra load carrying elements.
If the tail arm was required to be longer, the fuselage would have to be longer as well.

Another factor impacting the shape is the flight speed. However, this only becomes visible when moving in trans- and supersonic flight regimes. When reaching those speeds, the fuselage has to be designed with the

[2] https://aircraftextrusion.com/aircraft_extrusion/2024_extrusion/, conducted on [18-01-2021]
[3] https://www.azom.com/amp/article.aspx?ArticleID=12107, conducted on [18-01-2021]

Whitcomb area rule in mind, where the cross sectional area of the entire aircraft has to stay as constant as possible, to reduce the formation of shocks[4].

Therefore, the fuselage design was attributed by other subsystems and has no impact on its own.

6.6. Requirement Compliance

To see if the designed fuselage satisfies the given requirements, a compliance matrix was created, which can be found in Table 6.4. As can be seen, the design fulfills all requirements.

Table 6.4: Compliance matrix for the fuselage

Requirement ID	Description	Method of compliance	Requirement met?
Fuselage			
LAA-SUR-SAF-1	The aircraft shall be fitted with two zero-zero ejection seats.	see subsection 6.4.1	✓
LAA-SUR-VIS-1.1	The cockpit shall provide the pilot 280 degrees horizontal visual range	see Figure 6.2	✓
LAA-SUR-VIS-1.2	The cockpit shall provide the pilot 30 degrees downward visual range when looking straight ahead	see Figure 6.2	✓
LAA-SUR-VIS-1.3	The cockpit shall provide the pilot 70 degrees downward visual range when looking to the sides	see Figure 6.2	✓
LAA-STR-WPN-1.1	The aircraft shall feature a board canon to engage ground targets.	see Figure 6.1	✓
LAA-STR-CRW-1.1	The aircraft shall be able to fit two crew members.	see Figure 6.2	✓
LAA-SUR-PRJ-1.1	The aircraft shall be able to survive, according to table Table 2.1, impact of projectiles.	see subsection 6.4.1 and [8]	✓*

[4] https://history.nasa.gov/SP-4219/Chapter5.html, conducted on [18-01-2021]

7
Wing Design

In this chapter the design of the wing is discussed. First, the resulted design is shown and discussed. After which the functions, requirements and risks for the wing design are discussed. With these in mind the wing was designed, the approach of the design is explained in Section 7.4. The required area is calculated using the wing loading diagram. After this the airfoil selection, aileron sizing and flap sizing are discussed. Finally the sensitivity analysis and verification & validation is performed, in which the compliance with the earlier stated requirements is checked.

7.1. Design Overview

The overall shape and structure of the wing is shown in Figure 7.1. The wing spans 18.8 m, and has a surface area of 50.6 m^2. For the high lift devices, double-slotted Fowler flaps were selected. They span 4.3 m, at 35% of the chord starting from the fuselage. The ailerons span 4 m, at 35% of the wing chord, and are located as close as possible to the wing tips.

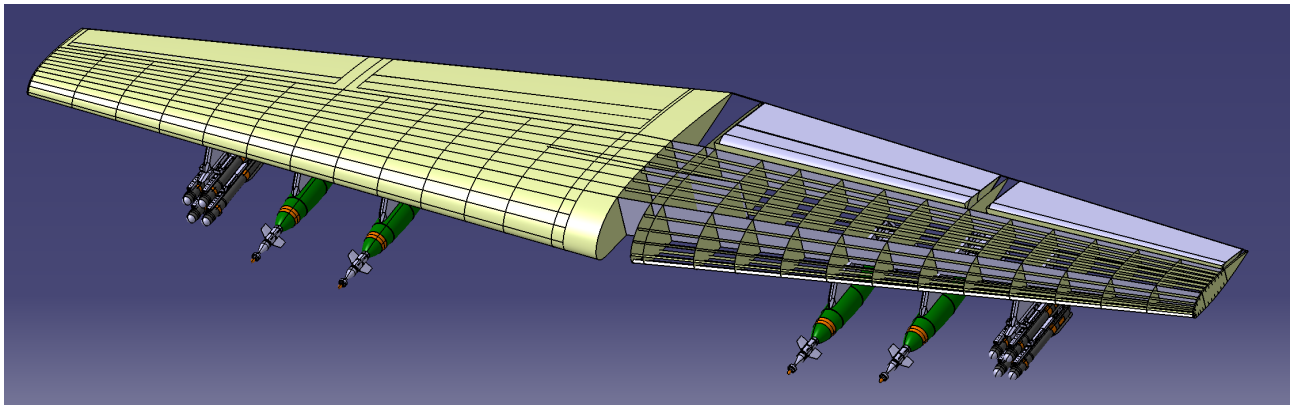

Figure 7.1: Geometry of the A-20 wing

7.2. Functional Analysis

In an earlier design stage, the requirements for the aircraft were set up. Table 7.1 presents the requirements applicable to the wing design. There are some additional requirements regarding the aileron and high lift device sizing. There are discussed in subsection 7.2.1 and subsection 7.2.2 respectively.

Table 7.1: List of requirements for the Light Attack Aircraft

Requirement ID	Description	Type	Source
LAA-PAY-RCS-1.1	The aircraft shall be able to carry a reconnaissance pod.		chapter 2
LAA-PER-SER-1.1	The service ceiling shall be higher than 9 144 m (30 000 ft).	Key & Driving	User
LAA-PER-FEM-1.1	The cruise distance during a ferry mission shall be at least 1 666.80 km (900 nmi).	Key & Driving	User
LAA-PER-DSM-1.1	Descent to 914.40 m (3 000 ft) shall be completed within 20 minutes of the initial climb to the cruise altitude.	Key	User
LAA-PER-DSM-2.1	The aircraft shall be able to loiter 4 hours on station without dropping the armament.	Key	User

Table 7.1: List of requirements for the Light Attack Aircraft

Requirement ID	Description	Type	Source
LAA-PER-DSM-3.1	The aircraft shall have reserve fuel sufficient for climb to 914.40 m (3 000 ft) and loiter for 45 minutes after the design mission completion.	Key	User
LAA-PER-DSM-3.3	The aircraft shall have a cruise altitude above 3 048 m (10 000 ft)	Key & Driving	User
LAA-PER-DSM-4.1	The aircraft shall be able to land over a 15.28 m (50 ft) obstacle within a distance of 1 219.2 m (4 000 ft) at most and at a density altitude up to 1 828.80 m (6 000 ft) on runways with California bearing ratio 5.	Key & Driving	User
LAA-PER-DSM-4.2	The aircraft shall be able to take off over a 15.28 m (50 ft) obstacle within a distance of 1 219.2 m (4 000 ft) at most and at a density altitude up to 1 828.80 m (6 000 ft) on runways with California bearing ratio 5.	Key & Driving	User
LAA-STR-WPN-2.1	The payload attachment system shall include at least 4 NATO standard hardpoints and/or rail launchers.	Stakeholder & Driving	section 2.1

7.2.1. Roll requirements

To size the ailerons of the aircraft, a requirement for the roll rate of the aircraft was found, which was done over defined handling qualities. Handling quality levels and the corresponding required roll rate were found in Table 7.2. As the A-20 is an attack aircraft, it has to possess level IVA handling qualities [13]. Thus, it has to be able to perform a 90 degree roll in 1.3 seconds.

Table 7.2: Required roll performance according to handling quality class [13]

Handling quality level	Required roll performance
I	60°in 1.3 s
II	45°in 1.4 s
III	30°in 1.5 s
IVA	90°in 1.3 s
IVB	90°in 1.0 s
IVC	90°in 1.7

7.2.2. High lift device requirements

The airfoil and wing shape provide a maximum lift coefficient $C_{L_{max}}$. However, during takeoff and landing, a higher $C_{L_{max}}$ is required, in order to keep the takeoff and landing speed low. This also reduces the takeoff and landing distance. To achieve this, high lift devices like leading and trailing edge flaps can be used. To size the flaps, the required difference in $C_{L_{max}}$, $\Delta C_{L_{max}}$, for takeoff and landing was determined first. During the airfoil selection, a $C_{L_{max}}$ of 1.6 was determined, while a value of 2.0 and 2.6 for takeoff and landing were chosen during the Class I weight estimate. Based on that, a $\Delta C_{L_{max}}$ of 0.4 and 1.0 is required during takeoff and landing, respectively.

7.3. Risk Analysis

The risks concerning the wing design are shown in Table 7.3. In the design process, all risks were taken into consideration. RIS-023 was mitigated by taking the required altitude, and climb rate into account in the T/W - W/S diagram. RIS-025 was mitigated by taking the payload as a starting point for the weight estimation, which directly influences the wing sizing. The structure was designed appropriately, and should be sized in the future. Since the service ceiling was not a limiting factor in the T/W - W/S diagram, RIS-026 was

mitigated.

Table 7.3: Wing related technical risks

ID	Label	Risk	Seq.	Cause	Prob.	Imp.
RIS-025	T	Aircraft can't carry the payload of 3 000 lbs	a	Wings do not generate enough lift	2	5

7.4. Design Approach

During the design of the wing several steps were taken to determine the final geometry of the wing. The methods used to decide on this are explained in this section.

7.4.1. Wing/Thrust loading

To determine the wing dimensions required, a thrust and wing loading diagram (T/W-W/S diagram) was constructed. From this graph, the critical wing and thrust loading for stall speed, take off, landing, maximum cruise speed, and climb were determined. The loading diagram was constructed using the methods shown in Roskam [4], and is shown in Figure 7.2. In the graph, the vertical, yellow line represents the maximum wing loading at stall conditions. In this particular case, the stall speed is chosen to be the stall speed in landing configuration at a density altitude of 6000 ft, as it was the most critical condition, i.e. the permitted wing loading was the lowest. The stall speed during landing in turn is related to the approach speed by Equation 7.1, where V_{S_L} is the stall speed in landing configuration and V_A the approach speed. The maximum allowable approach speed is determined over the allowable landing length s_{FL}. The relation is given by Equation 7.2. The wing loading can't be higher than the determined loading, so the design point is on or left of the stall line.

$$V_A = 1.2 \cdot V_{S_L} \tag{7.1}$$

$$s_{FL} = 0.3 \cdot V_A^2 \tag{7.2}$$

The red line represents the relationship between the thrust and wing loading at cruise speed and altitude, with a selected aspect ratio of 7. The design point should be on, or above this line. The green line relates the thrust and wing loading in take off conditions, considering the required runway length at 6 000 ft altitude. The design point should be on, or above this line. The thrust loading will be further discussed in Chapter 9.

Looking at the the thrust and wing loading diagram, the take off requirements, and stall speed determine the design point for the thrust and wing loading.

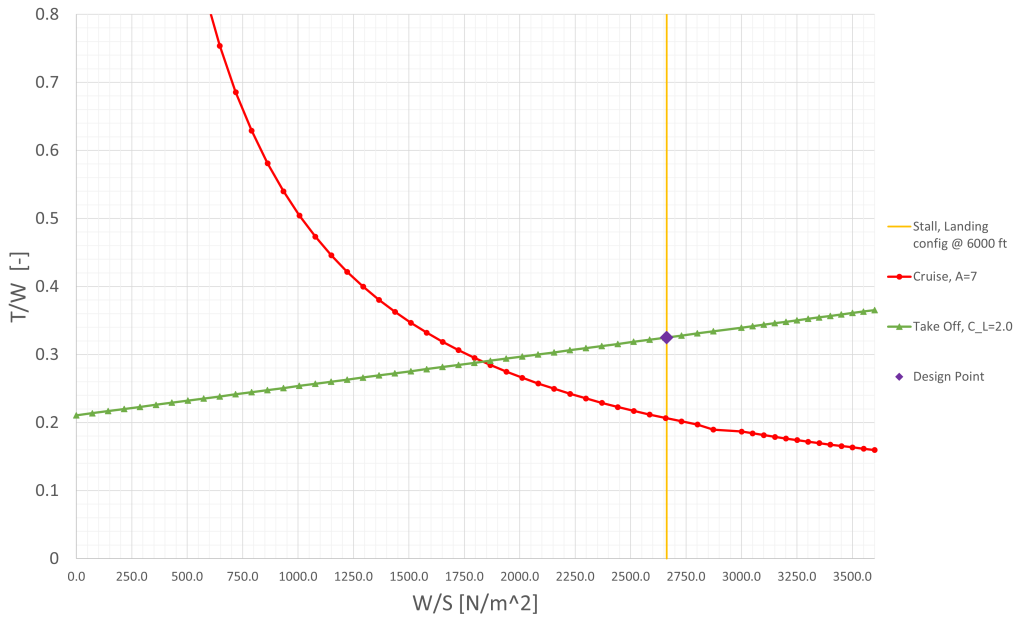

Figure 7.2: T/W-W/S diagram of the A-20

7.4.2. Wing sizing

The required wing area S of 50.5 m^2 was calculated using Equation 7.3 using the take off weight W_{TO} determined in chapter 5, and W/S from the design point (purple) in Figure 7.2.

With the determined wing area, and chosen aspect ratio A, the wing geometry was designed. A mid-wing configuration was the starting point. Using the aspect ratio and the wing area, the wing span b was determined using Equation 7.4.

$$S = \frac{W_{TO}}{W/S} \quad (7.3) \qquad b = \sqrt{S \cdot A} \quad (7.4) \qquad \lambda = 0.2 \cdot (2 - \Lambda_{c/4} \cdot \frac{\pi}{180}) \quad (7.5)$$

Next, the sweep angle of the quarter-chord line $\Lambda_{c/4}$ was determined to be 0°, since the aircraft cruises at Mach 0.6, which means that it does not reach transsonic speeds and no sweep is required.. The taper ratio (λ) of the wing was calculated using Equation 7.5 [14].

λ was used to calculate the root chord c_r and tip chord c_t of the wing using Equation 7.6 and Equation 7.7 respectively. The thickness over chord ratio t/c was determined as 0.18.

$$c_r = \frac{2S}{(1+\lambda) \cdot b} \quad (7.6) \qquad c_t = \lambda \cdot c_r \quad (7.7)$$

According to Raymer[5], a dihedral angle Γ of 3°should be used for an unswept mid-wing configuration. The wing geometry is summarized in Table 7.4.

Table 7.4: Dimensions of the main wing

parameter	value	unit
S	50.5	[m^2]
b	18.8	[m]
MAC	2.85	[m]
c_r	3.84	[m]
c_t	1.54	[m]
λ	0.4	[-]
$\Lambda_{c/4}$	0	[°]
Γ	3	[°]

7.4.3. Airfoil selection

In order to size the aileron and flaps, the airfoil of the wing was chosen. From the airfoil selection different parameters, such as the wing lift curve slope, wing zero lift drag and design lift coefficient, were needed in the sizing of the control surfaces.

The airfoil selection started at choosing a design lift coefficient, which was chosen as the lift coefficient used in the loiter part of the mission, as this is the most fuel intensive part of the mission. A design lift coefficient of 0.68 was chosen. The thickness of the airfoil was also calculated in the Class I sizing, the thickness ratio was determined to be 0.18. Using a NACA 5 digit airfoil generator from *Airfoil Tools*[1], an airfoil was generated, as a result the NACA 44018 was selected.

7.4.4. Aileron Sizing

To find the roll rate p, a constant roll rate is assumed. Thus, p was found by using Equation 7.8 with ϕ being the roll angle and t being the time to reach ϕ

$$p = \frac{\phi}{t} \quad (7.8)$$

[1] http://airfoiltools.com/airfoil/naca5digit, conducted on [17-12-2020]

To derive the required aileron size, the roll damping of the wings, the aileron effectiveness, aileron deflection, and flight speed were considered. This was done by using Equation 7.9. $C_{l_{\delta_\alpha}}$ is a coefficient describing the rolling moment change due to aileron deflection δ_α. C_{l_p} is a coefficient effectively describing the roll damping of the wings, while V is the airspeed in meters per second and b is the wingspan in meters.

$$p = -\frac{C_{l_{\delta_\alpha}}}{C_{l_p}} \cdot \delta_\alpha \cdot \frac{2 \cdot V}{b} \tag{7.9}$$

$C_{l_{\delta_\alpha}}$ was calculated using Equation 7.10. C_{l_α} is the lift rate coefficient of the chosen airfoil and S is the wing surface in square meter. The limits of the integral are the beginning and end of an aileron in spanwise direction. As the required roll rate is quite high, the ailerons are placed outboard for maximum effect. They have an offset of 10 cm from the wingtip, to provide some space for hinge mechanisms. This is the value b_2. The value for b_1 has to be chosen such that $C_{l_{\delta_\alpha}}$ is big enough to yield the desired roll rate. The variable y is the spanwise distance, measured along the y-axis, which is aligned with the wingspan. The function $c(y)$ represents the chord function, i.e. the chord length of the wing depending on the spanwise location. τ was found by using the graph in Figure 7.3. For the ailerons, a relative chord length of 0.35 was chosen, again to maximize the effect. This leaves 5% of the chord length between the rear spar and the aileron, to accommodate the hinge mechanism. This leads to a value of 0.56 for τ.

$$C_{l_{\delta_\alpha}} = \frac{2 \cdot C_{l_\alpha} \cdot \tau}{S \cdot b} \cdot \int_{b_1}^{b_2} c(y) \cdot y \, dy \tag{7.10}$$

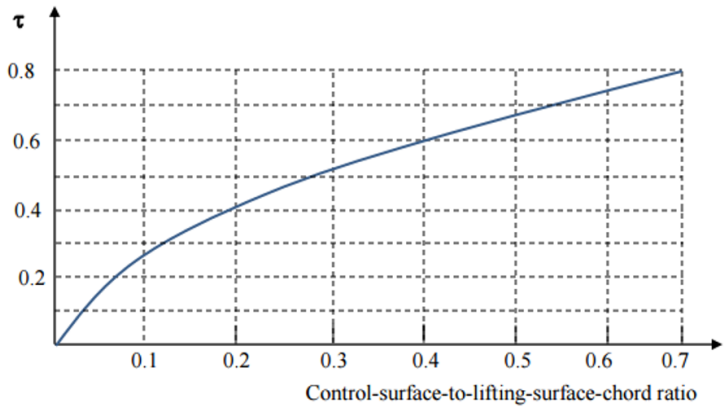

Figure 7.3: τ depending on the control surface chord to wing chord ratio [13]

C_{l_p} was found by using Equation 7.11. The only new value in this equation is C_{d_0}, which is the zero-lift drag coefficient of the chosen airfoil.

$$C_{l_p} = -\frac{4 \cdot C_{l_\alpha} + C_{d_0}}{S \cdot b^2} \cdot \int_0^{b/2} c(y) \cdot y^2 \, dy \tag{7.11}$$

The handling quality level IVA, requires a roll rate of 69.2 deg/s. This roll rate has to be reached during all stages of flight. Upon inspection of Equation 7.9, one finds that the roll rate is lower, the lower the airspeed is. Thus, to size the ailerons for the most critical flight condition, the airspeed is assumed to be the flapped stall speed at sea level of 40.9 m/s (~ 80 kts). Using the above described equations, one then finds a required aileron span of 4.1 m, while having a symmetric deflection of 30 degrees. This leads to a single aileron area of 2.9 m^2.

There are multiple ways of augmenting the roll of the aircraft. One option is the addition of spoilers to use them as spoilerons. Spoilerons have the advantage, that they can negate the adverse yaw effect of ailerons. This makes the aircraft easier to fly, as it leads to a partial decoupling of roll and yaw. It also makes the integrated guns easier to target, as small roll corrections do not lead to a yawing moment and thus do not bring the guns off target. Furthermore, the ailerons could be made smaller, while achieving the same roll rate.

However, the addition of spoilers would add more moving parts, which leads to an increase in weight, complexity and cost, while impacting the reliability negatively. This also increases the required maintenance time and cost. Another way of augmenting the roll, is using the tail control surfaces as tailerons. However, this requires a mixing of control surfaces, which in turn requires a more complex control and flight augmentation system. It would also reduce the elevator authority if roll and pitch are used at the same time, which then requires bigger elevators. The flaps could be used as well, making them flaperons. However, as calculations in subsection 7.4.5 show, the aircraft requires more complex flap systems, that typically are less suitable for the use as flaperons due to their slow deployment speed.

Lastly, it has to be considered if it even is necessary to augment the roll to reduce aileron size. The ailerons are very large, but when visually comparing them to ailerons of similar aircraft (A-10, Super Tucano), one finds that they are very comparable in proportion. On the other hand, a reduction in aileron size would increase the available area for flaps, allowing the use of simpler flap systems. However, as discussed in subsection 7.4.5 it would not significantly reduce the flap complexity. Thus, a roll augmentation was not further considered.

7.4.5. Flap Sizing

Based on the previously determined $\Delta C_{L_{max}}$, the required wing area that is effected by flaps S_{wf} was determined, using Equation 7.12 [14].

$$\Delta C_{L_{max}} = 0.9 \cdot \Delta C_{l_{max}} \cdot \frac{S_{wf}}{S} \cdot cos\Lambda_{\text{hinge line}} \tag{7.12}$$

S is the actual wing area in square meters, $\Lambda_{\text{hinge line}}$ is the sweep angle of the hinge line in degrees and $\Delta C_{l_{max}}$ is the difference in maximum profile lift coefficient due to the change of shape of the profile due to flap deployment. Typical values for $\Delta C_{l_{max}}$ for different flap systems were found in Table 7.5.

Table 7.5: Typical values for $\Delta C_{l_{max}}$ for different flap systems [13].

Flap type	$\Delta C_{l_{max}}$
Plain flap	0.9
Slotted flap	1.3
Fowler flap	$1.3 \cdot c'/c$
Double slotted Fowler flap	$1.6 \cdot c'/c$
Triple slotted Fowler flap	$1.9 \cdot c'/c$

Upon inspection, it becomes apparent, that the values of $\Delta C_{l_{max}}$ of Fowler flaps are dependent on the ratio c'/c. This is because a Fowler flap not only deflects downwards, but also extends backwards, effectively increasing the chord length c, yielding a new chord length c'. This new chord length was found by using Equation 7.13. Here, c is the chord length in meters and Δc the previously mentioned chord extension due to flap deployment.

$$c' = c + \Delta c \tag{7.13}$$

Assuming a relative chord length of 0.25 for simple flap systems and 0.35 for complex systems like Fowler flaps, one can use the graph shown in Figure 7.4, when typical flap deflections are known. Typical flap deflections for takeoff and landing depending on flap type were found in Table 7.6.

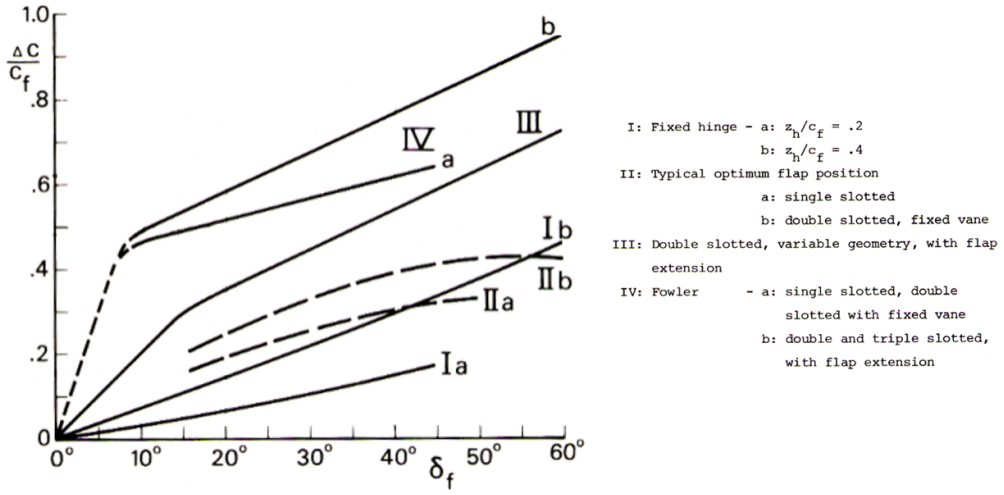

Figure 7.4: Typical $\Delta c/c_f$ values for different flap systems at varying deflection angle δ [13]

Table 7.6: Typical values for flap deflection during takeoff and landing for different flap systems [14].

Flap type	δ_{TO} [°]	δ_{LD} [°]
Plain flap	20	60
Slotted flap	20	40
Fowler flap	15	40
Double slotted Fowler flap	20	50
Triple slotted Fowler flap	20	40

Over the deflection angle one now can find a value for c'/c for each flap type, which in turn results in a value for $\Delta C_{l_{max}}$. Then, the previously determined required values for $\Delta C_{L_{max}}$ were used to find the required wing area that is effected by flaps S_{wf}, by using Equation 7.12. The required areas per type and scenario are found in Table 7.7. Plain flaps were excluded, as the required affected wing area would become too big, and thus also the span that is occupied by flaps. This could be compensated for by using leading edge high lift devices. However, those would increase complexity and cost, while reducing reliability when operating in harsh environments.

Table 7.7: Required wing area that is effected by flaps S_{wf} per flap type and scenario.

Flap type	$S_{wf_{TO}}$ [m^2]	$S_{wf_{LD}}$ [m^2]
Slotted flap	17.4	43.5
Fowler flap	14.8	35.9
Double slotted Fowler flap	11.8	27.2
Triple slotted Fowler flap	10.0	23.6

One has to keep in mind that not the entire wing span is available for flaps, as a part is covered by ailerons and another part lies within the fuselage. Taking both into account and integrating the chord function over the span, one finds an available wing area of 27.3 m^2, which means that there is just enough surface and span available for double slotted Fowler flaps. Double slotted Fowler flaps provide a compromise: they provide more lift than a normal slotted flap, while also being more efficient as they are adding considerably less drag [14]. This comes at cost of increased complexity compared to simpler flap systems. However, the use of simpler flap systems only is possible when used in combination with leading edge high lift devices and/or when reducing the aileron size (see subsection 7.4.4), which increases the complexity again. Another way of reducing the flap size or complexity is the use of the ailerons as flaps, making them flaperons. However, this could render the aircraft uncontrollable in roll during flapped stall conditions. Thus, this option was not further considered and double slotted Fowler flaps were chosen. They take up 35 % of the chord, leaving a

space of 5% of the chord between flap and rear spar to accommodate the hinge mechanism. Together with the required area, one finds the span of a single flap to be 4.3 m measured from the fuselage.

7.4.6. Structure

Given that this aircraft is equipped with a wet wing, the main structural components of the wing are spars, ribs, skin, stringer and the fuel tanks. Ribs give the cross sectional shape of the wing, help to increase the buckling stress carried by the skin as well as distributing the stress in the overall structure. The spars take up the load exerted on the wing and resist bending and torsion. Furthermore, longitudinal stringers are used to help the skin in carrying the buckling stress[15].
In terms of architecture, the aircraft has a multi-spar construction. There are 2 spars running along the wing span. To support the main landing gear, there is a third spar, which extends from the wing root to the MLG structure. Similar aircraft were analyzed to determine the ribs configuration. The aircraft has 14 ribs per wing. There is a rib at every location where a load is introduced, such as the hard points, landing gear, and control surfaces. By looking at similar aircraft, it was decided to use self sealing conformal fuel bladders as fuel tanks inside the wing[10]. Figure 7.5 shows the structure of the wing.
In terms of material selection, aluminum 2024 is selected for the spars where a high tensile strength, shear modulus and fatigue strength is required. For ribs, aluminum 5052 was selected. This alloy is known for its application for welded joints, corrosion resistance, and light weight[2]. The skin and control surfaces are made carbon epoxy composite that are made by hand lay up, which are one of the cheapest methods in aerospace industry. Another advantage of this method is that it is relatively easy to achieve different thicknesses using this method and at the same time, achieve a uniform resin distribution. [16].

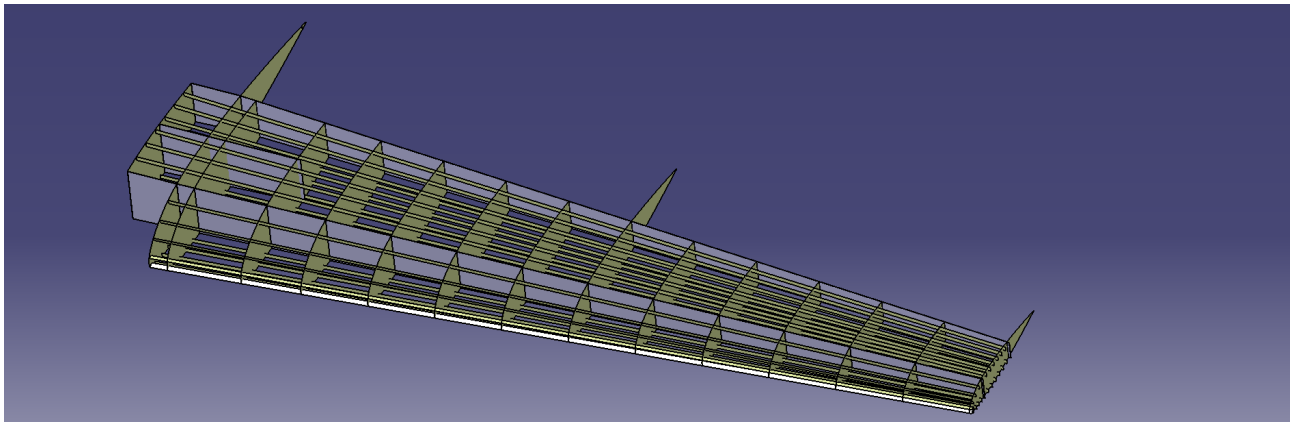

Figure 7.5: Catia render of the wing structure

7.5. Sensitivity Analysis

The wing sizing is dependent on the aircraft weight, speed and altitude requirements at different flight phases, and the selected airfoil. The speed and altitude requirements and selected airfoil are unlikely to change. The weight however, is dependent on the sizing of each component of the aircraft. Weight therefore has a large influence on the wing sizing. A 10% increase in weight results in a 10% increase in wing area, and a 4.8% increase in wing span and MAC. The sizing of high lift devices and control surfaces was done after the wing sizing.

7.6. Verification and Validation

The T/W - W/S diagram, and wing sizing were verified and validated in chapter 7 of the midterm report, and have not changed since. For the flap and aileron sizing, the calculations were checked multiple times by hand. A sanity check was performed comparing the flap, and aileron size with similar aircraft. The ailerons are large, but considering the high requirement of the roll rate, not too large. It also makes sense that the aircraft requires large, relatively complex flaps, since the runway requirements are steep.

[2] https://www.aalco.co.uk/datasheets/Aluminium-Alloy-5052-H32-Sheet-and-Treadplate_138.ashx, conducted on [13-01-2021]

7.7. Requirement Compliance

To give an overview of whether the wing requirements are met, a compliance matrix is presented in Table 7.8.

Table 7.8: Compliance matrix for the wing

Requirement ID	Description	Method of compliance	Requirement met?
LAA-PAY-RCS-1.1	The aircraft shall be able to carry a reconnaissance pod.	subsection 7.4.6	✓
LAA-PER-SER-1.1	The service ceiling shall be higher than 9 144 m (30,000 ft).	subsection 7.4.1	✓
LAA-PER-FEM-1.1	The cruise distance during a ferry mission shall be at least 1 666.80 km (900 nmi).	subsection 7.4.1	✓
LAA-PER-DSM-1.1	Descent to 914.40 m (3 000 ft) shall be completed within 20 minutes of the initial climb to the cruise altitude.	subsection 7.4.1	✓
LAA-PER-DSM-2.1	The aircraft shall be able to loiter 4 hours on station without dropping the armament.	subsection 7.4.1	✓
LAA-PER-DSM-3.1	The aircraft shall have reserve fuel sufficient for climb to 914.40 m (3 000 ft) and loiter for 45 minutes after the design mission completion.	subsection 7.4.1	✓
LAA-PER-DSM-3.3	The aircraft shall have a cruise altitude above 3 048 m (10 000 ft)	subsection 7.4.1	✓
LAA-PER-DSM-4.1	The aircraft shall be able to land over a 15.28 m (50 ft) obstacle within a distance of 1 219.2 m (4 000 ft) at most and at a density altitude up to 1 828.80 m (6 000 ft) on runways with California bearing ratio 5.	subsection 7.4.1	✓
LAA-PER-DSM-4.2	The aircraft shall be able to take off over a 15.28 m (50 ft) obstacle within a distance of 1 219.2 m (4 000 ft) at most and at a density altitude up to 1 828.80 m (6 000 ft) on runways with California bearing ratio 5.	subsection 7.4.1	✓
LAA-STR-WPN-2.1	The payload attachment system shall include at least 4 NATO standard hardpoints and/or rail launchers.	subsection 7.4.6	✓

8
Empennage Design

In this chapter the empennage design is discussed. To design the empennage accordingly first the loading diagram and x-plot had to be found. After this was done the geometry of the empennage was known, the design was verified against the set requirements.

8.1. Design Overview

In Figure 8.1 the overall shape of the empennage is presented. The entire empennage uses a symmetric NACA-0010 airfoil, according to the source[1] which gives a range. The horizontal stabilizer has a span of 7.93 m and an aspect ratio of 5.8. The horizontal tail has a constant chord of 1.37 m over the entire span. The vertical tails have a span of 2.74 m and an aspect ratio of 2.67. The vertical tails have a root chord equal to the chord of the horizontal tail and has a taper ratio of 0.5.

The horizontal tail is fitted with two elevators which both span 3.57 m over 25% of the chord. The vertical tails are likewise fitted with rudders spanning 2.46 m over 25% of the chord.

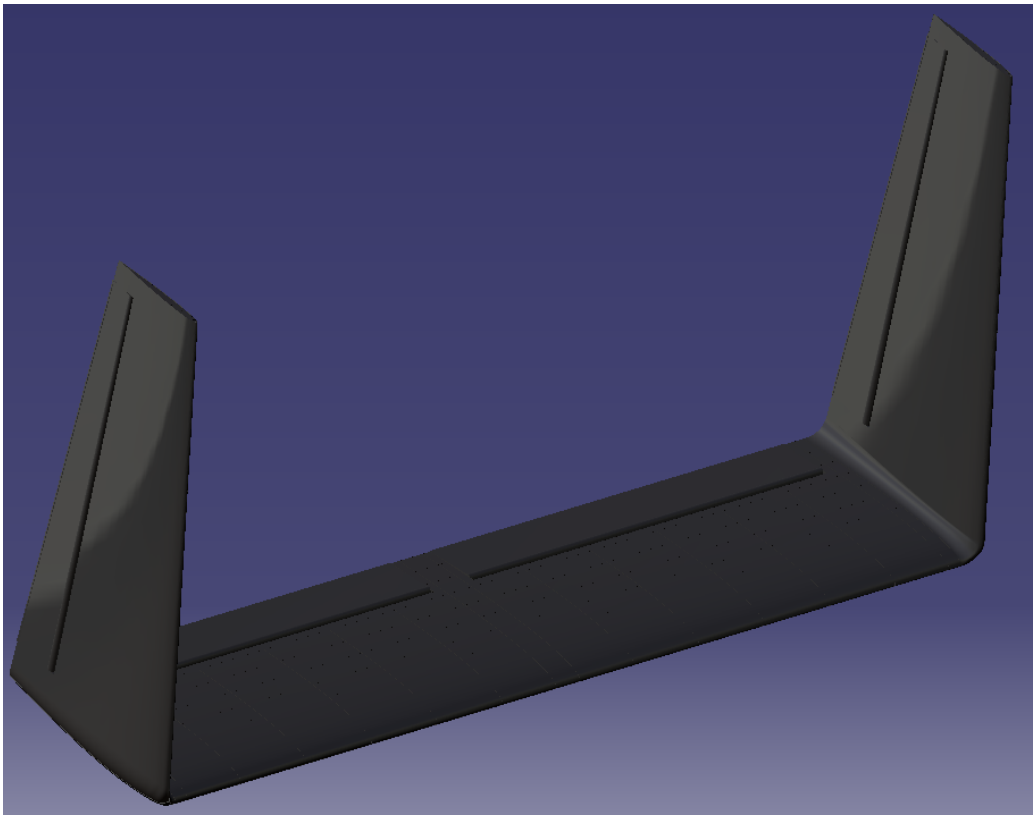

Figure 8.1: Catia render of the empennage

8.2. Functional Analysis

The empennage of the aircraft had to be sized properly for the aircraft to be controllable as well as stable. Not all military aircraft have to be stable, since the stability can be artificially managed by Proportional-Integral-Derivative (PID) feedback control as stated in chapter 16 of Raymer [5]. This is also typically the case for aircraft like the F-16 [14].

[1] https://www.fzt.haw-hamburg.de/pers/Scholz/HOOU/AircraftDesign_9_EmpennageGeneralDesign.pdf, conducted on [15-01-2021]

The empennage is sized with regard to the center of gravity (c.g.) and is also dependent on the wing position. For the controllability and stability requirements to be met, the c.g. range of the aircraft, for a certain wing position, should lie between the X-plot lines, which will be further discussed in section 8.4.

Figure 8.2 gives the functional breakdown structure of the empennage. The main function of the aircraft is divided into controlling the aircraft and stabilizing the aircraft. The empennage can control the aircraft in pitch and yaw. The pitch is typically controlled by the elevator on the horizontal tail surface, while the yaw is controlled by the rudder on the vertical tail surface.
While controlling the aircraft, the empennage must also provide stability to the aircraft. Regarding stability, there are two kinds; static and dynamic stability. Both of these kinds have different properties in the longitudinal and lateral direction. For this reason, the stability and control characteristics have been added. These characteristics were evaluated on their derivative with respect to the influence (stability: angle of attack, side slip, roll rate, yaw rate; control: rudder deflection).

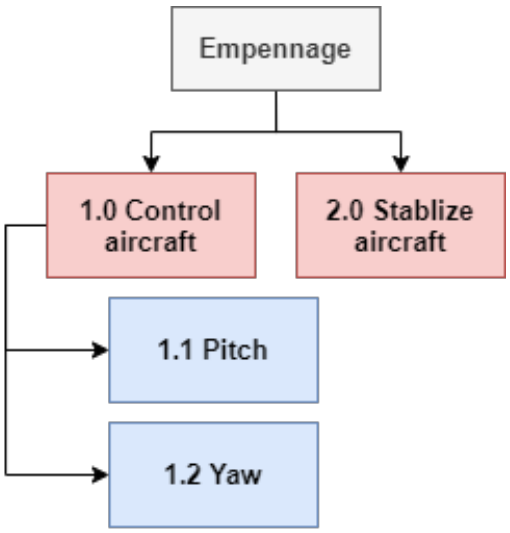

Figure 8.2: Functional Breakdown Structure of the Empennage Design

8.3. Risk Analysis

In preceding reports, there have been no specific risks determined regarding the empennage design. However, during the application of the methods in section 8.4, it showed that some aspects were overlooked.

The H-tail effectiveness was initially not considered. However, according to Roskam [17], the aspect ratio of the horizontal and vertical tail have to be multiplied by 1.5 for its effective aspect ratio. This aspect ratio increased the stability and controllability region seen in Figure 8.6.

Furthermore, the combination of bank angle and scrape angle should be checked with the angle of attack. This was checked with the Catia render and showed that with the initial landing gear sizing, it did not meet the scrape angle and bank angle. The strut length in chapter 10 had been adjusted to accommodate for these angles.

Lastly, the elevator and rudder deflection have to checked whether they do not collide when deflected. If they do collide, then a cut-out will be required in the control surfaces. Consequently, this reduces the area of the control devices and should be accounted for. The identification and consideration of these risk during the designing of the aircraft was considered to be enough to mitigate the risks.

8.4. Design Approach

The empennage design was sized by a combination of a loading diagram and an X-plot. The loading diagram shows the c.g. of several loading configurations of the aircraft with regards to the wing position, while the X-plot analyzes the stability and control of the aircraft. The combination of the two plots gives a position of the wing and the horizontal tail surface area.

8.4.1. Loading Diagram

The loading diagram analyzes several loading scenario's with regards to payload attached or unattached to the hard points and the fuel. Item 1 in the list below, portrays the standard mission profile, while items 2 and 3 sketch the worst-case scenario's of the loading diagram.

1. Sufficient ammo for it to be depleted after 55 seconds, using two integrated guns and the remainder of the payload weight attached to the hard points (i.e. 864 kg ammo 497 kg bombs).
2. Only the ammo for the integrated gun is considered (i.e. 1361 kg of ammo).
3. The maximum weight of the payload is attached under under the hard points (i.e. 1361 kg of bombs or 1361 kg of podded fuel tanks used for a ferry mission).

A combination of loading procedures was used to plot a loading diagram. It was assumed that there is no specific loading procedure for the military aircraft. Hence, A different plot was observed, unlike the one seen in SEAD lecture weight and balance, where a "window-aisle" procedure is used for commercial aircraft [18].

The payload on the hard points are placed on the same longitudinal position. They are typically located from the leading edge spar till the trailing edge spar. The bombs attached to those hard points have to protrude out from the wing planform for sufficient clearance. Therefore, the c.g. location of the payload attached to the hard points are assumed to be located at the front spar of the Mean Aerodynamic Chord (i.e. 2% of the MAC).

Equation 8.1 gives an equation of the c.g. shift per weight component. The OEW was used as starting value. Afterwards several combination of the items (i.e. the ammo, the fuel and the payload attached on the hard points) are used as item. For each new contribution, the weight and the location of the previous calculation was used as input for the subscript "old".

$$x_{cg_{new}} = \frac{x_{cg_{old}} \cdot m_{old} + x_{cg_{item}} \cdot m_{item}}{m_{old} + m_{item}} \tag{8.1}$$

For the fuel location, Equation 8.2 gives the lateral fuel c.g. location with respect to the fuselage symmetric line. It is considered that the fuel is stored between the spars (located at 20% and 60% of the local wing chord), whereby the longitudinal c.g. position of the fuel stored in the wing is located in the middle of the spars (40 % of the local wing chord). The S_1 and S_2 can be seen from Figure 8.3, which shows a reference image of a wingbox.

$$y_{cg_{fuel}} = b \cdot \alpha_{fuel} = b \cdot \frac{b}{4} \cdot \frac{S_1 + 3S_2 + 2\sqrt{S_1 S_2}}{S_1 + S_2 + \sqrt{S_1 S_2}} \tag{8.2}$$

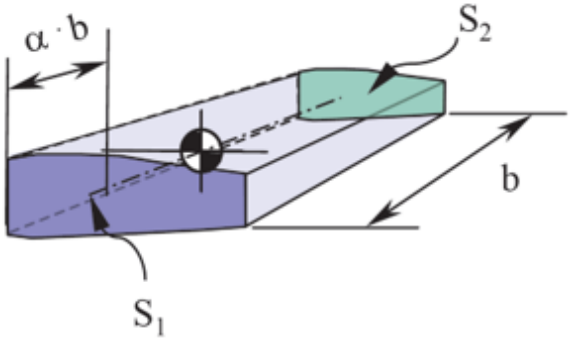

Figure 8.3: Reference wingbox for the lateral fuel c.g. location [18]

An additional margin of 2% was multiplied after all scenario's was plotted for the outer values, in order to account for c.g. variations due to landing gear retracting, and other movable items. This yielded the maximum and minimum locations of the c.g. locations.

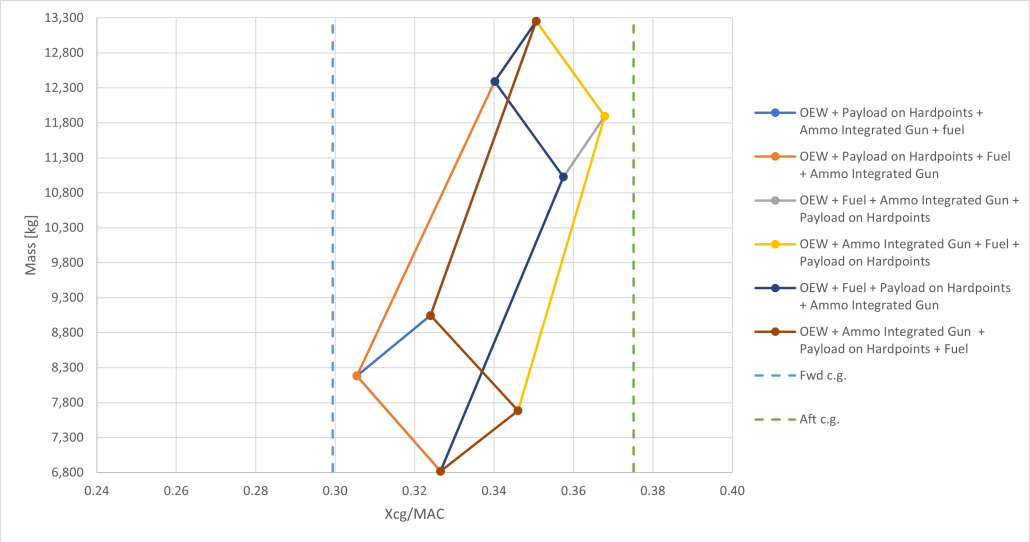

Figure 8.4: Loading diagram of the six possible load paths.

Finally, a graph was made using the maximum and minimum location as mentioned above and was plotted according to variable wing positions, by changing the x_{LEMAC} for several positions, a c.g. range diagram was created.

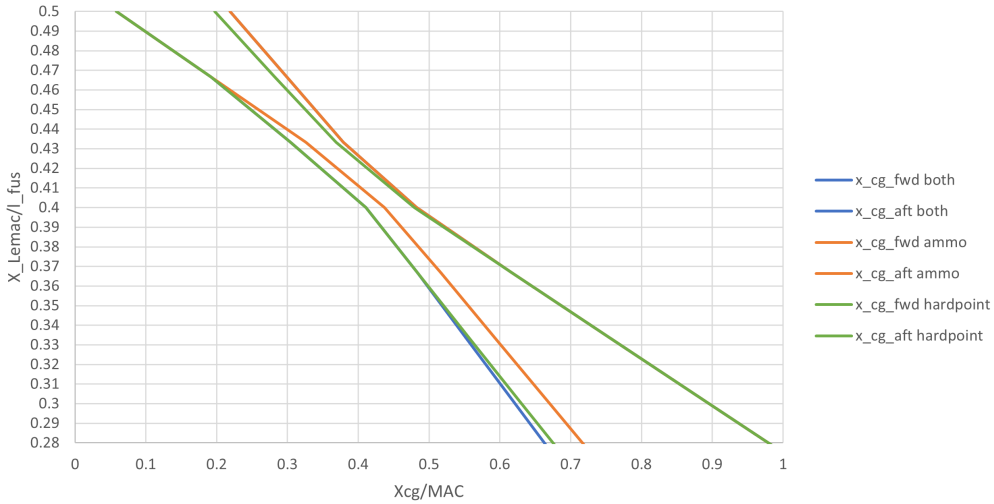

Figure 8.5: c.g. range diagram considering three different loading scenarios for different wing positions.

8.4.2. X-plot

The X-plot in figure Figure 8.6 presents the controllability line and the stability lines of the aircraft. There are two stability lines, one without stick-fixed static margin (S.M.), and one including a S.M. The S.M. is usually applied to account for stick-free stability and stick forces. However, in this aircraft a fly-by-wire system is applied, so the stick forces are not considered. Therefore, a S.M. of 5% was chosen to account for the stick-free stability. The controllability line and the stability lines were created using Equation 8.3 and Equation 8.4, where $\bar{x}_{cg}$ is the variable, following the steps as presented in the SEAD lectures [18]. The input values for the controllability and stability equations are given in Table 8.1 and Table 8.2 respectively.

$$\frac{S_h}{S} = \frac{\bar{x}_{cg} + \frac{C_{m_{ac}}}{C_{L_{A\text{-}h}}} - \bar{x}_{ac}}{\frac{C_{L_h}}{C_{L_{A\text{-}h}}} \frac{l_h}{\bar{c}} \left(\frac{V_h}{V}\right)^2} \tag{8.3}$$

Table 8.1: Input values Equation 8.3

Parameter	Value
$C_{m_{ac}}$	-0.508
$C_{L_{A\text{-}h}}$	2.6
$\bar{x}_{ac}$	0.207
C_{L_h}	-0.629
l_h	6.78
$\bar{c}$	2.85
$\left(\frac{V_h}{V}\right)^2$	0.85

$$\frac{S_h}{S} = \frac{\bar{x}_{cg} - \bar{x}_{ac} - S.M.}{\frac{C_{L_{\alpha_h}}}{C_{L_{\alpha_{A\text{-}h}}}} \left(1 - \frac{d\varepsilon}{d\alpha}\right) \frac{l_h}{\bar{c}} \left(\frac{V_h}{V}\right)^2} \tag{8.4}$$

Table 8.2: Input values Equation 8.3

Parameter	Value
$\bar{x}_{ac}$	0.213
S.M.	0.05
$C_{L_{\alpha_h}}$	5.57
$C_{L_{\alpha_{A\text{-}h}}}$	5.60
$\frac{d\varepsilon}{d\alpha}$	0.534
l_h	6.78
$\bar{c}$	2.85
$\left(\frac{V_h}{V}\right)^2$	0.85

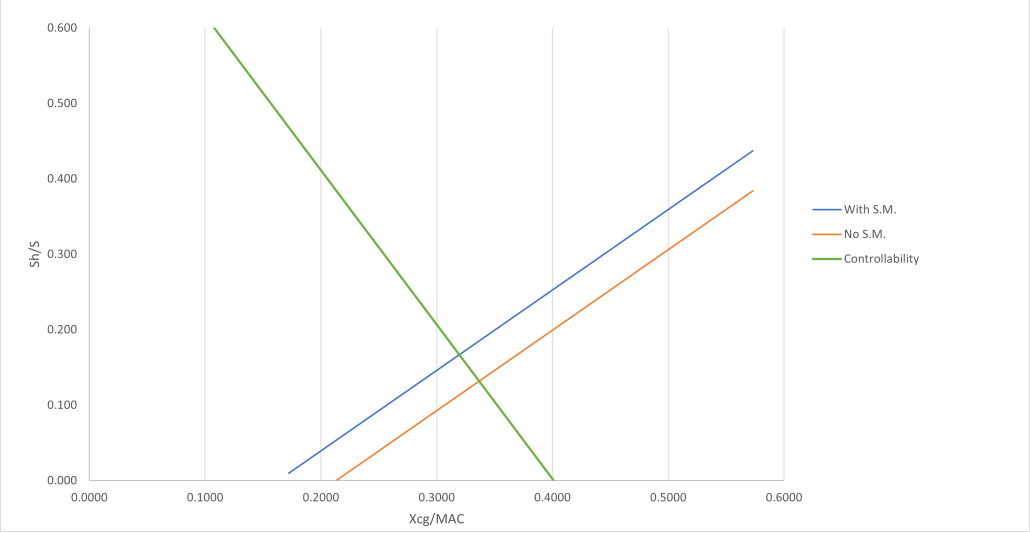

Figure 8.6: X-plot for the final configuration of the aircraft.

The c.g. of the aircraft should be on the right of the controllability line for the aircraft to be controllable and on the left of the stability line including S.M. to be stable. To see when the c.g. fits between the X-plot, the

c.g. range diagram is laid on top of the X-plot. Then the c.g. range diagram is shifted up or down to fit the most forward and most aft c.g. on the X-plot lines, this results in the minimal required tail size and a x_{LEMAC} appropriate to that size. After finding these values, a new iteration on the class I and class II estimations were done. After which the same process with the c.g. plot and the X-plot was carried out and 5 more iterations were performed. After the first iteration, it was concluded that it would be beneficial to increase the fuselage length to 15 meters to reduce the tail size. The final iteration then led to a x_{LEMAC} at 6.55 m as measured from the nose and a horizontal tail to wing surface ratio of 0.22. The X-plot and the corresponding c.g. range diagram can be seen in figure 8.7.

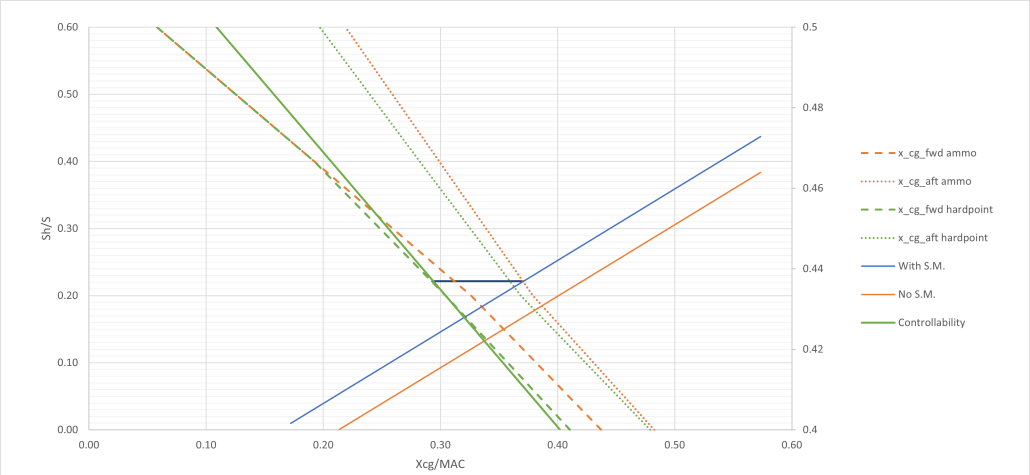

Figure 8.7: X-plot including c.g. range diagram.

8.4.3. Structural overview

Similar to the wing structure mentioned in Subsection 7.4.6, the structure of both horizontal and vertical stabilizers were determined by referring to aircraft with similar empennage overall design[10]. For the vertical stabilizers, it is decided to have 5 ribs along the stabilizers. These ribs are put perpendicular to the longitudinal axis of the rudder. There are also 2 spars running from root of the vertical stabilizer to the tip and are parallel to the longitudinal axis of rudder. There are 4 dual sets of stringers between the first and second spar helping to distribute the load to ribs and spars. The same allocation of spars and stringers are applied to the horizontal stabilizers, except for the ribs, where these have one more. The empennage structure is visually presented in Figure 8.8

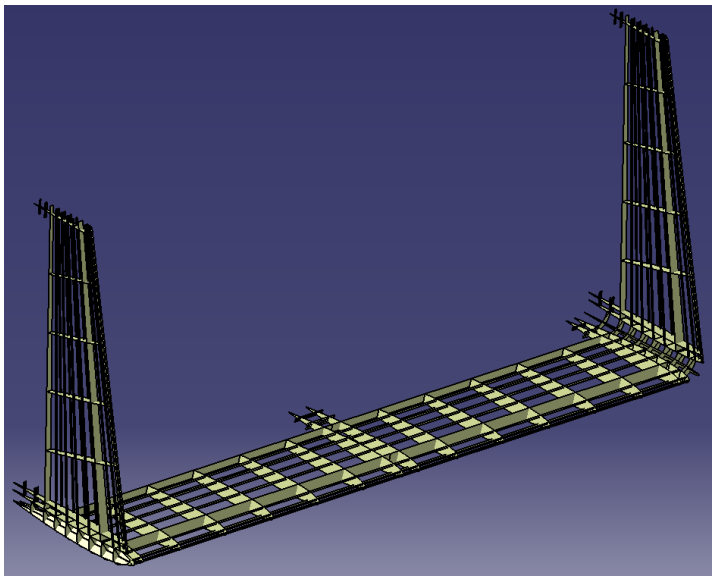

Figure 8.8: Catia render of the empennage structure

In terms of materials, for the same reasons mentioned in Subsection 7.4.6, aluminum 7075 and aluminum 5052 are selected spars and ribs respectively. The material for both vertical and horizontal stabilizers' inboard surfaces is Titanium grade 5, to protect the structure from hot emission gasses from the engine. The selected material for the rudders and elevators is Polyphenylene Sulfide (PPS). This is a carbon fiber composite with a thermoplastic resin and is already used in other aircraft such as Gulfstream G650. This choice is made for the sake of sustainability as thermoplastics are known to be more recyclable than composites with theromset resin such as epoxy [2]. Furthermore the outboard of the stabilizers' skin is made from the same carbon epoxy material mentioned in Subsection 7.4.6.

8.5. Sensitivity Analysis

In section 8.4, a few parameters were assumed. In the sensitivity analysis these input variables are given a slight change, in order to see how the corresponding output values change.

For the loading diagram, the c.g. location of the the hard point positions, the ammo position and the fuel location were changed, as these numbers were assumed. The Table 8.3 shows the sensitivity analysis given the changes.

The locations that were used as sensitivity analysis for the c.g. ranges show that the forward and aft c.g. increase or decrease accordingly with the change that was made for the input variables. For the top row, the initial values were used with a 2% margin. The values given in the other rows are shown without the 2% margin. The 2% margin was not given here, in order to see whether they fall within the given margin.

Table 8.3: sensitivity analysis of c.g. range

Initial values with 2 %margin				
$x_{cg_{payload,hardpoint}}$	$x_{cg_{ammo}}$	$x_{cg_{fuel}}$	**Forward c.g. [%MAC]**	**Aft [%MAC]**
7.121	7.976	7.713	0.293	0.370
changes in $x_{cg_{payload,hardpoints}}$			(on TE spar, TEMAC, LEMAC respectively) without 2% margin	
$x_{cg_{payload,hardpoint}}$	$x_{cg_{ammo}}$	$x_{cg_{fuel}}$	**Forward c.g. [%MAC]**	**Aft [%MAC]**
8.262	7.976	7.713	0.318	0.387
6.551	7.976	7.713	0.265	0.363
9.402	7.796	7.713	0.318	0.438
changes in $x_{cg_{ammo}}$			(on LE spar, TE spar, respectively) without 2% margin	
$x_{cg_{payload,hardpoint}}$	$x_{cg_{ammo}}$	$x_{cg_{fuel}}$	**Forward c.g. [%MAC]**	**Aft [%MAC]**
7.121	7.713	7.713	0.270	0.352
7.121	9.402	7.713	0.299	0.399
changes in $x_{cg_{fuel}}$			(on 30%, 50%, 35%, 45% of the local chord respectively) without 2% margin	
$x_{cg_{payload,hardpoint}}$	$x_{cg_{ammo}}$	$x_{cg_{fuel}}$	**Forward c.g. [%MAC]**	**Aft [%MAC]**
7.121	7.976	7.413	0.298	0.338
7.121	7.976	8.013	0.299	0.401
7.121	7.976	7.563	0.298	0.344
7.121	7.976	7.863	0.299	0.382

8.6. Verification and Validation

In this section, the verification and validation of the tools, used to determine the empennage sizing in section 8.4, is carried out. It also gives the integration of Class-I, Class-II, c.g. analysis and X-plot, as a consequence of the empennage sizing.

8.6.1. Verification and Validation of c.g. analysis

As verification for the weight components, all possible loading procedure was added. These were then checked whether, after adding all components, the c.g. location converge to the same point. An example of this convergence can be seen from Figure 8.4.

[2] https://insights.globalspec.com/article/12596/thermoplastic-composites-for-aerospace-applications, conducted on [15-01-2021]

Similarly, the contribution of the c.g. location were checked and whether they impact the loading diagram as expected. When increasing the weight of a component ahead of the $x_{cg_{oew}}$, the c.g. location of the combined load must shift forwards (to the LEMAC). When the weight of a component behind the $x_{cg_{oew}}$ was increased, it was observed that the c.g. location of the combined load was shifted aft.
Additionally, when moving the c.g. location of a component towards the LEMAC, the combined c.g. location shifted forwards. While moving the c.g. location of a component towards the trailing edge of the mean aerodynamic chord (TEMAC), the combined c.g. location shifted backwards.
These results showed that the weight components were adopted correctly into the calculations and shift the c.g. location accordingly with component c.g. location and weights.

Another aspect that was checked, was regarding the loading order as observed in the loading diagram. For commercial airlines, a typical loading procedure is adopted (window seating rule). However, for military aircraft there is no significant procedure to be taken into account. The hot-pit refueling also further emphasizes on having no strict loading order, as the aircraft has to re-arm and re-fuel simultaneously. This was taken into account for the loading diagram, by taking into account all loading procedures (the variety of loading procedures are observed in Figure 8.4. This then takes into account a wider array of c.g. margins.

Regarding the sensitivity analysis that was carried out, some values represented fall outside the c.g. range (with 2% margin). However, these values are justified to be never the case of the aircraft and do not pose any threats to the balance of the aircraft. First regarding the c.g. ranges outside for shifting the payload on the hard points. For the changes in $x_{cg_{payload,hardpoints}}$ it is highly unlikely that the c.g. locations are located in front of the LE spar or behind/at the TE spar. Moreover, as the payload on the hard points (for example bombs) must protrude the wing planform for a small section due to clearances, the initial assumption of the c.g. location to be placed on the front spar is taken as reasonable.

For the changes in $x_{cg_{ammo}}$ the ammo for the integrated gun is also unknown. However, given the fact that the guns themselves are placed behind the LEMAC, the ammo must be stored close to this location. Additionally, the ammo location is considered a design choice. Hence, it should be placed, such that it falls within the initially set c.g. range.
Despite this being a design choice, certain factors had not been considered for the integration of the entire design. For example, when adding the ammo at the pre-determined location, the fuel tanks inside the fuselage, the landing gear and the available cross-sectional area of the fuselage at this location should also be considered.
As future recommendation, these should be taken into account.

Lastly, it was assumed that the c.g. location of the fuel is placed 40% of the local chord (the location of this local chord in lateral direction was calculated using Equation 8.2). Given the upwards dihedral, the fuel is depleted from the tip to the root, which means the c.g. location of the fuel moves backwards (when looking at the wing planform). According to Table 8.3, a c.g. location shift forwards would still fall within the margin that was given, which is the opposite direction of what would be the case. However, considering that there is little sweep and the fuel tanks themselves are rectangular, the c.g. would not shift drastically, and thus not fall beyond the 45% of the local chord.

8.6.2. Integration of Class-I, Class-II, c.g. analysis and X-plot

As a final check, all procedures have been followed from the first class estimation, the second class estimation, the c.g. curve and finally, the X-plot. The methods used for first class estimation and second class estimation have already been checked in previous steps of this project and are assumed to be verified and validated. Adding the contribution of the current step, all steps were followed and seen if the components converge to a same point.

9
Propulsion Unit Design

As the aircraft enters service in 2025, this gives little time for engine manufacturers to build a new engine. Therefore, the chosen engine is based on an existing engine with modifications. This chapter explains the engine sizing method.

9.1. Design Overview

The two most realistic design options for the propulsion system were a turboprop and a turbofan. The turbofan was selected because of its smaller size. The turboprop engines had required very large diameter propellers (>3 m), which heavily impacts the placement of the engines and the aircraft ground performance. Having more freedom when it comes to the engine placement, allows to protect the engines better of enemy weapon fire. Furthermore, turbofan engines are capable of reaching a higher cruise speeds. As the required cruise speed of Mach 0.6 is on the edge of what is possible with turboprop engines, the turbofan was chosen. The propulsion system was designed with survivability in mind. The aircraft has two engines, so it is still able to fly in case one engine is hit, or fails. The engines are mounted between wing and tail, and high on the fuselage to avoid ingestion of dirt/debris on the austere field. The engines are covered by the wing (or tail) when looking at the airplane from the ground under an angle. This makes them harder to target than wing-mounted engines. Furthermore, the hot exhaust is partially covered by the horizontal tail plane, which reduces the susceptibility to heat-seeking missiles from the ground. To reduce the heat signature even more, a mixer was added, which mixes the hot gases from the engine core with the colder gases from the bypass flow. An added benefit of the mixer is a reduction in noise generation and an increase in efficiency, at the cost of extra weight.

9.2. Functional Analysis

The function of the propulsion system is to provide the required thrust in all flight phases. It should be reliable, and as economical as possible. Furthermore, the propulsion system shall adhere to the requirements shown in Table 9.1.

Table 9.1: List of requirements for the propulsion system

Requirement ID	Description	Type	Source
LAA-PER-DSM-4.2	The aircraft shall be able to take off over a 15.28 m (50 ft) obstacle within a distance of 1 219 m (4 000 ft) at most and at a density altitude up to 1 829 m (6 000 ft) on runways with California bearing ratio 5.	Key & Driving	User
LAA-PAP-POW-2.1	The engine shall meet all the requirements of the specification throughout the complete operating envelope without exceeding any limits.		JSSG-2007A [19]
LAA-TEC-RDY-1.1	Critical technologies shall be above NASA's technology readiness level (TRL) 8 in 2020.	Key & Driving	User
LAA-SUR-ENG-1.1	The aircraft shall be able to safely land with an engine failure.		JSSG-2010-7

9.3. Risk Analysis

The technical risks applicable to the propulsion design are shown in Table 9.2. RIS-049B was mitigated by adding a mixer to the exhaust, and the engine placement. Furthermore, by including two engines, the impact of the risk is reduced due to redundancy. RIS-050 was mitigated by the engine placement, and protection around the engine.

Table 9.2: Risks regarding engine design

ID	Label	Risk	Seq.	Cause	Prob.	Imp.
RIS-035: Aircraft cannot provide close-air support.						
RIS-049	T	The aircraft is too susceptible when flying low.	b	Heat signature of aircraft is too visible.	2	5
RIS-050	T	Aircraft is too vulnerable when flying low.	a	Protection is not sufficient for close attacks.	1	4
			b	Critical areas badly protected.	1	4

9.4. Design Approach

To determine the required thrust, one has to go back to the wing and thrust loading diagram discussed in chapter 7, shown in Figure 7.2. To construct the green line of the graph, the takeoff requirements had to be considered. LAA-PER-DSM-4.2 states that the aircraft shall be able to takeoff over an obstacle withing a distance of 4 000 ft. This is mostly impacted by the thrust and wing loading. The allowable wing loading already was determined in chapter 7, leaving only the thrust loading.

Equation 9.1 directly relates the takeoff distance s_{TO} to the allowable ground run s_{TOG}. The allowable ground run is shorter than the takeoff distance, since the takeoff distance also includes and air born phase up to the obstacle. For military aircraft, the relation between s_{TOG} and the Thrust-to-Weight ratio (TWR) is given by Equation 9.2, with ρ being the air density at takeoff altitude, $C_{\text{L}_{\text{max}_{\text{TO}}}}$ as the maximum lift coefficient in takeoff configuration, C_{D_0} being the zero lift drag coefficient, T being the thrust and μ_{G} as the friction coefficient of the ground.

$$s_{\text{TO}} = 1.66 \cdot s_{\text{TOG}} \tag{9.1}$$

$$s_{\text{TOG}} = \frac{k \cdot \left(\frac{W}{S}\right)_{\text{TO}}}{\rho \left(C_{L_{\text{max}_{\text{TO}}}} \cdot \left(k_2 \cdot \left(\frac{T}{W}\right)_{\text{TO}} - \mu_{\text{G}} \right) - 0.72 \cdot C_{\text{D}_0} \right)} \tag{9.2}$$

The factor k is given by Equation 9.3, where λ_{e} is the bypass ratio of the engine.

$$k = 0.75 \cdot \left(\frac{5 + \lambda_{\text{e}}}{4 + \lambda_{\text{e}}} \right) \tag{9.3}$$

The ground friction coefficient μ_{G} stems from the required California Bearing Ratio stated in LAA-PER-DSM-4.2. A value of 0.17 was chose, which corresponds to a soaked and very soft grass field [20].

To construct the red line of the wing and thrust loading diagram, the cruise performance had to be considered as well. The required TWR is determined by using Equation 9.4.

$$\frac{T_{\text{TO}}}{W_{\text{cruise}}} = \left(\frac{\rho_0}{\rho} \right)^{3/4} \left[\frac{C_{D_0} \frac{1}{2} \rho V^2}{\left(\frac{W_{\text{cruise}}}{S}\right)} + \left(\frac{W_{\text{cruise}}}{S} \right) \frac{1}{\pi A e \frac{1}{2} \rho V^2} \right] \tag{9.4}$$

As the cruise condition clearly is no the limiting factors when it comes to the thrust loading, it will not be further elaborated on.

The required thrust (T) of 44 kN was determined from the design point on the wing/thrust loading diagram, discussed in subsection 7.4.1, using Equation 9.5. As the aircraft features two engines, the required thrust per engine is 22 kN. The engines were sized, based on a reference engine with similar thrust, the HTF7000 by Honeywell. An initial "rubber sizing" was done by directly scaling the size and weight from the reference engine, by the reference engine thrust compared to the required thrust. The engine nacelle was sized according to the methods of Torenbeek [14]. The total length of the engine is 2.8 m, and the diameter is 0.89 m, including nacelle. The bypass ratio of 4.5 is the same as the reference engine.

$$T = \frac{W_{\text{TO}}}{T/W} \tag{9.5}$$

9.5. Requirements Compliance

To give an overview of whether the wing requirements are met, a compliance matrix is presented in Table 9.3.

Table 9.3: List of requirements for the propulsion system

Requirement ID	Description	Method of Compliance	Require met?
LAA-PER-DSM-4.2	The aircraft shall be able to take off over a 15.28 m (50 ft) obstacle within a distance of 1 219 m (4 000 ft) at most and at a density altitude up to 1 829 m (6 000 ft) on runways with California bearing ratio 5.	section 9.4	✓
LAA-PAP-POW-2.1	The engine shall meet all the requirements of the specification throughout the complete operating envelope without exceeding any limits.	section 9.4	✓
LAA-TEC-RDY-1.1	Critical technologies shall be above NASA's technology readiness level (TRL) 8 in 2020.	section 9.1	✓
LAA-SUR-ENG-1.1	The aircraft shall be able to safely land with an engine failure.	section 9.1	✓

10 Landing Gear Design

In this chapter first a brief description of the obtained design is given, after which the functions, requirements and risks are discussed which were taken into account during the design. Afterwards, the design approach is discussed. This section aims to give the reader insight on the steps taken to achieve the obtained design. Finally the sensitivity analysis and verification and validation are discussed to conclude this chapter.

10.1. Design Overview

To size the landing gear, there are three major components to be considered; location, struts length and tire dimension. The nose landing gear was set to be 3.5m in front of the c.g. and the main landing gear to be 0.45 m behind the c.g.. Furthermore, the track of the main landing gear was set to be 4.2 m, which is the distance between the two main landing gear. Moreover, the strut length for nose and main landing gear were set to be 2.2 m and 2.1 m. The calculations used for the values above were to maintain static stability on ground and to ensure the aircraft fulfills the certification requirements. Lastly, the tire dimension was determined by the contact loads and runway surface. The nose landing gear is fitted with two 6.00-6 tires. The main landing gears are both in double-bogie configuration, with four 8.50-10 tires per strut.

10.2. Functional Analysis

In this section the functional analysis and the requirements are given for the landing gear.

The landing gear must foremost provide means for the aircraft to land on. Also, it should allow for a landing on unprepared runways with a California Bearing Ratio (CBR) of 5. Furthermore, during flight it should be stored such that the drag is minimized. Apart from that, it should provide stability when landing and maneuvering on the ground, i.e. the aircraft should not tip over. Additionally, the aircraft must be able to maneuver, while on the ground. Lastly, the landing gear must be easily maintainable, so common defects can be repaired quickly.

From the functions, several requirements were determined, which are given in Table 10.1. In this table the requirement ID and its description is given.

Table 10.1: List of requirements for landing gear

Requirement ID	Description	Function source
Landing gear		
LAA-PER-DSM-4.1	The aircraft shall be able to land over a 15.3 m (50 ft) obstacle within a distance of 1219 m (4 000 ft) at most and at a density altitude up to 1828.80 m (6 000 ft) on runways with California bearing ratio 5.	User
LAA-PER-DSM-4.2	The aircraft shall be able to take off over a 15.3 m (50 ft) obstacle within a distance of 1219 m (4 000 ft) atmost and at a density altitude up to 1829 m (6 000 ft) on runways with California bearing ratio 5.	User
LAA-STR-LDG-1.1	Landing gears shall permit rapid replacement of main wheels, tail wheels, or nose wheels.	Functional analysis
LAA-STR-LDG-2.1	The aircraft front landing gear shall be able to steer on the ground.	Functional analysis

10.3. Risk Analysis

Previously determined technical risks depending on the landing gear can be found in Table 10.2. Due to the scrape angle requirement, explained in the section below, the aircraft is rather high. Therefore it can not be stated that the risk is mitigated. It is recommended to do a more elaborate investigation and trade-off, in future design stages, towards a solution for this risk.

Table 10.2: Specified risks for the landing gear

ID	Label	Risk	Seq.	Cause	Prob.	Imp.
RIS-036: Aircraft cannot be maintained (properly).						
RIS-055	T	Aircraft is not easy to access for maintenance.	a	Landing gear is too high.	1	4

10.4. Design Approach

First, the configuration of the landing gear was determined. It was decided to use a conventional tricycle configuration with a steerable nose landing gear. This allows to steer on the ground, while giving a high ground clearance and an advantageous load distribution. It was decided to make the landing gear retractable, which drastically reduces drag in flight. The nose landing gear is stored in the fuselage under the cockpit, while the main landing gear is stored in fairings under the wing. All gear legs fold forward, so that in case of a hydraulics failure, they can be released so gravity and the air stream lock the landing gear in place.

Afterwards, the longitudinal position of the main landing gear was determined. For that, the line going through the most aft c.g. and the point of ground contact of the main landing gear, has to be at an angle of less than 15°, as shown in Figure 10.1a. If the landing gear is too far aft, it becomes difficult to rotate around the pitch axis during takeoff. If is is too far to the front, the aircraft can tip over onto its tail. Additionally, the tail strike angle has to be considered as well, so that the tail does not strike the ground when flying at a high angle of attack or when performing a cross wind landing with a bank angle. Just before the landing, the aircraft flies at an angle of attack of 13°. Furthermore, a bank angle of 8° was accounted for, as it brings the horizontal tail closer to the ground. These angles together lead to a required tail strike angle of 20°. Considering all aforementioned points, a ground clearance of 1.5 m, with respect to the bottom of the fuselage, and a distance of 0.5 m between main landing gear and aft c.g. were chosen. After that, the wheel base, or spacing between the gear legs of the main landing gear, was determined. This is done to make sure, that the aircraft does not tip over laterally, when maneuvering on the ground. The wheel base was determined using Figure 10.1b. It was determined to be 4.2 m wide.

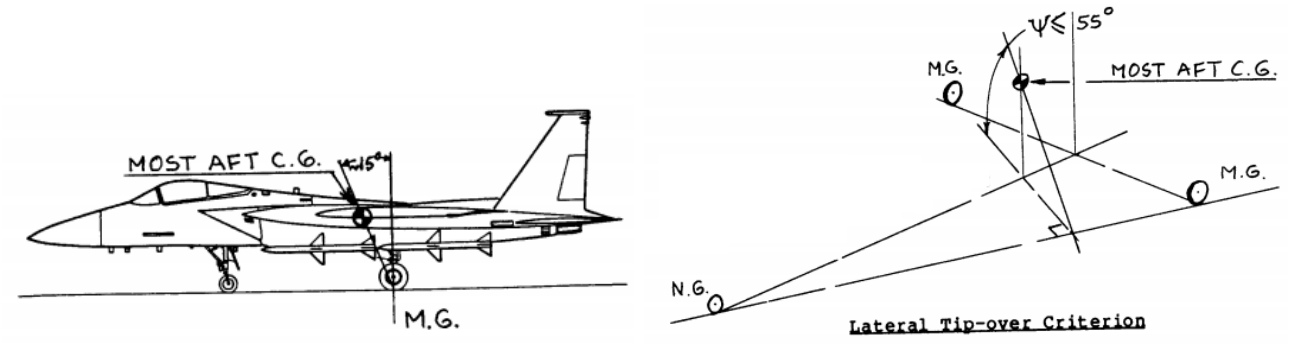

(a) Estimation of the longitudinal position of the main landing gear

(b) Landing gear positioning using the tip-over criterion

Figure 10.1: Landing gear positioning [21]

Once the position of the main landing gear was determined, the load per gear strut was calculated by using Equation 10.1 and Equation 10.2 [21]. The distance of the nose landing gear with respect to the aft c.g., l_n has to be chosen such that the nose landing gear carries at least 8% of the aircraft weight, to assure

controllability. Considering this, an l_n of 3.5 m was chosen.

$$P_n = \frac{W_{TO} \cdot l_m}{n_{s_n} \cdot (l_m + l_n)} \tag{10.1}$$

$$P_m = \frac{W_{TO} \cdot l_n}{n_{s_m} \cdot (l_m + l_n)} \tag{10.2}$$

Next, requirements LAA-PER-DSM-4.1 and LAA-PER-DSM-4.2 were analyzed with regards to the CBR of 5. The CBR is a measure to define how much force is needed to push a defined test objective 2.5 mm into the ground while controlling the rate. This values is compared to the standard of crushed rock (13.44 kN). The ratio is given as a number in percent. A CBR of 5 means, that 670 N is needed to push a cylinder, with a diameter of 50 mm, 2.5 mm into the ground, which is extremely low when considering the mass of an aircraft. Based on that, the maximum allowable tire pressure onto the ground p was determined using Equation 10.3, with p_s being the reference value for crushed rock. This yields an allowable pressure of 3.5 kg/cm^2. The tire pressure should be equal or smaller than p to not sink into the soil.

$$CBR = \frac{p}{p_s} \cdot 100\% \tag{10.3}$$

Using the maximum tire pressure, the load per gear leg, and Figure 10.2, the amount of tires can be selected. The amount of wheels has to be chosen, such that the intersection of static load per tire and inflation pressure lie on the line of an existing tire.

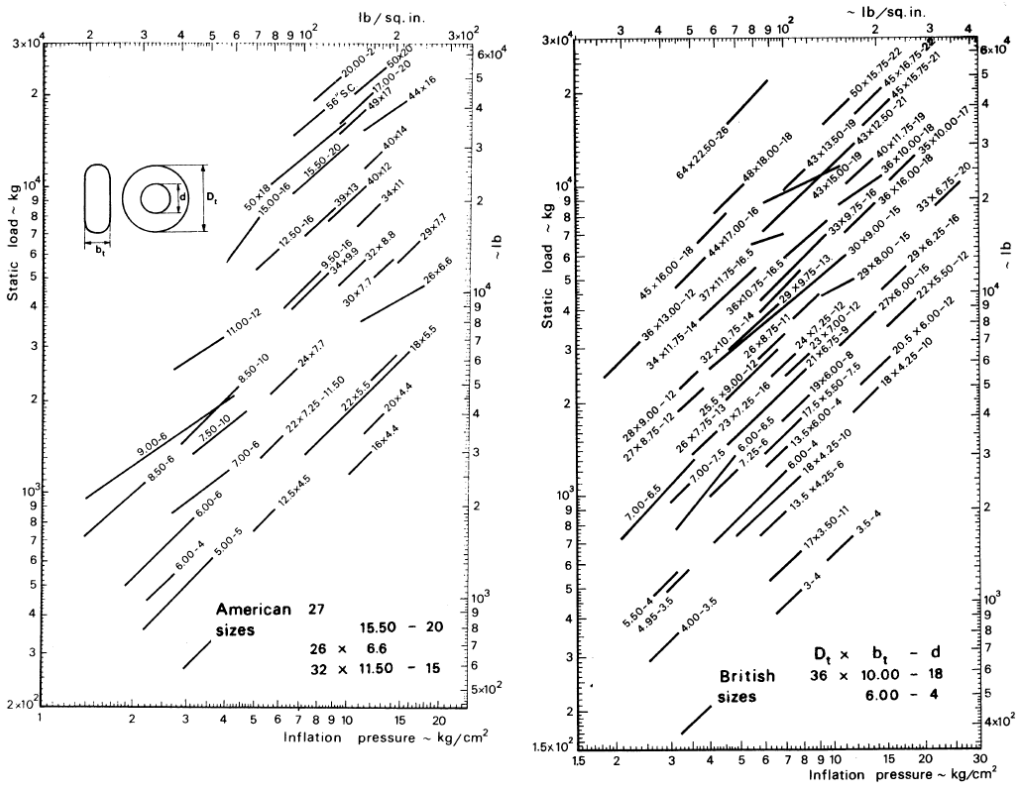

Figure 10.2: Tire dimension graph from Torenbeek [14]

The choice of the amount of wheels was done by a trade off. More wheels mean a more complex and bulkier landing gear assembly, less wheels result in larger individual tires. As a result, two 6.00-6 tires have been chose for the nose landing gear. Four 8.50-10 tires have been chosen for each main landing gear leg.

10.5. Sensitivity Analysis

To see the impact for a different amount of wheels, a sensitivity analysis was made. The results can be found in Table 10.3. At first, the amount of nose wheels was reduced to one, while keeping the amount of main wheels constant. After that, the amount of nose wheels was set to its original number of two and the amount of main wheels was halved to four. The tire size changes due to varying amounts of wheels, then

was compared to the initial sizes. It showed that the size of the tires increased by about 25-50% when the amount of tires were halved.

Since the tires already were very big and the landing gear assemblies were very bulky, the amount of wheels was kept unchanged.

Table 10.3: Sensitivity analysis of landing gear tire size. For better size comparison, the tire sizes dimensions were converted to meters.

Initial tire size			
# Nose wheels	Tire size nose wheels: outer tire diameter [m] X tire width [m]	# Main wheels	Tire size main wheels: outer tire diameter [m] X tire width [m]
2	0.45 X 0.15	8	0.65 X 0.25
Reducing number of nose wheels			
# Nose wheels	Tire size nose wheels	# Main wheels	Tire size main wheels
1	0.65 X 0.25	8	0.65 X 0.25
Reducing number of main wheels			
# Nose wheels	Tire size nose wheels	# Main wheels	Tire size main wheels
2	0.45 X 0.15	4	0.82 X 0.31

10.6. Requirements Compliance

In this section the evaluation of the chosen design is given using a compliance matrix, presented in Table 10.4. Requirements that have been fulfilled, are marked with a check mark.

Since no brakes have been designed and the landing length was addressed by choosing a corresponding approach speed, the only part of LAA-PER-DSM-4.1 and LAA-PER-DSM-4.2 that concerns the landing gear, is the CBR requirement. The CBR requirement has been addressed by choosing the right amount and size of the tires. LAA-STR-LDG-1.1 was satisfied by choosing commercial off-the-shelf wheels, that are non permanently mounted to the landing gear. A wheel can easily removed and replaced. LAA-STR-LDG-2.1 was addressed by choosing a conventional tricycle configuration with a steerable nose landing gear.

Table 10.4: Compliance matrix for the landing gear

Requirement ID	**Description**	**Method of compliance**	**Requirement met?**
Landing gear			
LAA-PER-DSM-4.1	The aircraft shall be able to land over a 15.28 m (50 ft)obstacle within a distance of 1 219.2 m (4 000 ft) at most and at a density altitude up to 1 829 m (6 000 ft) on runways with California bearing ratio 5.	Maximum pressure of 3.5 kg/cm^2, section 10.4	✓
LAA-PER-DSM-4.2	The aircraft shall be able to take off over a 15.28 m (50 ft) obstacle within a distance of 1 219.2 m (4 000 ft) at most and at a density altitude up to 1 828.80 m (6 000 ft) on runways with California bearing ratio 5.	Maximum pressure of 3.5 kg/cm^2, section 10.4	✓
LAA-STR-LDG-1.1	Landing gears shall permit rapid replacement of main wheels, tail wheels, or nose wheels.	Off-the-shelf, removable wheels	✓
LAA-STR-LDG-2.1	The aircraft front landing gear shall be able to steer on the ground.	Steerable nose landing gear	✓

11 Additional Subsystems

Now that the aircraft has been scaled and all geometric values are known, the subsystems can be designed. Although most of these subsystems are generally not visible when looking at an aircraft, they should still be included and thought off. In this chapter the fuel system, hydraulic system, electrical system, environmental control system, data handling system and the telecommunication system is discussed. First the design of the systems is discussed after which function, requirement and risk analyses are discussed. The chapter is finalized with a design approach and an verification and validation of this approach and the designs.

11.1. Design Overview

In this section the design overview of each additional subsystem will be given. Every subsystem discusses a different system and the resulting design.

11.1.1. Fuel System

The fuel system configuration was mainly determined by the location of the fuel and the location of the engines. The fuel was considered to be located in the wings and fuselage, while the engines are located above the wings and are mounted on the fuselage, as could be seen in the three-view drawing in section 4.3.

It was chosen to have a fuel pump system in order to ensure a constant fuel flow to the engines and APU. In Figure 11.1 a schematic of the fuel system is given, do note that this is a simplified schematic to give a general overview of the system.

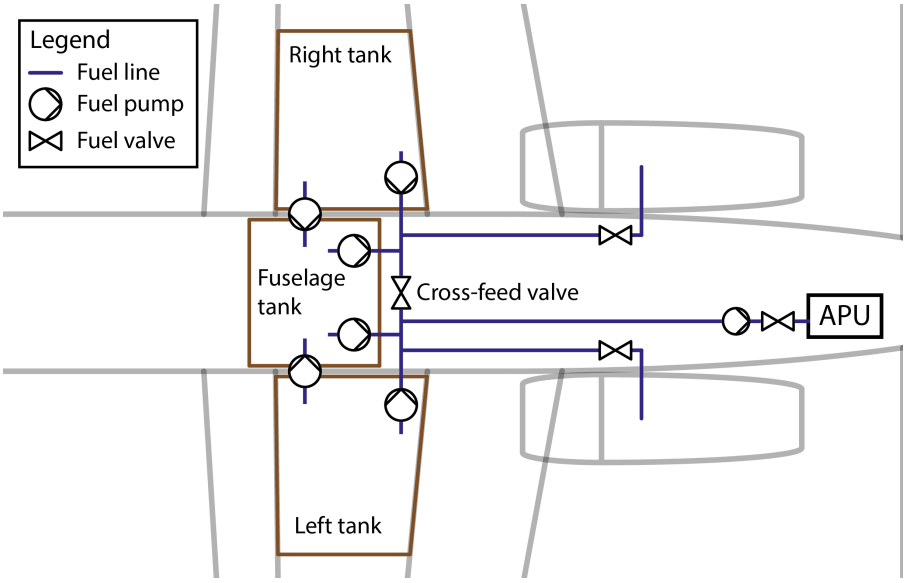

Figure 11.1: Simplified schematic of the fuel system

11.1.2. Hydraulic System

The hydraulic system is used to actuate several aircraft components. For this aircraft, the hydraulic system is designed to actuate control surfaces, landing gears, braking and steering. An Electric-Hydrostatic Actuation (EHA) system was chosen as the hydraulics system, which consist of multiple, self-contained hydraulic systems at the actuation points and is controlled by an EHA-processor (EHA-CPU). In Figure 11.2 an overview of the electric-hydraulic system can be found, the electric system will be further elaborated in the next section.

11.1.3. Electrical System

The electrical system provides electricity throughout the aircraft. The hydraulic system is also dependent on the electrical system, so redundancy is key. To ensure redundancy, two separate system have been implemented into the aircraft. Each system consists of a power delivery system (PD), a battery and the flight control computer (FCC), connected to this is the EHA processor (EHA-CPU) for the hydraulic actuation. The cockpit power is distributed in the cockpit-distributor (CD). For power generation two starter-generators (S/G) are implemented on the engines. For auxiliary power, an auxiliary power unit (APU) is fitted at the rear of the aircraft. The starter-generators are connected to each PD, the FCCs can be powered by both PDs. An overview of the electric-hydraulic system can be found in Figure 11.2, the redundant electrical lines are indicated as dotted lines.

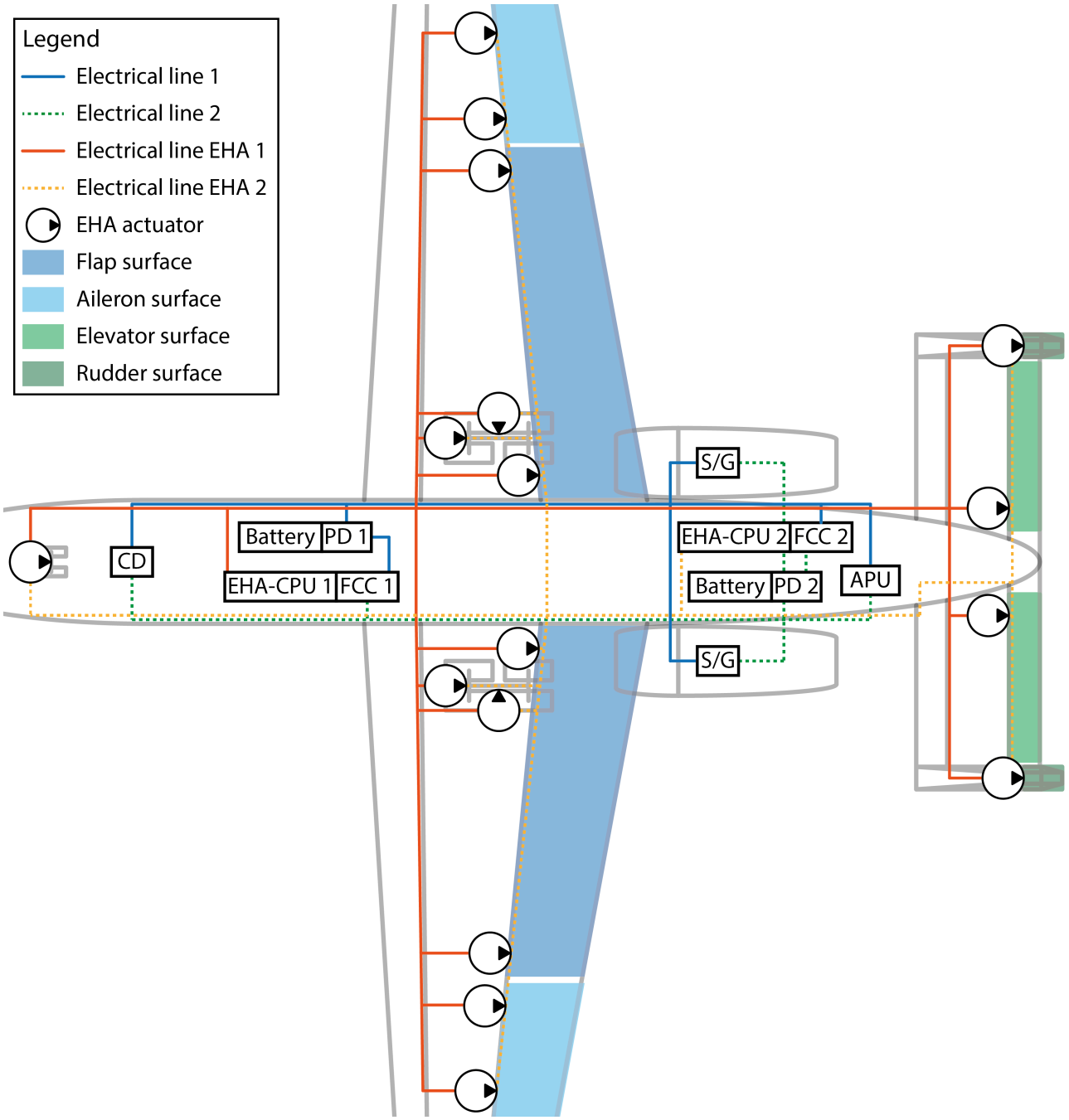

Figure 11.2: Schematic of the electric-hydraulic system

11.1.4. Environmental Control System

The overall function of the environmental control system (ECS) is to provide pressurization and thermal control of the cabin for the crew.

Even though the cabin is pressurized, the crew will still be equipped with an oxygen mask. The reason for this is that it can supply pressured air during high load maneuvers, giving a higher g tolerance [22]. Furthermore, it can supply the crew with oxygen in case of emergency, like a pressure drop in the cockpit, an internal fire, or when operating in hazardous environments (exposure to chemical, biological, radiological or nuclear hazards). The masks also contain microphones for enhanced communication.

For the thermal control system it was found that it is desired to keep the cockpit temperature below 28 °C [23]. The ECS system works collaboratively with a pneumatic system known as Engine Based Air System (EBAS), which uses bleed air from the engine. In addition to that, the cabin is also equipped with pressure valves to regulate the interior pressure by entering high pressure bleed air [24].

11.1.5. Data handling system and avionics

The data handling and avionics system consists of sensors, data processors, actuators and distributors. The chosen system architecture for this aircraft is a federated architecture. In this type of system, the hardware of the control system is distributed over the locations of application, while the software is centralized. It should also be mentioned that even though in Figure 11.2 there is more than one computer for data handling and control, there is still a central software for data processing. These computers work in parallel for the sake of redundancy. A federated structure is not the lightest architecture, but it is still lighter than a system in which both hardware and software are centralized. In comparison to other configurations, this control system is also known to be cheaper and easier to maintain because it is easier to reach the localized hardware [25].

It was decided to fit the A-20 with a fly-by-wire system. This was done to allow for an augmentation of the flight behaviors. This comes in handy in case control surfaces are hit, because the system can compensate by using the other control surfaces. This increases redundancy and reduces pilot work load in case of a damage. Furthermore, it allows to use control surfaces without trim tab, as the control surfaces can be adjusted accordingly, without that the pilot has to handle the load. Lastly, it allows for the use of PID controllers, as discussed in section 13.7.

Due to the technological advancements of the past years, data became more important than ever before. This shift also occurred in the designing of attack aircraft. It has even evolved so much that a fighter jet pilot's main job is not flying the plane, but employing it according to test pilot Randy "Laz" Gordon [1]. However, as the RFP for this project is to design an *best-value* aircraft for asymmetrical-warfare a trade-off should be done on which subsystem is required for the aircraft. In some cases, the extra performance is worth the cost, sometimes it is not.

From the mission and threat analysis performed in chapter 2, it is clear that the designed aircraft will mainly fight in asymmetrical warfare scenarios. Hence, enemy attack aircraft, advanced anti-aircraft systems and high-end radar systems were not considered to be a threat. However, from interviews with Richard Helsdingen, former F-16 pilot of the Royal Netherlands Air Force, it became clear that a pilot feeling safe in the aircraft is a big contributing factor as well. However, also to this point there are multiple sides as stated by Pascal Smaal, a current F-35 pilot of the Royal Netherlands Air Force. The feeling of safety can come from two aspects; either being stealthy enough to not be noticed (like an F-35) or to be robust enough to keep flying while being shot (like an A-10). This feeling of safety was taken into account during the trade-off of the several subsystems chosen in this chapter.

In Figure 11.3 a high-level data-handling block diagram is shown, the main structure and interaction of the diagram is based on the F-35's sensor fusion [26]. The F-35 was chosen as a reference for the possibilities of data handling, as it is currently using one of the most advanced sensor integration systems on the market. Below the individual components are discussed.

- **Satellite**: Satellites are used for multiple purposes. They often are used for surveillance and reconnaissance as well as data transfer. Surveillance and reconnaissance can be split into two main types: imaging systems and electronic reconnaissance systems. During imaging reconnaissance, images of areas, landscapes, building, troops, etc. are taken by using optical or radar systems. During electronic reconnaissance, communication is intercepted and analyzed to gather information. Further-

[1] Guest lecture at MIT https://www.youtube.com/watch?v=Evhrk5tY-Yo, conducted on [04-01-2021]

more, these are shared within the data platform and can give a good overview (e.g. over enemy troop strength, location and movement).

- **Ground based assets**: Ground based assets consist of ground troops, ground vehicles and ground based radars. They process and generate data, such as target location and target profile. Those assets then communicate with the aircraft via radio or satellite link.
- **Other aircraft**: Other military aircraft process and generate data, such as target location, target profile and weapons available. This enables target sharing and weapons coordination. Furthermore, this is typically communicated via radio frequency or satellite link.
- **General sensor suite**: A number of 'general' sensors have to be used in the aircraft and will be discussed briefly in this overview. A discussion on which type/ model of the sensor will be used is omitted, as this is perceived to be out of the scope of the report. The sensors discussed will be a pitot tube, pressure sensors, flow sensors,thermometers and accelerometers. A pitot tube is a device that measures the stagnation and statics pressure to calculate the fluid flow velocity by utilizing Bernoulli's equation [2]. Pressure sensors can be for a lot of different purposes from measuring the air pressure outside of the aircraft to measuring the pressure inside of the hydraulics system. Flow sensors will mainly be used in the fuel system, where it gives the pilot an indication on the amount of fuel it uses during flight. Thermometers exist in a lot of shapes and sizes, hence they can be used for a lot of different measurements on the aircraft. A couple of these applications are: fuel temperature, engine in- / outlet temperatures and cockpit temperatures. To determine the position/attitude of the aircraft accelerometers are used, to support the GPS system. Furthermore, they are used to determine the loads the aircraft and crew are experiencing, which allows to limit the maneuvers to the maximum allowed value.
- **Altimeter**: An altimeter is a device used to measure or calculate the altitude of an object above a fixed level. This can be accomplished via pressure measurement, laser, radar and GPS [3]. However, the most common type of altimeter being used in aviation is the barometric altimeter.
- **FQIS/ FCMS**: Fuel quantity indication systems (FQIS) and fuel control and monitoring systems (FCMS) are almost identical systems, measuring the amount of fuel aboard of the aircraft. However the FCMS is a bit more advanced as it also controls the amount of fuel in different tanks. As stated in the previous subsection, a pumped system is used i.e. a FCMS.
- **CVR**: The Cockpit Voice Recorder (CVR), is a device which logs the conversation between the pilots on to the flight recorder. However, the FAA has no jurisdiction over military aircraft and therefore it is not required for military aircraft to adhere to the FAA rules of having a flight recorder[4]. Nonetheless, it was chosen to include a CVR for both data storage in case of a crash and training purposes.
- **Stick input**: The stick input was induced by the pilot via a side stick, in which the side stick sensor measure the deflection of the stick and pass the signal to the flight system processor.
- **Throttle setting**: For the throttle setting it was chosen to use conventional thrust levers. As the aircraft has two engines two levers will be included allowing for differential thrust.
- **GPWS**: Ground Proximity Warning System (GPWS) is a system which alerts the pilot when the aircraft flies too close to the ground or an obstacle in front of the aircraft[5]. Since the A-20 is a ground attack aircraft, a GPWS obviously is necesarry.
- **Radar**: Radar utilizes radio frequency to measure the distance, angle and velocity of objects. It is mainly used to detect things such as other aircraft, weather and terrain. A typical radar system consists of a transmitter, receiver and processor. As the A-20 is not designed for air-to-air combat, the radar does not have to provide tracking/locking capabilities, which simplifies the radar system. The

[2] https://www.grc.nasa.gov/www/k-12/VirtualAero/BottleRocket/airplane/pitot.html, conducted on 04-01-2021
[3] https://www.uavnavigation.com/support/kb/general/general-system-info/introduction-altimeters, conducted on 04-01-2021
[4] https://www.faa.gov/about/mission/activities/, conducted on 04-01-2021
[5] https://unitingaviation.com/news/safety/ground-proximity-warning-systems/, conducted on 04-01-2021

final radar system chosen/designed shall be in line with the MIL-STD-469B [27], which gives a thorough description of the requirements on military radar systems.

- **GPS**: The Global Positioning System (GPS), is a location technology that utilizes the run time of signals and trigonometry to identify the user's location at any time. Depending on the amount of connected satellites and the feasible amount of post processing, the position can be measured in the millimeter range. A GPS systems has to be included to effortlessly determine the position of the aircraft and to navigate to the mission area and/or target. Furthermore, the aircraft needs an interface to send GPS locations to the payload, as bombs like the JDAM or cruise missiles like the JASSM need a GPS coordinate of their target.
- **MAW**: Missile Approach Warning (MAW) systems can notify the crew of launched and approaching missiles. To do that, they either can use a Doppler radar system, or detect invisible light, like infrared or ultraviolet, emitted from the missiles. The radar systems can precisely determine the direction and speed of incoming missiles. However, they require complex and heavy on board systems. Infrared systems can detect the heat of the missile motor, even after it burned out. Depending on the speed of the missile, they can also detect the friction heat of the missile it self. The downside is, that they can easily be irritated by the sun or other hot objects on the ground. Furthermore, infrared systems are very sensitive to weather conditions, as water strongly absorbs infrared light. Ultraviolet MAW systems can not be irritated by the sun or ground objects, as they are 'sun-blind', i.e. they ignore the spectrum stemming from the sun. They use the UV light that comes from the hot exhaust of the missile motor. The downside is, that they cannot detect a missile after the motor has burned out. Considering that the A-20 will fly the majority of its missions close to the ground and that MANPADs are the only threat when it comes to missiles, long range missiles with long coast phases can be neglected. Thus, I can be assumed that the motor of the missile is burning for the majority of the (very short) flight, which alleviates the major drawback of UV MAW systems. Thus, a sun-blind UV MAW system will be fitted to the A-20.
- **Camera**: Cameras on the aircraft can be used for multiple reasons. One reason to include the cameras is to reach the set requirement of the pilots' visibility (30 degree down and forward looking, 70 degrees down and sideways looking), which could not be reached with the cockpit design. Hence, multiple fixed cameras will be included to increase the pilots field of view, giving them the ability to 'see through the aircraft'. Cameras can also be used for reconnaissance missions. They can provide intelligence on enemy forces and the terrain, which allows for a mapping of entire regions. As the A-20 also shall perform reconnaissance missions, it was fitted with a gimballed camera system with high power optics. It also can be used to acquire targets. The system is placed in the nose of the aircraft, under the cockpit. It sits in a fuselage cutout, covered by glass, similar to the camera system of the F-35. This way it has an unobstructed view, while being protected and creating less drag.
- **FLIR**: Forward-looking infrared (FLIR), is a technique which uses infrared radiation, to create either images or video. This allows the user to find heat signatures in their surroundings[6]. This type of imagery can be used when operating under low visibility conditions or when trying to identify targets. From the interview with Pascal Smaal (F-35 pilot), it became apparent that many of the aircraft's missions will typically be executed during night time. Hence, a FLIR system is a necessity, as it is vital to perform missions. Again, the system also can be used for reconnaissance missions, allowing for the mapping of terrain at night, or the identification of enemy units. The FLIR system is housed in the same gimbal mechanism as the optical camera.
- **LiDAR**: Light Detection And Ranging (LiDAR) is a comparable technology to radar, however instead of radio waves it uses laser pulses to measure the distance of objects. LiDAR is mainly used for 3D imaging of surfaces, which is useful during a reconnaissance mission. Thus, a LiDAR system is included as well.
- **Data fusion processor**: The data fusion processor is an on-board computer which receives both data from the aircraft and data from outside the aircraft. After combining this data, the processor shares it

[6] https://www.sciencedirect.com/topics/engineering/forward-looking-infrared, conducted on 04-01-2021

with the system processor.[26]

- **Aircraft system processor**: The aircraft system processor is the on-board computer which stores and presents the data. It also receives the data the pilot puts in and communicates this with the previously discussed system [26]. It also filter the combined data from the fusion processor. This fusion and filtering of data is essential, because it provides the crew with a full overview, increasing situational awareness, while not overwhelming them with a large amount of data.
- **Data storage**: The data from the previously discussed sensors might be a very valuable asset during warfare. Therefore, the data stream coming from the sensor needs to be captured. As a sensor can not be halted, the data recorder needs to handle the continuous throughput of data coming from the sensors. Modern architectures either use gigabit or 10 gigabit Ethernet [7]. It was chosen to use an internal 10 gigabit network, to have more room for future updates. Assuming a full utilization during the entire mission, this leads to a potentially needed storage space of 27 TB for a 6 hour mission.
- **User interface**: The data gathered of course has to be visualized for the pilot. Modern day advancements allow for a glass cockpit[8]. However, digital instruments in the cockpit are not the only way of giving the pilot the data that is needed. The aircraft could feature a Head-Up Display (HUD), giving the pilot all the important information needed while flying the aircraft. Lockheed Martin and others took it a step further and placed it in the visor of the helmet. They also included some other functionalities, like 'looking through the aircraft' and seeing the surroundings. Although the helmet is much more expensive than a normal HUD, from the interview with Pascal Smaal (F-35 pilot) it became apparent that for CAS missions, the helmet is worth it, considering the enhanced situational awareness. Hence, it was chosen to feature a modern helmet instead of an HUD.
- **Flight system processor**: The flight system processor is an on-board computer which is dedicated to the flight performance of the aircraft.
- **Pilot**: The pilot is the nerve center of the aircraft. The purpose of all the processor and sensors mentioned above are to assist the decision making process of the pilot. Furthermore, once an input has been induced by the pilot the aircraft will adjust the aerodynamic characteristic or weapons deployment accordingly.

11.1.6. Telecommunication

The following sections describe the telecommunication systems of the A-20 Chimera.

Air to ground telecommunication

This covers communicating with the ground troops as well as operation leaders and air traffic controllers. One of the used data links is TADIL-A/Link 11 which is a NATO standard. It is an encrypted link used to communicate real time radar data. Another utilized band is Link 16. It is used for near-real time transferring of encrypted texts, pictures and voice, which is a necessity for a modern fusioning of data as described in subsection 11.1.5.

Air to air telecommunication

To be able to communicate with other aircraft, the A-20 also is equipped with a transmitter and receiver for the L-band. It's one of the standard bands used in aviation. In case encrypted communication is required, link 16 can be used again.

[7] https://www.curtisswrightds.com/applications/aerospace/data-recording-storage/, conducted on 04-01-2020
[8] https://www.nasa.gov/centers/langley/news/factsheets/Glasscockpit.html, conducted on 04-01-2021

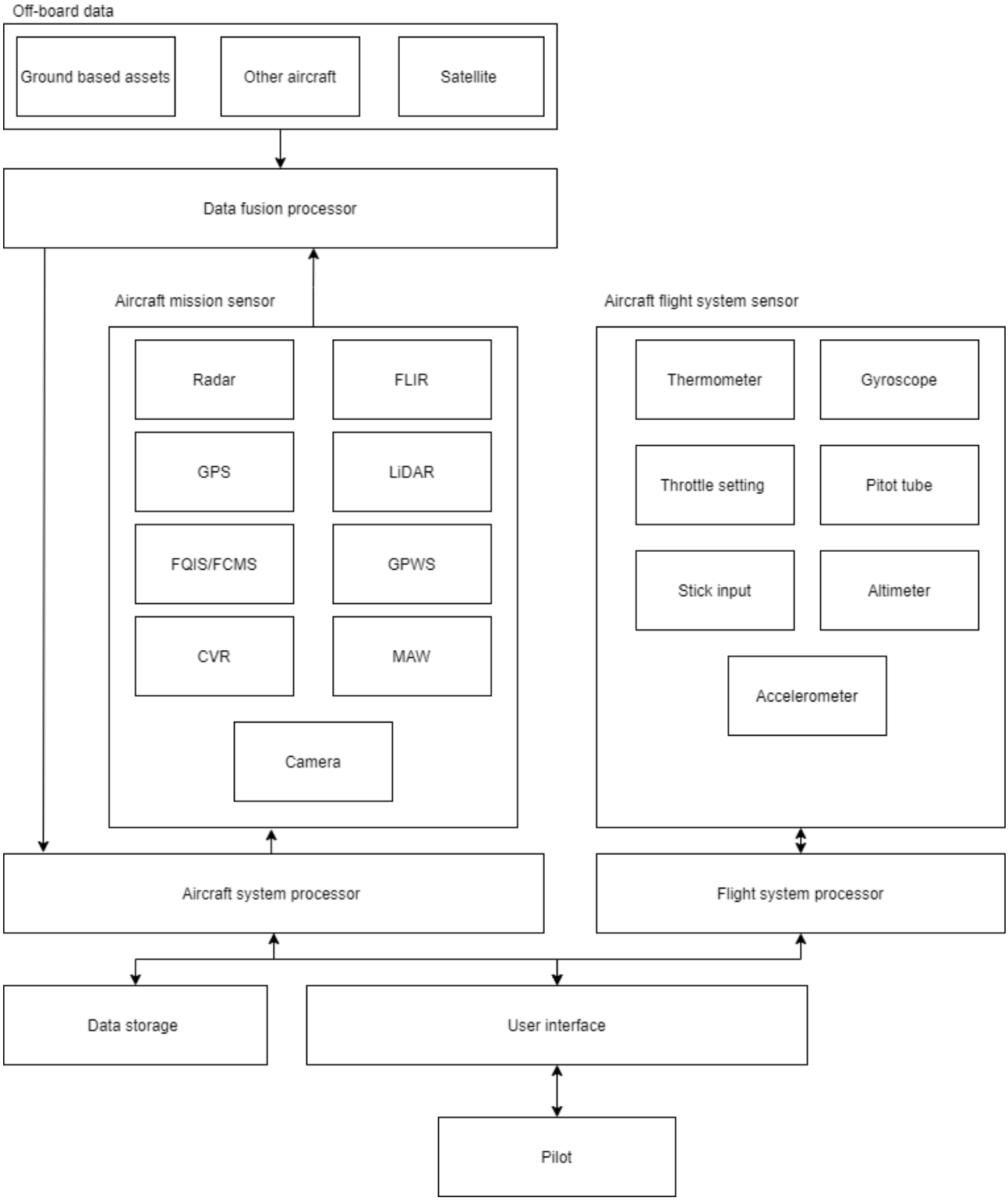

Figure 11.3: Data handling diagram

11.2. Functional Analysis

In this section the functional analysis and the requirements are given for each subsystem. In Figure 11.4,Figure 11.5 and Figure 11.6 the functions of each subsystem are given in a diagram, from these the requirements of these subsystem are determined and presented in Table 11.1.

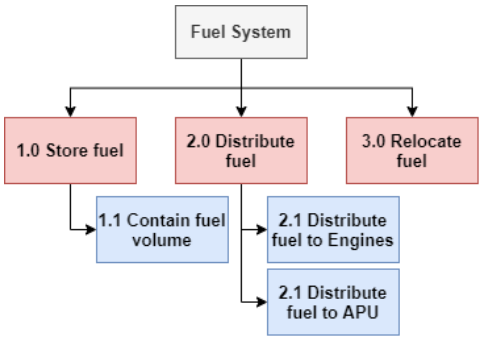

Figure 11.4: Function diagram of the fuel system

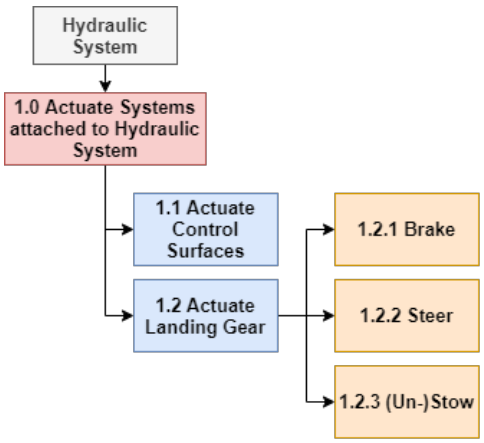

Figure 11.5: Function diagram of the hydraulic system

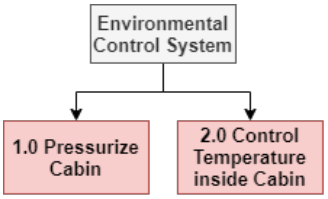

Figure 11.6: Function diagram of the environmental control system

From the functions, several requirements can be determined, which are given in Table 11.1. In this table the requirement ID and its description is given, as well as which function it comes from.

Table 11.1: List of requirements for the additional subsystems

Requirement ID	Description	Function source
Fuel System		
LAA-PER-DSM-2.1	The aircraft shall be able to loiter 4 hours on station without dropping the armament.	User
LAA-PER-DSM-3.1	The aircraft shall have reserve fuel sufficient for climb to 914.40 m (3,000 ft) and loiter for 45 minutes after the design mission completion.	User
LAA-PAP-POW-3.1	Upon receiving a signal from the air vehicle for stopping, the engine shall terminate fuel flow in any operating condition.	Functional analysis
LAA-PAP-FUE-1.1	The aircraft shall be able to move the center of gravity in order to stabilize itself.	Functional analysis
Hydraulic System		
LAA-SUR-HYD-1.1	In the event of a hydraulic failure, the aircraft shall be able to land safely while protecting aircraft occupants without causing lethal injuries.	Functional analysis
Electrical System		
LAA-PAP-POW-1.1	The aircraft shall have a power unit to provide enough energy to power the onboard systems.	Functional analysis
LAA-SUR-POW-1.1	The aircraft shall contain an emergency power source.	Functional analysis
Environmental Control System		
LAA-SUR-CAB-1.1	The aircraft shall have a cabin pressure ranging from 410 to 670 mmHg	Functional analysis
LAA-SUR-CAB-1.2	The aircraft shall have a cabin temperature of a maximum of 28 °C	Functional analysis

11.3. Risk Analysis

The risk that are specific to the additional subsystems can be found in Table 11.2. During the design process steps were taken to mitigate these risks. For RIS-042 redundancy in the subsystems was considered, as explained in section 11.1. This redundancy added more components to the design, however as they are

added for redundancy the components are not unnecessary. Therefore, it was considered that RIS-053.b is mitigated. RIS-055.c was not considered during designing yet, it therefore is recommended that during preliminary design a thorough research towards the maintenance hatches is performed.

Table 11.2: Specified risks for the fuel, hydraulic, electrical and environmental control systems

ID	Label	Risk	Seq.	Cause	Prob.	Imp.
RIS-021: Aircraft does not reach the required service life hours.						
RIS-042	T	Aircraft does not survive attack of foe.	b	Aircraft is not well protected against defined threats.	1	5
RIS-036: Aircraft cannot be maintained (properly).						
RIS-053	T	Systems are too complex to maintain.	b	System has an unnecessary high amount of components.	2	3
RIS-055	T	Aircraft is not easy to access for maintenance.	c	Multiple sub-systems are integrated in one structure.	3	4

11.4. Design Approach

In this section the design approach of each of the subsystems is given. In each design approach it is discussed what options could be chosen.

11.4.1. Fuel System

There are two options for fuel systems, a gravity-feed system and a fuel-pump system.[9] The gravity-feed system uses, as the name suggests, gravity to feed the fuel to the engines. The fuel-pump system is used when the engines are located above the fuel tanks. As this is the case, the fuel-pump system is chosen. Next to this, as the aircraft is an attack aircraft, which can experience high maneuver loads, the fuel pump is needed in order to ensure to constant feed of fuel to the engines. The fuel system consists of the following elements; the fuel tanks, fuel lines & fittings, fuel valves, electric pump and engine-driven pump.[10]. All of these components will be discussed in the following paragraphs.

First up, the fuel tanks. As mentioned earlier, the fuel tanks are partly located inside the wings, part of the fuel tank will be located inside the fuselage. This was chosen in order to reduce the possibility of the fuel tank being hit in combat. The fuel tank inside the wings are used in the first part of each mission, such that during loiter only the fuel tank inside the fuselage has fuel inside.

The second element is the fuel lines & fittings. In order to connect the different fuel tanks to the engines and with a "cross-feed" connection to each other[11], fuel lines have to be taken into account. Fittings need to be considered which can be easily disconnected when the aircraft is disassembled for transport, which will be discussed in more detail in section 16.2. The third element, the fuel valves, is used in order to select from which tank fuel is taken, to shut off fuel flow to the engines or to open the cross-feed.

The fourth element is the fuel filter. Before entering the motor, the fuel enters a strainer to have moisture and any other unwanted materials removed. After that, these materials will be stored at the bottom of the fuel tank in a sump, an area which can be drained during each pre-flight check[12].

The last element in the fuel system is fuel pump. There are two types of pumps; the transfer pump and the boost pump. The transfer pump is used for transfer of fuel between different tanks, the boost pump will provide the engines with fuel [28].

11.4.2. Hydraulic System

Looking at the similar aircraft and current trends, it was decided to use Electro-Hydrostatic Actuation system. It is a pre-integrated hydraulic system located in several parts of aircraft where actuation is required.

[9] https://www.flightliteracy.com/aircraft-fuel-systems-part-one/, conducted on [06-01-2021]
[10] https://www.aircraftsystemstech.com/2017/05/aircraft-fuel-system-components.html, conducted on [06-01-2021]
[11] https://www.aircraftsystemstech.com/2017/06/types-of-aircraft-fuel-pumps.html, conducted on [06-01-2021]
[12] https://www.flightliteracy.com/aircraft-fuel-systems-part-one/#:~:text=Aircraft%20with%20fuel%2Dpump%20systems,reliability%20to%20the%20fuel%20system., conducted on [06-01-2021]

The system is self-contained and only needs electrical power in order to operate. In addition, the system aids to reduce the aircraft weight, thanks to the scaled size for each point of actuation, which can results in a saved weight of up to 5 kg per actuator[13]. The reason for this lighter weight is that in comparison to other systems, the EHA system does not need a centralized hydraulic power supply system or hydraulic lines, the system is driven by its own motor.

As mentioned, the EHA system requires electrical power to operate. The power is provided by a generator and the APU, which will be discussed in further detail in subsection 11.4.3. As there are two systems that can provide power to the system, this will add redundancy. It was chosen to have redundant actuators at the ailerons and flaps in order to still be used when one actuation point fails. The main landing gear also has redundant actuators. Next to this redundancy, the total hydraulic system will be more reliable, as each actuation point has its own hydraulic system. If one hydraulic system fails, other hydraulic systems in the aircraft are still able to operate, which will make this system more reliable.

11.4.3. Electrical System

As discussed earlier, the power for the aircraft is generated by two starter-generators and an APU. The starter-generator is used in order to start the engines with the help of the APU and batteries. When the engines reach a self-sustaining speed, the starter-generator is used for generation of power. This start-up sequence can be done within 5 minutes.

The APU is a second power source for the aircraft electrical system. As the hydraulic system is powered by the Flight Control Computer, it is necessary to ensure there is enough power to be used in all flight stages. As discussed before, the APU is also used in order to start the engines.

11.4.4. Environmental Control System

The pressurization of the cabin is chosen to increase linearly with increasing height. This is for having a lower stress on the airframe. Throughout the research, it was decided that the pressure of the cabin will follow the trend of an average fighter aircraft which is as follows: the cabin is under-pressurized for altitudes up to 8 000 ft (2.43 km), for altitudes higher than that, the pressurization system will keep the cabin pressure at the pressure of 8 000 ft which is 10.92 psi, or 565 mmHg[14].

It is recommended to take a closer look at the design of the thermal control system, in future design stages.

11.5. Requirement Compliance

In this section the evaluation of the chosen design is given using a compliance matrix, presented in Table 11.3. In the compliance matrix each requirement is given, which were presented in Table 11.1, in the third column the method of compliance is given, the fourth column shows if the requirement is met by using a check mark.

For future recommendations, the thermal control system can be designed in more detail at a later stage.

Table 11.3: Compliance matrix for the additional subsystems

Requirement ID	Description	Method of compliance	Requirement met?
Fuel System			
LAA-PER-DSM-2.1	The aircraft shall be able to loiter 4 hours on station without dropping the armament.	chapter 7	✓
LAA-PER-DSM-3.1	The aircraft shall have reserve fuel sufficient for climb to 914.40 m (3 000 ft) and loiter for 45 minutes after the design mission completion.	chapter 7	✓

[13] https://www.mobilehydraulictips.com/electrohydraulic-actuation-technology-improving-global-aviation-industry/, conducted on [08-01-2021]

[14] https://www.highskyflying.com/are-fighter-jets-pressurized/, conducted on [11-01-2021]

Table 11.3: Compliance matrix for the additional subsystems

Requirement ID	Description	Method of compliance	Requirement met?
LAA-PAP-POW-1.1	The aircraft shall have a power unit to provide enough energy to power the onboard systems.	Not sized, but possible, Figure 11.1	N/A
LAA-PAP-POW-3.1	Upon receiving a signal from the air vehicle for stopping, the engine shall terminate fuel flow in any operating condition.	Not specified in this design stage	N/A
LAA-PAP-FUE-1.1	The aircraft shall be able to move the center of gravity in order to stabilize itself.	Cross-feed, Figure 11.1	✓
Hydraulic System			
LAA-SUR-HYD-1.1	In the event of a hydraulic failure, the aircraft shall be able to land safely while protecting aircraft occupants without causing lethal injuries.	Redundancy, subsection 11.4.2	✓
Electrical System			
LAA-PAP-POW-1.1	The aircraft shall have a power unit to provide enough energy to power the onboard systems.	Not sized, but possible, Figure 11.1	N/A
LAA-SUR-POW-1.1	The aircraft shall contain an emergency power source.	The APU, subsection 11.4.3	✓
Environmental Control System			
LAA-SUR-CAB-1.1	The aircraft shall have a cabin pressure ranging from 410 to 670 mmHg	565 mmHg, Not sized, but discussed, subsection 11.4.4	N/A
LAA-SUR-CAB-1.2	The aircraft shall have a cabin temperature of a maximum of 28 °C	Not sized, but discussed, subsection 11.4.4	N/A

12
Drag Analysis

In this chapter the drag analysis performed for the final conceptual design is discussed. First it is discussed how the first order drag analysis was performed, of which the result were used in the iterative sizing process. After that the approach for the second order drag analysis is explained, after which the methods used is explained in more detail. Finally this chapter will conclude with the results obtained from the second order drag analysis, followed by a verification of the method.

12.1. First Order Drag Analysis

In the first order estimations, done in the midterm report, Equation 12.1 was used to calculate the drag of the aircraft. This drag then was used in the determination of the L/D of the aircraft in both cruise and loiter. From Equation 12.1 it becomes apparent that the drag coefficient exist from two components, i.e. zero lift drag (C_{D_0}) and lift induced drag.

$$C_D = \left(C_{D_0} + \frac{C_L^2}{\pi A e} \right) \tag{12.1}$$

Where C_{D_0} was determined using Equation 12.2. Where the wetted area wa sestimated using Equation 12.3 [14] and an assumed skin friction coefficient (C_{fe}) of 0.004.

$$C_{D_0} = C_{fe} \frac{S_{wet}}{S} \tag{12.2}$$

$$S_{wet} = \pi \bar{D}_f \left(L_f - 1.3 \bar{d}_{fus} \right) + (S_w)_{net} \left\{ 2 + 0.5 (\overline{t/c})_w \right\} + k_{fair} \cdot b_{cw} \cdot c_r + 2 \cdot (S_h + S_v) \tag{12.3}$$

Where the variables have the following meaning.

- $S_{w_{net}}$ is the net exposed area of the wing.
- b_{cw} represents the center section span.
- c_r represents the root chord.
- k_{fair} is a correction factor for the fairing.
- S_h and S_v are the surfaces of horizontal and vertical tails.

12.2. Second Order Drag Analysis

Roskam suggest that for a second order drag analysis, the drag coefficient of the aircraft can be split up in separate components of the aircraft, see Equation 12.4[17]. Where the components of Equation 12.4 are explained in the list below.

$$C_D = C_{D_{wing}} + C_{D_{fus}} + C_{D_{emp}} + C_{D_{np}} + C_{D_{flap}} + C_{D_{gear}} + C_{D_c} + C_{D_{store}} + C_{D_{trim}} + C_{D_{int}} + C_{D_{misc}} \tag{12.4}$$

- $C_{D_{wing}}$: Wing drag coefficient
- $C_{D_{fus}}$: Fuselage drag coefficient
- $C_{D_{emp}}$: Empennage drag coefficient
- $C_{D_{np}}$: Nacelle/ pylon drag coefficient
- $C_{D_{flap}}$: Flap drag coefficient
- $C_{D_{gear}}$: Landing gear drag coefficient

- C_{D_c}: Canopy drag coefficient
- $C_{D_{stores}}$: Stores drag coefficient
- $C_{D_{trim}}$: Trim drag coefficient
- $C_{D_{int}}$: Interference drag coefficient
- $C_{D_{misc}}$: Miscellaneous drag coefficient

As drag is depending on a lot of factors such as speed, altitude, aircraft configuration etc.. The drag has been predicted for four different aircraft configurations, which allowed for an analysis on the sensitivity of different objects creating drag.

- **clean**: Where the aircraft is flying clean (without stores), at cruise conditions.
- **stores**: Where the aircraft is flying with stores, at cruise conditions.
- **landing gear**: Where the aircraft is flying with stores and landing gear out, at maximum approach speed.
- **flapped**: Where the aircraft is flying with stores, landing gear out and flaps deflected.

The clean configuration was chosen as it would be the optimal case for lowest drag the aircraft would encounter, since it would be flying without stores and flap deflection. For the same reasoning the flapped configuration was chosen, as this would yield the maximum drag force during a mission. Stores and landing gear configurations were chosen to see the effect of the individual components.

1. It was assumed that the aircraft is designed following the area rule, described by Roskam VI chapter 4.3.4 [17]. Due to this assumption the interference drag coefficient can be neglected for all flight stages.
2. It was assumed that there are no extra items mounted on the outside aircraft, i.e. no targeting pods, camera's, etc.. This assumption makes that the miscellaneous drag coefficient can be neglected.
3. Because the shape of the canopy is integrated in the shape of the fuselage, it was assumed that the canopy does not create any extra drag. Hence the canopy drag coefficient can be neglected.
4. From the trim calculations it became apparent no elevator deflection was needed to fly in trimmed conditions, hence it was assumed that trim drag could be neglected.
5. For all configurations a constant weight was assumed, which was set equal to the weight of the aircraft at the beginning of the respective flight stage. For the clean and stores configuration the cruise weight was assumed, for landing gear and flapped the maximum landing weight (130 kN) was assumed as this would be the most extreme case.
6. The air viscosity (μ), used in the calculations for the Reynolds number, was assumed to be constant.
7. For all calculations it was assumed that the aircraft is only flying at subsonic speeds, as the cruise speed was set to be roughly 0.6 M. This assumption was later validated, using the dog-house plots discussed in chapter 14.
8. It was assumed that the wing, fuselage and horizontal tail are the only components creating lift. Hence, the lift induced drag component for all the other components are neglected.
9. It was assumed that the stores mounted on the wings are MK-82 bombs. As this is a rather general bomb used in the weight class specified by the RFP [29]. [1]
10. During landing it was assumed that the flaps would only be extended, after the C_L required to fly exceeded the $C_{L_{max_{clean}}}$. The flap deflection required for the extra C_L, was assumed to be linear with the extra C_L created.
11. It was assumed the landing gear would only be deployed after a speed of 250 kts, as this was found to be a reasonable speed[2].

[1] https://www.af.mil/News/Art/igphoto/2000424176/, conducted on 16-01-2021
[2] https://contentzone.eurocontrol.int/aircraftperformance/details.aspx?ICAO=A10, conducted on 16-01-2021

As stated before the drag coefficient is partly determined due to the lift induced drag, which is dependent on C_L as becomes clear from Equation 12.9. From Equation 12.8 it becomes clear that C_L depends on speed. Furthermore, as explained in subsection 12.3.1 the C_f coefficient is dependent on the speed as well. Hence, for all configurations the speeds were varied from stall speed to a speed which could still be consider subsonic (V = 210 m/s ≈ 0.65M).

12.3. Method

In this section the method, used to find the different drag coefficients, is explained. The method is based on Roskam VI chapter 4 [17], with some simplifications discussed in the section above. For the upcoming formula's all area's were obtained from the 3D model created in CATIA, unless stated otherwise.

12.3.1. Wing drag coefficient

As stated before both the zero lift drag coefficient and the lift induced drag coefficient were calculated for the wing. Hence the wing drag coefficient can be calculated using Equation 12.5.

$$C_{D_{wing}} = C_{D_{0_W}} + C_{D_{L_W}} \tag{12.5}$$

The zero lift drag coefficient is calculated using Equation 12.6.

$$C_{D_{0_W}} = (R_{wf})\,(R_{LS})\left(C_{f_w}\right)\left\{1 + L'(t/c) + 100(t/c)^4\right\} S_{wet_W}/S \tag{12.6}$$

Where t/c and S were obtained from the wing sizing as explained in chapter 7.

- R_{wf} is the wing/fuselage interference factor, which was determined using figure 4.1 presented in Roskam VI page 24 [17].
- R_{LS} is the lifting surface correction factor, which was determined using figure 4.2 presented in Roskam VI page 24 [17].
- C_{f_w} is the skin friction coefficient of the wing, which was determined using the Reynold number, calculated using Equation 12.7, and figure 4.3 in Roskam VI page 25 [17].
- L' is the airfoil thickness location parameter, using the airfoil selected in subsection 7.4.3 and Roskam VI page 26 [17], it was determined to be 1.2.
- S_{wet_W} is the wetted area of the wing.

$$R_N = \frac{\rho V l}{\mu} \tag{12.7}$$

$$C_L = \frac{2W}{\rho V^2 S} \tag{12.8}$$

Where l is the specific length of the object for which the Reynolds number is calculated.

For the lift induced drag coefficient Equation 12.9 was used.

$$C_{D_{L_W}} = \left(C_{L_W}\right)^2/\pi Ae + 2\pi C_{L_W}\epsilon_t \upsilon + 4\pi^2\epsilon_t^2 w \tag{12.9}$$

Since the wing is designed without a twist angle (ϵ_t), only the first term was calculated. Where C_{L_W} is the lift coefficient produced by the wing. Roskam suggest that this can be calculated using $C_{L_W} = 1.05C_L$ [17], where C_L was calculated using Equation 12.8. Furthermore, A and e where found in chapter 7.

12.3.2. Fuselage drag coefficient

For the calculations of the fuselage drag coefficient the same structure was used as in the previous section, see Equation 12.10.

$$C_{D_{\text{fus}}} = C_{D_{0_{\text{fus}}}} + C_{D_{L_{\text{fus}}}} \tag{12.10}$$

For the zero lift drag coefficient, Equation 12.11 was used.

$$C_{D_{0_{\text{fus}}}} = R_{\text{wf}} C_{f_{\text{fus}}} \left\{1 + 60(l_f/d_f)^3 + 0.0025(l_f/d_f)\right\} S_{\text{wet}_{\text{fus}}}/S + C_{D_{b_{\text{fus}}}} \tag{12.11}$$

Where l_f and d_f were determined in chapter 6, the factor $C_{D_{b_{\text{fus}}}}$ was calculated using Equation 12.12 and the other factors are explained below.

- R_{wf} is the wing/fuselage interference factor, Roskam suggest that this is equal to one for just a fuselage [17].
- $C_{f_{\text{fus}}}$ is the skin friction coefficient of the fuselage, which was determined using the Reynold number, calculated using Equation 12.7, and figure 4.3 in Roskam VI page 25 [17].
- $S_{\text{wet}_{\text{fus}}}$ is the wetted area of the fuselage.

$$C_{D_{b_{\text{fus}}}} = \frac{0.029\,(d_b/d_f)^3}{\left(C_{D_{0_{\text{fus-base}}}}\,(S/S_{\text{fus}})\right)^{0.5}}\,(S_{\text{fus}}/S) \tag{12.12}$$

Where $C_{D_{0_{\text{fus-base}}}}$ is calculated using the first term of Equation 12.11 and d_b is the fuselage base diameter, which was obtained from CATIA. For the lift induced drag coefficient of the fuselage Equation 12.13 was used.

$$C_{D_{L_{\text{fus}}}} = 2\alpha^2 S_{b_{\text{fus}}}/S + \eta c_{d_c} \alpha^3 S_{\text{plf}_{\text{fus}}}/S \tag{12.13}$$

Where α is the angle of attack of the aircraft, the other factors are explained below.

1. $S_{b_{\text{fus}}}$ is the base area of the fuselage.
2. $S_{\text{plf}_{\text{fus}}}$ is the planform area of the fuselage.
3. η is the ratio of drag for a finite cylinder to that of an infinite cylinder, this ratio was determined using Roskam VI figure 4.19 [17].
4. c_{d_c} is the steady state cross-flow drag coefficient, obtained from Roskam VI figure 4.20 [17].

12.3.3. Empenage drag coefficient

To determine the empenage drag coefficient the sum of the drag coefficient for the individual components was found, see Equation 12.14. As stated earlier, it is assumed only the horizontal tail creates a lift component. Hence, the lift induced drag component for the vertical tail is omitted in this calculation.

$$C_{D_{\text{emp}}} = \sum_i \left\{\left(C_{D_{0_{\text{emp}}}}\right)_i + \left(C_{D_{L_{\text{emp}}}}\right)_i\right\} \tag{12.14}$$

Where the $C_{D_{0_{\text{emp}}}}$ was computed in the same manner as the $C_{D_{0_W}}$, with the correct substitution of the empenage components where wing specific components were used. The lift induced drag of the horizontal tail was calculated using Equation 12.15.

$$C_{D_{L_W}} = \left\{ \left(C_{L_h}\right)^2 / \pi Ae \right\} (S_h / S) \tag{12.15}$$

Where the C_{L_h} was calculated using a method provided by Roskam VI page 68 [17] and chapter 8.

12.3.4. Nacelle drag coefficient

The nacelle drag coefficient was determined in two steps, first the nacelle and pylon drag coefficient were determined, see Equation 12.16. The second step was to determine the interference caused due to the fuselage-pylon-engine structure, see Equation 12.17. After these drag coefficients were determined they were summed and multiplied by two.

$$C_{D_{np}} = C_{D_n} + C_{D_p} \tag{12.16}$$

Where C_{D_n} was determined using the method described in subsection 12.3.2. For C_{D_p} the method in subsection 12.3.1 was used.

$$C_{D_{n_{int}}} = F_{a_2} \left(C'_{D_n} - 0.05 \right) (S_n / S) \tag{12.17}$$

Where C'_{D_n} was determined using Roskam VI figure 4.42 [17], S_n is the maximum frontal area of the nacelle and F_{a_2} was set to 1 by suggestion of Roskam [17].

12.3.5. Flap drag coefficient

The flap drag coefficient has been calculated using Equation 12.18, this method differs a bit from the previous methods. Here the drag coefficient is build up from the flap profile drag increment ($C_{D_{prof_{flap}}}$), the induced drag increment ($C_{D_{i_{flap}}}$) and the interference drag increment ($C_{D_{int_{flap}}}$).

$$C_{D_{flap}} = \Delta C_{D_{prof_{flap}}} + \Delta C_{D_{i_{flap}}} + \Delta C_{D_{int_{flap}}} \tag{12.18}$$

Where $C_{D_{prof_{flap}}}$, $C_{D_{i_{flap}}}$, $C_{D_{int_{flap}}}$ were calculated using Equation 12.19, Equation 12.20 and Equation 12.21 respectively.

$$C_{D_{prof_{flap}}} = C_{d_{p_{\Lambda=0}}} \cos \Lambda S_{wf} / S \tag{12.19}$$

Where $C_{d_{p_{\Lambda=0}}}$ is the two-dimensional profile drag increment, which was determined using Roskam VI figure 4.47 [17]. The other variables have been determined in earlier stages of the design, such as S_{wf} which has been determined in subsection 7.4.5.

$$C_{D_{i_{flap}}} = K^2 \left(\Delta C_{L_{flap}} \right)^2 \cos \Lambda \tag{12.20}$$

Where $\Delta C_{L_{flap}}$ is the incremental lift coefficient due to the flaps, which as stated before was assumed to be the difference between the C_L required and the $C_{L_{max_{clean}}}$. The factor K is a constant which was determined using Roskam VI figure 4.52 and 4.53 [17].

$$\Delta C_{D_{int_{flap}}} = K_{int} \Delta C_{D_{prof_{flap}}} \tag{12.21}$$

Where Roskam suggest to use 0.25 for fowler flaps and 0.4 for slotted flaps [17] and $C_{D_{prof_{flap}}}$ was determined using Equation 12.19.

12.3.6. Landing gear drag coefficient

Since the landing gear is retractable the landing gear drag coefficient was only determined for the landing configuration. Where a maximum speed was assumed (250 kts), where the landing gear would be extended. To determine this drag coefficient Equation 12.22 was used.

$$C_{D_{\text{gear}}} = \sum_i \left\{ \left((C_{\text{D}_{0_{\text{gear}}}})_\text{i} + p_\text{i} C_\text{L} \right) (S_{\text{gear}})_\text{i} / S \right\} \tag{12.22}$$

Where $C_{\text{D}_{0_{\text{gear}}}}$ is the zero lift drag coefficient of the landing gear, which was determined using Roskam VI figure 4.58 and 4.59 [17]. p_i is a factor which was determined using Roskam VI figure 4.61 [17].

12.3.7. Stores drag coefficient

The stores on the wing of the aircraft, i.e. the bombs and landing gear fearing, are calculated using section 14.2. Where the $C_{D_{\text{store}}}$ is calculated using the method in subsection 12.3.2.

$$C_{D_{\text{stores}}} = \sum_\text{i} \left\{ (K_{\text{store}})_\text{i} \left(C_{D_{\text{store}}} \right)_\text{i} \right\} \tag{12.23}$$

Where K_{store} is 0.7 for the semi-submerged landing gear fearing and 1.3 for the bombs, see Roskam VI figure 4.69/4.70 [17].

12.4. Sensitivity Analysis

Using the method as explained before and the input variables stated in Appendix A, four different drag polars were plotted, shown in Figure 12.1 and Figure 12.2. From the drag polars and Table 12.1 the effect of the added objects to the different configurations becomes clear. For the landing gear configuration it was observed that the starting point is shifted tot he right, this is due to the maximum speed assumed for landing gears out. Which is lower then the maximum speed used for the other configurations, resulting in a higher required C_L. For the flapped configuration the y-axis is given another range, this is due to the assumption that the flaps are extended, only after the $C_{\text{L}_{\text{max}_{\text{clean}}}}$ is reached.

The trend lines in Figure 12.1 and Figure 12.2 are plotted such that the values C_{D_0} and e could be determined from it. In Table 12.1 the values found for the different configurations are listed.

Table 12.1: Values found from trend lines of the drag polars.

Configuration	C_{D_0}	e
Clean	0.017	0.76
Stores	0.028	0.76
Landing gear	0.043	0.78
Flapped	$0.061\Delta C_\text{L} + 0.038$	0.57

Where the formula for the flapped configuration is due to the dependency of the profile drag on the flap deflection angle. Which, as stated before, was assumed to vary linearly with the ΔC_L required.

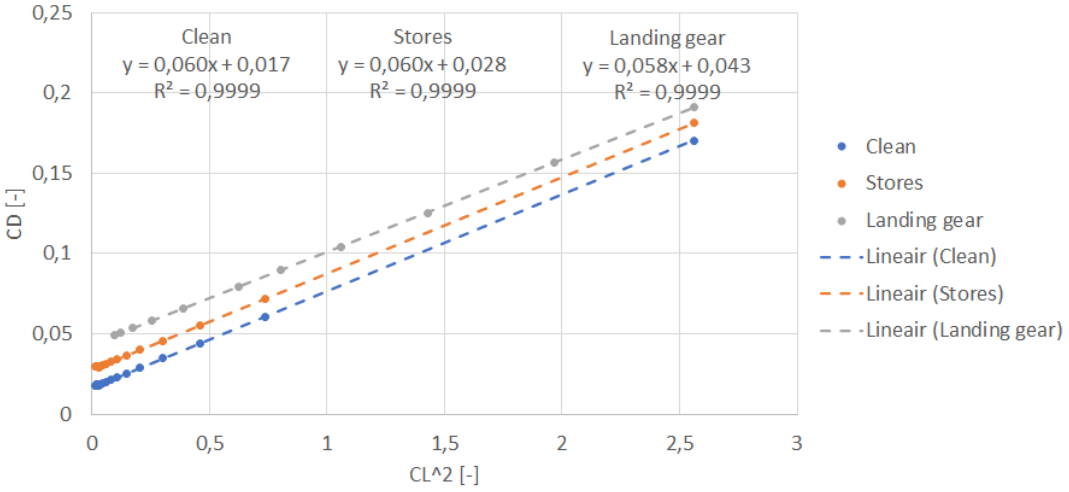

Figure 12.1: Drag polar for the clean, stores and landing gear configuration.

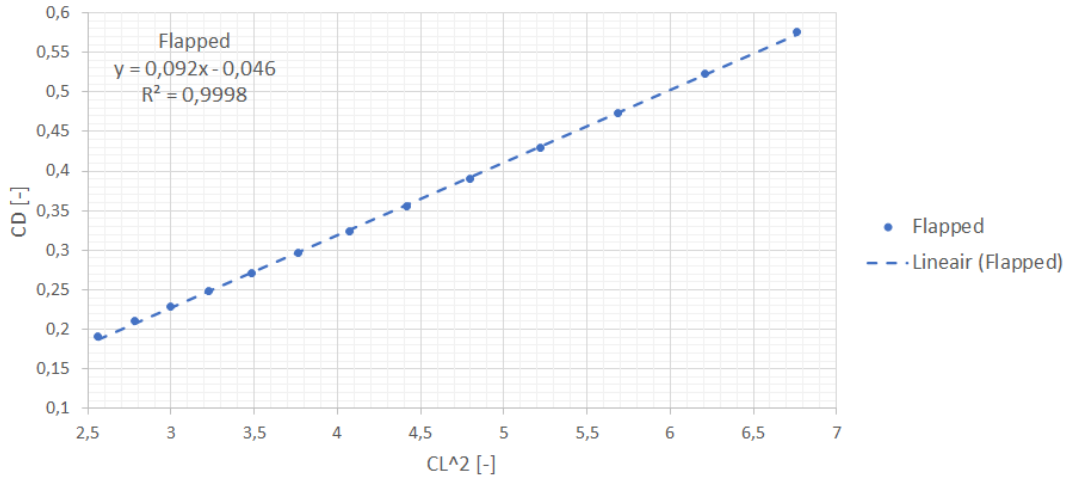

Figure 12.2: Drag polar for the flapped configuration.

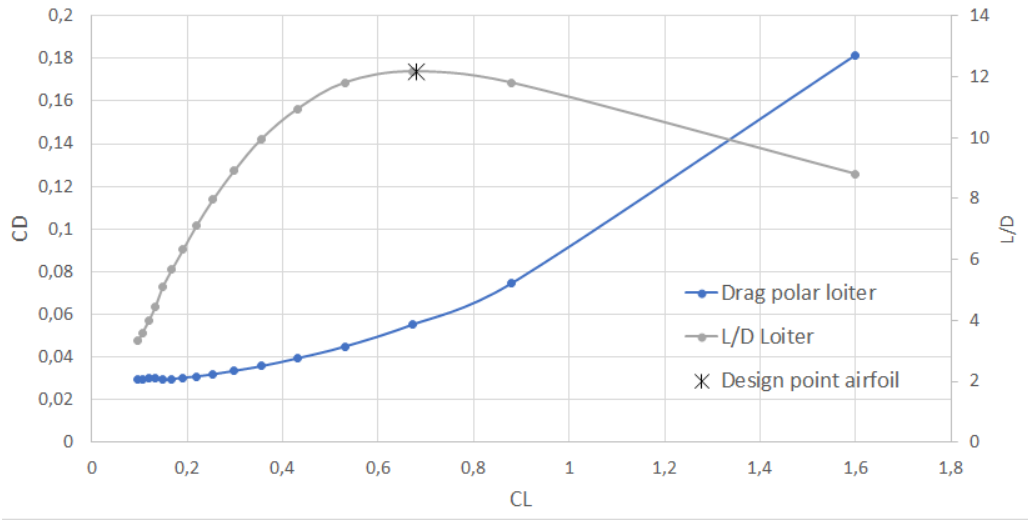

Figure 12.3: Drag polar and L/D curve for loiter configuration.

12.5. Verification and Validation

In subsection 7.4.3 it is explained how the airfoil was selected. Here it was stated that the airfoil should have a design lift coefficient of 0.68, as this would yield an optimal L/D during the loiter phase. Hence, from the second order drag estimation the drag polar and the corresponding L/D curve were plotted in Figure 12.3. On this curve the airfoil design point (0.68, L/D_{max}) was plotted. It was observed that the design point indeed coincides with the L/D curve, and hence verifies the airfoil selection.

The first step that was taken to verify the results from the drag estimation method used, was inspecting the resulting values. This was done by comparing the C_{D_0} used in the first order drag estimation with the value obtained from the second order weight estimation. If the difference would be too large, the equations used on the program would be checked for syntax errors. The second step was to pick a configuration and check if the calculated value in the program were equal to hand calculated values. This step also aimed to reduce the amount of syntax errors. The final step to verify the program was to plot both the first order estimated drag polar and the second order estimated drag polar for the cruise configuration. Of which the result is shown in Figure 12.4. It can be seen in this graph that the difference between the two lines grows with increasing C_L. A possible explanation for this is assumption 8, stated in section 12.2, which underestimates the lift induced drag. Another explanation for the difference is the underestimation of the wetted area in the first order analysis.

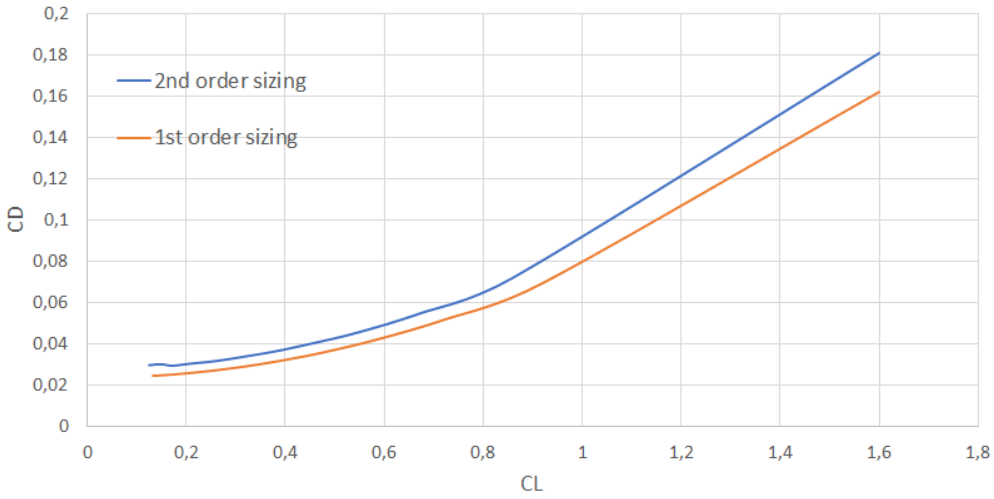

Figure 12.4: Comparison of the first and second order drag analysis.

Due to the amount of assumptions made in this method, it is recommended that a more thorough analysis would be performed in future design steps. Where a computational fluid dynamics (CFD) analysis of the 3D model might be performed to investigate more exactly what the effect of certain features might be. Which eventually could be verified by a wind-tunnel experiment, confirming the actual drag created in different configurations.

13
Stability and Control Analysis

In order to operate an aircraft safely, the pilot should know whether it is stable and controllable. This chapter analyses the control and stability characteristics of the aircraft. First the requirements and risks regarding this topic are discussed. Following a distinction is made in static and dynamic stability. Firstly the static stability is evaluated in longitudinal and lateral direction, respectively. Secondly the dynamic control and stability is conducted with a description of the pilots handling qualities. Finally a sensitivity analysis, and verification and validation of the used tools are described.

Throughout the chapter not all formulas are provided in this section to keep the chapter brief. The most important formulas are provided with their results. The formulas required to calculate intermediate values can be found in Roskam part VI[17].
The arrows in Figure 13.1 and Figure 13.2 are used as convention for the positive direction. These conventions are used throughout the entire chapter. For each static stability derivative, the results are given, along with its contribution and the method to calculate the values. In some tables, the expected or required sign is given that indicate a stable aircraft. This sign is shown between curly brackets and next to the derivative. Lastly, the stability and control analysis was done for three different flight phases:

- **Loiter**: This is the loiter phase where the aircraft is performing a mission, meaning that the altitude, velocity, and mass are 3,000 ft, 86.19 m/s, and 12.2 tons, respectively. Furthermore, it was assumed that the aircraft flies in a clean configuration.
- **Cruise**: For the cruise phase, an altitude of 10,000 ft, the MTOW of 13.7 tons and the cruise velocity of 201.3 m/s were used. Just as for the loiter phase, it was assumed that the aircraft flies in a clean configuration.
- **Landing**: In this phase, the aircraft is approaching the runway with a density altitude, velocity and mass of 6,000 ft 52.9 m/s and 13.3 tons, respectively. The mass was taken from the situation when the aircraft must land immediately after take off.

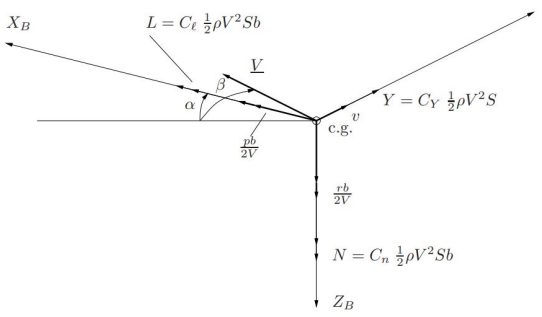

Figure 13.1: Asymmetric force and moments [30]

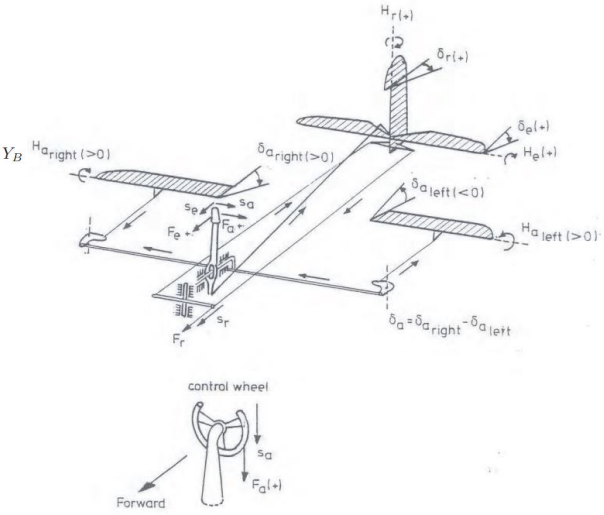

Figure 13.2: The positive direction of control deflections, control forces, control surface deflections and hinge moments [30]

13.1. Requirements

The requirements given in Table 13.1 are not directly related to the empennage, but do involve the empennage sizing. Therefore, they have been included in this section. Some requirements however, directly involve the stability and control characteristics elucidated in chapter 13.

Regarding stability and control, several additional requirements were created. Some requirements already existed in preceding reports, but additional requirements were added to put a certain stability and control characteristic in mind.

These requirements involve the integration of all subsystems of the aircraft. In the subsequent chapters, they are evaluated using the requirements.

Table 13.1: List of requirements for landing gear

Requirement ID	Description	Source
Stability and Control		
LAA-SAC-STA-1.1	The aircraft shall be able to stabilize itself stick free.	JSSG-2001b [1]
LAA-SAC-STA-1.2	The aircraft shall be longitudinally static stable for all phases of the mission profile.	
LAA-SAC-STA-1.3	The aircraft shall be laterally static stable for all phases of the mission profile.	
LAA-SAC-DYN-1.1	The aircraft shall have level 1 handling qualities for short period at all phases of the mission profile	MIL-F-8785C
LAA-SAC-DYN-1.2	The aircraft shall have level 1 handling qualities for phugoid period at all phases of the mission profile	MIL-F-8785C
LAA-SAC-DYN-1.3	The aircraft shall have level 1 handling qualities for aperiodic roll at all phases of the mission profile	MIL-F-8785C
LAA-SAC-DYN-1.4	The aircraft shall have level 1 handling qualities for dutch roll at all phases of the mission profile	MIL-F-8785C
LAA-SAC-DYN-1.5	The aircraft shall have level 1 handling qualities for aperiodic spiral at all phases of the mission profile	MIL-F-8785C
Performance		
LAA-PER-STK-1.1	The maximum stick forces shall not exceed 133 N (30 lbs).	MIL-F-8785C

13.2. Risk Analysis

Regarding the requirements that have been set, there are some risks involved for the design on parameters that may cause the requirement not to be reached.

Table 13.2: Specified risks for the aircraft stability

ID	Label	Risk	Seq.	Cause	Prob.	Imp.
RIS-041: Aircraft is statically unstable.						
RIS-056	T	The rolling moment due to sideslip (C_{l_β}) is positive	a	insufficient sweep	2	4
			b	insufficient sweep	2	4
RIS-057	T	The yawing moment due to sideslip (C_{n_β}) is negative	a	small contribution of the vertical tailplane	2	4
			b	small contribution of the wing	2	4
			c	large contribution of the fuselage	2	4
			d	insufficient sweep	2	4
RIS-058	T	The rolling moment due to roll rate is positive	a	small contribution of the wing	2	4

Table 13.2: Specified risks for the aircraft stability

ID	Label	Risk	Seq.	Cause	Prob.	Imp.
			b	small contribution of the vertical tailplane	2	4
RIS-059: Aircraft is dynamically unstable.						
RIS-060	T	Aircraft does not reach level 1 handling qualities for short period motion	a	The short period motion is insufficiently damped	1	2
RIS-061	T	Aircraft does not reach level 1 handling qualities for phugoid period motion	a	Large C_L is required, causing insufficient damping	2	4
RIS-062	T	Aircraft does not reach level 1 handling qualities for aperiodic roll motion	a	Dihedral angle of the aircraft too small	2	4
RIS-063	T	Aircraft does not reach level 1 handling qualities for dutch roll motion	a	Insufficient vertical tail.	2	4
RIS-064	T	Aircraft does not reach level 1 handling qualities for aperiodic spiral motion	a	Insufficient dihedral	3	4
			b	Insufficient vertical tail surface area	3	4
			c	C_L required is too large	3	4

There have been no risks set regarding the controllability of the aircraft. The signs of the control derivatives are directly related between the design and the derivatives. Hence, for a conventional aircraft should not have impacts to the change in signs.
The magnitude of the derivative may differ depending on its size and impact the performance of the aircraft. However, regarding the stability, the aircraft is not influenced by these parameters. These risks are mitigated by adjusting parameters that cause these risks.

13.3. Longitudinal Static Stability

In this section, the longitudinal static stability characteristics of the aircraft is described. The following section describes the longitudinal stability with respect to the clean-configuration (situated at cruise condition, Mach=0.613), and the flaps extended condition (situated in at landing condition, Mach=0.144). The neutral point for static pitch stability was calculated using Equation 13.1.

$$\bar{x}_{\text{np}} = \frac{C_{L_\alpha}\bar{x}_{\text{ac}_\text{w}} - C_{m_{\alpha_{\text{fus}}}} + \eta_\text{h}\frac{S_\text{h}}{S_\text{w}}C_{L_{\alpha_\text{h}}}\frac{\partial\alpha_h}{\partial\alpha}\bar{x}_{\text{ac}_\text{h}}}{C_{L_\alpha} + \eta_\text{h}\frac{S_\text{h}}{S_\text{w}}C_{L_{\alpha_\text{h}}}\frac{\partial\alpha_h}{\partial\alpha}} \tag{13.1}$$

The terms found in Equation 13.1 are calculated/found using the methods found in Roskam, DATCOM and the Aerospace Design and Systems Engineering Elements (ADSEE) and Systems Engineering and Aerospace Design (SEAD) Lectures provided at the Faculty of Aerospace Engineering of Delft University of Technology, or are provided by (resulting) design choices in preceding chapters. C_{L_α} in particular is required throughout this chapter and was calculated using Equation 13.2 with the inputs as given in Table 13.3 for the three different flight conditions used in this chapter: loiter, cruise, and landing.

$$C_{\text{L}_\alpha} = C_{\text{L}_{\alpha_{\text{A-h}}}} + C_{\text{L}_{\alpha_\text{h}}}\frac{S}{S_\text{h}}\left(1 - \frac{d\epsilon}{d\alpha}\right)\left(\frac{V_\text{h}}{V}\right)^2 \tag{13.2}$$

Table 13.3: Input values Equation 8.3

Parameter	Value loiter	Value cruise	Value landing
$C_{L_{\alpha_{A\text{-}h}}}$ [rad^{-1}]	4.86	5.60	5.42
$C_{L_{\alpha_h}}$ [rad^{-1}]	4.90	5.57	4.84
S [m^2]	50.6	50.6	50.6
S_h [m^2]	10.6	10.6	10.6
$\frac{d\epsilon}{d\alpha}$ [-]	0.463	0.534	0.517
$\left(\frac{V_h}{V}\right)^2$ [-]	0.85	0.85	0.85
C_{L_α} [rad^{-1}]	5.36	6.06	5.84

For the flaps extended configuration, a correction was added to include the contributing effects of the flaps to the lift curve, which increases the lift curve slope, increases the maximum achievable lift and also changes the angle of attack at zero-lift. These calculations were provided by the ADSEE. [17] [13]

Here, it is assumed that the aerodynamic center of the wing and the horizontal tail is located at 25% of the MAC and 25% of the MAC of the horizontal tail surface, respectively.

Finally, Equation 13.3 is used to calculate the pitching moment [17].

$$C_{m_\alpha} = C_{L_\alpha}(\bar{x}_{ac} - \bar{x}_{cg}) \tag{13.3}$$

For both cases, the most aft c.g. was taken, as this is the most limiting case. The c.g. locations was derived using the calculations presented section 8.4. When the c.g. is ahead of the neutral point, a positive static margin is given, which leads to a longitudinally statically stable aircraft (i.e. negative C_{m_α}). This means that, if the aircraft has an increase in angle of attack, the aircraft will naturally pitch in the opposite direction. The resulting values are provided in Table 13.4

Table 13.4: Longitudinal Static Stability

Configuration	C_{m_α} {-} [rad^{-1}]
Loiter	-0.856
Cruise	-0.895
Landing	-0.699

13.4. Lateral Static Stability

In this section, the lateral static stability derivatives due to sideslip, yaw-rate and roll-rate are given. Additionally, the contributions to these derivatives are noted down.

13.4.1. Stability Derivatives With Respect to Sideslip Angle

In this subsection, the method to calculate the stability derivatives with respect to sideslip angle are presented. In the method, only the most important formula were added where the terms and contributions to this term are explained. Lastly, the values for these stability derivatives are given in Table 13.5.

- C_{y_β}: is the sideforce due to sideslip derivative and its main contribution comes from the vertical tail. The wing and the fuselage have a small contribution to the side force. This term is generally negative as the vertical tail experiences a force in the opposite direction as given in the convention (Figure 13.1).
- C_{l_β}: is the rolling moment due to sideslip derivative and it is affected by the dihedral, sweep and wing configuration. A positive dihedral and sweep both contribute to a negative C_{l_β}. This derivative is preferred negative, so there is a negative relation between the sideslip angle, β, and rolling moment, C_l.

- C_{n_β}: is the yawing moment due to sideslip derivative, which is preferred positive. It is also called the "weathervane stability", "weathercock" or "static directional stability". It is affected by the vertical tailplane (due to the moment arm of the normal force), the wing configuration, the fuselage and the sweep.

The equation required to compute the sideforce due to sideslip is given by Equation 13.4. $C_{y_{\beta_w}}$ is the contribution from the wing and is mainly a result form the dihedral angle, $C_{y_{\beta_f}}$ is the contribution from the fuselage and $C_{y_{\beta_v}}$ is the contribution from the vertical tail, which has the highest contribution.

$$C_{y_\beta} = C_{y_{\beta_\mathrm{w}}} + C_{y_{\beta_\mathrm{f}}} + C_{y_{\beta_\mathrm{v}}} \tag{13.4}$$

In Equation 13.5 the first term represents the contribution of wing-fuselage and is mainly contributed by the sweep and dihedral. The second term is the contribution of the horizontal tail and is mainly governed by the horizontal tail dihedral. The third term is the contribution of the vertical tail and is due to contributions of C_{y_β} and the arm that is created between fuselage and c.g. location.

$$C_{l_\beta} = C_{l_{\beta_{\mathrm{wf}}}} + C_{l_{\beta_\mathrm{h}}} + C_{l_{\beta_\mathrm{v}}} \tag{13.5}$$

In Equation 13.6, the first represents the contribution of the wing. Its contribution is mostly important at high angles of attack. However, for preliminary design this value was chosen as zero. The second term is the contribution of the fuselage, which is dependent on the Reynold's number and fuselage length. The third term is the contribution of the vertical tailplane, which is due to the moment arm created between the c.g. and the vertical tailplane, and the acting sideforce ($C_{y_{\beta_v}}$).

$$C_{n_\beta} = C_{n_{\beta_\mathrm{w}}} + C_{n_{\beta_\mathrm{f}}} + C_{n_{\beta_\mathrm{v}}} \tag{13.6}$$

The resulting values are given in Table 13.5. The values are either positive or negative accordingly with the description given at the beginning of the subsection. Therefore, the lateral stability of the aircraft with sideslip is stable.

Table 13.5: Lateral stability derivatives with respect to sideslip angle

Configuration	C_{y_β} {-} [rad^{-1}]	C_{l_β} {-} [rad^{-1}]	C_{n_β} {+} [rad^{-1}]
Loiter	-0.438	-0.086	0.123
Cruise	-0.438	-0.083	0.122
Landing	-0.427	-0.072	0.131

13.4.2. Stability Derivatives With Respect to Roll Rate

In this subsection, the stability derivatives with respect to roll rate are given. The expected values, the contributing factors to these values and the resulting values are given.

- C_{y_p}: is the side force due to roll rate derivative and is only caused by the vertical tailplane. This term is generally small and is negative (The sideslip causes the vertical tail to be pushed into the flow, which causes a normal force in negative Y-direction as seen from Figure 13.1).
- C_{l_p}: is the rolling moment due to roll rate derivative and is caused by the main wing, which causes a negative C_{l_p} value (this is the roll damping). The vertical tailplane induces an additional negative C_{l_p}, increasing the roll damping. The horizontal tailplane also has another contribution to the roll damping.
- C_{n_p}: is the yawing moment due to roll rate derivative and is mainly contributed by the sweep of the wing and vertical tail. A positive roll rate results in a negative yawing moment and results in a negative C_{n_p} value.

Equation 13.7 is caused by the contribution of the arm created between the c.g. and the vertical tailplane and the $C_{y_{\beta_v}}$.

$$C_{Y_p} = 2C_{Y_{\beta_v}}(z_v \cos(\alpha) - l_v \sin(\alpha))/b \tag{13.7}$$

In Equation 13.8, the first term is the contribution of the wing and is contributed by the dihedral, the lift curve of the wing and wing drag contribution. The second term is due to the horizontal tail contribution and is affected by the horizontal tail sizing. The last term is due to the vertical tail contribution, which is due to the arm created between c.g. and vertical tail and $C_{y_{\beta_v}}$.

$$C_{l_p} = C_{l_{p_w}} + C_{l_{p_h}} + C_{l_{p_v}} \tag{13.8}$$

In Equation 13.9, the first term represents the yaw due to roll rate derivative of the wing and is mainly caused by the wing sweep. The second term is the yaw due to roll rate derivative caused by the vertical tail. This is due to the arm that is created between the c.g. and the vertical tailplane and $C_{y_{\beta_v}}$. At cruise conditions, these terms reduce to zero, due to no wing twist, no flap deflection and no angle of attack. For landing configuration, there is a contributing factor by both.

$$C_{n_p} = C_{n_{p_w}} + C_{n_{p_v}} \tag{13.9}$$

At the beginning of this subsection, the expected or required sign for the lateral stability derivatives are given. Given the values due to roll rate, seen in Table 13.6, is laterally stable. For cruise, the yawing moment stays neutral at cruise configuration.

Table 13.6: Lateral stability derivatives with respect to roll rate

Configuration	C_{y_p} {-} [rad^{-1}]	C_{l_p} {-} [rad^{-1}]	C_{n_p} {-} [rad^{-1}]
Loiter	-0.092	-0.494	0.000
Cruise	-0.092	-0.499	0.000
Landing	-0.017	-0.513	-0.337

13.4.3. Stability Derivatives With Respect to Yaw Rate

In this section, the method to calculate the stability derivatives with respect to yaw rate is described, along with its contributing factors. At the end, the values for these stability derivatives are given for the aircraft.

- $\boldsymbol{C_{y_r}}$: is the sideforce due to yaw rate derivative and is mainly caused by the vertical tail. This term is generally positive, as the yaw introduces a sidewash on the vertical tail, which results in a positive force in the Y-direction (see Figure 13.1).
- $\boldsymbol{C_{l_r}}$: is the rolling moment due to yaw rate derivative and is caused by the main wing (due to velocity differential over the wing span, creating difference in lift) and the vertical tailplane (due to the vertical moment arm). Both contribute to a positive C_{l_p}.
- $\boldsymbol{C_{n_r}}$: is the yawing moment due to yaw rate derivative and is caused by yawing moment due to yaw rate derivatives of the wing and the vertical tailplane. This derivative is generally negative, due to the vertical tailplane producing a positive force in Y-direction resulting in a negative yawing moment around the c.g. (see Figure 13.1).

The contribution terms in Equation 13.10 is due to the arm created between the c.g. location and the position of the vertical tail. Additionally, $C_{y_{\beta_v}}$ also contributes to the sideforce due to yaw rate derivative.

$$C_{y_r} = -2(C_{y_{\beta_v}})(l_v \cos(\alpha) + z_v sin(\alpha))/b \tag{13.10}$$

The first term in Equation 13.11 is the contribution of the wing. The second term is the contribution of the vertical tail.

$$C_{l_r} = C_{l_{r_w}} + C_{l_{r_v}} \tag{13.11}$$

In Equation 13.12, the first term represents the contribution of the wing and the second represents the contribution of the vertical tail.

$$C_{n_r} = C_{n_{r_w}} + C_{n_{r_v}} \tag{13.12}$$

In Table 13.7, the resulting values regarding the lateral stability due to yaw rate derivatives are given. Given the description of the expected or required sign of the values, the aircraft is laterally stable with respect to yaw rate.

Table 13.7: Lateral stability derivatives with respect to yaw rate

Configuration	C_{y_r} {+} [rad^{-1}]	C_{l_r} {+} [rad^{-1}]	C_{n_r} {-} [rad^{-1}]
Loiter	0.269	0.736	-0.180
Cruise	0.269	0.220	-0.174
Landing	0.276	1.737	-0.216

13.5. Longitudinal Dynamic Stability

In this section the longitudinal dynamic stability of the aircraft is described. For the longitudinal direction two motions are described: the short period motion and the phugoid. To approximate the derivatives described in this section, Roskam book part VI was used [17]. The symmetric equations of motion in longitudinal direction are described in Equation 13.13.

$$\begin{bmatrix} C_{X_u} - 2\mu_c D_c & C_{X_\alpha} & C_{Z_0} & 0 \\ C_{Z_u} & C_{Z_\alpha} + \left(C_{Z_{\dot{\alpha}}} - 2\mu_c\right) D_c & -C_{X_0} & C_{Z_q} + 2\mu_c \\ 0 & 0 & -D_c & 1 \\ C_{m_u} & C_{m_\alpha} + C_{m_{\dot{\alpha}}} D_c & 0 & C_{m_q} - 2\mu_c K_Y^2 D_c \end{bmatrix} \begin{bmatrix} \hat{u} \\ \alpha \\ \theta \\ \frac{q\bar{c}}{V} \end{bmatrix} = \underline{0} \tag{13.13}$$

13.5.1. Short Period Motion

The short period motion is characterized by its heavily damped oscillation, which occurs no longer than a few seconds. In the following calculations the airspeed was assumed to be constant. The symmetric equations of motion of Equation 13.13, thus reduce to Equation 13.14.

$$\begin{vmatrix} C_{Z_\alpha} + \left(C_{Z_{\dot{\alpha}}} - 2\mu_c\right)\lambda_c & C_{Z_q} + 2\mu_c \\ C_{m_\alpha} + C_{m_{\dot{\alpha}}}\lambda_c & C_{m_q} - 2\mu_c K_Y^2 \lambda_c \end{vmatrix} = 0 \tag{13.14}$$

The parameters and derivatives is explained in the following way:

- $\boldsymbol{\mu_c}$: is described by the following formula:

$$\mu_c = \frac{m}{\rho \cdot S \cdot \bar{c}} \tag{13.15}$$

  In Equation 13.15, m is the mass of the airplane, ρ the air-density, S the wing area and $\bar{c}$ the mean aerodynamic chord.

- $\boldsymbol{K_Y^2}$: is the non-dimensional radius of gyration about the Y-axis and was calculated with the following formula:

$$K_Y^2 = \frac{I_{yy}}{m\bar{c}^2} \tag{13.16}$$

  In Equation 13.16, I_{yy} is the moment of inertia about the Y-axis, which was computed in Equation 5.2.

- $\boldsymbol{C_{Z_\alpha}}$: is the aerodynamic angle-of-attack derivative in the Z-direction. In the case of aircraft this is the lift due to angle-of-attack. For this derivative the assumption was made that the main wing is the main contribution to the lift created.

- $\boldsymbol{C_{Z_{\dot{\alpha}}}}$: is the lift derivative due to the rate of the angle of attack. It was calculated by using Equation 13.17, where the lift, represented by subscript L, acts in the negative z-direction [17]. In the calculation, the angle of attack of the wing was assumed to be zero during cruise.

$$C_{L_{\dot{\alpha}}} = 2\left(C_{L_{\alpha_h}}\right)\eta_h\left(\bar{V}_h\right)\cdot\frac{d\epsilon}{d\alpha} \tag{13.17}$$

  In Equation 13.17 $C_{L_{\alpha_h}}$ represents the lift curve slope of the horizontal tail as calculated in Table 13.3. Secondly, η_h is the the horizontal tail ratio to the wing dynamic pressure and was calculated by using formula 8.37 of Roskam part VI [17]. Thirdly $\bar{V}_h$ is the horizontal tail volume coefficient as a ratio to to the MAC. Finally $\frac{d\epsilon}{d\alpha}$ is the downwash gradient at the horizontal tail.

- $\boldsymbol{C_{m_\alpha}}$: is called the static longitudinal stability coefficient. It was described and evaluated in section 13.3.

- $\boldsymbol{C_{m_{\dot{\alpha}}}}$: is known as the pitching moment due to the rate of the angle of attack. It was computed in Equation 13.18 [17]. It was assumed that the horizontal tail is the only contribution to this derivative.

$$C_{m_{\dot{\alpha}}} = -2\left(C_{L_{\alpha_h}}\right)\eta_h\left(\bar{V}_h\right)\cdot\left(\bar{x}_{ac_h} - \bar{x}_{cg}\right)\frac{d\epsilon}{d\alpha} \tag{13.18}$$

  By observation many terms of Equation 13.18 are the same as the terms of Equation 13.17, therefore their explanations are found above. For $\bar{x}_{cg}$, the location of the most aft c.g. was chosen, since that would lead to the most extreme case for the stability.

- $\boldsymbol{C_{Z_q}}$: is the lift due to pitch rate. To compute this derivative Equation 13.19 was used[17].

$$C_{L_q} = C_{L_{q_w}} + C_{L_{q_h}} \tag{13.19}$$

  As is shown in Equation 13.19, the lift due to pitch rate has two contributions of both the wing and the horizontal tail surface. By inspection it is clear that the main wing is the largest contributing factor to this derivative.

- $\boldsymbol{C_{m_q}}$: is the pitching moment due to the pitch rate. It was calculated by Equation 13.20 [17].

$$C_{m_q} = C_{m_{q_w}} + C_{m_{q_h}} \tag{13.20}$$

  It should be noted however that the formula for the wing contribution was whited out in the first print of Roskam part VI. Therefore, a similar approach as for previous coefficients was followed, leading to Equation 13.21:

$$C_{m_{q_w}} = -2\cdot C_{L_\alpha}\cdot\left(\bar{x}_{ac} - \bar{x}_{cg}\right) \tag{13.21}$$

The values of the above described derivatives are found in Table B.1. To evaluate the handling characteristics of the short period motion, the eigenvalues have to found. This leads to the following set of equations.

$$A = 2\cdot\mu_c\cdot K_Y^2\cdot\left(2\cdot\mu_c - C_{Z_{\dot{\alpha}}}\right) \tag{13.22}$$

$$B = 2\cdot\mu_c\cdot K_Y^2\cdot C_{Z_\alpha} - \left(2\cdot\mu_c - C_{Z_q}\right)\cdot C_{m_{\dot{\alpha}}} - \left(2\cdot\mu_c - C_{Z_{\dot{\alpha}}}\right)\cdot C_{m_q} \tag{13.23}$$

$$C = C_{Z_\alpha}\cdot C_{m_q} - \left(2\cdot\mu_c - C_{Z_q}\right)\cdot C_{m_\alpha} \tag{13.24}$$

The equations described in Equation 13.22 are then used to find the eigenvalues with the following equation [30].

$$\lambda_{c_{1,2}} = \xi_c \pm j\eta_c = \frac{-B \pm j\sqrt{4AC - B^2}}{2A} \tag{13.25}$$

For the handling qualities of the short period motion it is important to compare the damping coefficients to the boundaries set in MIL-F-8785-C [31]. The damping coefficient was found by using Equation 13.26.

$$\zeta = -\frac{\xi_c}{\sqrt{\xi_c^2 + \eta_c^2}} \tag{13.26}$$

The damping ratios of the short period motion were evaluated in both cruise, corresponding to category B, and landing, corresponding to category C [31]. In order to achieve handling qualities level one a comparison was made in Table 13.8. In this comparison and throughout the rest of this section, level 1 is defined, according to MIL-F-8785C[31], as "Flying qualities clearly adequate for the mission Flight Phase". Level 2 is described as "Flying qualities adequate to accomplish the mission flight phase, but some increase in pilot workload or degradation in mission effectiveness, or both, exists". Finally level 3 is described as "Flying qualities such that the airplane may be operated safely but the pilot workload is excessive or mission effectiveness is inadequate, or both. Category A flight phases can be terminated safely, and category B and C flight phases can be completed". Furthermore, MIL-F-8785C describes a difference in airplane categories, where light attack aircraft fit in category IV. All handling qualities are thus taken for this category.

Table 13.8: Short period motion handling qualities

Flight Phase	Level 1	Level 2	Level 3
Category A & C	$0.35 \leq \zeta \leq 1.3$	$0.25 \leq \zeta \leq 2.0$	$0.15 \leq \zeta$
Loiter	$\boldsymbol{\zeta = 0.89}$		
Landing	$\boldsymbol{\zeta = 0.89}$		
Category B	$0.30 \leq \zeta \leq 2.0$	$0.20 \leq \zeta \leq 2.0$	$0.15 \leq \zeta$
Cruise	$\boldsymbol{\zeta = 0.71}$		

13.5.2. Phugoid Motion

The phugoid motion of an airplane is a large period motion described by a large variation in air-speed, pitch angle and altitude. During this motion, the rate of the angle of attack was considered to be constant as well as the slope of the pitch rate. Leading to the following simplification of Equation 13.13.

$$\begin{bmatrix} C_{X_u} - 2\mu_c D_c & C_{X_\alpha} & C_{Z_0} & 0 \\ C_{Z_u} & C_{Z_\alpha} & 0 & 2\mu_c \\ 0 & 0 & -D_c & 1 \\ C_{m_u} & C_{m_\alpha} & 0 & C_{m_q} \end{bmatrix} \begin{bmatrix} \hat{u} \\ \alpha \\ \theta \\ \frac{q\bar{c}}{V} \end{bmatrix} = \underline{0} \tag{13.27}$$

In Equation 13.27 the derivatives are explained as follows:

- $\boldsymbol{C_{X_u}}$: is the drag due to the airspeed. It was approximated by using the relationship described in Equation 13.28.

$$C_{X_u} = -2 \cdot C_D \tag{13.28}$$

- $\boldsymbol{C_{X_\alpha}}$: is the drag due to the angle of attack, described in Equation 13.29[17]. It should be noted that in the equation the drag acts in the negative x-direction.

$$C_{D_\alpha} = \left(\frac{2 \cdot C_{L_1}}{\pi \cdot A \cdot e} \right) \cdot C_{L_\alpha} \tag{13.29}$$

  As described in section 12.4, the drag polar were considered to be parabolic, which validates that Equation 13.29 can be used. In Equation 13.29, C_{L_α} is the lift curve slope, e the oswald efficiency factor and C_{L_1} is the steady state lift coefficient.

- $\boldsymbol{C_{Z_u}}$: is the lift due to the airspeed. A value was found using Equation 13.30 [17]. During steady state flight it was assumed that the main wings are the sole contribution to the lift coefficient.

$$C_{L_u} = \frac{M^2 \cdot \cos \Lambda_{c/4}{}^2 \cdot C_{L_1}}{1 - M^2 \cdot \cos \Lambda_{c/4}{}^2} \tag{13.30}$$

  In Equation 13.30, M represents the Mach number. Since during cruise, loiter and landing a subsonic mach is obtained, it is excepted to use the equation for all three cases. Secondly the angle of sweep was taken at quarter chord.

- C_{m_u}: is the pitching moment due to the airspeed. It was calculated by using Equation 13.31 [17]. The same assumption for the lift coefficient was made as described above for steady state flight.

$$C_{m_u} = C_{L_1} \cdot \frac{\partial \bar{x}_{ac}}{\partial M} \tag{13.31}$$

The numerical values for the coefficients was found in Table B.1. To evaluate the handling qualities of this motion the damping ratio was computed using Equation 13.26 and in case of a level three handling quality the double-amplitude time has to be computed using Equation 13.32.

$$T_2 = -\frac{\log 2}{\xi_c} \cdot \frac{\bar{c}}{V} \tag{13.32}$$

The comparison, of the double amplitude time or the damping ratio of the phugoid, with the MIL-F-8785F specifications was performed in Table 13.9.

Table 13.9: Phugoid motion handling qualities

Flight Phase	**Level 1**	**Level 2**	**Level 3**
All categories	$\zeta \geq 0.04$	$\zeta \geq 0.0$	$T_2 \geq 55[s]$
Loiter	$\boldsymbol{\zeta = 0.92}$		
Cruise	$\boldsymbol{\zeta = 0.16}$		
Landing	$\boldsymbol{\zeta = 1.0}$		

From Table 13.9 it becomes clear that during all flight phases the desired handling quality of level 1 was met. However, it is still advised to make use of an auto-throttle. This not only is beneficial for the pilot workload but also for sustainability reasons since it reduces the amount of fuel used [32].

13.5.3. Eigenvalue Locations

This subsection investigates the eigenvalues of the motions in longitudinal direction, which are presented in Figure 13.3.

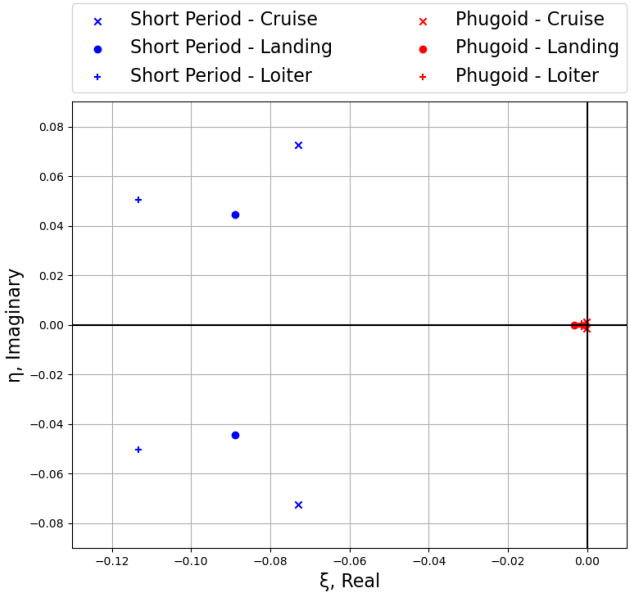

Figure 13.3: Representation of the eigenvalues of the motions in longitudinal direction

For the short period, represented by the color blue, the imaginary components of the eigenvalues are situated around the ±0.06 line. Furthermore, it can be seen that the imaginary part is largely related to the lift curve slope, C_{L_α}, leading to landing having the smallest imaginary part. This can also be seen in Table 13.8, where the damping ratio for the landing is the largest closely followed by the loiter. Secondly for

the phugoid, it was seen that the eigenvalues are located close to the origin. The real value for all three configurations is located at the negative side of the axis, meaning the phugoid will be damped, as shown in Table 13.9. Finally it must be noted that during landing the imaginary part of the eigenvalue is equal to zero, leading to a damping coefficient of 1.

13.6. Lateral Dynamic Stability

In this section the lateral dynamic stability is described. Three motions are described in the lateral direction: the aperiodic roll, the Dutch roll, and the aperiodic spiral.

The characteristic equation for the asymmetric motions are found in Equation 13.33. For computing the characteristic parameters, there are no changes with respect to the longitudinal motions, if the mean aerodynamic chord is replaced by the wing span. The eigenvalues for the lateral motions are indicated as λ_b. In order to give a first approximation, some assumptions were made:

- C_{Y_p} was set to zero since it is a relatively small derivative.
- C_{Y_r} is very small relative to $4\mu_b$ and hence neglected.
- The non-dimensional product of inertia K_{XZ} is relatively small compared to K_X^2 and K_Y^2 and thus omitted.

The first two assumptions are acceptable since the aircraft has a straight wing with a small dihedral[30].

$$\begin{bmatrix} C_{Y_\beta} + \left(C_{Y_{\dot\beta}} - 2\mu_b\right) D_b & C_L & C_{Y_p} & C_{Y_r} - 4\mu_b \\ 0 & -\frac{1}{2}D_b & 1 & 0 \\ C_{l_\beta} & 0 & C_{l_p} - 4\mu_b K_X^2 D_b & C_{l_r} + 4\mu_b K_X Z D_b \\ C_{n_\beta} + C_{n_{\dot\beta}} D_b & 0 & C_{n_p} + 4\mu_b K_{XZ} D_b & C_{n_r} - 4\mu_b K_Z^2 D_b \end{bmatrix} \begin{bmatrix} \beta \\ \varphi \\ \frac{pb}{2V} \\ \frac{rb}{2V} \end{bmatrix} = 0 \tag{13.33}$$

13.6.1. Aperiodic Rolling Motion

An aperiodic roll motion occurs when the aircraft has a roll rate such that the damping moment counteracts the rolling moment induced by the ailerons. This leads to a constant roll rate because no resultant rolling moment acts on the aircraft. A few assumptions were made, in order to compute the eigenvalue. The first assumption was that the aircraft only rolls about the longitudinal axis. Thus the columns corresponding the angle of sideslip and non-dimensional yaw rate disappeared from the equation. Secondly, from the first assumption it was concluded that the roll angle does not occur anymore in the remaining equation, which resulted in the approximate solution Equation 13.34 [30].

$$\left(C_{l_p} - 4\mu_b K_X^2 D_b\right) \frac{pb}{2V} = 0 \tag{13.34}$$

Replacing the differential operator D_b, resulted in the real eigenvalue:

$$\lambda_b = \frac{C_{l_p}}{4\mu_b K_X^2} \tag{13.35}$$

Where μ_b, the relative density for asymmetric motions, is computed in the same way as described in Equation 13.15. However, here the wing span was used instead of the mean aerodynamic chord. K_X^2 is the non-dimensional radius of gyration about the X-axis, which was computed the same way as in Equation 13.16. The moment of inertia I_{yy}, as given in section 5.3, was replaced by I_{xx} and the mean aerodynamic chord $\bar{c}$ was replaced by the wing span[30].

With the value of C_{l_p} given in subsection 13.4.2, the eigenvalue was computed. In order to check to what level of acceptability the aircraft is related to, the time constant had to be determined. Table 13.10 shows the maximum values for the roll-mode time constant per category and level. The time constant was determined by Equation 13.36 [30].

$$\tau = -\frac{1}{\lambda_b}\frac{b}{V} \tag{13.36}$$

In Table 13.10, the results are presented of the handling qualities for the aperiodic roll. As is seen, the aircraft complies with the level 1 flying quality for all three flight phases.

Table 13.10: Aperiodic roll motion handling qualities [31]

Flight Phase	**Level 1**	**Level 2**	**Level 3**
Category A	$\tau \leq 1.0$	$\tau \leq 1.4$	
Loiter	$\boldsymbol{\tau = 0.34}$		
Category B	$\tau \leq 1.4$	$\tau \leq 3.0$	$\tau \leq 10.0$
Cruise	$\boldsymbol{\tau = 0.18}$		
Category C	$\tau \leq 1.0$	$\tau \leq 1.4$	
Landing	$\boldsymbol{\tau = 0.58}$		

13.6.2. Dutch Roll Motion

When a Dutch roll occurs, the aircraft yaws and rolls in an oscillatory way, where the yaw lags the roll by a quarter period. It is a periodic mode in which the aircraft side-slips, yaws, and rolls. A few assumptions were made to obtain an approximation for the eigenvalues. Firstly, it was assumed to discard the rolling component. Consequently, φ and $\frac{pb}{2V}$ were set to zero, thus the corresponding columns in Equation 13.33 disappear. Since the rolling moment remains in balance, the rolling moment equation was omitted. Furthermore, the $C_{n_{\dot{\beta}}}$ and $C_{Y_{\dot{\beta}}}$ derivatives were neglected. This resulted in Equation 13.37.

$$\begin{bmatrix} C_{Y_\beta} - 2\mu_b D_b & -4\mu_b \\ C_{n_\beta} & C_{n_r} - 4\mu_b K_Z^2 D_b \end{bmatrix} \begin{bmatrix} \beta \\ \frac{rb}{2V} \end{bmatrix} = \underline{0} \tag{13.37}$$

Again, by replacing the differential operator, the eigenvalues were computed by finding the coefficients for the characteristic equation Equation 13.25.

$$\begin{aligned} A &= 8\mu_b^2 K_Z^2 \\ B &= -2\mu_b \left(C_{n_r} + 2K_Z^2 C_{Y_\beta}\right) \\ C &= 4\mu_b C_{n_\beta} + C_{Y_\beta} C_{n_r} \end{aligned} \tag{13.38}$$

Where K_Z^2 is the non-dimensional radius of gyration about the Z-axis, which was computed in the same way as K_X^2 and with the moment of inertia about the Z-axis, I_{zz}.

With the values for the stability derivatives, given in section 13.4, the eigenvalues were computed for the Dutch roll. In addition to the damping ratio ζ, the aircraft also needs to meet the requirement for the eigenfrequency ω_n. The values for these handling qualities, given in Table 13.11, are the minimum values that should be exceeded. The eigenfrequency was found by using Equation 13.39 [30].

$$\omega_n = \omega_0 \sqrt{1-\zeta} \tag{13.39}$$

$$\text{where} \quad \omega_0 = \sqrt{\xi^2 + \eta^2}\frac{V}{b} \tag{13.40}$$

For all three phases the aircraft complies with the level 1 handling qualities. However, it should be noted that the level 1 handling quality in category A, specifically for a ground attack phase, has a higher requirement when it comes to the damping ratio [31].

Table 13.11: Dutch roll motion handling qualities [31]

Flight Phase	Level 1	Level 2	Level 3
Category A	$\zeta \geq 0.19$, $\omega_n \geq 1.0$[rad/s]	$\zeta \geq 0.02$, $\omega_n \geq 0.4$[rad/s]	$\zeta \geq 0.0$, $\omega_n \geq 0.4$[rad/s]
Loiter	$\boldsymbol{\zeta = 0.19}$, $\boldsymbol{\omega_n = 2.0}$		
Category B	$\zeta \geq 0.08$, $\omega_n \geq 0.4$[rad/s]	$\zeta \geq 0.02$, $\omega_n \geq 0.4$[rad/s]	$\zeta \geq 0.0$, $\omega_n \geq 0.4$[rad/s]
Cruise	$\boldsymbol{\zeta = 0.16}$, $\boldsymbol{\omega_n = 4.2}$		
Category C	$\zeta \geq 0.08$, $\omega_n \geq 1.0$[rad/s]	$\zeta \geq 0.02$, $\omega_n \geq 0.4$[rad/s]	$\zeta \geq 0.0$, $\omega_n \geq 0.4$[rad/s]
Landing	$\boldsymbol{\zeta = 0.20}$, $\boldsymbol{\omega_n = 1.2}$		

13.6.3. Aperiodic Spiral Motion

A spiral motion occurs when an aircraft slowly rolls, yaws and sideslips, which will increase over time. In order to approximate the eigenvalue, following assumption was made. Since the motion is usually very slow, it was assumed that all linear and angular accelerations were negligible. This implied that $D_b\beta = D_b\frac{pb}{2V} = D_b\frac{rb}{2V} = 0$. This resulted in the simplified matrix given in Equation 13.41.

$$\begin{bmatrix} C_{Y_\beta} & C_L & 0 & -4\mu_b \\ 0 & -\frac{1}{2}D_b & 1 & 0 \\ C_{l_\beta} & 0 & C_{l_p} & C_{l_r} \\ C_{n_\beta} & 0 & C_{n_p} & C_{n_r} \end{bmatrix} \begin{bmatrix} \beta \\ \varphi \\ \frac{pb}{2V} \\ \frac{rb}{2V} \end{bmatrix} = \underline{0} \tag{13.41}$$

This characteristic equation reduced to first order due to the many zeros, of which the solution of the eigenvalue is given by:

$$\lambda_{b4} = \frac{2C_L\left(C_{l_\beta}C_{n_r} - C_{n_\beta}C_{l_r}\right)}{C_{l_p}\left(C_{Y_\beta}C_{n_r} + 4\mu_b C_{n_\beta}\right) - C_{n_p}\left(C_{Y_\beta}C_{l_r} + 4\mu_b C_{l_\beta}\right)} \tag{13.42}$$

The values given in section 13.4 for the stability derivatives and the lift coefficient calculated with Equation 12.8 resulted in the real eigenvalue for the spiral. In order to state the level of handling quality of the aircraft for the roll mode, the time to double amplitude was calculated by using Equation 13.43 [30]. This value must exceed the minimum values per level given in Table 13.12.

$$T_2 = \frac{\ln(2)}{\lambda_b}\frac{b}{V} \tag{13.43}$$

Table 13.12 shows the handling quality levels for the three phases. Only during cruise the aircraft reaches level 1. For the loiter and landing phase, level 3 and no level were reached, respectively. This is not desirable, hence a Proportional-Integral-Derivative (PID) controller was designed, as described in section 13.7, in order to make sure the aircraft can safely operate during those phases.

Table 13.12: Aperiodic spiral motion handling qualities [31]

Flight Phase	Level 1	Level 2	Level 3	> Level 3
Category A & C	$T_2 \geq 12$[s]	$T_2 \geq 8$[s]	$T_2 \geq 4$[s]	
Loiter			$\boldsymbol{T_2 = 5.0[s]}$	
Landing				$\boldsymbol{T_2 = 1.8[s]}$
Category B	$T_2 \geq 20$[s]	$T_2 \geq 8$[s]	$T_2 \geq 4$[s]	
Cruise	$\boldsymbol{T_2 = 70.0[s]}$			

13.6.4. Eigenvalue Locations

This subsection investigates the eigenvalues of the motions in lateral direction, which are presented in Figure 13.3.

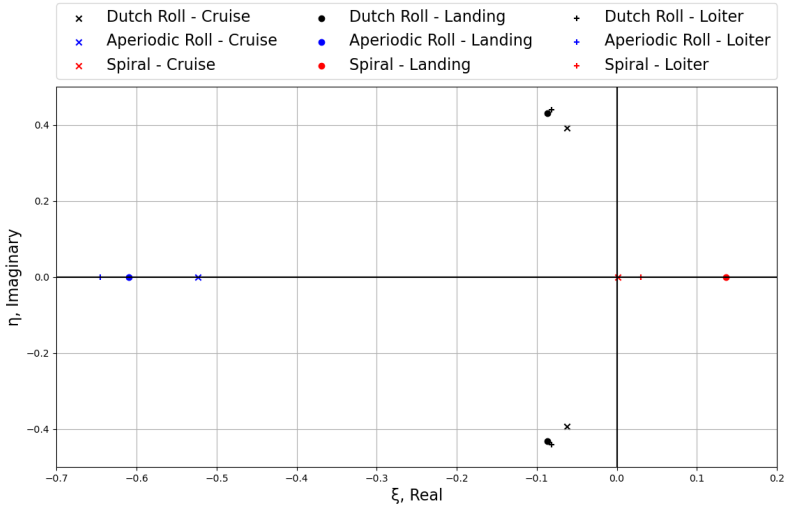

Figure 13.4: Representation of the eigenvalues of the motions in lateral direction

For the Dutch roll mode, represented in black, it becomes clear that how larger the absolute value of the imaginary part is, the sooner the motion will damp out. This is can also be concluded from Table 13.11, in which it can be see that the dutch roll damping coefficient is lowest during cruise. Secondly, for the aperiodic roll, represented in blue, the real eigenvalue is located relatively far from the origin. This leads to a higher time constant as can be seen in Table 13.10. The fact that the time constant is highest for the landing phase, is related to the lower airspeed. Finally for the aperiodic spiral, represented in red, it was observed that the eigenvalues are situated on the positive side of the real axis, leading to an unstable motion. A more positive eigenvalue, as can be seen for the landing phase, leads to a more unstable spiral. When the spiral is unstable, it is important that the double amplitude time is sufficiently large, as shown for the boundary values in Table 13.12.

13.7. PID Controller for Aperiodic Spiral

In order to support the pilots when entering an aperiodic spiral during flight, a PID controller was designed. Since a spiral is caused by a change in bank angle of the aircraft due to a disturbance, the PID controller supports the ailerons to counteract the roll rate and bank angle, and thus the spiral motion.

In Figure 13.5 the block scheme of the PID controller is shown as a double closed loop system. The feed forward path starts with a step input, which may be a gust or input from the pilot for example that changes the bank angle of the aircraft, starting a roll moment. Next is the PID controller, which uses the three gain values, the proportional, integral, and derivative, which gives an input to the second PID controller. This second PID controller then gives an command to the aileron actuators to deflect to a certain angle. The actuator then applies the aileron deflection, which will be applied to the aircraft. Subsequently, a corresponding bank angle and roll rate come from the aircraft dynamics as a result. Finally, two feedback paths were applied, where the outer loop gives feedback for the bank angle and the inner loop for the roll rate. The inner loop was designed to let the PID controller converge faster. Within both feedback paths, a sensor was used. It was assumed that these sensors have a transfer function equal to 1, meaning that the measurement of the back angle or roll rate by the PID controller is perfect.

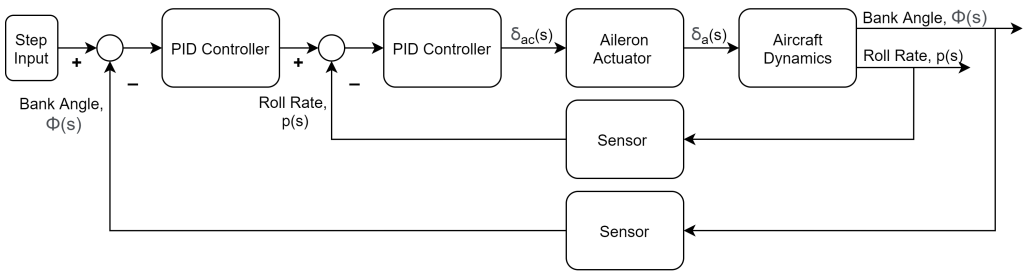

Figure 13.5: Block scheme of the PD controller for the bank angle and roll rate.

For simplicity, a first order system was made for the actuator aileron, where the transfer function was determined by the time constant τ. This value was assumed to be between 0 and 0.5, where a larger time constant represents a slower response [33]. The value for τ was then put in Equation 13.44.

$$\frac{\delta_a(s)}{\delta_{ac}(s)} = \frac{1}{\tau s + 1} \tag{13.44}$$

In the same manner the transfer function for the aircraft dynamics block was found by using the time constant τ which was calculated for stall conditions in Equation 13.36 with the eigenvalue from the aperiodic roll λ_b. With the aileron deflection from the aileron actuator block as input and the value for τ in Equation 13.44, the bank angle, ϕ, and roll rate, p, were computed.

After the transfer functions were determined, the gains of the PID controllers were tuned. Iterations were performed while using different terms of the PID controllers. It was found that with two PD controllers, the step responses converged fastest without overshooting too much. Adding the integral term, resulted in a slightly lower overshoot, but also a slower step response. In Figure 13.6, the step responses with different time constants for the aileron actuator are plotted. It can be seen that for a higher actuator time constant, the controller represents a slower response.

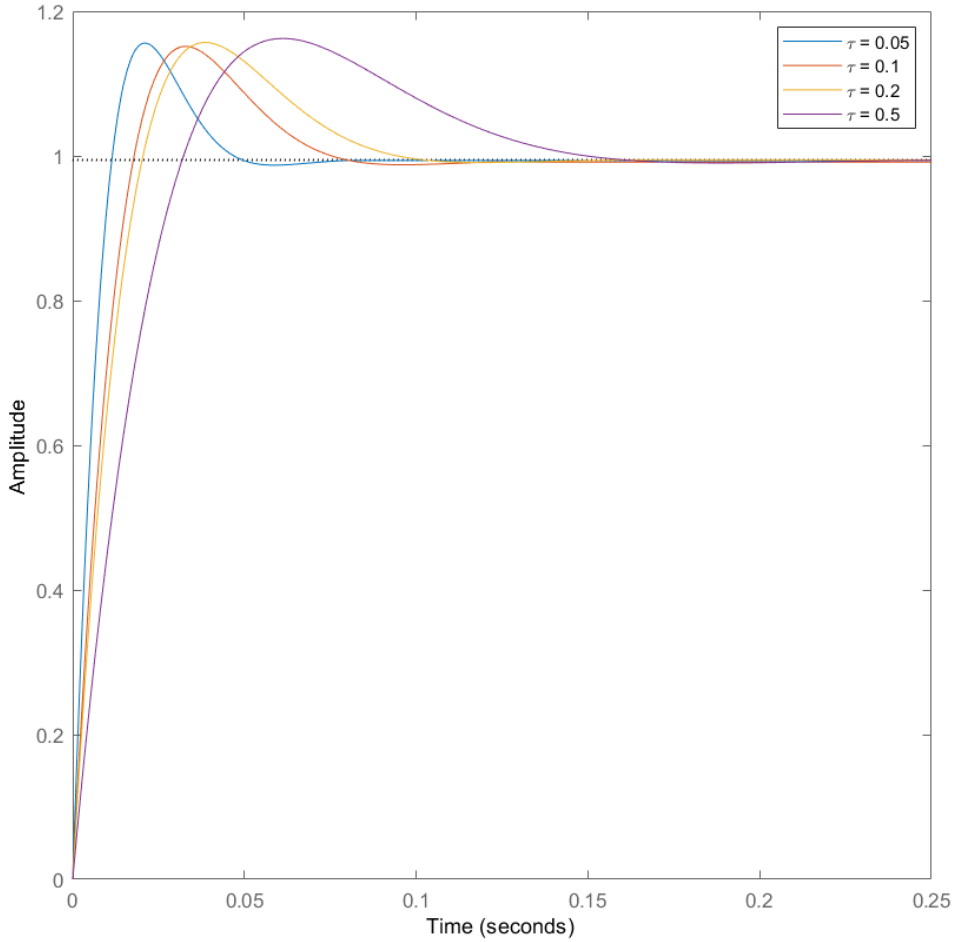

Figure 13.6: Step response PD controller for different actuator time constants

It can be concluded that this PD controller will be able to make sure to counteract a roll moment within a short amount of time. Resulting in a reduced workload for the pilot, since the aircraft will not get into a spiral. However, the PD controller is not finished as of yet. It is a simplified controller that has to be tested in the future. Additionally it was assumed that the sensor gives a perfect measurement of the roll rate and

bank angle. In practice, this is not the case and probably a rate-integrating gyroscope will be used. This will result in a slower response of the system.

13.8. Control Derivatives due to Elevator, Aileron and Rudder

To complete the stability and control analysis, the control derivatives of the control surfaces had to be determined. These derivatives were calculated using the equations as provided by Roskam [17]. Only elevators, ailerons, and rudders had to be evaluated, since no other control surfaces are implemented on the aircraft. For all control derivatives, they were analyzed for cruise configuration and landing configuration. At the end of each subsection, the resulting control derivatives are given.

13.8.1. Elevator Control Derivatives

In this subsection, the method to compute the control derivative due to flap deflection are given with the final results.

Equation 13.45 shows the equation for the drag due to elevator derivative. Equation 13.46 shows the equation for the lift due to elevator derivative. Equation 13.47 shows the equation for the moment due to elevator derivative.

$$C_{D_{\delta_r}} = \alpha_{\delta_e} \cdot C_{D_{i_h}} \quad (13.45) \qquad C_{L_{\delta_e}} = \alpha_{\delta_e} \cdot C_{L_{i_h}} \quad (13.46) \qquad C_{m_{\delta_e}} = \alpha_{\delta_e} \cdot C_{m_{i_h}} \quad (13.47)$$

Table 13.13: Control derivatives due to elevator deflection

Configuration	$C_{D_{\delta_e}}$ [+]	$C_{L_{\delta_e}}$ [+]	$C_{m_{\delta_e}}$ [-]
Cruise	0.522	1.100	-1.348
Landing	0.522	0.956	-1.348

13.8.2. Aileron Control Derivatives

In this subsection the control derivatives with respect to the aileron deflection in cruise and landing conditions are discussed, and their final values are presented.

- $\boldsymbol{C}_{Y_{\delta_a}}$: is the side force due to aileron deflection. This is neglected, since the ailerons are not in close proximity of the vertical tail.
- $\boldsymbol{C}_{l_{\delta_a}}$: is the rolling moment due to aileron deflection. A positive aileron deflection should result in a rolling motion in the negative direction.
- $\boldsymbol{C}_{n_{\delta_a}}$: is the yawing moment due to aileron deflection. A positive aileron deflection should result in a positive yawing moment.

$C_{l_{\delta_a}}$ was calculated using equation Equation 13.48. Here $(C_{l_\delta})_{\text{left}}$ and $(C_{l_\delta})_{\text{right}}$ are the contributions from the left and the right aileron respectively.

$$C_{l_{\delta_a}} = (C_{l_\delta})_{\text{left}} + (C_{l_\delta})_{\text{right}} \quad (13.48)$$

Equation 13.49 shows the equation used for calculating the $C_{n_{\delta_a}}$ where C_{L_W} is the lift curve slope of the wing and K_a is a correlation constant for the yawing moment due to aileron deflection as presented by Roskam [17].

$$C_{n_{\delta_a}} = K_a C_{L_W} C_{l_{\delta_a}} \quad (13.49)$$

In Table 13.14 the final values of the control derivatives due to aileron deflection are given. $C_{l_{\delta_a}}$ and $C_{n_{\delta_a}}$ have signs as expected, which means the aircraft reacts to an aileron deflection as conventional.

Table 13.14: Control derivatives due to aileron deflection

Configuration	$C_{Y_{\delta_a}}$ [+]	$C_{l_{\delta_a}}$ [-]	$C_{n_{\delta_a}}$ [+]
Cruise	0	-0.401	0.009
Landing	0	-0.401	0.103

13.8.3. Rudder Control Derivatives

In this subsection, the control derivative due to a positive rudder deflection is given. In this section the same convention as shown in Figure 13.1 and Figure 13.2 was used. Therefore, a positive rudder deflection results in a negative yawing moment.

- $\boldsymbol{C_{Y_{\delta_r}}}$: is the side force due to rudder deflection. When the rudder is deflected positively, the vertical tail surface experiences an angle of attack. This causes a positive force in the y-direction.
- $\boldsymbol{C_{l_{\delta_r}}}$: is the rolling moment due to rudder deflection. A positive value means that a positive rudder deflection, causes a positive rolling moment.
- $\boldsymbol{C_{n_{\delta_r}}}$: is the yawing moment due to rudder deflection. A positive rudder deflection should result in a yawing moment in the negative direction.

$C_{Y_{\delta_r}}$ was calculated using Equation 13.50 with constants k' and K_b in combination with the lift effectiveness and the ratio of the area of the vertical tail and the wing.

$$C_{Y_{\delta_r}} = \left(C_{L_{\alpha_v}}\right)\left(k' K_b\right)\left(\frac{c_{l_\delta}}{(c_{l_\delta})_{\text{theory}}}\right)(c_{l_\delta})_{\text{theory}}\left(\frac{S_v}{S}\right) \tag{13.50}$$

Equation 13.51 gives $C_{l_{\delta_r}}$, which is dependent on $C_{Y_{\delta_r}}$ and the normalized position of the aerodynamic center of the vertical tail.

$$C_{l_{\delta_r}} = \left(\frac{z_v \cos(\alpha) - l_v \sin(\alpha)}{b}\right) C_{Y_{\delta_r}} \tag{13.51}$$

Equation 13.52 is similar to Equation 13.51. However, the horizontal distance is considered instead of the vertical distance.

$$C_{n_{\delta_r}} = -\left(\frac{l_v \cos(\alpha) + z_v \sin(\alpha)}{b}\right) C_{y_{\delta_r}} \tag{13.52}$$

The resulting values in Table 13.15 are positive/negative according to the description given. Therefore, the aircraft reacts as expected to a rudder deflection and is stable for a δ_r contribution.

Table 13.15: control derivatives due to rudder deflection

Configuration	$C_{Y_{\delta_r}}$ [-]	$C_{l_{\delta_r}}$ [-]	$C_{n_{\delta_r}}$ [-]
Cruise	1.586	0.197	-0.578
Landing	1.271	0.022	-0.489

13.9. Sensitivity Analysis

This section describes the sensitivity analysis of the dynamic motions in cruise phase. Each of the changed parameters were performed using the one factor at a time (OFAT) approach. Firstly the effect of the dihedral angle was investigated by increasing it from 3° to 6°. Secondly the vertical tail area was increased by 50%. Thirdly the effect of the weight was investigated, to see the handling qualities when no armament is attached. Fourthly aspect ratio of the wing was increased from 7 tot 8. Finally a quarter chord sweep of 20° was applied to the main wing.

Table 13.16: Sensitivity analysis stability and control in cruise phase

Parameter	Short period	Phugoid	Aper. roll	Dutch roll	Spiral
No changes	$\boldsymbol{\zeta = 0.71}$	$\boldsymbol{\zeta = 0.16}$	$\boldsymbol{\tau = 0.18}$	$\boldsymbol{\zeta = 0.16, \omega_n = 4.2}$	$\boldsymbol{T_2 = 70[s]}$
Increase Γ by 3°	$\zeta = 0.71$	$\zeta = 0.16$	$\tau = 0.18$	$\zeta = 0.16$, $\omega_n = 4.2$	$T_2 = 190$ [s]
Decrease S_v by 50%	$\zeta = 0.73$	$\zeta = 0.16$	$\tau = 0.18$	$\zeta = 0.16$, $\omega_n = 2.3$	$T_2 = 135$ [s]
Weight without stores	$\zeta = 0.72$	$\zeta = 0.18$	$\tau = 0.18$	$\zeta = 0.16$, $\omega_n = 4.2$	$T_2 = 97$ [s]
AR wing increase by 1	$\zeta = 0.72$	$\zeta = 0.16$	$\tau = 0.17$	$\zeta = 0.16$, $\omega_n = 4.2$	$T_2 = 74$ [s]
$\Lambda_{c/4}$ increase to 20°	$\zeta = 0.89$	$\zeta = 0.17$	$\tau = 0.18$	$\zeta = 0.15$, $\omega_n = 4.7$	$T_2 = 67$ [s]

When looking at the results of the sensitivity analysis, no big changes occurred for the short period motion. Only when increasing the quarter chord sweep, the damping ratio increases. For all cases this motion stayed in flying quality level 1. The same applies for the phugoid and aperiodic roll, no big changes were found for all cases. For the Dutch roll, in two cases there was a relatively large change. Firstly, when the dihedral angle was increased, the eigenfrequency lowered, which is not beneficial for the flying quality. However, it was still well above the requirement for level 1. Secondly, when the quarter chord sweep was increased, the eigenfrequency increased, which was beneficial for the flying quality.

In general, the sensitivity analysis showed that the aircraft was well designed for these four motions. However, the sensitivity analysis showed some interesting cases for the aperiodic spiral. For almost every case, the time to double amplitude increased, except for the case where sweep was increased. Since the spiral was not in the desired level of flying quality for the loiter and landing phase, these changes were not implemented into the design as of yet for some require a new iteration process. This must be looked into in the future.

13.10. Verification and Validation

A first step of verifying the results for the derivatives obtained, was by inspection. Chapter 11 of Roskam part VI provides examples of stability derivatives [17]. An example similar to the design of the A-20 *Chimera* was used to make a first comparison. Both the sign of the derivative and the order of magnitude were inspected to gain a first insight whether the result could be trusted. Secondly, the python program that is used to calculate the eigenvalues of the lateral and longitudinal motions, was verified by filling in the example values provided in the Flight dynamics reader [30]. The eigenvalue, and the damping ratio of both the short period motion as the phugoid, were compared to the results provided in the reader.

13.11. Requirement Compliance

Table 13.17 shows which requirements were complied with by a checkmark if it is and an empty space if not. Note that the checkmarks with a [*] do have an extra explanation below the table.

Table 13.17: List of requirements for stability and control

Requirement ID	Description	Method of compliance	Compliance
Stability and Control			
LAA-SAC-STA-1.1	The aircraft shall be able to stabilize itself stick free.	subsection 8.4.2	✓*
LAA-SAC-STA-1.2	The aircraft shall be longitudinally static stable for all phases of the mission profile.	Table 13.4	✓
LAA-SAC-STA-1.3	The aircraft shall be laterally static stable for all phases of the mission profile.	Table 13.6, 13.5 and 13.7	✓
LAA-SAC-DYN-1.1	The aircraft shall have level 1 handling qualities for short period at all phases of the mission profile	Table 13.8	✓

Table 13.17: List of requirements for stability and control

Requirement ID	Description	Method of compliance	Compliance
LAA-SAC-DYN-1.2	The aircraft shall have level 1 handling qualities for phugoid period at all phases of the mission profile	Table 13.9	✓
LAA-SAC-DYN-1.3	The aircraft shall have level 1 handling qualities for aperiodic roll at all phases of the mission profile	Table 13.10	✓
LAA-SAC-DYN-1.4	The aircraft shall have level 1 handling qualities for dutch roll at all phases of the mission profile	Table 13.11	✓
LAA-SAC-DYN-1.5	The aircraft shall have level 1 handling qualities for aperiodic spiral at all phases of the mission profile	Table 13.12	✓*
Performance			
LAA-PER-STK-1.1	The maximum stick forces shall not exceed 133 N (30 lbs).	section 13.11	✓*

Requirement LAA-PER-STK-1.1 was not complied with, since this was not evaluated. The reason why this was not checked, is due to the application of a fly-by-wire system. This implied that the pilot provides a stick-input, which is not directly proportional to the elevator deflection. Hence, the maximum stick force has become less important to what needs to be achieved.

Requirement LAA-SAC-STA-1.1 was indirectly met due to the 5% stability margin, mentioned in section 8.4, which takes into account the stick-free stability with respect to stick-fixed stability.

Requirement LAA-SAC-DYN-1.5 was complied with after the design of a PID controller. Since the aperiodic spiral did not comply with the desired level 1 handling quality at first during the landing and loiter phase, a PID controller was designed in section 13.7. This PID controller is not entirely finished as of yet, however, it was proven to work. For a future recommendation, it is necessary to continue with this design.

14
Aircraft Performance Analysis

When designing an attack aircraft, performance is a key feature. Hence, a thorough analysis was executed to find the payload range and payload combat radius diagram, the flight envelope and several performance diagrams. First, the payload range and payload combat radius diagram are discussed, after which the method to compute the load factor envelope is elucidated and the diagram is given, then the specific excess power plots for several flight configurations are given. Finally the chapter will end with a verification of the methods and some future recommendations.

14.1. Range Diagrams

This section includes the approach and the results for both payload range and payload combat radius diagrams.

14.1.1. Payload Range Diagram

The range of an aircraft is heavily influenced by the payload and fuel on board. Therefore, to represent the relationship between these variables, a payload-range diagram was constructed In Figure 14.1a. Point A illustrates the range of the aircraft with zero fuel weight and maximum payload. As the fuel weight increases so does the range of the aircraft, moving horizontally right from point A.
Once point B has been reached, the aircraft is at MTOW with maximum payload and maximum fuel weight. In order to increase the range further, the payload has to be reduced while maintaining maximum fuel weight.
Point C shows the range at 60% payload capacity, which is required for the ferry mission listed in the request for proposal (RFP). The graph shows that the aircraft outperforms the requirement. This is due to the fact that the payload range diagram includes the range credits from the loiter phase of the flight. Therefore, in subsection 14.1.2 the payload combat radius diagram is displayed, which gives a more accurate representation of range during mission. Lastly, point D shows the maximum range without payload.

14.1.2. Payload Combat Radius Diagram

Similar to the payload range diagram mentioned in subsection 14.1.1, the combat radius is heavily influence by the payload and fuel on board. The payload combat radius diagram represent the relationship between these variables, which is shown in Figure 14.1b. However, unlike the payload range diagram, the payload combat radius diagram has excluded the 4 hours and 45 minutes loiter range credit. This is because the aircraft remains in the same region during the loiter phase. Furthermore, the combat radius is a more accurate representation of range during mission, since during operation the aircraft has travel to and from the battlefield. Therefore, the combat radius was determined by dividing the range by 2.

Similar to payload range diagram, point A represents the combat radius of the aircraft with zero fuel weight and maximum payload. Furthermore, as fuel weight increases so does the combat radius of the aircraft. Moreover, point B illustrates the combat radius when the aircraft is at MTOW with maximum payload and fuel weight. In addition, point C shows the maximum combat radius without payload. Lastly, the vertical line represents the design mission combat range as set by requirements, which can be found in section 2.4.

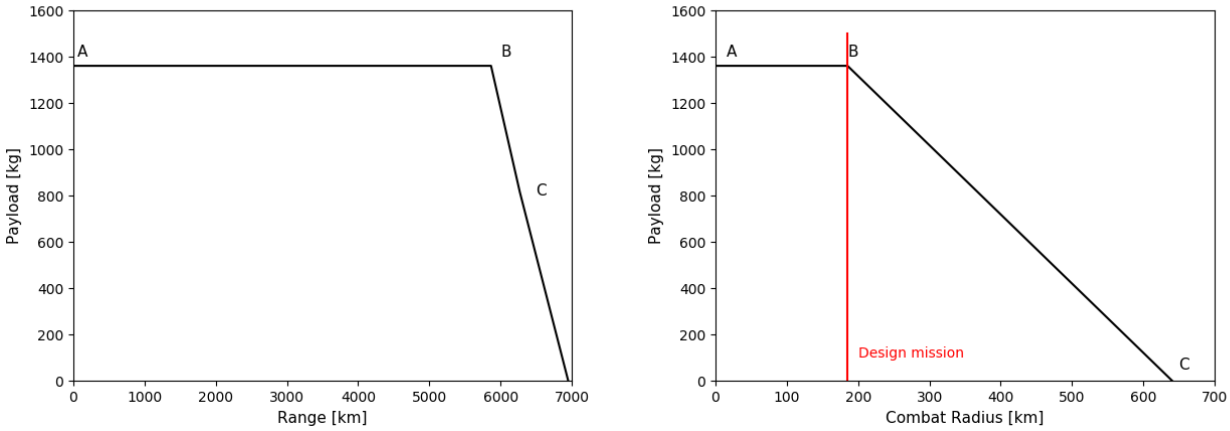

(a) Payload range diagram.

(b) Payload combat radius diagram excluding range credit.

Figure 14.1: Range diagrams for the A-20 Chimera.

14.2. Load Factor Envelope

The load factor envelope is a graph which provides information about the combination of speeds and load factors, which the aircraft should be able to sustain. The diagram is build up from two sources of load factors. The first load factors are due to maneuvering, which is explained in the first subsection. The second source of a load factor are gust loads, which are discussed in the second subsection. Finally, the flight envelope will be presented in Figure 14.2.

14.2.1. Maneuverability

When an aircraft is maneuvering it usually accelerates in a certain direction as well. This acceleration is often described in g-forces. For an aircraft in a symmetrical flight at constant speed the g-force is equal to one. However, it should be able to withstand higher loads while the aircraft is maneuvering, of which the highest load the aircraft has to withstand is the limit load. For an attack aircraft the MIL-A-8861 specifies that the design limit load of an attack aircraft should be 7.5. Hence, this number was used in the construction of the maneuvering diagram. [34]

To construct the line from 0 to A in Figure 14.2, Equation 14.1 was used [35], where V_{MS} is the minimum stall speed in clean configuration, and V the equivalent airspeed (EAS) of the aircraft. However, due to structural limits the load factor can't be allowed to keep increasing, hence a n_{max} has to be chosen. As mentioned before a limit load of 7.5 from the MIL-A-8861 standard was chosen [34]. Using Equation 14.2, the speed at which the curve should stop was determined.

$$n = \frac{V^2}{V_{MS}^2} \tag{14.1}$$

$$V_A = V_{MS}\sqrt{n_1} \tag{14.2}$$

The line from 0 to H was determined using the same method. However, a smaller negative limit load was used as can be seen in Figure 14.2. From MIL-A-8861 it was determined to be -3 [34]. Crossing the curves 0 to A or 0 to H would result in stall, hence the vertical line in the beginning of the envelope. This vertical line represents the stall speed at 1g.

Point C on the V-n diagram represents the cruise speed, this speed was determined during the Class 1 sizing to be 201.3 m/s. When converted to EAS the cruise speed becomes 173.0 m/s. Point D is the design diving speed, which was calculated using MIL-A-8860 and Anderson [34, 36]. In the MIL-A-8860 document it is stated that the dive speed needs to be 120% of the maximum achievable speed. The maximum speed was calculated by equating the thrust available to the thrust required. This led to a maximum cruise speed (at cruise altitude) of 230 m/s or an EAS of 170 m/s, which then resulted in a dive speed of 240 m/s (EAS). For point F in the diagram, the cruise speed is used, from which a straight line is drawn to point E. Which was determined by the limiting gust loads, which will be discussed in the following subsection.

The small red flight envelope in Figure 14.2 is the load factor envelope for the aircraft when flaps are extended. The lines were made using the same method as explained above. However, for a flap extended flight the aircraft has a lower limit load. Which is specified by MIL-8860B to be 2. The limit speed for flap extended flight was specified to be $1.75V_s$, using the same document. [34]

14.2.2. Gust Loads

When flying through turbulent air, symmetrical vertical gusts subject the aircraft. The immediate effect due to this is an increase or decrease in the angle of attack. This effect will change the load factor and generate a gust load. The gust load might exceed the maneuver load and thus alter the V-n diagram. The gust load factors were computed by Equation 14.3, where K_w is the gust alleviation factor given in Equation 14.4 [35]. Since gust velocity profiles are not sharp-edged but more uniformly shaped, the gust alleviation factor accounts for this. It is based on the mass ratio, given in Equation 14.5 for subsonic speeds [27, 35].

$$n = 1 \pm K_w \frac{dC_L}{d\alpha} \frac{\rho_0 U_e V_e S}{2W} \tag{14.3}$$

$$K_w = \frac{0.88\mu_g}{5.3 + \mu_g} \tag{14.4}$$

$$\mu_g = \frac{2W}{\rho g \bar{c} \frac{dC_L}{d\alpha} S} \tag{14.5}$$

According to MIL-A-8861B, the aircraft must be able to withstand particular positive and negative gust velocities [34]. As is shown in Figure 14.2, three different positive and negative gust velocities (gray dotted lines) were considered. Gust velocities at the design cruising speed were assumed to be 15 m/s equivalent speed at altitudes between sea level and 20 000 ft. From 20 000 ft to 50 000 ft, these gust velocities were reduced linearly to 7.5 m/s. For the design driving speed, positive and negative gusts of 8 m/s were also considered at altitudes between sea level and 20 000 ft. Lastly, a gust velocity of ±20 m/s was considered for rough air gusts at altitudes between sea level and 20 000 ft. This maximum gust velocity determines the design speed for maximum gust velocity V_B, which is the speed that causes the aircraft to stall at the assumed maximum gust velocity. [35]

When looking at Figure 14.2, one can see that the gust loads limit the flight envelope only for the negative gust velocity of 7.5 m/s, i.e. point E.

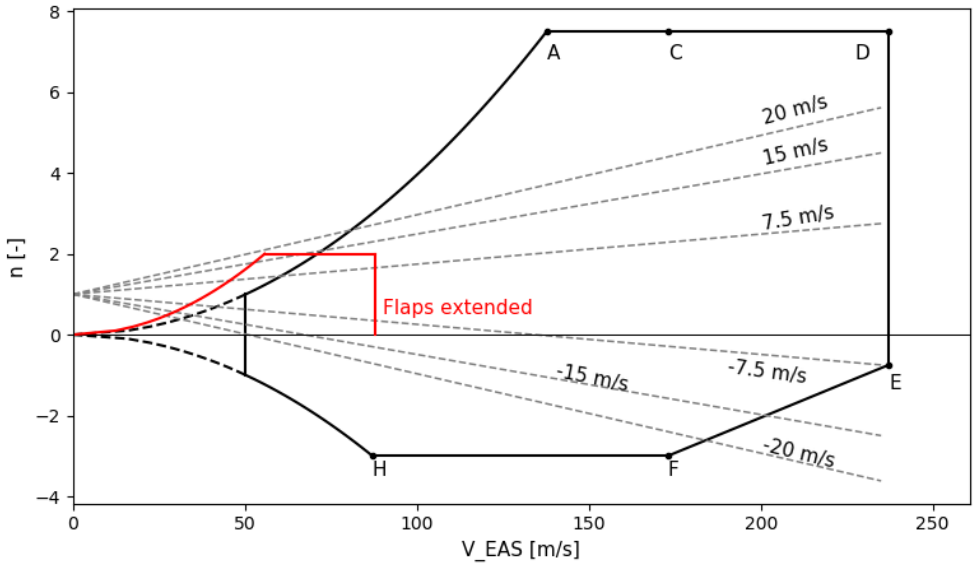

Figure 14.2: V-n diagram for the designed aircraft.

14.3. Specific Excess Power Diagrams

In order to evaluate the performance of the aircraft, a 'specific excess power diagram' was made. In the diagram the altitude is shown on the vertical axis, while the true airspeed is shown on the horizontal axis. On

this plot the specific excess power (P_s) is given as a contour plot. The specific excess power is the excess power divided by the weight of the aircraft, as defined in Equation 14.6. P_s was used for acceleration, to climb or for sustained turns, all for a specified weight, thrust and configuration. The configuration determines the maximum lift coefficient and zero-lift drag coefficient.

14.3.1. Approach

For the specific excess power the thrust and drag are to be calculated, both depend on the altitude. The thrust available, T_{av}, dependents on the air density and is calculated in Equation 14.7 and Equation 14.8 for the troposphere and tropopause, as defined in the International Standard Atmosphere (ISA), respectively [35, p.126-127].

$$P_s = \frac{T_{av} - D}{W} * V \quad (14.6) \qquad \frac{T_{av}}{T_0} = \left[\frac{\rho}{\rho_0}\right]^{0.75} \quad (14.7) \qquad \frac{T_{av}}{T_s} = \frac{\rho}{\rho_s} \quad (14.8)$$

In order to calculate the drag, the drag coefficient was calculated from the zero-lift drag, as calculated in chapter 12, and lift coefficient which is calculated for the speed, air density and specified weight, as can be seen in Equation 14.9 and Equation 14.10.

Additionally, the stall speed was calculated for each altitude and the $C_{L_{max}}$ as per the specified configuration, as can be seen in Equation 14.11.

$$C_L = \frac{2W}{\rho V^2 S} \quad (14.9) \qquad C_D = C_{D_0} + \frac{C_L^2}{\pi A R e} \quad (14.10) \qquad V_s = \sqrt{\frac{2W}{\rho C_{L_{max}} S}} \quad (14.11)$$

For the different flight stages, the configuration data is given in Table 14.1.

Table 14.1: Configuration for different flight stages

	W [kN]	$C_{L,max}$ [-]	C_{D_0} [drag counts]	V [m/s]	h [m]
Take off	130	2.0	760	61	1 800
Cruise, stores	130	1.6	280	200	3 000
Loiter, stores	120	1.6	280	86	910
Landing	100	2.6	1200	50	1 800

14.3.2. Results

From the configurations and equations given in the previous section, the specific excess power diagrams can be made. In this section a brief description of the a specific excess power diagram is given, after which a table with results of all configurations is given.

In Figure 14.3a the specific excess power diagram of the take off configuration is given. The stall speed for the specific configuration is indicated with a blue line, also known as the lift limit line. Values with negative specific excess power and the area left of the lift limit line are both grayed out, as there is no sustained flight possible in these areas. The red dot in the excess power plots represent the speed and altitude for each configuration, as given in Table 14.1.

In Table 14.2 the results for each flight stage are given. In the table the specific excess power at the design point is given, the maximum P_s and the speed of this maximum P_s is given as well. The last two columns give the stall speed and maximum speed at the altitude given in Table 14.1. The P_s diagrams of the take off, cruise, loiter and landing configurations are given in Figure 14.3a, Figure 14.3b, Figure 14.3c, and Figure 14.3d, respectively.

Table 14.2: Results from the specific excess diagrams for the different flight stages

	P_s [m/s]	$P_{s,max}$ [W/N]	$V_{Ps\ max}$ [W/N]	V_{stall} [m/s]	V_{max} [m/s]
Take off	9.7	12	86	51	140
Cruise, stores	13	23	140	59	230
Loiter, stores	22	28	130	52	230
Landing	11	13	68	39	110

14.4. Turn Rate Diagrams

From the performance graphs as explained above, the specific excess power for a given altitude and speed combination can be determined. From this the optimal climb rate of the aircraft can be found. However, excess power can also be used for turning. To investigate what the turn performance of the A-20 Chimera is, two excess power plots were made as shown in Figure 14.4.

The red lines in Figure 14.4 are the specific excess power lines, ranging from -40 [m/s] at the top, to 25/20 [m/s] at the bottom, cruise with stores and loiter with stores respectively. The green lines represent constant load factor lines, where the x-axis represents the 1-g line. The blue lines represent the turn radius for the given combination of speed and turn rate. The left black line represents the stall speed at different turn rates, the left black line is determined by the maximum speed of the aircraft.

The stall line (left black line), the stall speed for a given load factor was calculated using Equation 14.2. With the obtained speed the corresponding turn rate, ω, was calculated using Equation 14.12. The power limit line, the vertical black line, was obtained from the calculations shown in the precious section.

$$\omega = \frac{57.3 \cdot g}{V}\sqrt{n^2 - 1} \tag{14.12}$$

$$R = \frac{\omega}{V} \tag{14.13}$$

The constant load factor lines were calculated using Equation 14.12, where the load factor was kept constant while the speed varied. Using the ultimate load factor found in subsection 14.2.1, the corner velocities were found to be 160 m/s for cruise configuration, as seen in Figure 14.4a, and 142 m/s for the loiter configuration, as seen in Figure 14.4b.

The turn radius lines were found using Equation 14.13. For the specific excess power lines first the turn rate was found for a given combination of load factor and speed. For the same values of load factor and speed the specific excess power was calculated, using Equation 14.6. Where the drag was multiplied with the load factor. This resulted in the obtained contour lines, shown in Figure 14.4.

It was chosen to plot both loiter and cruise (in stored condition), as these are the main flight stages in which the maneuverability is most important.

14.5. Verification and Validation

For both the flight envelope analysis and the performance diagram analysis tools were created to calculate and plot the needed values. Hence a verification of these tools was carried out, to make sure the obtained values and information was correct.

For both tools the first steps taken to verify, were aimed to find syntax errors in the plugged in equations. First step taken to find these errors was to have a sanity check of the output values. Second step was to take a point for which the values were hand calculated and checked if these values compared to the output values for the same point. These steps were assumed to be enough to verify the plugged in equations.

To validate the obtained plots, aircraft data would be needed, combined with their performance diagram. However, the combination of both data and plots were hard to find. Therefore the plots have not been validated with a real life case. A future recommendation would be to obtain this data and complete a thorough validation of the tools and methods used. Another future recommendation would be to create a turn rate versus speed plots. These plots would provide information about the combination of speed, g-loads and

turn-rates at specific excess power levels. From these graphs it could be made clear if the aircraft would provide a sufficient turn rate in different scenarios.

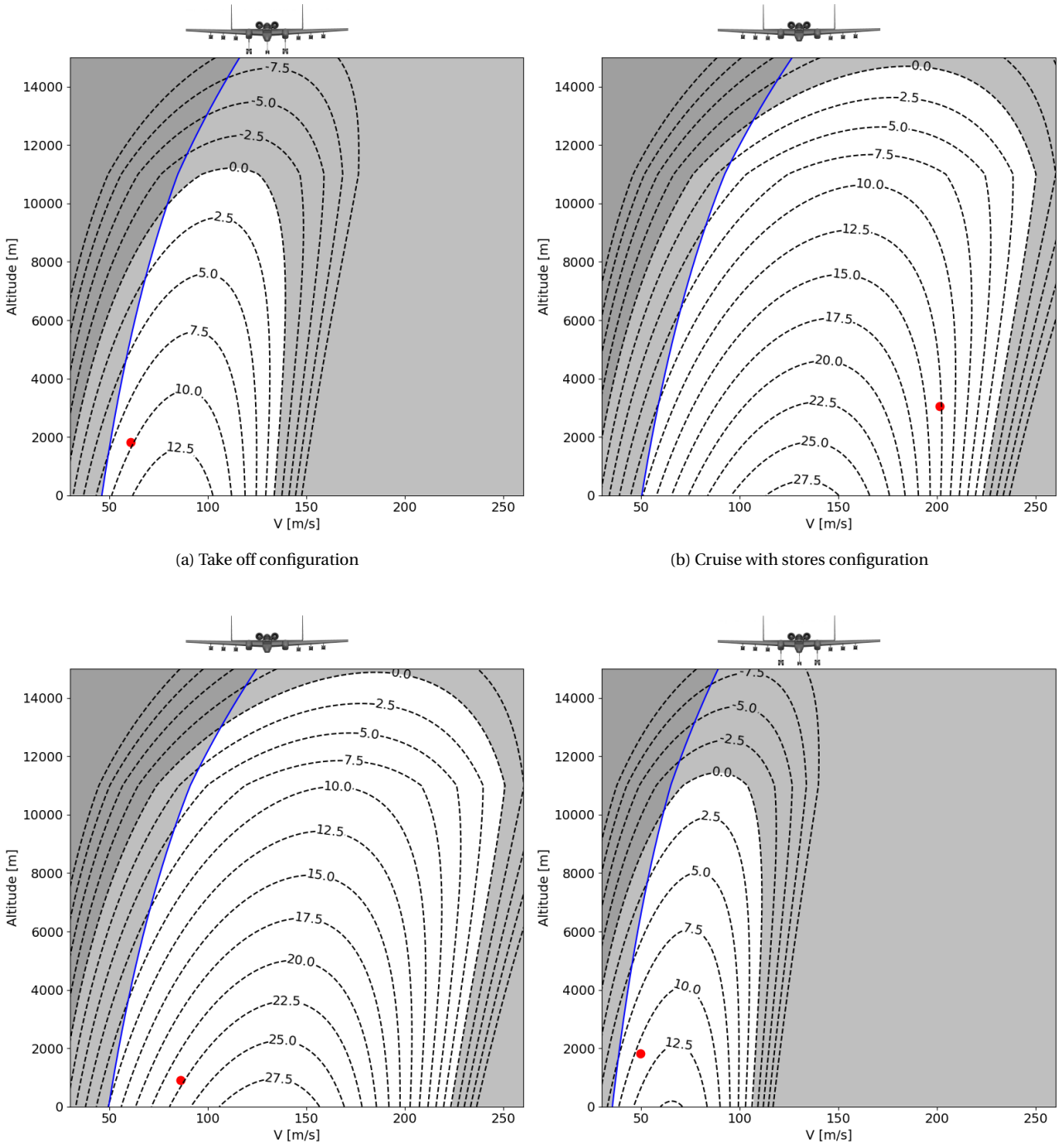

(a) Take off configuration

(b) Cruise with stores configuration

(c) Loiter with stores configuration

(d) Landing configuration

Figure 14.3: Specific excess power diagrams

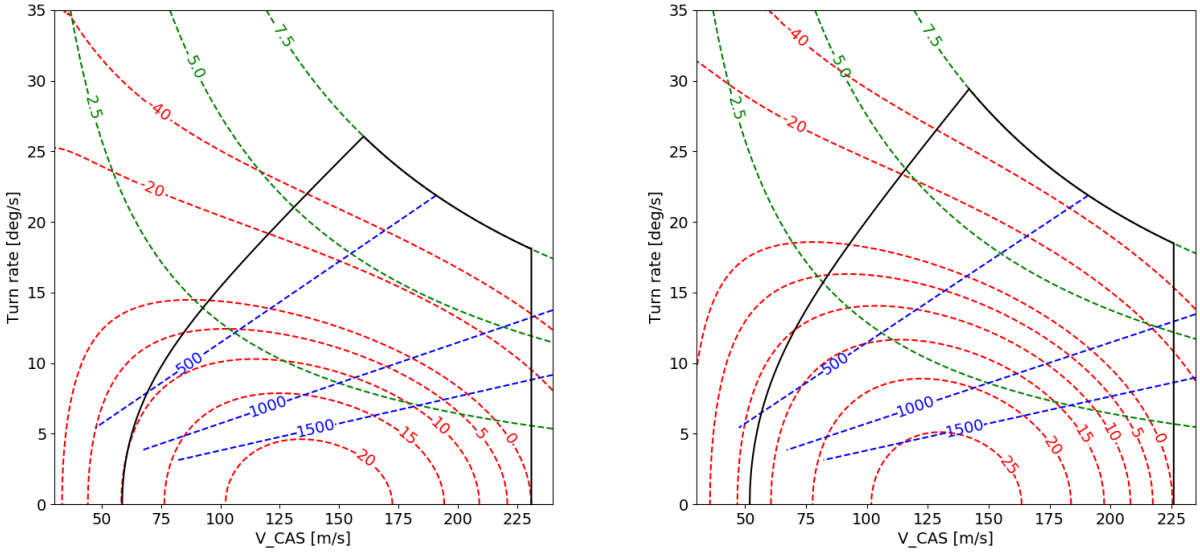

(a) Cruise with stores configuration

(b) Loiter with stores configuration

Figure 14.4: Turn rate diagrams

15 Budget Breakdown and Resource Allocation

In this chapter the budget breakdown and resource allocation are presented. First the budget breakdown is given, after which the resource allocation is performed.

15.1. Budget Breakdown

In order to keep an overview on the quality of the project, a Technical Performance Measures (TPM) model was created during the baseline report. In this model, the most important parameters are included with a contingency margin. During each design phase, the contingency factor decreases for each design phase and is used, such that the actual value in a design phase lies within the contingency margin. In the case that it lies outside, then it can be re-evaluated, such that the parameters of the aircraft converges to the target value.

Table 15.1 shows the identified contingencies related to technical performance parameters. For each technical performance parameter a relative importance is given at the right column of Table 15.1. The relative importance is decided, based on the user requirements.

The target values found in Table 15.1 are gives as result of reference light attack aircraft, used in the baseline report. However, the actual numbers are reliant on other factors, such as range and endurance.

In the baseline report, the parameters were; MTOW, OEW, payload mass, mission range, mission endurance, ferry range, required runway length and cost.

However, in this report some parameters that were directly driven from the requirements were removed. On the ground that they are requirements, they are used as input for other calculations. Finally, some more specific parameters have been added. In later stages, the contingency can be used to check the variance between result, expected and results from the previous design phase.

In case, a target value was not given for the parameters listed below, they have been left blank and only the estimated value is given with the contingency for further phases.

15.1.1. Technical Performance Measures for values in Baseline Report

In this subsection, the TPM estimated values are given with regards to the baseline report. Payload mass has been kept as parameter, due to the fact that this value was increased as design choice.

Table 15.1: Budget allocation Contingency

Parameter	**Target value**	**Estimated Value in Conceptual Design**	**Relative Error**
MTOW	$5.5{\cdot}10^3$ kg	$13.7{\cdot}10^3$ kg	150%
OEW	$2{\cdot}10^3$ kg	$7.3{\cdot}10^3$ kg	265%
Payload mass	1361 kg	2225 kg	63%
(Production) Cost	16.5 mln$	10 mln$	40%

Initially, the values given above have a conceptual contingency factor of 50%, 50%, 30% and 20%, respectively. Given that the initially assumed target values and contingency margins are highly under/over estimated, it makes sense that the estimated values are not within this range. For further analysis The estimated values can be used for a better assumed target value along with a new contingency margin.

15.2. Resource Allocation

In this section, the division of the resources are written down that was used during this project and how they were used.

Labor per member: Given that the team consists out of 10 people, the labor must be divided effectively, such that each work load is set as equal. In the project plan, the pros and cons of each team member with its expertise was discussed, in order to identify which project managing and technical role fits best.

Computational Aid: Several tools were used to enhance calculations. *Python* and *Microsoft Excel* were most optimal for situations where a lot of calculations were required, rather than doing everything by hand. These tools also gave a visual representation of the resulting values.
Additionally, *Catia* was used to make a model of the aircraft.

Working Time: The timespan of this DSE is limited by 10 weeks, so effective use of these 10 weeks is key. The DSE was already split up, such that there is a project plan to get a basic laout of the group and the approach that was taken, baseline for the product, midterm for working out several concepts and final for working out the best concept from midterm in detail. The gantt chart gave a good approximate for the working time required per task. Additionally, *Click-up* was used to keep overview of the tasks to be assigned, to be worked on, to be reviewed and finished [1].

[1] app.clickup.com, conducted during Fall DSE 2020

16
Operations & Logistics Plan

In this chapter, the kind of operations and logistics that are considered throughout the project are discussed. The practicality of the aircraft, mentioning what values it offers to the air forces and what aspects of it make it a unique aircraft are covered.

16.1. Operations

Interviews with two fighter pilots gave insight on the kind of operations that are desired to be performed by the aircraft. These operations were one of the fundamental factors in the design of the aircraft. The A-20 is capable of "hot pit refueling and rearming". Hot pit refueling is a refueling method that occurs with engines still running and its operational purpose to have the aircraft ready to take off as soon as possible. In general, the time taken for hot pit refueling is 66% of refueling with engines turned off[1]. On top of that, rearming is another operational performance which covers providing the aircraft with new supplies of ammunition for weapons. This depends on the type and quantity of the ammunition for the aircraft. In the interview with the F-35 pilot it was found out that the rearming process for an average fighter aircraft takes around 5 minutes per hard point. Given that the aircraft has 3 hard points per wing, this means that rearming the whole wing will take about 15 minutes.
Another important operational matter is providing the support for ground troops. However, this is already taken care of during setting the requirements and trade off criteria and class-I sizing. Furthermore, this report has focused on flight conditions such as cruise, loiter, climb or descent.

16.2. Logistics Plan

One of the key challenges to operate from an austere field is logistics. This includes the transportation of the aircraft itself as well as the equipment and crew required to deploy the aircraft for combat missions. However, this usually involves traveling long distances, which is costly and complicated.

To transport the aircraft to the austere field two methods are available; transport under its own power or deliver via carriers such as cargo aircraft, ships, trains, as well as trucks.

Transport under its power may require either aerial refueling or intermediate stops. This allows minimal downtime for the aircraft, since no reassembling is required once arriving at an austere field. Due to aerial refueling being a costly method for transfer (as will be mentioned in subsection 19.4.3), this logistic options for transferring the aircraft was discarded.

On the other hand, delivery by carrier is the most cost effective method of transportation, since the infrastructure required already exists and no aerial refueling or intermediate stops are required. However, there are restrictions on the weight and dimensions of the cargo, due to the ratings and dimensions of ISO shipping containers used within the shipping industry. Therefore, the cargo is subjected to a dimension and weight below 16.154m X 2.591m X 2.896m and 25440 kg [2]. These containers can also be transported by train or truck, this can further make use of readily existing infrastructure.
In the event of quick deployment, specialized carries such as the C-17 *Globemaster* or A400M *Atlas* are used, since the cargo bay of both aircraft can comfortably accommodate the container's dimension. Either way, the aircraft has to be disassembled and reassembled after arrival. Therefore, a modular design is required to reduce the assembly time. As a side benefit, maintenance on austere field can be simplified. Instead of fixing the broken part on site, the broken modular can be replaced by a spare and shipped back to the factory for maintenance.

For assembly and disassembly of the aircraft, the most important factors are first maintaining the structural integrity of the aircraft and then being able to fit those components inside the containers with the given

[1] https://www.airforce-technology.com/news/usaf-practises-hot-pit-refuelling-technique/, conducted on [04-01-2021]
[2] http://containertech.com/container-sales/53ft-high-cube-container-domestic/, conducted on [13-01-2021]

dimensions. Furthermore, it needs to be mentioned that the assembly methods are independent of how the aircraft shall be transferred as the dimensions of the container will remain the same. The aircraft is modular in several locations which are shown in Figure 16.1. During the assembly procedure, all of these components are bolted to each other. Below each of these locations are mentioned:

- **Along the wings' span**: These lines are shown with the green color on Figure 16.1. These lines are located on the main spar that connects the leading edge to the rest of the wing and extends from the wing root to the wing tip. The front section of this cut includes edge structure as well as the landing storage. The rear section include the rest of the wing structure as well as the hard point and actuator system for main landing gears.
- **Wing fairings to the fuselage**: These dashed lines are shown with the red color on Figure 16.1 and basically include the wing fairing structure.
- **Engine pylons**: These lines are shown with the purple color on Figure 16.1. On these lines the engines are connected to the pylons.
- **Horizontal stabilizers**: These lines are shown with the white color on Figure 16.1.
- **Vertical stabilizers**: After dismantling the horizontal stabilizers, now it is time for the vertical stabilizers. These are shown with blue color in Figure 16.1.

According to the group's estimation, it would take 2 containers with dimensions mentioned above to fit in all of aircraft's components. Both the big section and smaller sections of the wings are fitted in one container. This adds up to 4 items in the first containers which are all put diagonally. The other container includes the fuselage, engines, horizontal and vertical stabilizers.

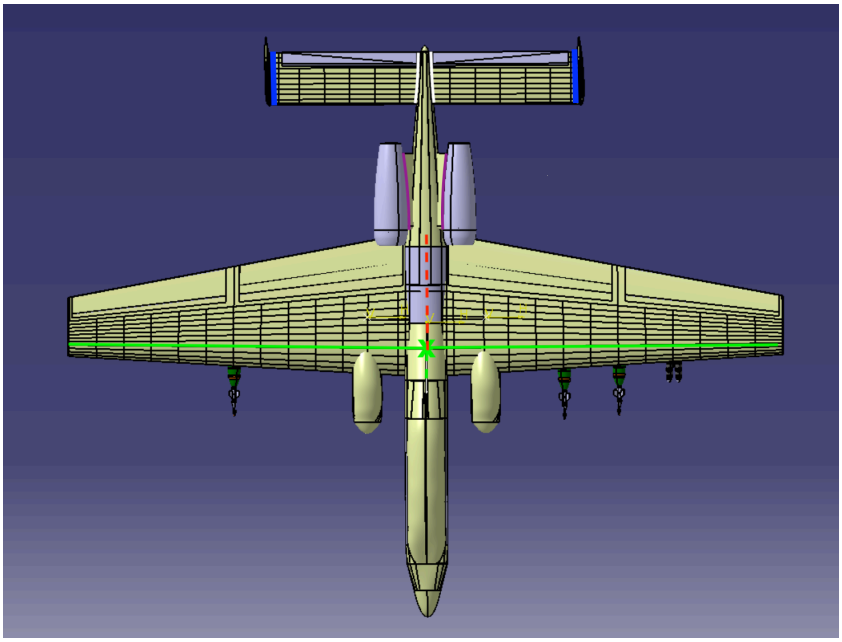

Figure 16.1: Top view of the aircraft with assembly and dismantling lines

Additional containers should be used to transport spare parts of the aircraft. The orientation of these components depend on the component type and its quantity which is different per each customer. Lastly, the fuel can be transported to the end user via a range of transportation platforms, such as pipelines, trucks, barge and rail. The logistics required to deliver the fuel from supplier to end user is displayed in Figure 16.2.

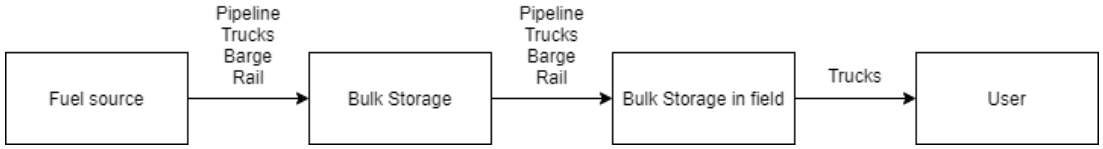

Figure 16.2: Logistic diagram of fuel from supply to end user [37]

17
Production & Assembly Plan

This chapter covers the steps that have to be taken in order to manufacture this aircraft. After that it is explained how components are joint together based on their materials. During deciding on the assembling methods the type of the aircraft and its operational environment have also been considered.

17.1. Production Plan

Figure 17.1 represents the manufacturing steps in order to make the aircraft. Cells colored in blue are the most detailed elements in this figure. These cells add up together to form the purple cells, which together with other individual purple cells make form the yellow regions. All items in the yellows regions must be first manufactured so that the production can move to the next steps. Furthermore, these yellow regions add up to individual yellow cells to make each subsystems which are colored in green. Finally the subsystems are grouped together to form the aircraft.

As can be seen from Figure 17.1, each subsystem is first manufactured as an individual item and then combined with other subsystems. The same logic can be applied even to smaller components of a subsystem: smaller components of a certain subsystem are first made and then combined with other components of that subsystem. The design, format and the level of content depth of this production plan was chosen based on a production line scheme of F-35[1]. However, it needs to be mentioned that even though A-20 is a different class of fighter than F-35, it still has a modern production plan that also applies for this aircraft. This scheme allows several manufacturing companies to take part in the production of the aircraft. This is advantageous for this type of production plan, because the companies that produce a subsystem or a section of the subsystem have a lot of expertise in this area. In other words, if the aircraft has its parts manufactured by several expert companies, its quality is expected to be better than if only one manufacturer makes everything [2]. As explained in section 19.2, it was decided to have 830 aircraft produced which takes around 10 million man hours. This means that it takes around 12 000 man hours for a singe aircraft. To speed up the total manufacturing process per aircraft, several subsystems should be made parallel to each other as they do not affect one other directly for the initial production steps.

[1] https://www.f-16.net/forum/download/file.php?id=16554, conducted on [16-01-2021]

[2] https://www.economicshelp.org/blog/147528/economics/benefits-of-being-a-multinational-company/, conducted on [18-01-2021]

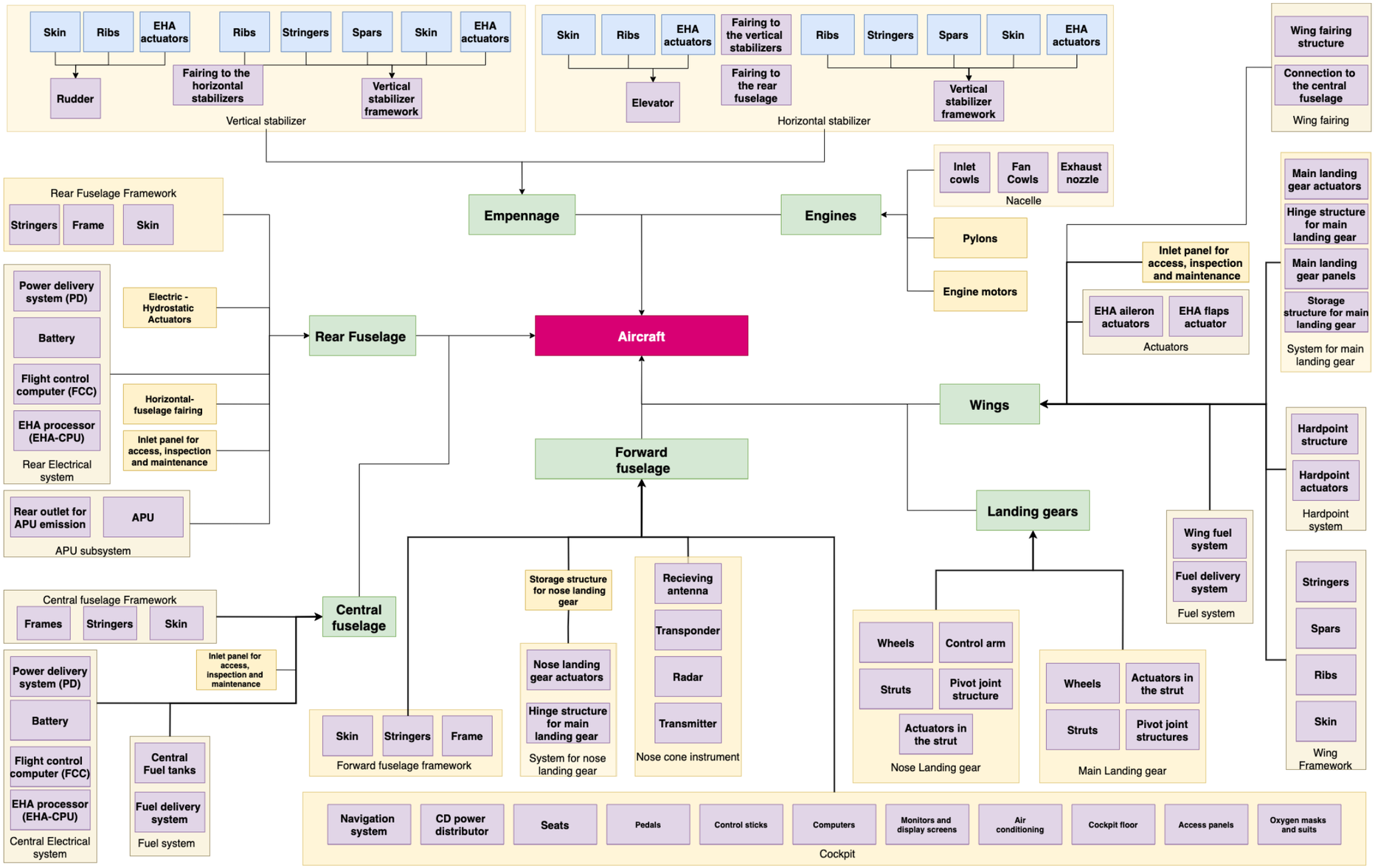

Figure 17.1: Step/Production Plan

17.2. Assembly of Components

In terms of assembling methods, it is dependent on the materials and structures of the assembly. For joining aluminum alloys to skin, it was decided to use 3M Scotch-Weld Epoxy Adhesives. This choice was based on the fact that this kind of adhesives is known to provide a strong and permanent bond between aluminum and carbon fiber composites. Furthermore, this joint type is still able to function under vibrations and impacts. 3M Scotch-Weld Epoxy Adhesives are also known to have a relatively high tensile and shear strength and are resistant against water intrusion[3].

To connect the aluminum structures together, the joining method is Gas Tungsten Arc Welding. These joint configurations are widely used in aerospace industry and are preferable for their high strength and resistance against corrosion[4]. This all led to decision to use this method to connect ribs, spars and stringers of the wings and stabilizers. Using the same reasoning, this method is also used to connect the stringers and frames of the fuselage. For aluminum joints that are located at inspection or assembly points, it was decided to use fasteners. This allows components to be removed or replaced more easily. The material of fasteners is coated steel as this avoids the corrosion of aluminum at the joint[5]. Examples of such joints are at the wing or empennage fairing or where the engines meet the pylons. For the sake of fail safe, it is decided to have the drilled head configuration for these bolts. This means that safety wires will pass through the bolts to make sure the joint still functions in case of failure[6].

To join composite materials, scarf adhesive joints (SAJs) were chosen. This variety of bonds are favorable as they have no eccentricity along the load path and provide better surfaces in terms of aerodynamics compared to other adhesives. To install composite panels for inspection panels or assembly structures, the selected joining method is bolting. In addition to bolts, for the sake of a fail-safe design, it was decided to use nuts and washers. With reference to most popular joint configurations for composites in aerospace, it is decided to have the bolts made of titanium alloys and have nuts and washers made from stainless steel [38].

[3] https://www.3m.com/3M/en_US/bonding-and-assembly-us/structural-adhesives/, conducted on [17-01-2021]

[4] http://www.mechanicalengineerblog.com/2019/03/31/advantages-disadvantages-gas-tungsten-arc-welding-gtaw/, conducted on [26-01-2021]

[5] https://www.ascensionfasteners.com/blog/which-fastener-materials-work-with-aluminum-without-corroding-it, conducted on [26-01-2021]

[6] https://www.eaa.org/eaa/aircraft-building/builderresources/while-youre-building/building-articles/basic-construction/safety-wiring-and-other-failsafe-precautions?, conducted on [26-01-2021]

18
RAMS Analysis

This chapter describes the RAMS analysis of the aircraft. RAMS stand for Reliability, Availability, Maintainability and Safety and will be described in this respective order in the chapter. Their interrelation is described in Figure 18.1.

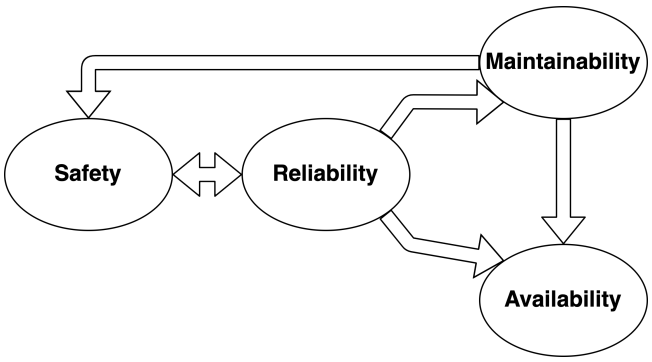

Figure 18.1: Relationship representation of the RAMS analysis [39]

It can be seen that maintainability ensures that the aircraft can be operated safely and that it is available when needed. Secondly, there is a direct interrelation between safety and reliability. It means that in order to be reliable for the pilot to operate it shall be safe and vice versa. Finally, it can be observed that that the availability flows from the other three parameters. This is due to the fact that all other parameters should be ensured in order to be available when needed.

18.1. Reliability

Reliability is determined by the risk mitigation and system reliability. Risk mitigation is the approach to reduce the chance and effect of possible failure(s), which had taken place throughout the design phase, as shown in the risk analysis sections above. The system reliability is determined by its components and the redundancy. Reliability of components can only be identified by extensive testing, which consequently is not feasible during the conceptual phases of aircraft development. As a result, the redundancy has been considered as the primary choice of improving reliability. For redundancy of the system, all critical components on board have at least one back up, as explained in the chapters above. This minimizes the impact of system failure, since there is a back up component to carry out its function.

18.2. Availability

The aircraft was designed to be a ground support aircraft with quick response capabilities. For this aircraft to be effective, it has to be accessible to ground troops at all times. However, the availability of the aircraft is highly dependent on the maintenance schedule. Hence, predictive maintenance is crucial to maintain a high level of operational readiness. In addition to the aircraft itself, the maintenance of ground infrastructures is as important as the aircraft. Therefore, ground infrastructure such as the runway, shall be inspected regularly.

18.3. Maintainability

As mentioned in section 16.2, the aircraft was designed with modularity in mind. In the event of major failure of a specific module, it will not be repaired on location, but replaced by a spare component. This reduces the down time of the aircraft. Furthermore, the aircraft has an expected service life of over 25 years, therefore, the availability and serviceability of spare parts is critical as well. Especially when the end of its service life is approaching, since the manufacturing of spare parts will be downsized.

In addition to repair maintenance, predictive maintenance such as wear items replacement and lubrication replacement, should be carried out as the maintenance schedule states. Predictive maintenance is a preventive measure against component failure, since the component is replaced before the failure point. This action improves the availability of the aircraft as stated in section 18.2, which leads to additional cost savings.

18.4. Safety

Safety is about how the aircraft responds in case of a possible hazard or failure. Given that the aircraft operates in a very hazardous environment, it is important to have the hazards defined. A hazard is any factor that threatens the aircraft or the pilot. These threats have already been covered in subsection 2.1.2. For failure, there are already verification and validation procedures done for the tools and designed subsystems of the aircraft. On top of these methods, some popular safety testing methods should also be done on the aircraft. The definition of safety in systems engineering also covers the protection of the aircraft, pilots and the people on the ground. For instance a PID controller was chosen to assist the pilots during landing, since without the controller the pilot would have an excessive workload. The workload could ultimately lead to a crash of the aircraft. Furthermore, the pilots are protected by armor around the cockpit and have ejection seats in case of emergency. One of the method to inspect safety of the aircraft is the Failure Mode, Effect, and Criticality Analysis (FMECA) method. It aims to evaluate the aircraft's safety and reliability. In this process all failure modes are mentioned and how they affect the aircraft and its subsystems. It is recommended to the operator to perform this globally known test on the aircraft few times during its operation [39].
Fail safe design is a parameter that is considered through out this conceptual design, which aims to minimize the damage to the system when a component fails. For instance as already mentioned in subsection 11.1.3, if an actuator on a control surface fails, backup systems will compensate for this loss. Another example can be the power delivery components: if PD1 fails to deliver power to an actuation point, PD2 will take over the power delivery.

19 Production Quantity and Cost Analysis

In this chapter, the buyer's behaviour was investigated, to find which factors influence the buyer's decision. Ultimately, these affect the production quantity, of which the estimation is explained in the chapter after. Lastly, the cost analysis explains the method of cost estimation, and estimates the cost for production, service use, and a more detailed subsystem cost analysis.

19.1. Buyer's Behavior

The buyer's decision has different stages; the problem recognition, the information search, the alternative evaluation and the purchase decision[1]. In this section each of these stages will be discussed.

19.1.1. Problem Recognition

The decision begins with problem recognition, which in this case is the need to fill in the gap for an aircraft that is able to satisfy a certain MNS, and states as follows: *To provide close air support to ground forces from short, front-line, austere fields at short notice, while being affordable.*
The second stage is the information search, and looks at products that are available on the market, and the manufacturers that provide them. In section 3.3, a number of manufacturers is listed.
For the alternative evaluation, the buyer compares each product. The buyer's rationale is based on several factors; the marketing stimuli, environmental stimuli and the buyer's characteristics.
Lastly, the purchase decision is made. In the following paragraphs, the buyer's rationale is further explained with regards to an attack aircraft and the buyer, which in this case would be the government acquiring a military aircraft.[1]

19.1.2. Marketing Stimuli

The product, price, place and promotion stimulates the buyer into selecting their product. Therefore, looking at what a company has to offer is influential to the buyer's behavior. Regarding "product", in section 3.4, it showed that there is more demand for multirole aircraft.
Section 3.3 showed that the price was a determining factor for a buyer to choose an aircraft. The manufactured location is another important role for the buyer. Additional to the political influence, the region at which it is manufactured has impact on its logistics (i.e. how should the aircraft be transported).[1]

19.1.3. Environmental Stimuli

The environmental stimuli consists of political, economic and technological influences. For every armed aircraft that is to be purchased, political views should also be taken into account. Together with the air force of a country, the government makes decisions on which aircraft will be purchased and how many of them. In line with the political views, the state of the economy influences these decisions. typically, a country with a financially healthy economy is able to spend more money on military reinforcement or innovation if desired. Lastly, technology also influences the decision making of the buyer. With the change in the past decades from symmetric to asymmetric warfare, the level of technology plays an important role when it comes to deciding the right product to be purchased. On the other hand, new and more advanced technological products are also very interesting to purchase in order to keep up with the technology in the world. A modern day example for that is the F-35[1].

19.1.4. Buyer's Characteristics

The buyer's characteristics can be categorized into attitude, motivation, perception and knowledge. First of all, for an air force, attitude means the way a country would like to profile itself. Having a large amount of aircraft can scare off potential enemies and is therefore a show of power. Secondly, the buyer's motivation can be found in the purpose of the product. A light attack aircraft might be needed for warfare and the protection of freedom. Thirdly, the perception of the buyer can be found in the feeling of potential threads from other countries. An example of this can be found in Israel that increased its defense budget to buy 25

[1] https://en.wikipedia.org/wiki/Consumer-behaviour, conducted on 17-12-2020

new F-35's. This decision was preceded by the news that the United States agreed to sell multiple F-35's to Saudi-Arabia, which could lead to potential threats [2]. Finally, the in-house knowledge can be an argument to buy or not to buy a product. The lack of knowledge for the usage of the product may induce higher costs, since extra training is needed. The training of F-35 pilots for example can only be followed in the US, England, Japan, Korea and Australia [3] [1].

19.1.5. Buyer's Response

Finally, the buyer's response is categorized into product choice, brand choice, purchase timing, and purchase amount. Based on the previously mentioned stimuli, the decision on the type of product can be made. Next, the choice has to be made what exact product will be purchased and from which company. As described in section 3.3, Lockheed Martin has the biggest market share within the fighter aircraft industry and therefore probably more reliable compared to a new company producing a new fighter aircraft. Furthermore, the purchase timing can have a big influence on the buyer. At times where war is uprising or the type of warfare is changing, the demand for certain fighter aircraft can increase. Lastly, depending on the need, price, characteristics, and other features of the product, the buyer decides on the amount of products. [1]

19.2. Production Quantity

Based on the competitors mentioned in section 3.3 and buyer's behavior in section 19.1, the expected quantity of aircraft to be sold is estimated in this subsection. This value was used in the cost analysis of the aircraft, which is discussed in section 19.4. For this, first the reference aircraft from Table 3.1 that are still in service were selected. These aircraft were initially the A-10 Thunderbolt, Eurofighter, F-16, F-4 Phantom II and F-35A. However, after initial analysis, the Eurofighter was decided to be neglected as its unit price is drastically higher with respect to other aircraft [4] .

It is found that out of 716 produced A-10s, 282 of them are still active today[5]. These aircraft were manufactured at least 37 year ago and have received updates since. The USA, in which the A-10 is manufactured, has decided not to sell the A-10 to other countries, despite the success of the A-10. It was found that the US is planning to keep the A-10 in-service until late 2030, and is already looking for a replacement[6]. As a rough estimate for the production quantity, it considered to sell 100 aircraft to the U.S. airforce as a replacement for the A-10s in the current fleet.

The next reference aircraft is F-16, for which out of 4600 aircraft, around 3000 units are still active today[7]. As is presented in section 19.4 the unit selling price of group's aircraft will be significantly lower than F-16. Additionally, the upgrade costs of F-16 is remarkably high; for instance the Greek air force has signed a contract of $ 1.5 billion to upgrade 84 of its F-16 to the latest F-16V edition, which is the most advanced version [8]. This means an upgrade per F-16 aircraft is worth almost 18 million which is even more expensive than the fly away cost of the A-20, which is calculated in section 19.4.
This budget logic not only applies to the F-16, but it is also true for F-35. For instance, UK has recently halved the number of its purchased F-35s [9]. Next to economical factors, political factors can also influence the customer's behavior as mentioned in section 19.1. For instance, the Venezuelan air force is equipped with F-16s. However, due to current political tensions between Venezuela and the USA, maintenance of these aircraft will be challenging [10]. Because of the above reasoning, the group is confident that it can re-

[2] https://www.forbes.com/sites/sebastienroblin/2020/09/18/, conducted on [04-01-2021]
[3] https://www.f35.com/about/life-cycle/training, conducted on [04-01-2021
[4] https://www.reuters.com/article/us-aerospace-belgium/belgium-picks-lockheeds-f-35-over-eurofighter-on-price-idUSKCN1MZ1S0, conducted on [04-01-2021]
[5] https://www.airforcetimes.com/news/your-air-force/2019/08/13/a-10-re-winging-completed-will-keep-warthog-in-the-air-until-late-2030s/ conducted on [04-01-2021]
[6] https://www.defensenews.com/air/2019/10/25/air-force-officially-buying-light-attack-planes/, conducted on [04-01-2021
[7] https://news.lockheedmartin.com/2018-06-25-Lockheed-Martin-Awarded-Contract-to-Build-F-16-Block-70-Aircraft-for-Bahrain, conducted on [04-01-2021
[8] https://www.dw.com/en/lockheed-martin-to-upgrade-greeces-f-16-fighter-jets/a-51815309, conducted on [04-01-2021
[9] https://www.pesmedia.com/f-35-tempest-fighter-jet-08092020/, conducted on [04-01-2021
[10] https://www.state.gov/the-united-states-sanctions-maduro-aligned-officials-of-venezuelas-military-counterintelligence-agency, conducted on [04-01-2021

place at least 400 F-16s and even F-35 orders.
The next reference aircraft is the F-4 Phantom II. Looking at current countries with active F-4 phantoms in their air force [11], it is estimated that there are 146 units of this aircraft are still in service. The manufacturing of the F-4 has stopped 40 years ago, so most customers are looking for a replacement of this aircraft. Currently, the F-15 Strike Eagle is known to be a replacement for F-4s. However, given the unit cost of F-15 Strike Eagle is at least $80 million[12], a replacement of 90 units was considered.
Next to replacing the above mentioned aircraft, it is also possible to sell the aircraft to new customers, as the light attack aircraft is able to take off and land from austere airfields with limited length. An example of potential new customers are countries that are economically weaker such as African, South American or Eastern European countries. A prediction of 200 aircraft to be sold to such customers is made. Adding all these target quantities up, that leads to an expected value of 830 aircraft to be sold to the fighter aircraft market.

19.3. SWOT Analysis

In this section, a SWOT analysis is carried out in which several elements are divided under external and internal categories and then categorized depending on whether they are harmful or helpful for the marketing of the aircraft. This is visualized in Table 19.1. The factors in Table 19.1 shall help the group to make appropriate design and marketing decisions.

Table 19.1: SWOT-analysis of the market analysis

	Positive	**Negative**
Internal	Strengths: • Design from scratch: all component can be adjusted to project needs. • Similar products available to provide example. • Cheap labor: the members of the group are students. • Free consultancy from experts in the field. • Ideas are not constrained by experience.	Weaknesses: • Lack of contact with the potential clients. • Lack of budget and time in comparison to potential competitors. • Lack of pre-existing relationship with potential suppliers. • Lack of professional resources to assist the development process.
External	Opportunities • System upgrades of aircraft to adept into niche markets. • Once acquired by a NATO member state, the product becomes more appealing to member states. • Large client base. • Limited competition.	Threats • Change in requirements set by current battlefield demand. • COVID-19 leads to potential defense budget cut. • COVID-19 government policy leads to delay in project progress. • Change in threats faced by the aircraft. • Advancements in development of shoulder launched missiles.

19.4. Cost Analysis

This section describes the cost analysis method used to determine the price of the aircraft. Firstly, the costs of several engineering and design stages are estimated. Secondly, the break-even point and return on investment are discussed. Afterwards, the operational and maintenance costs are analyzed. Next, the subsystems of aircraft are compared with each other in terms of cost. Finally, the aircraft is compared with other aircraft in terms of cost.

[11] https://nationalinterest.org/blog/buzz/its-hard-believe-f-4-phantom-still-flying-after-60-years-112186, conducted on [04-01-2021

[12] https://www.airspacemag.com/military-aviation/shocking-resurrection-f-15-180974446/, conducted on [04-01-2021

19.4.1. Cost Estimation Method

To estimate the cost of the production of the aircraft, the method presented by Gudmundsson's was performed [40]. This method is based on the "Development And Production Costs of Aircraft" (DAPCA) method, specifically DAPCA-IV, which is used to estimate Research, Development, Testing & Evaluation (RDT&E) costs. On top of that, the DAPCA method was also used to estimate engineering, tooling, and manufacturing labor hours. With these values the total production cost of the aircraft have been estimated.

Gudmundsson's equations were required to perform the cost estimation for the aircraft [40]. For this, W_E, maximum speed, and the amount of aircraft planned to be produced were required as inputs. The engine cost per unit was estimated using the maximum thrust per engine and amount of engines per aircraft. Lastly, the avionics cost was estimated as a percentage of the flyaway cost. According to Raymer, the avionics for airliners cost about 5%-25% of the flyaway cost, depending on how sophisticated the system is [5]. Military avionics system are generally more advanced and the value for this aircraft is thus assumed to be 30%.

Since the values of DAPCA are from 1986, the costs should be adjusted to account for inflation. Gudmundsson already adjusted the values to 2012. However, since the designed aircraft will enter service in 2025, the values had to be adjusted to that year. Therefore, the Consumer Price Index (CPI) was used[13]. The average CPI growth over the period of 1982 to 2020 was calculated, and used to predict the CPI growth factor, which was approximately 1.39 for the period of 2012-2025.

Some extra factors were included to account for complexity and the usage of composites. Complex flap systems, pressurized cabins, and tapered wings add complexity to the design which increases the cost. The usage of composites increases the costs too, an estimation of the percentage of the aircraft that is made out of composites was made. Figure 19.1 shows that the composite usage for fighter aircraft is often under 20%, this has to do with the costs and properties of composites. Generally composites are more expensive to use, and the properties of composites make it harder to apply them in certain situations. Composites are still applied where skin does not have to be reinforced and on control surfaces, such as the elevators and rudders [41]. With these things in mind, it was estimated that approximately 10% of the aircraft will be made out of composites.

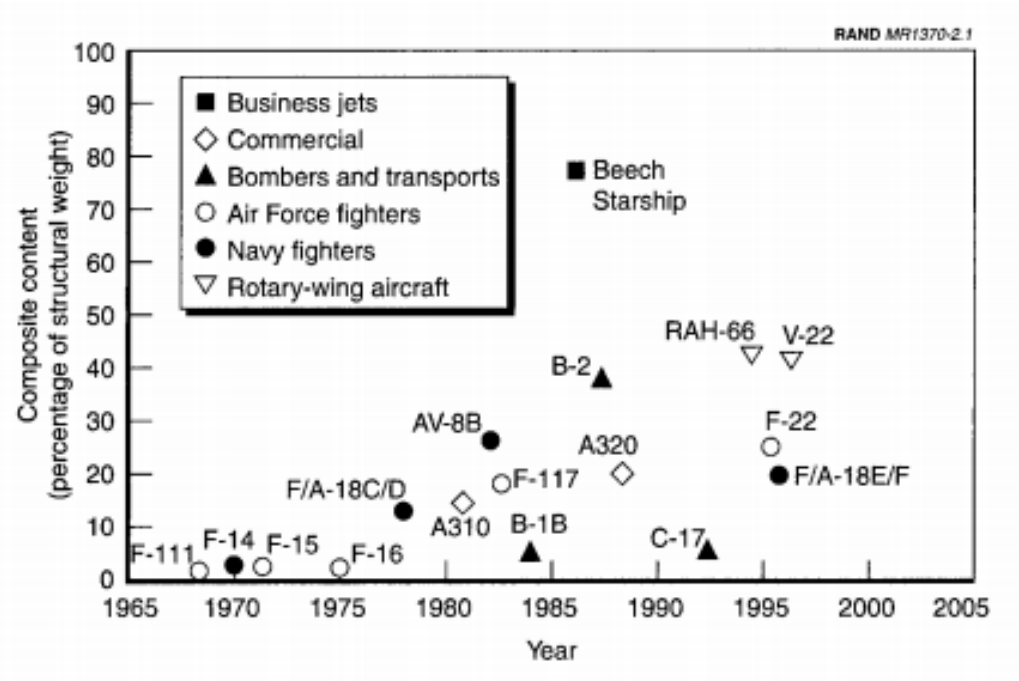

Figure 19.1: Graph presenting usage of composites in different aircraft [41].

In Table 19.2 the outcome of the adjusted DAPCA-IV method is presented. Furthermore, the costs in this table divide into two general groups: recurring costs and non-recurring costs.

[13] https://www.bls.gov/regions/mid-atlantic/data/consumerpriceindexhistorical_us_table.htm, conducted on [18-12-2020]

Non-recurring cost are those that are documented once during the whole production program such as the engineering and development, flight test operations, and tooling costs. Recurring costs are costs that depend on the quantity of production such as the manufacturing, quality control, materials and equipment, and liability costs.
That being said, it also needs to be mentioned that in Table 19.2, certification costs are the total costs to develop the aircraft, and the total cost to produce is the total production cost per unit. The liability cost covers the risk of accidents during production, it was estimated to be 15% of the production cost. The minimum selling price to cover all the cost with the planned amount of aircraft, is the sum of the certification cost per unit, the production cost, and the liability cost. Lastly a quantity discount factor (QDF) was included in the table, as also used in Gudmundsson. A discount factor of 5% was assumed which resulted in the QDF for 830 unit being equal to 0.61. This would mean that a discount on the engines, avionics and liability cost of 39% would be applied. However, since this would be optimistic, the worst case scenario where there would be no QDF, was considered.

It should be noted that the software is not taken into account for determining the cost estimation. This is due to the fact that the DAPCA-IV method is from 1986, which doesn't take into account the software development costs. As future recommendation, these values should also be included, in order to get a better understanding of the certification cost.

Table 19.2: Cost analysis as presented in the DAPCA-IV method

	Man-hours [h]	**Rate [$ / h]**	**Total Cost [2025 USD]**	**Cost per unit [2025 USD]**	
Engineering	3 million	90	0.74 billion	0.9 million	
Development support			42 million	51 thousand	
Flight test operations			7.9 million	9.4 thousand	
Tooling	1.4 billion	60	0.26 billion	0.31 million	
Certification cost			**1.0 billion**		
Manufacturing	10 billion	50	1.5 billion	1 8 million	
Quality Control			0.21 billion	0.25 million	
Material/equipment			0.22 billion	0.27 million	
Units produced in 5 years				830	
Quantity Discount Factor (QDF)				0.61	
				Without QDF	**With QDF**
Engines				2.9 million	1.8 million
Avionics				2.3 million	1.4 million
Liability cost				1.1 million	0.69 million
Total cost to produce				**7.6 million**	**4.6 million**
Minimum selling price				**10 million**	**6.6 million**

19.4.2. Break-Even Point

As can be seen in table Table 19.2, a minimum selling price for the aircraft was calculated. The price was determined such that the break-even point is reached when all units produced in 5 years, are sold. From a business point of view, this induces a lot of risk and will not result in any profit. Therefore, it is useful to make an analysis of the break-even point and how it shifts with the increase of the selling price. The outcome of this analysis is presented in Figure 19.2. The fixed cost of the aircraft are the certification cost and the variable cost represent the cost per aircraft.

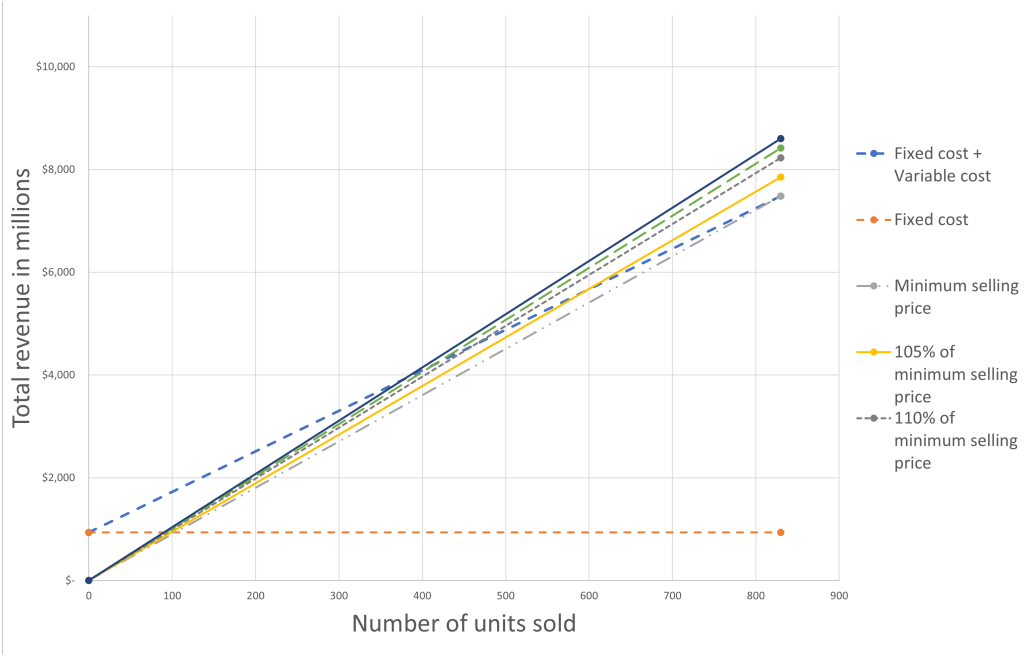

Figure 19.2: Break-even point compared to the fixed + variable costs

From Figure 19.2, the intersections from the different lines with the cost line represent the break-even points. From this, the amount of aircraft that have to be sold was determined. In addition, the graph also shows the return on investment (ROI). The ROI is calculated by dividing the total revenue by the total costs. The aforementioned values are represented in Table 19.3.

Table 19.3: Break-even point and ROI for different selling prices

Price per unit [mln 2025 US$]	Break-even amount	ROI
9.96	830	0%
10.5	600	5%
11.0	470	10%
11.2	420	12.5%
11.5	380	15%

Finally a selling price had to be chosen. The selling price of the aircraft is $10.96 million. With this selling price, the break-even point is at approximately 56% of the estimated sales volume of 830 units. This covers risks involved with the market. For example, if the US government would not buy any to replace the A-10 fleet, the margin would still be big enough to make the sales profitable. Hence, even if the aircraft is performing worse than expected on the market, the break-even point will still be met. In case the full estimated volume gets sold, the profit would amount to $ 830 million, which equals to a ROI of 10%.

19.4.3. Estimating Transportation Cost

As was mentioned in Section 16.2, three methods may be used for the transportation of the aircraft: aerial refueling, transferring the aircraft in containers on ships or transporting it in aircraft like the C-17. Throughout the research over these transport methods, it was found that transporting the aircraft in containers is a much cheaper method. It was found that transferring a container from New York to London will cost about $ 2 500 [14]. This means that based on the dimensions of the containers which are mentioned in Section 16.2 and given that two containers are required per aircraft, the transport cost of one aircraft would be $ 5 000. On the other hand, only the jet fuel of aerial refueling aircraft for the same distance will be at least $ 27 000 [15]. Given that affordability is an important factor in trade off and design of this aircraft, this cheap method of transfer gives an advantage to the product in terms of logistic cost and marketing.

[14] https://www.icontainers.com/, conducted on [18-12-2020]
[15] https://thepointsguy.co.uk/guide/cost-of-fueling-an-airliner/, conducted on [18-12-2020]

19.4.4. Estimating Operational Cost

This section represents the operational and maintenance costs of the aircraft. The same approach was taken as in subsection 19.4.1, using the adapted DAPCA-IV method from Gudmundsson [40]. The overhaul price of the engine was estimated to be 30% of the total cost of the engine based on data gained from Pratt&Whitney[16]. The assumption was made that this value holds for comparable sized engines like the Honeywell HTF7000 as was chosen in chapter 9. The estimated Time Between Overhauls (TBO) for a comparable engine is 3000 flight hours[17]. However since this aircraft is used in military conditions, the TBO is shorter due to more intensive use of the aircraft, therefore a TBO of 2000 flight hours was assumed. According to requirement LAA-TIM-SER-1.2 the aircraft has to fly 15,000 hours over a service life of 25 years, which results in flying an average of 600 hours per year. With these values, the overhaul cost per year were calculated, which are presented in Table 19.4.

The maintenance cost are dependent on the amount of flight hours, the flight hours to maintenance hours ratio, and the wage of the mechanics. The flight hours to maintenance hours ratio is related to the complexity of the aircraft, more complex systems take more time to maintain. The wage of the mechanics according to Gudmundsson was $53-$67, the average of $60 was assumed and corrected with the CPI as mentioned in subsection 19.4.1. This resulted in the maintenance cost per year as presented in Table 19.4.

Loan and insurance costs are not applicable and the fuel cost will be more accurately estimated with another method. The fuel cost was calculated using the fuel weight for the design mission as provided by the weight estimation performed in chapter 5. It is assumed that all of the fuel will be consumed during a flight. A mission is also assumed to equal 5.5 flight hours, with an average of 600 flight hours per year. This means approximately 109 flights are performed per aircraft each year. Combined with the assumed cost of the JP-8 fuel, which was approximately $0.78 per liter in 2020[18], the fuel cost per year was calculated, as presented in Table 19.4. However, note that fuel prices fluctuate a lot, and that fuel prices on remote locations may drastically increase to up to $100 per liter[19]. Therefore, depending on the location, the cost per flight hour may increase from $1 100 up to $96 000 per flight hour due to fuel cost. This fuel cost would however be the same for any aircraft, thus even though the cost increase is so large, the cost of comparable aircraft would drastically increase as well. In comparison the Super Tucano costs $1 000 per flight hour, an AT-6 roughly $2 500 per flight hour ,and the A-10 $20 000 per flight hour[20]. This means the operational cost of this aircraft are relatively cheap.

With the before mentioned yearly cost, the total cost per year for operations of the aircraft was calculated. Since it is known that the aircraft will on average fly 600 hours per year, the cost per flight hour was calculated as well. These values too, are represented in Table 19.4.

Table 19.4: Operational and maintenance costs

Cost factor	Cost [2025 US$]
Engine overhaul	880 thousand
Maintenance cost per year	21 thousand
Fuel cost per year	450 thousand
Total operational and maintenance cost per year	640 thousand
Total cost per flight hour	1100

19.4.5. Subsystem Cost Analysis

Figure 19.3 represents the ratio of costs with respect to each subsystem of the aircraft. The source for the

[16] https://www.pwc.ca/en/products-and-services/services/maintenance-programs-and-solutions/pwcsmart-maintenance-solutions/pwcsmart-pt6a/flat-rate-overhaul-program, conducted on [18-12-2020]

[17] https://www.guardianjet.com/jet-aircraft-online-tools/aircraft-brochure.cfm?m=Cessna/Textron-Bravo-62, conducted on [18-12-2020]

[18] https://www.dla.mil/Portals/104/Documents/Energy/Standard%20Prices/Petroleum%20Prices/E_2019Oct1PetroleumStandardPrices_190928.pdf?ver=2019-09-30-072433-663, conducted on [18-12-2020]

[19] https://thehill.com/homenews/administration/63407-400gallon-gas-another-cost-of-war-in-afghanistan-, conducted on [18-12-2020]

[20] https://www.csis.org/too-little-too-much-or-lot-little-air-force-oa-x-light-attack-program, [conducted on 26-01-2021]

construction of this figure is a study that has gathered data and regression equations from several military aircraft [42]. Based on these data and equations, a model is made which produces the cost of each subsystem based on its weight. Then Figure 19.3 was made which compares subsystems in terms of their cost. As can be seen from this figure, the main contributions to the cost of the aircraft come from the wing, fuselage, and propulsion units. On top of that, the combination of the fixed equipment with the furnishing and instruments also has a large contribution to the cost. This is to be expected as those are the most labor intensive parts of the aircraft, and require the most material.

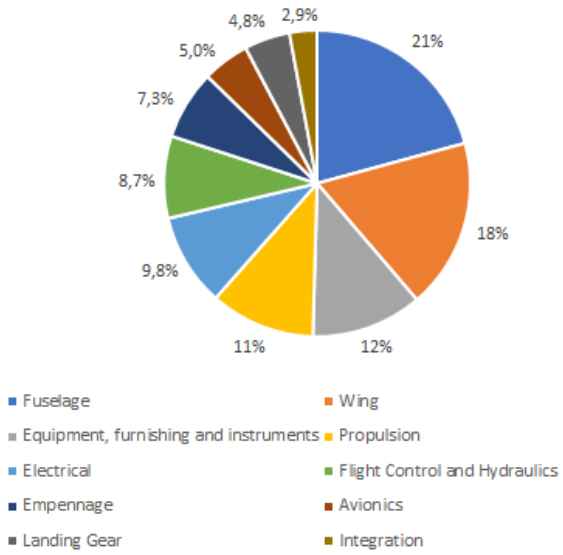

Figure 19.3: Cost breakdown per subsystem of the aircraft

19.4.6. Comparison to Competitors

Figure 19.4 compares the aircraft with respect to its competitors in terms of empty weight and cost as found in Table 3.1. The figure also includes a line of showing the expected cost of any empty weight based on these data. Obviously it is desired to be below this line as that means the group is offering a relatively cheap aircraft. Following that reasoning, the aircraft indeed is relatively cheap compared to aircraft of around the same weight. One heavier aircraft is even cheaper, this is the Sepecat Jaguar. However, noted should be that there is quite some fluctuations in the prices which makes this trend line inaccurate with a R^2 of 0.59.

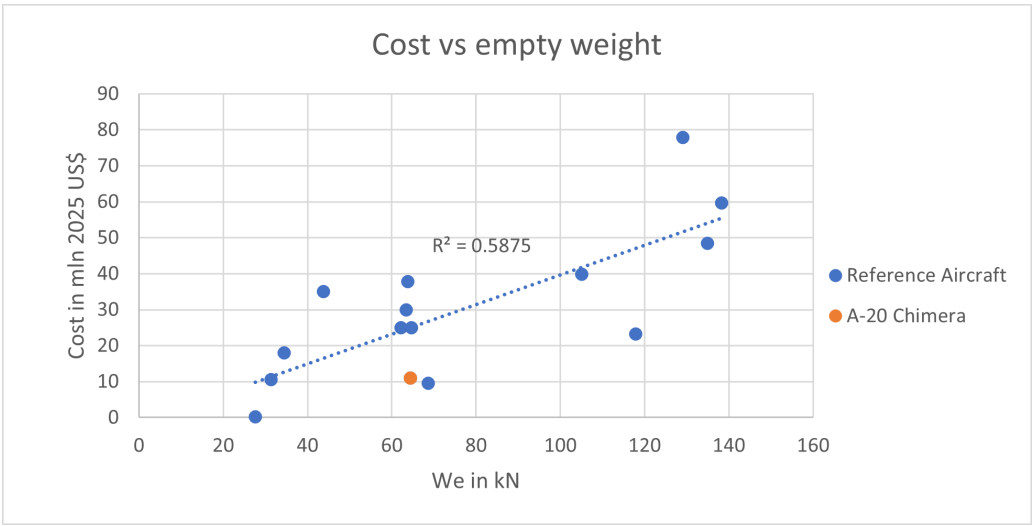

Figure 19.4: Cost versus empty weight plot

20 Sustainability Strategy

In this chapter the sustainability approach is discussed. Five different types of sustainability are discussed. First the environmental sustainability is discussed, after that the end-of-life approach is presented, then the technological sustainability is explained. The financial sustainability is discussed afterwards and finally the impact of the aircraft on social sustainability is presented.

20.1. Environmental Sustainability

The three main contributions to the environmental sustainability are the operative emissions, production emissions, and the material selection.

The main contributor to the operative emissions is fuel consumption. There are multiple ways of reducing fuel consumption. One of the ways is to improve fuel efficiency, however due to not designing a new engine for this aircraft, this factor is only influenced by the engine choice. Another way to reduce the fuel consumption is reducing drag on the aircraft. To reduce skin friction drag, passive turbulent drag reduction methods can be implemented, like riblets or large eddy breakup devices[43]. For this aircraft riblets will be implemented on the top of the wing and on the fuselage, this could reduce the drag with up to 15% [44]. The effects of riblets are in more detail shown in Figure 20.1. Lastly, the weight of the riblets is roughly equivalent to the weight of the paint it replaces [45]. Furthermore, to reduce lift-induced drag, high aspect ratios for the wing and the horizontal tail were chosen.

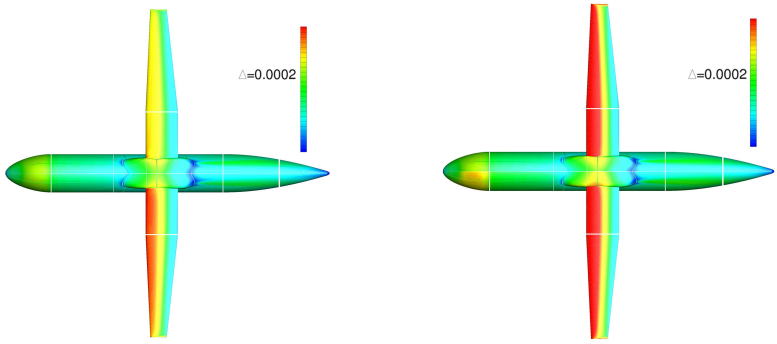

Figure 20.1: Effect of riblets on skin friction drag [44].

Before the aircraft flies its mission, it first has to be transported to the specified location. As in more detail explained in section 16.2, shipment of the aircraft in shipping containers is chosen as main means of transportation. This allows for large amount of aircraft and spare parts to be shipped to a location at the same time. Furthermore, these containers can also be transported by train or truck, this offers flexibility in transport all over the world with readily existing infrastructure. On top of that it also contributes to lowering emission of greenhouse gasses, especially compared to using for example a C-17 to transport the aircraft, or flying there by itself. This is further substantiated by Table 20.1[1] , where the difference between emission of different modes of transport is presented.

Table 20.1: Grams of CO_2 emitted per tonnes-km for different modes of transport

Mode of transport	Deep-sea	Rail	Road	Airfreight
g CO_2/tonnes-km	8	22	62	600

[1] https://www.ecta.com/resources/Documents/Best%20Practices%20Guidelines/guideline_for_measuring_and_managing_co2.pdf, conducted on [18-01-2021]

Another contribution to greenhouse gasses is due to emissions from production. For the production of aluminum and composites, a lot of CO_2 is emitted. For example, 24-31 kg of CO_2 is produced to produce 1 kg of carbon fiber[46]. To reduce the carbon footprint of the production, production methods should be sustainable and optimized to reduce waste of material which also relates to lean manufacturing [47]. Also the material choice affects the CO_2 production, as for example producing aluminum as primary metal requires as much as 20 times more energy than production of aluminum as secondary metal[48].

Material selection exceeds just the impact on the emission of greenhouse gasses. When taking a look at rare earth mining for example, it shows water pollution in nearby areas. This spreads to worsened living conditions for local communities, which should be prevented[49]. Therefore, even though these rare earth metals may have a positive effect on the design, it does not weigh up to the negative environmental impact as a consequence.

20.2. End-of-Life Sustainability

After the aircraft has concluded its service, the aircraft should be disposed of. The disposal of the aircraft should already be considered during the design process. Recycling and re-using components should be considered as these have a lower environmental impact than for example discarding them on landfills, incineration, or other means of destroying the components.

Re-using parts is the most sustainable approach as this does not involve any additional processes. The components are at the end-of-life taken out of the aircraft and used in another aircraft or other system. Parts can also be used as spare parts for similar aircraft that are still in service. This reduces the amount of parts that have to be produced or repaired. However, since parts can drastically change due to innovation, it is hard to predict what parts will be re-usable at the time.

Therefore, planning for recyclability, even for parts that seem re-usable, is important. The more that can be recycled, the less material is wasted. Also, as mentioned before for example the production of aluminum as secondary metal is beneficial as the required energy is much lower. An issue in the aerospace industry is however, that a lot of aluminum alloys that are used in aircraft are not cost-effective to recycle[48]. Aluminum 20 and 50 series are readily recyclable, therefore, to increase the recyclability of this aircraft, it will mainly exist of those aluminum types as already discussed throughout the report.

Composites are harder to recycle than metals, especially in the case of thermoset resins. Thermoplastic resins would be easier to recycle, however composites with thermoplastic resins are not yet applicable to main structures. Thermoset composites are recyclable as well, they are however more likely to be incinerated due to a lack of recycling processes[50]. On top of that, some resins are hazardous to the environment and should be carefully disposed of. These properties were taken into account when selecting composite materials.

20.3. Technological Sustainability

To ensure that the aircraft will stay relevant throughout its projected service life of 25 years, systems should be either update-able or replaceable. This allows the aircraft to adapt to newer technology and innovations. This ability to adapt also increases flexibility in deploying the aircraft on newly designed missions.

Being able to replace parts is also beneficial for maintenance purposes. Easy access to parts which may need regular replacements, like braking systems, decreases the work load of maintenance. As explained in chapter 10, the braking system makes use of carbon brakes to further reduce required maintenance on this particular system. Additionally, as discussed in chapter 16, one of the benefits of the container shipment is that spare parts can easily be included in shipping. This means that broken parts can be send back for repairment while spare parts are readily available. This saves time in maintenance such that aircraft are ready for operation at shorter notice. Another benefit of the shipping, is that the aircraft was designed to be modular. This results in more easily replacing parts which are already detachable for shipment.

The systems of the aircraft should also be update-able. Flight computers may have to be updated to comply with new regulations or new parts. Also the pilots helmet, which will display the HUD as explained in chapter 11, may have to be updated during the aircraft's service life.

20.4. Financial Sustainability

The financial sustainability of the aircraft includes the production cost and the operational costs. The production cost can be reduced by efficient use of material, which reduces the waste and thus the total amount required. The efficiency of the production process can also be influenced by contracting different specialized companies to produce subsystems, which increases overall quality as well[2]. This increase in quality would reduce the amount of maintenance required on subsystems, which then decreases the maintenance cost.

The operational costs can be decreased mainly by improving on maintenance or reducing fuel costs, since these two factors account for roughly 60% of the total operational cost of military aircraft [51]. The fuel cost are directly coupled to the consumption, which is already taken into account in section 20.1. The maintenance cost are too already partially discussed in section 20.3, they can however be even be further decreased by properly training maintenance technicians. By training maintenance technicians, the quality and reliability of their work increases, decreasing accidents and incidents, and will thus reduce the frequency of maintenance required for subsystems[52].

20.5. Social Sustainability

To make the project socially sustainable, the situation of the employees and their working place should be considered. Employees should be educated regularly to keep a high level of knowledge. With a higher level of knowledge, the resulting product will be of higher quality. More knowledgeable employees are more productive, more adaptable and are more likely to come up with innovative ideas[53]. On top of that, the health of workers also has a big influence on their productivity. Health can be improved by providing access to good healthcare and stimulating balanced diets as well as spreading information on prevention of health issues. Both these measures can positively influence the further lives of the workers, even beyond this project.

Secondly safety on the work floor is an important factor on social sustainability. By providing a safe environment to work in, the productivity of workers can improve[54]. Workers can focus at the tasks at hand and have less worries about potential hazards. The safety of the workers exceed just the physical safety on the working place, also psychological safety play an important role. Employees should feel accepted and should be able to express themselves to prevent any psychological issues. When one does not feel accepted, their mental health can decline. This can lead to distraction which can introduce safety issues for both themselves as well as those around them. This can however also lead to resignation of the employee, which can cause a decline in production.

The last aspect of social sustainability that will be covered is noise. The noise levels produced by aircraft can be high. Even though one of the functions of this aircraft is to intimidate enemy forces by flying low and producing noise, this is not always desired. This would for example not be desirable when having to operate near civilian domains. However, not only civilians are impacted by the noise levels, military personnel is as well. Important is to note that for military aircraft, noise reduction should not be at the cost of performance, therefore options are limited.

The most important parts of the flight where noise is an issue are take off, low altitude flight, and landing. To help reduce noise from the engines, chevron nozzles or a mixer can be implemented which will decrease noise levels during take off and landing[3]. The option of adding a mixer was chosen for this design. In addition, low altitude flight should be performed at minimum speed to reduce noise levels from the jet engines[55], this however is only applicable in training when necessary, as this could endanger missions.

The noise from jet engines can also introduce acoustic fatigue into structures[55]. This gives another reason to reduce noise levels, as this can result in more maintenance, which in turn leads to more costs and possibly more materials required. It can thus be concluded that reducing noise helps the sustainability of the aircraft on multiple levels, environmental, financial, and social.

[2] https://www.economicshelp.org/blog/147528/economics/benefits-of-being-a-multinational-company/, conducted on [18-01-2021]

[3] https://www.nasa.gov/topics/aeronautics/features/bridges_chevron_events.html, conducted on [16-01-2021]

21
Post-DSE activities

This chapter layout the project design & development logic for the A-20 *Chimera* project. Project design & development logic represent the logical order for the post DSE activities to be executed, which is shown in Figure 21.1 and Figure 21.3 till Figure 21.6.

21.1. Post DSE Work Breakdown Structure

Up till now, the project covered the entire conceptual phase of the aircraft development process. The next steps had been divided into five different phases, preliminary design, detailed design, manufacturing, operation & service and end of life. Each individual phase had been further analyzed and broken down into smaller tasks, which is shown in Figure 21.1. In Figure 21.1, the red boxes represent the different phases of the post DSE period, the blue boxes represent top level tasks and the green boxes represent the sub level tasks. Furthermore it needs to be mentioned that as it can be seen from Figure 21.1, the first red cell is numbered with 2. The reason is that the first stage is conceptual design, which is basically what this is report is all about. Moreover, this diagram represents the time duration that has been allocated to each cell. The time duration was governed by the requirements LAA-TIM-SER-1.1[1] and LAA-TIM-SER-1.2[2].

21.2. Post DSE Work Flow Diagram

Based on the work breakdown structure, a work flow diagram is made which is represented in Figure 21.2. Same as the work breakdown structure, the green color represents the most detailed steps in this diagram. These cells form the blue cells which combine to red cells. As it can be seen from this figure, there are several tasks that can be done at the same time.

21.3. Post DSE Project Gantt Chart

Based on the work breakdown structure and work flow diagram mentioned in section above, the a Gantt chart was made, which is shown in Figure 21.3.

[1] The aircraft shall enter service in 2025

[2] The aircraft shall have a service life of at least 15,000hours over 25 years

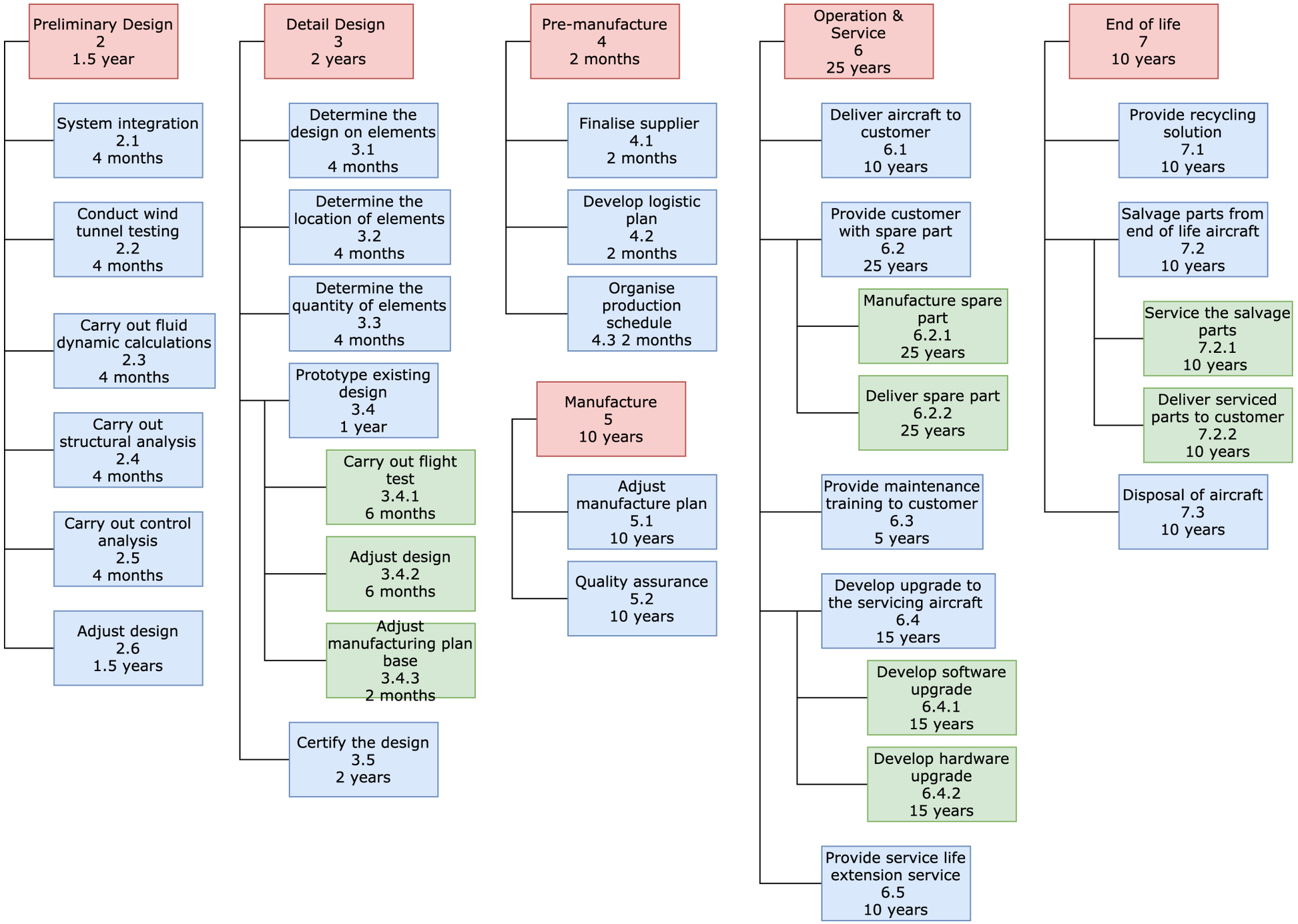

Figure 21.1: Work Breakdown structure of Post DSE activities

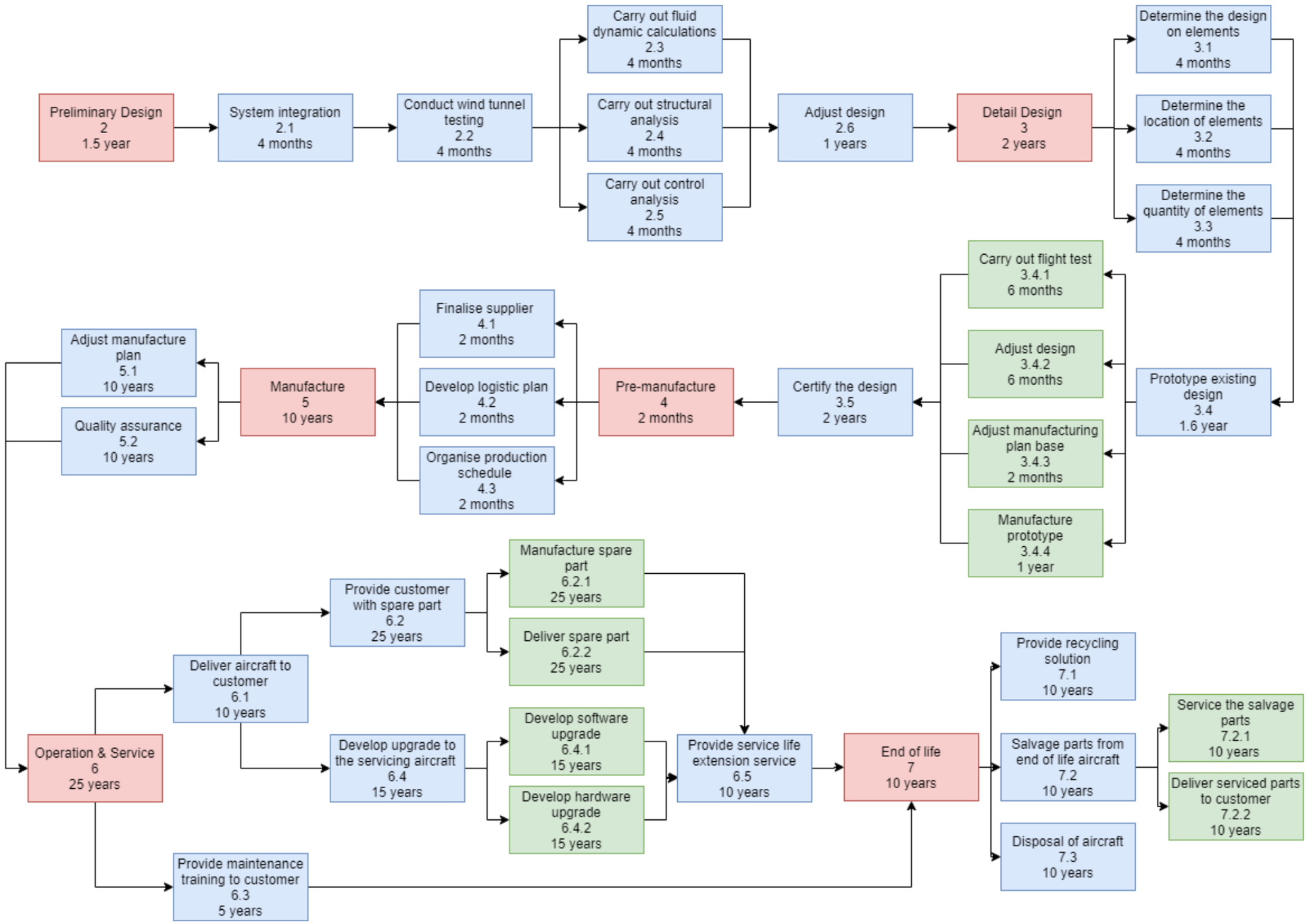

Figure 21.2: Work flow diagram of Post DSE activities

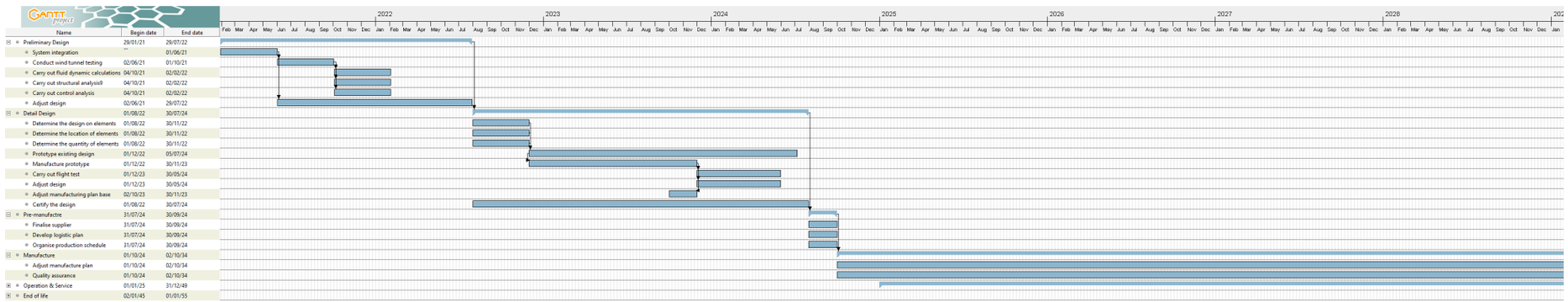

Figure 21.3: Gantt chart for Post DSE activities

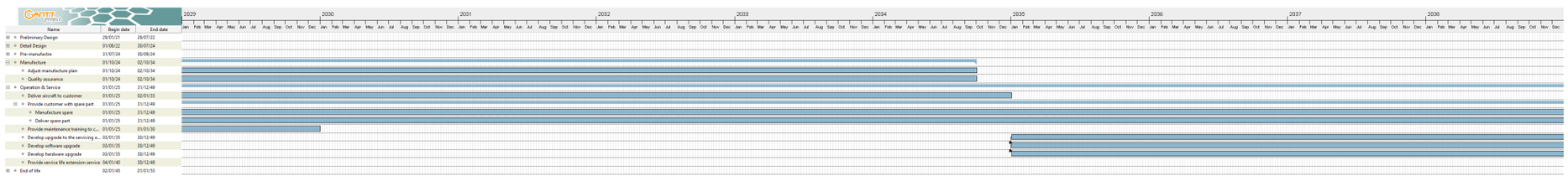

Figure 21.4: Gantt chart for Post DSE activities

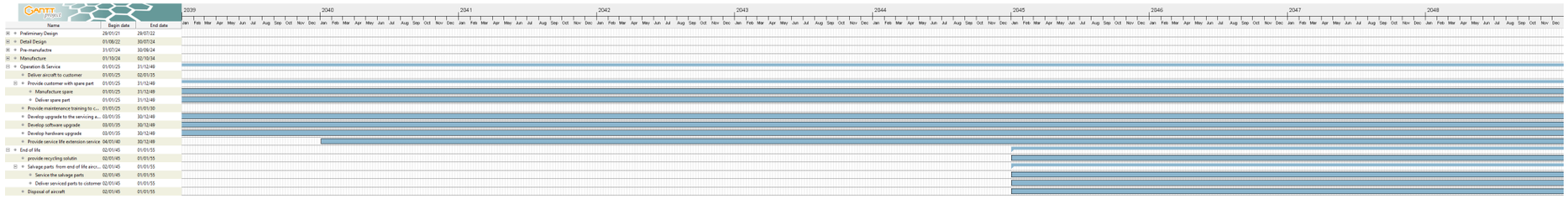

Figure 21.5: Gantt chart for Post DSE activities

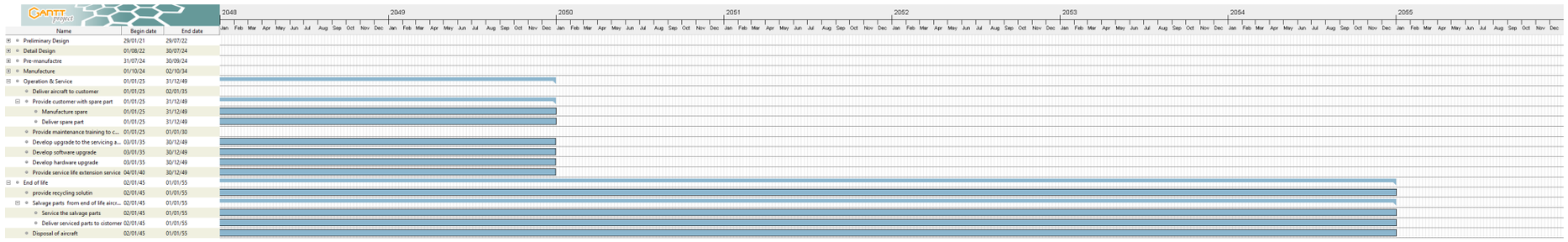

Figure 21.6: Gantt chart for Post DSE activities

22 Compliance to User Requirements & Future Recommendations

In this chapter an overview is presented of the user requirements and if they have been complied with in section 22.1. Furthermore, the future recommendations are described in section 22.2.

22.1. User Requirements Compliance Table

The user (the AIAA) has setup several requirements that impact the design. These requirements are listed below and ticked off whether the requirements are met.

Table 22.1: Compliance check of list of user requirements for the Light Attack Aircraft given by the AIAA

Requirement ID	Description	Method of compliance	Compliance Check
Payload			
LAA-PAY-WTH-1.1	The aircraft shall be able to carry 1360.78 kg (3000 lbs) of armament.	section 5.1	✓
Performance			
LAA-PER-SER-1.1	The service ceiling shall be higher than 9,144 m (30,000 ft).	subsection 7.4.1	✓
LAA-PER-FEM-1.1	The cruise distance during a ferry mission shall be at least 1,666.80 km (900 nmi).	subsection 7.4.1	✓
LAA-PER-DSM-1.1	Descent to 914.40 m (3,000 ft) shall be completed within 20 minutes of the initial climb to the cruise altitude.	subsection 7.4.1	✓
LAA-PER-DSM-2.1	The aircraft shall be able to loiter 4 hours on station without dropping the armament.	subsection 7.4.1	✓
LAA-PER-DSM-3.1	The aircraft shall have reserve fuel sufficient for climb to 914.40 m (3,000 ft) and loiter for 45 minutes after the design mission completion.	subsection 7.4.1	✓
LAA-PER-DSM-3.3	The aircraft shall have a cruise altitude above 3.048 km (10,000 ft)	subsection 7.4.1	✓
LAA-PER-DSM-4.1	The aircraft shall be able to land over a 15.28 m (50 ft) obstacle within a distance of 1219.2 m (4,000 ft) at most and at a density altitude up to 1828.80 m (6,000 ft) on runways with California bearing ratio 5.	subsection 7.4.1, section 10.4	✓
LAA-PER-DSM-4.2	The aircraft shall be able to take off over a 15.28 m (50 ft) obstacle within a distance of 1219.2 m (4,000 ft) at most and at a density altitude up to 1828.80 m (6,000 ft) on runways with California bearing ratio 5.	subsection 7.4.1, section 10.4	✓
Power and Propulsion			
LAA-PAP-DSM-1.1	Warm-up shall take no longer than 5 minutes.	For future recommendation	N/A
LAA-PAP-DSM-1.2	Shutdown shall take no longer than 5 minutes.	For future recommendation	N/A

Table 22.1: Compliance check of list of user requirements for the Light Attack Aircraft given by the AIAA

Requirement ID	Description	Method of compliance	Compliance Check
Time			
LAA-TIM-SER-1.1	The aircraft shall enter service in 2025.	Figure 21.3-Figure 21.6	✓
LAA-TIM-SER-1.2	The aircraft shall have a service life of at least 15,000 hours over 25 years.	Upgrades and service life extension, Figure 21.2	✓
Technology			
LAA-TEC-RDY-1.1	Critical technologies shall be above NASA's technology readiness level (TRL) 8 in 2020. & Driving	chapter 9, chapter 11	✓
Structures			
LAA-STR-WPN-1.1	The aircraft shall feature a board canon to engage ground targets.	section 6.4	✓
LAA-STR-CRW-1.1	The aircraft shall be able to fit two crew members.	section 6.4	✓

22.2. Future Recommendations

Due to time constraints it was not always possible to address all encountered issues fully. For example, it turned out that the aircraft is not stable in spiral mode. It was concluded that a PID was needed. However, there was not enough time to tune the PID controller. Thus, it remains as a recommendation for the future. This, and other recommendations are collected in the following sections. They are split into recommendations regarding general aircraft design, i.e. physical structure, and performance analysis.

In the additional subsystems design, schematic diagrams were made for the fuel, hydraulic and electrical systems. These can be worked out in further detail in a later design stage. Next to this, the environmental control system was not designed, only thought about. In future design stages this system can be designed in more detail.
This also ties into the fuselage design. During future design stages, the subsystems should be integrated into the fuselage.

As stated in chapter 12 it is recommended that the C_{D_0} of the flapped configuration should be checked for errors, as it seems that the trend line is off. It was also recommended that the drag analysis would be verified with a CFD analysis.

In order to make sure the aircraft is in level 1 handling quality for all eigenmotions in all flight phases, a thorough PID controller has to be designed for the aperiodic spiral motion. The basis for this PID controller has been designed, next is adding a sensor and update the transfer functions.

As a future recommendation for the performance analysis, more detailed analysis can be carried out. First up could be the turn rate performance in different flight stages and configurations.

23 Conclusion

The goal of this report was to present the steps that have been taken in the conceptual design phase of a light attack aircraft which can operate from short austere fields, the aircraft was named the A-20 *Chimera*.

A concept was worked out with an iterative Class II component weight estimation, which was implemented in the existing Class I sizing. Different subsystems, mainly the fuselage, wings, empennage, propulsion unit and landing gear, were designed separately. For each subsystem it was concluded that it would comply with the set requirements. Additional subsystems, such as the fuel, hydraulic, and electrical system were designed with redundancy in mind, which makes the aircraft safer to operate in CAS missions.

From the design stages, it was concluded that the aircraft can take off and land on austere fields and arrive at the mission location at short notice. In addition, the wing span provides enough space for six hardpoints next to two guns integrated within the fuselage, hence it was concluded that the A-20 is flexible when it comes to payload choice.

A challenge regarding the logistic plan was to come up with a way to transport the aircraft to mission location in a safe, efficient and cost effective way. It was concluded that the A-20 will be transported by delivery via a standard sized container, as this is the most cost effective way of transportation. Transport by other aircraft will only be used in the event of quick deployment.

From the stability and control analysis, it was concluded that the aircraft is statically stable. However, it is not fully dynamically stable. The phugoid motion and the aperiodic spiral motion in landing configuration did not comply with the desired level 1 handling qualities. This increases the workload for the pilot. Therefore, an auto-throttle and a PID controller had to be designed in order to counteract the phugoid motion and spiral motion respectively.

Performance diagrams were made in order to evaluate the flight configurations and their respective performance, from the diagrams it was concluded that each flight configuration was within their respective positive specific excess power range.

From the market and cost analysis a production quantity, and cost analysis was carried out. When producing 830 aircraft, a unit selling price of $11 million results in a break-even point at 600 units. In comparison to competitive aircraft the A-20 *Chimera* was found to be relatively cheap.

For environmental sustainability, fuel consumption reduction was achieved by reducing the drag by implementing riblets and the use of relatively high aspect ratio wings and horizontal tail, of 7 and 5.8 respectively. Next to this, the shipping of the aircraft in containers was concluded to be more environmentally and financially sustainable. Due to the use of mainly aluminum 20 and 50 series, parts of the aircraft were determined to be more recyclable. Moreover, it was concluded that reducing noise helps the sustainability of the aircraft on multiple levels; environmental, financial, and social.

In general, it was concluded that the A-20 'Chimera' is suitable to carry out missions from short, front-line, austere fields at short notice, while being affordable.

References

[1] D. of Defense, *Joint Service Specification Guide: Air Vehicle* (Department of Defense, United States of America, April 2004).

[2] S. D. Intelligence, *The global military fixed-wing aircraft market 20152025,* (2015).

[3] *The global military fixed-wing aircraft market 2015-2025,* (2015).

[4] J. Roskam, *Airplane Design Part 1: Preliminary Sizing of Airplanes* (Design, Analysis and Research Corporation, 1985).

[5] D. Raymer, *Aircraft Design: A Conceptual Approach* (AIAA, 2004).

[6] J. Roskam, *Airplane Design Part 5: Component Wieght Estimation* (Design, Analysis and Research Corporation, 1985).

[7] J. Roskam, *Airplane Design Part III: Layout Design of Cockpit, Fuselage, Wing and Empennage: Cutaways and Inboard Profiles* (Design, Analysis and Research Corporation, 1985).

[8] J. Marx, M. Portanova, and A. Rabiei, *Performance of Composite Metal Foam Armors against Various Threat Sizes*, Tech. Rep. (North Carolina State University, November 2020).

[9] M. Spick, *Great Book of Modern Warplanes* (Zenith Press, September 2000).

[10] D. R. Barrett, *A-X Overseer*, Tech. Rep. (Kansas University, 2017).

[11] A. Krakers, *Parametric Fuselage Design Integration of Mechanics and Acoustic & Thermal Insulation*, Tech. Rep. (TU Delft, September 2009).

[12] Y. C. J. Kyungtae Kim, *Adhesion enhancement and damage protection for carbon fiber-reinforced polymer (cfrp) composites via silica particle coating,* Composites: Applied Science and Manufacturing (2018).

[13] F. Oliviero, *Ae2111-ii aircraft design & system engineering elements part 2: Lecture slides,* (2020).

[14] E. Torenbeek, *Synthesis of Subsonic Airplane Design* (Delft University Press, 1982).

[15] S. Swedberg and M. Svalstedt, *Commercial Aircraft Wing Structure*, Tech. Rep. (Examenarbete Inom Technology, Grundniva, 2020).

[16] M. S. M. Mohammad R.M. Jamir, Mohammad S.A. Majid, *Natural lightweight hybrid composites for aircraft structural application*, Tech. Rep. (University Malaysia, 2020).

[17] J. Roskam, *Airplane Design Part VI: Preliminary Calculation of Aerodynamic, Thrust and Power Characteristics* (Design, Analysis and Research Corporation, 1987).

[18] F. Oliviero, *Ae3211-i systems engineering and aerospace design,* (2020).

[19] D. of Defense, *Joint Service Specification Guide: Engines, Aircraft, Turbine* (Department of Defense, United States of America, January 2004).

[20] G. Bock, C. Gerlach, H. Beauvais, W. Sarnes, and W. Mörchen, *Operations from unprepared & semi-prepared airfield*, Tech. Rep. (North Atlantic Treaty Organization Advisory Group for Aeronautical Research and Development, September 1960).

[21] J. Roskam, *Airplane Design Part 2: Preliminary Configuration Design and Integration of the Propulsion System* (Design, Analysis and Research Corporation, 1985).

[22] J. P. Lars P. Lauritzsen, *Pressure breathing in fighter aircraft for g accelerations and loss of cabin pressurization at altitude a brief review,* Canadian Journal of Anesthesia (2003).

[23] A. S. J. Shetty, C.P. Lawson, *Simulation for temperature control of a military aircraft cockpit to avoid pilots thermal stress,* CEAS Aeronaut Journal **6**, 319 (2015).

[24] P. K. P. Reddy, *Environmental control system of military aircraft, lca,* International Journal of Engineering Research and Technology (2013).

[25] M. egvi, K. Krajek, and E. Ivanjko, *Technologies for distributed flight control systems: a review,* Faculty of Transport and Traffic Sciences (2015).

[26] T. Frey, C. Aguilar, K. Engebretson, D. Faulk, and L. Lenning, *F-35 information fusion,* AIAA Aviation Forum (2018).

[27] D. of Defense (USA), *MIL-STD-469B: Department of Defense interface standard for radar engineering interface requirements, electromagnetic compatibility*, Tech. Rep. (Department of Defense, 1996).

[28] H. Gavel, *On Aircarft Fuel Systems, Conceptual Design and Modeling*, Tech. Rep. (Linköpings Universitet, 2007).

[29] AIAA, *AIAA 2021 Undergrad Team Aircraft Design RFP* (2020).

[30] A. in 't Veldt, *Ae3212-i: Aerospace flight dynamics,* (2019).

[31] *Military specifications: flying qualities of piloted airplanes,* (1980).

[32] R. M. Johnson, *Using an autothrottle to compare techniques for saving fuel on a regional jet aircraft*, Tech. Rep. (Iowa State University, 2010).

[33] J. S. Handa Xi, *Effects of Actuator Dynamics on Stabilization of High-Speed Planing Vessels with Controllable Transom Flaps*, Tech. Rep. (University of Michigan, 2005).

[34] D. of Defense (USA), *MIL-A-8861B: Military Specification Airplane Strength and Rigidity Flight Loads*, Tech. Rep. (Department of Defense, 1987).

[35] G. Ruijgrok, *Elements of Airplance Performance*, 2nd ed. (Delft Academic Press (VSSD), 2013).

[36] J. D. Anderson. Jr., *Introduction to Flight*, 8th ed. (McGraw-Hill Education, 2016).

[37] J. chiefs of staff, *Joint Bulk Petroleum and Water Doctrine*, Tech. Rep. (Department of the army, USA, 2016).

[38] M. C.T.McCarthy, *12 - Design and failure analysis of composite bolted joints for aerospace composites*, Tech. Rep. (Woodhead Publishing Series in Composites Science and Engineering, 2020).

[39] I. R. Hamann, *Systems engineering & technical management techniques,* System Integration , 90 (2006).

[40] S. Gudmundsson, *General Aviation Aircraft Design* (Butterworth-Heinemann, 2013).

[41] J. C. G. Obaid Younossi, Michael Kennedy, *Military Airframe Costs*, Tech. Rep. (RAND, 2001).

[42] J.L.Brikler and J. Large, *A method for estimating cost of the aircraft structural modification,* Journal of Cleaner Production (1981).

[43] M. Jahanmiri, *Aircraft Drag Reduction: An Overview*, Tech. Rep. (Chalmers University of Technology, 2011).

[44] P. Catalano, D. de Rosa, B. Mele, R. Tognaccini, and F. Moens, *Performance improvements of a regional aircraft by riblets and natural laminar flow,* Journal of Aircraft **57** (2019).

[45] W. H. D.W. Bechert, *Drag reduction with riblets in nature and engineering*, Tech. Rep. (Department of Turbulence Research, German Aerospace Center (DLR), Berlin, Germany, 2006).

[46] J. J. Cook and S. Booth, *"Carbon Fiber Manufacturing Facility Siting and Policy Considerations: International Comparison"*, Tech. Rep. (Clean Energy Manufacturing Analysis Center, June 2017).

[47] T. Melton, *The benefits of lean manufacturing: What lean thinking has to offer the process industries,* Chemical Engineering Research and Design , 662 (2005).

[48] S. K. Das and J. G. Kaufman, *Recycling aluminium aerospace alloys,* Light Metals 2007 , 1161 (2007).

[49] T. Z. Humsa and R. K. Srivastava, *Impact of rare earth mining and processing on soil and water environment at chavara, kollam, kerala: A case study,* Elsevier: Procedia Earth and Planetary science **11**, 566 (2015).

[50] V. R. Patlolla and R. Asmatulu, *Recycling and reusing fiber-reinforced composites.* Recycling: Technological Systems, Management Practices and Environmental Impact , 193 (January 2013).

[51] M. Boito, E. G. Keating, J. Wallace, B. DeBlois, and I. Blum, *Metrics to Compare Aircraft Operating and Support Costs in the Department of Defense*, Tech. Rep. (RAND Corporation, Santa Monica, CA, 2015).

[52] S. Dalkilic, *Improving aircraft safety and reliability by aircraft maintenance technician training,* Engineering Failure Analysis **82**, 687 (2017).

[53] B. A. Weisbrod, *Investing in human capital,* The Journal of Human Resources **1**, 5 (1966).

[54] T. Maudgalya, A. Genaidy, and R. Shell, *Productivityqualitycostssafety: A sustained approach to competitive advantagea systematic review of the national safety council's case studies in safety and productivity,* Human Factors and Ergonomics in Manufacturing & Service Industries **18**, 152 (2008).

[55] S. J. Nethery, *Military Aircraft and Airport Noise and Opportunities for Reduction without Inhibition of Military Missions*, Tech. Rep. (Environmental Protection Agency, 1973).

[56] R. W. Hess and H. Romanoff, *Aircraft Airframe Cost Estimating Relationships* (RAND, December 1987).

[57] R. Byers, J. Sorroche, M. Christopher, G. Shanks, and B. Hinkle, *Standard for: Link 11/11b simulation sisostd005-v13 draft,* Simulation Interoperability Standards Organization (2014).

[58] B. E. White, *Tactical data links, air traffic management and software programmable radios,* The Computer Journal (1999).

[59] R. Jain, F. Templin, and K.-S. Yin, *Analysis of l-band digital aeronautical communication systems: L-dacs1 and l-dacs2,* IEEE Xplore (2010).

[60] T. Okura, *Materials for Aircraft Engines*, Tech. Rep. (University of Colorado Boulder, 2015).

[61] Y. W. Kwon, *Strength of Composite Scarf Joints*, Tech. Rep. (Naval Postgraduate School, 2011).

[62] D. of Defense, *Joint Service Specification Guide: Air System* (Department of Defense, United States of America, October 2002).

[63] D. of Defense, *Joint Service Specification Guide: Aircraft Structures* (Department of Defense, United States of America, October 1998).

[64] D. of Defense, *Joint Service Specification Guide: Air Vehicle Subsystems* (Department of Defense, United States of America, November 2013).

[65] R. Dahiya and A. K. Singh, *Performance analysis of control techniques for roll movement of aircraft,* International Journal Of Engineering And Computer Science 5 , 19212 (2017).

A Appendix A: Drag Analysis

Table A.1: Input values for drag analysis.

Wing			**Fuselage**			**Empenage**			**Nacelle**		
S	50.6	[m^2]	S_{wet}	20.1	[m^2]	S_{wet_v}	5.8	[m^2]	N_l	2.8	[m]
$\Lambda_{0.25c}$	0	[rad]	l_f	15	[m]	S_{wet_h}	22.3	[m^2]	N_d	0.89	[m]
MAC	2.85	[m]	d_f	1.28	[m]	t/c	0.1	[-]	$S_{wet_{nac}}$	7.0	[m^2]
A	7	[-]	S_{fus}	2	[m^2]	MAC_v	1.1	[m]	S_{nac}	2.79	[m^2]
λ	0.4	[-]	$S_{b_{fus}}$	0.134	[m^2]	MAC_h	1.4	[m]	$S_{nac_{base}}$	0.80	[m^2]
e	0.84	[-]	$S_{fus_{plf}}$	13.316	[m^2]						
t/c	0.18	[-]									
L'	1.2	[-]									
S_{wet}	97.0	[m^2]									
Stores			**Flaps**			**Landing gear**			**Fearing**		
# of stores	6	[-]	S_{wf}	27.25	[m^2]	*Main*			F_l	2.75	[m]
S_{store}	0.86	[m^2]	b_{f_i}	1.2	[m]	S_{front}	1.87	[m^2]	F_d	0.82	[m]
$S_{b_{store}}$	0.19	[m^2]	b_{f_0}	9.8	[m]	width	0.64	[m]	S_{wet}	8.37	[m^2]
$S_{wet_{store}}$	0.13	[m^2]	b	18.8	[m]	height	1.25	[m]	$S_{fearing}$	1	[m^2]
K	1.3	[-]	K	0.23	[-]	*Nose*			$S_{fearin_{base}}$	0.34	[m^2]
			K_{int}	0.3	[-]	S_{front}	0.28	[m^2]			
						height	1.99	[m]			
						width	4.13	[m]			

B
Appendix B: Dynamic Stability

Table B.1 represents the derivative results described in section 13.5.

Table B.1: Longitudinal stability derivative data A20-Chimera

Longitudinal derivatives	Cruise	Landing	Loiter
C_{X_α}	-0.0881	-0.7826	-0.3293
C_{X_u}	-0.0944	-0.7139	-0.4156
C_{Z_α}	-5.5977	-4.2101	-5.3566
$C_{Z_{\dot{\alpha}}}$	2.1398	2.6279	2.4657
C_{Z_q}	-12.3350	-9.8499	-11.7716
C_{Z_u}	-0.0875	-0.0443	-0.0398
C_{m_α}	-0.8945	-0.6992	-0.8560
$C_{m_{\dot{\alpha}}}$	-4.7902	-5.7146	-5.5197
C_{m_q}	-7.1895	-7.9098	-8.633
C_{m_u}	0.0044	0.0077	0.0063

Secondly Table B.2 represents the derivative results described in section 13.6.

Table B.2: Lateral stability derivative data A20-Chimera

Lateral derivatives	Cruise	Landing	Loiter
C_{Y_β}	-0.4376	-0.4270	-0.4376
C_{l_β}	-0.0825	-0.0723	-0.0864
C_{l_p}	-0.4987	-0.5129	-0.4943
C_{l_r}	0.2202	1.7366	0.7355
C_{n_β}	0.1216	0.1310	0.1234
C_{n_p}	0.0000	-0.3365	0.0000
C_{n_r}	-0.1736	-0.2156	-0.1801